International Journal of Mathematical Analysis and Modelling

(Formerly Journal of the Nigerian Society for Mathematical Biology)

Volume 5, Issue 4 (Nov.), 2022

ISSN (Print): 2682 - 5694
ISSN (Online): 2682 - 5708

International Journal of Mathematical Analysis and Modelling (Formerly Journal of the Nigerian Society for Mathematical Biology)

Volume 5, Issue 4 (November), 2022

ISSN (Print): 2682 – 5694

ISSN (Online): 2682 - 5708

A publication of the Nigerian Society for Mathematical Biology

International Journal of Mathematical Analysis and Modelling
Volume 5, Issue 4, November 2022, Pages 1 – 13

Analytical Method for Estimation of Black-Scholes Equation of Option Pricing

I.U. Amadi[1] and B.E. Umoh[2]

Abstract

The attainment of any investments hinge on the value of options which impels the entire financial authority of every trader and Black-Scholes equation are well known prevailing mathematical instrument used for the estimations of stock option prices. Therefore, this paper, considered the concept of option pricing by means of Black-Scholes equation which governs the growth of option price with esteem to the expiration and cost of the fundamental asset. These equations were modified to assume a probability which measures risk-free interest rate of the underlying asset for Call and Put options. The Black-Scholes exact values and Modified Black-Scholes values were obtained and compared to close form prices. Finally, graphical solutions and interpretations of relevant parameters were well discussed.

Keywords: stock prices; Black-Scholes equation; call option; put option; error

1 Introduction

An option is a tool whose worth is derived from the principal asset which is otherwise known as financial derivative. This type of derivative does have anything in common with mathematical meaning of derivative. In other words, an option on underlying asset is a business between parties who come together to agree on either buying or selling an underlying asset at a determined strike price in the future for a fixed price. The cost of the option lies on the underlying asset, which is usually a stock, commodity, currency or an index [1]. The holder has the right but cannot be compelled to buy, for call option where European put option involves the ability to sell an asset for a certain charge at a prescribed date in the future. Options are known as "*in- the money*", "*at- the money*", or "*out- of the money*". If S is a stock price and K is the strike price, a call option is in- the money as soon as S >K, at- the money when S=K, and out -of –the- money when S<K. A put option is in the money as soon as S<K, at- the -money once S=K, and out- of- the money once S>K. Obviously, an option is exercised only when it is in- the money. In the nonappearance of transactions costs, an in-the money option is always exercised on the expiration date if it has not been exercised earlier [2].

[1]Corresponding Author. Department of Mathematics/ Statistics, Captain Elechi Amadi Polytechnic, Rumuola, Port Harcourt, Nigeria; Email: innocent.amadi@portharcourtpoly.edu.ng
[2]Department of Mathematics/ Statistics, Ignatius Ajuru University of Education, Rumuolumeni, Port Harcourt, Nigeria; Email: umohbella5@gmail.com

The relevance of options valuation was first demonstrated by Black-Scholes [3] when option faced difficulties in valuation of option at expiration. They used no-arbitrage argument to explain a partial differential equation which governs the growth of the option price with esteem to the expiration and cost of the fundamental Asset. The Black-Scholes equation has been used widely in many financial applications.

For instance, [4] studied implied volatility and implied risk free rate of return in solving systems of Black- Scholes equations. In their research they established that options prices provides important information for market participants for future expectations and market policies. In the same vain [5] analyzed BS formula for the valuation of European options; Hermite polynomials were applied. They concluded that BS formula can easily be achieved devoid of the use of partial differential equation. In another study of BS [6] considered the BS terminal value problem and observed that their proposed method is better, simple than the previous methods. In the work of [7] time varying factor were incorporated in the explicit formula for different aspect of options with the aim of providing exact solution for dividend paying equity of option. In considering the stability of stock market price of stochastic model,[8] applied Crank-Nicolson numerical scheme to BS model. The results showed stock prices being stable and its increasing rate of stock shares was obtained. Not quite long,[9] investigated the variation of stock market price using BS PDE. The convergence to equilibrium of growth rate and sufficient conditions for stability was achieved. However,[10] studied Black-Scholes model because of its biasness in mispricing options. They established a new technique of assessing pricing effects on the premise to reduce pricing bias.

In financial markets, investors and financial analysts are generally too interested on how to maximize profit over particular trading days, that is, the changes in the price of goods and services. Therefore, modeling a behavior of a stock exchange market can be made through its relative change of the unstable market variables in time so as to predict stock price fluctuation, advice investors and corporative owners who are working out for convenient ways to do business by issuing of stocks in their corporations. The origin of this work lies in the study of [11]. This is so since the path of the stock price method can be allied to his description of the random collision of some tiny particles with the molecules of the liquid he introduced, hence the name Brownian motion. Now, the market price behavior shows the characteristics as a stochastic process called "Brownian motion" or Wiener process with drift. It is an important example of stochastic processes satisfying a Stochastic Differential Equation (SDE) displayed in Figure 1.

The analytical approach of solving BS equation for option pricing is not a difficulty one. It becomes multifarious when some levels of probability measures are considered to assess riskless interest rate of the underlying asset in the model. This difficulty depends when the analytical approach is being determined; which is the novelty of this paper. To propose an analytical approach of BS equation; this will be comparable or possibly better than the original BS equation. The great encounter in the modification is the ability of coming up with some realistic assumptions that will be incorporated into the model.

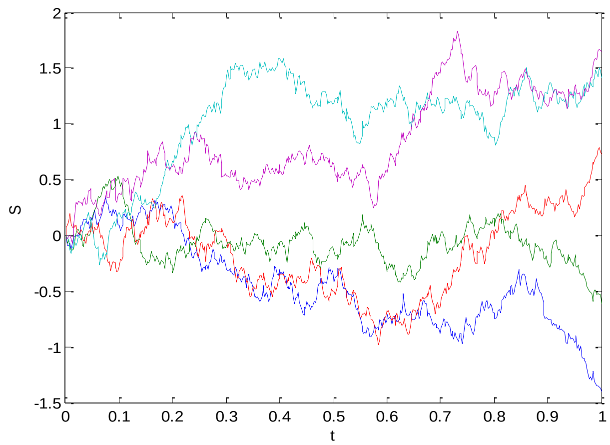

Figure 1: Sample trajectories of the stock price process following Black-Scholes Model

This study is aimed at modifying Black-Scholes equation such we obtain comparable results with BS. To this end, this type of work has not been seen elsewhere as these widens the area of application of problem of this nature.

For the purpose of this study the paper is arranged as follows: Section 2.1 presents the Mathematical preliminaries, problem formulation is seen in Subsection 2.1.1, method of solution is seen in Subsection 2.1.2, Results and discussion are seen in Section 3 and paper is concluded in Section 4.

2.1 Mathematical Preliminaries

Here we present some definitions as foundations of this mathematical finance models.

Definition 1. Probability space: This is a triple $(\Omega, \mathrm{F}, \tilde{A})$ where Ω represents a set of sample space, F represents a collection of subsets of Ω, while $\wp$ is the probability measure defined on each event $A \in \mathrm{F}$. The collection F is a σ -algebra or σ -field such as $\Omega \in \mathrm{F}$ and F is closed under the arbitrary unions and finite intersections. Hence it is called probability measure when the following condition holds.

(i) $\quad P(A) \geq 0 \;\; for\ all\ \; A \subset \Omega \qquad (1)$

(ii) $\quad P(\Omega) = 1 \qquad (2)$

(iii) $\quad A, B \subset \Omega,\; A \cap B = \phi \; then \; P(A \cup B) = P(A) + P(B) \qquad (3)$

Definition 2. Normal Distribution: A normal distribution function is a peculiar distribution in probability theory and is usually used for modeling asset returns. A normal distribution is used in the Black-Scholes Partial differential equation to value European options. A normal distribution depends on two parameters,[12].

Mean, $\mu \in \mathbb{R}$, is the expectation of a random variable normal distribution.

Variance , $\sigma^2 > 0$, deals with the magnitude of the spread from the mean.

In Black-Scholes formula, normal distributions are used. The cumulative distribution, usually denoted as $\phi(X)$, is the probability that X will be equal to or less than X ,expressed as $F_x(x) = P(X \leq x)$. A standard normal cumulative distribution function is defined as.

$$\phi(x) = \frac{1}{\sqrt{2\pi}} \int_{-\infty}^{x} e^{-\frac{t^2}{2}} dt \tag{4}$$

A normal distribution is a symmetric distribution, which means that it touches around a vertical axis of symmetry. Obviously, there is a connection between any given points with same distance to the vertical axis. This relationship is defined in equation 1.5.5

$$\phi(x) = 1 - \phi(-x). \tag{5}$$

Definition 3. A σ -algebra is a set F of subsets of Ω with the following axioms:

(i) $\phi, \Omega \in \mathrm{F}$ (6)

(ii) If $A \in \mathrm{F}, then\ A^c \in \mathrm{F}$ (7)

(iii) If $A_1, A_2, \ldots, \in \mathrm{F}, then \bigcup_{k=1}^{\infty} A_k, \bigcap_{k=1}^{\infty} A_k \in \mathrm{F}$ (8)

Clearly $A^c := \Omega - A$ is the complement of A.

Definition 4. If F is a σ -algebra in Ω, then Ω is called a measurable space and the members of F are called the measurable sets in Ω.

Definition 5. Let (Ω, M) be a measurable space .A map $\mu : \mathrm{M} \to \mathbb{R} = [0, \infty) \cup \{\infty\}$ is called a measure provided that

(i) $\mu(\phi) = 0$ (9)

(ii) $\mu\left(\bigcup_{n=1}^{\infty} A_n\right) = \sum_{n=1}^{\infty} \mu(A_n)$ (10)

Definition 5. Stochastic process: A stochastic process $X(t)$ is a relations of random variables $\{X_t(\gamma), t \in T, \gamma \in \Omega\}$, i.e, for each t in the index set T, $X(t)$ is a random variable. Now we understand t as time and call $X(t)$ the state of the procedure at time t . In view of the fact that a stochastic process is a relation of random variables, its requirement is similar to that for random vectors.

It can also be seen as a statistical event that evolves time in accordance to probabilistic laws. Mathematically, a stochastic process may be defined as a collection of random variables which are ordered in time and defines at a set of time points which may be continuous or discrete.

Definition 6. A stochastic process whose finite dimensional probability distributions are all Gaussian.(Normal distribution).

Definition 7. Random Walk: There are different methods to which we can state a stochastic process. Then relating the process in terms of movement of a particle which moves in discrete steps with probabilities from a point $x=a$ to a point $x=b$. A random walk is a stochastic sequence $\{S_n\}$ with $S_0=0$, defined by

$$S_n = \sum_{k-1}^{n} X_k \qquad (11)$$

where X_k are independent and identically distributed random variables

Definition 8: Stochastic Differential Equation (SDE)
Let $S(t)$ be the price of some risky asset at time t ,and μ ,an expected rate of returns on the stock and dt as a relative change during the trading days such that the stock follows a random walk which is govern by a stochastic differential equation.

$$dS(t) = \alpha S(t)dt + \sigma S(t)dW_t \qquad (12)$$

Where, α is drift and σ the volatility of the stock, W_t is a Brownian motion or Wiener's process on a probability space $(\Omega, \xi, \wp), \xi$ is a $\sigma-\text{algebra}$ generated by $W_t, t \geq 0$.

Theorem 1.1: (Ito's formula) Let $(\Omega, \beta, \alpha, \mathrm{F}(\beta)$ be a filtered probability space $X = \{X, t \geq 0\}$ be an adaptive stochastic process on $(\Omega, \beta, \alpha, \mathrm{F}(\beta)$ possessing a quadratic variation (X) with SDE defined as:

$$dX(t) = g(t, X(t))dt + f(t, X(t))dW(t) \qquad (13)$$

$t \in \Re$ and for $u = u(t, X(t) \in C^{1\times 2}(\Pi \times \square))$

$$du(t, X(t)) = \left\{\frac{\partial u}{\partial t} + g\frac{\partial u}{\partial x} + \frac{1}{2}f^2\frac{\partial^2 u}{\partial x^2}\right\}d\tau + f\frac{\partial u}{\partial x}dW(t) \qquad (14)$$

Using theorem 1.1 and equation (12) comfortably solves the SDE with a solution given below:

$$S(t) = S_0 \exp\left\{\sigma dW(t) + \left(\alpha - \frac{1}{2}\sigma^2\right)t\right\}, \forall t \in [0,1].$$

2.1.1 Problem Formulation
This Section modifies BS model and presents the tools that can analyze empirically the dynamics of option pricing. In particular, we compare the results of original BS and that of modified one for the purpose of prediction and other capital investments. However, assuming there are N stocks in the capital market. Let $S_i,\ i = 1, 2, \ldots, N$ be the initial stock prices for T trading days. Since Black-Scholes equation is based on seven assumptions, we therefore, incorporate the probability of riskless asset. However, the seven assumptions are:

The asset price has characteristics of a Brownian motion with μ and σ as constants, the transaction costs or taxes are not allowed, the entire securities are absolutely divisible, dividend is not permitted during the period of the derivatives, unacceptable of riskless arbitrage opportunities, the security trading is constant, the option is exercised at the time of expiry for both call and put options.

Nevertheless, the dynamics of option pricing is given by the partial differential equation as follows:

$$\frac{\partial V}{\partial t}+\frac{1}{2}\sigma^2 S^2\frac{\partial^2 V}{\partial S^2}+rS\frac{\partial V}{\partial S}-rV=0. \tag{15}$$

To eliminate the price process in (15) slightly gives the Black-Scholes analytic formula for Call and Put options:

The analytic formula for the prices of European call option is given as follows

$$\left.\begin{aligned} C &= SN(d_1)-Ke^{-rt}N(d_2)\\ d_1 &= \frac{\ln\left(\frac{S}{K}\right)+\left(r+\frac{\sigma^2}{2}\right)T}{\sigma\sqrt{T}}\\ d_2 &= d_1-\sigma\sqrt{T} \end{aligned}\right\} \tag{16}$$

where C is Price of a call option, S is price of underlying asset, K is the strike price, r is the riskless rate , T is time to maturity, σ^2 is variance of underlying asset, σ is standard deviation of the (generally referred to as volatility) underlying asset, and N is the cumulative normal distribution.

Similarly, the formula for prices of European put option is given as

$$P = SN(d_1)-Ke^{-rt}N(d_2) \tag{17}$$

where P is the price of a put option and the meaning of other parameters remain the same as in (16) see [13] , [14] and [15] etc.

In option trading and capital investment, profit making is not known in advanced but is an uncertain stochastic variable. We therefore use ϕ_t to measure the probability levels of risk-free interest rate, r of the underlying asset which motivates to define as:

$$(1-\phi_t) \tag{18}$$

(18) Is the probability of risk free interest rate .Hence, it is a statistics concept that carries a major significance in financial mathematics. Therefore, using (18) modifies the BS equation as follows:

$$\left.\begin{aligned} C &= SN(d_1) - Ke^{-rt}(d_2) \\ d_1 &= \frac{\ln\left(\frac{S}{K}\right) + r\left((1-\phi_t) + \frac{\sigma^2}{2}\right)\tau}{\sigma\sqrt{\tau}} \\ d_2 &= d_1 - \sigma\sqrt{\tau} \end{aligned}\right\} \tag{19}$$

Similarly, the formula for prices of European Put option is given as

$$P = SN(d_1) - Ke^{-rt}N(d_2). \tag{20}$$

3 Results and discussion

This Section presents the simulated results for the problem stated in Subsection 2.1.1. The graphical results are implemented using MATLAB programming software.

Table 1: Comparing the performance of the Black-Scholes exact values and Modified Black-Scholes(MBS) for European Call Option when initial stock prices are 60 and 70 with K = 25, r = 0.2 and T = 1 , $\phi_t = 0.03$.

Sigma	So = 60, E = 25, ϕ =0.03			So =70, E =25,r=0.2		
	BS Exact Values	MBS Exact Values	Relative Error	BS Exact values	MBS Exact Values	Relative Error
0.25	39.5317	39.5317	0.0000	49.5317	49.5317	0.0000
0.3	39.5322	39.5322	0.0000	49.5318	49.5318	0.0000
0.35	39.5353	39.5353	0.0000	49.5325	49.5325	0.0000
0.4	39.5469	39.5469	0.0000	49.5361	49.5361	0.0000
0.45	39.5750	39.5750	0.0000	49.5476	49.5476	0.0000
0.5	39.6277	39.6276	0.000003	49.5736	49.5736	0.0000
0.55	39.7106	36.7106	0.0000	49.6208	49.6208	0.0000
0.6	39.8273	36.8273	0.0000	49.6946	49.6945	0.000002
0.65	39.9788	36.9756	0.00008	49.7985	49.7984	0.000002
0.7	40.1643	40.1642	0.000002	49.9342	49.9341	0.000002
0.75	40.3820	40.3819	0.000002	50.1020	50.1019	0.000002
0.8	40.6295	40.6294	0.000002	50.3009	50.3008	0.000002
0.85	40.9038	40.9037	0.000002	50.5291	50.5290	0.000002

0.9	41.2022	41.2021	0.000002	50.7846	50.7845	0.000002
0.95	41.5216	41.5215	0.000002	51.0650	51.0648	0.000004
1.0	41.8593	41.8592	0.000002	51.3675	51.3674	0.000002

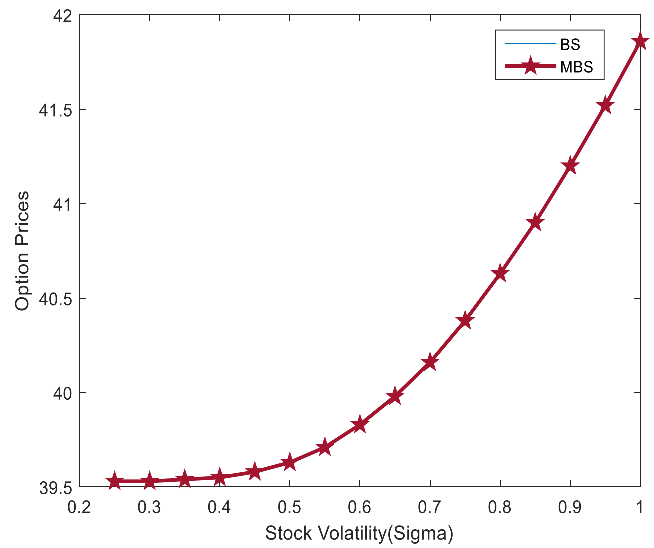

Figure 2: Profiles of BS and MBS for call option when initial stock price is 60.

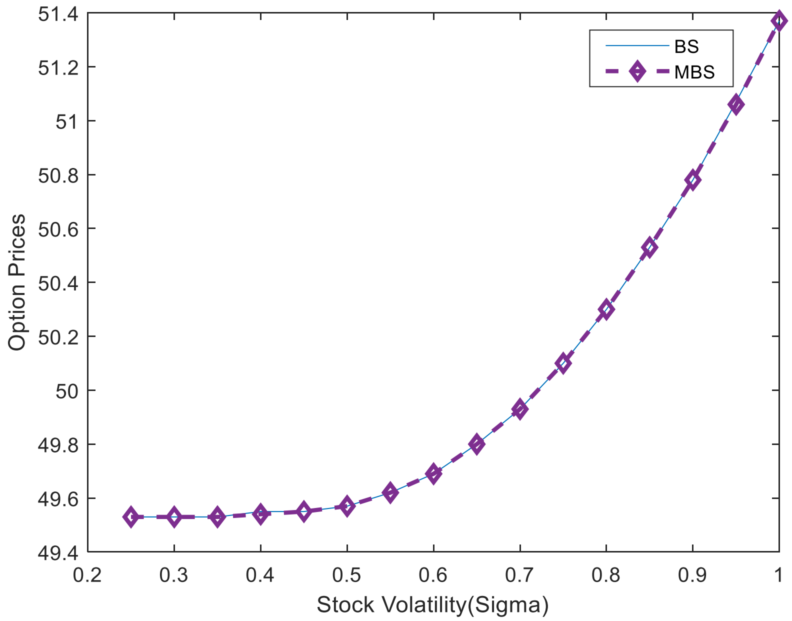

Figure 3: Profiles of BS and MBS for call option when initial stock price is 70.

Table 2: Comparing the performance between the Black-Scholes exact values and Crank-Nicolson finite difference method for European Put Option when initial stock prices are 60 and 70with K = 100, r = 0.2 and T = 1, $\phi_t = 0.03$.

Sigma	$S_o = 60$, $K = 100$, ϕ =0.03			$S_o = 70$, $K = 100$		
	BS Exact values	MBS Exact Values	Relative Error	BS Exact Values	MBS Exact Values	Relative Error
0.25	22.7672	22.7663	0.0004	14.9160	14.9143	0.0001
0.3	23.4960	23.4951	0.00004	16.1862	16.1847	0.0001
0.35	24.3677	24.3667	0.0053	17.5121	17.5107	0.00009
0.4	25.3408	25.3399	0.00004	18.8713	18.8701	0.00006
0.45	26.3860	26.3852	0.00003	20.2504	20.2492	0.00006
0.5	27.4826	27.4818	0.00003	21.6405	21.6395	0.00005
0.55	28.6158	28.6150	0.00003	23.0357	23.0348	0.00004
0.6	29.7745	29.7738	0.00003	24.4317	24.4309	0.00003
0.65	30.9508	30.9502	0.00003	25.8252	25.8244	0.00003
0.7	32.1384	32.1378	0.00002	27.2137	27.2130	0.00003
0.75	33.3325	33.3319	0.00021	28.5950	28.5944	0.00002
0.8	34.5291	34.5285	0.00002	29.9675	29.9669	0.00002
0.85	35.7250	35.7245	0.00001	31.3296	31.3290	0.00002
0.9	36.9177	36.9172	0.00001	32.6800	32.6794	0.00002
0.95	38.1049	38.1045	0.00001	34.0175	34.0170	0.00001
1.0	39.2848	39.2844	0.00001	35.3412	35.3407	0.00001

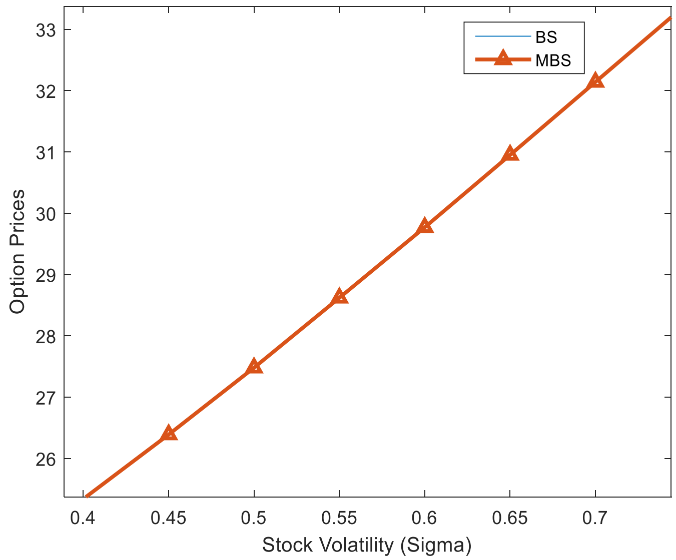

Figure 4: Profiles of BS and MBS for put option when initial stock price is 60.

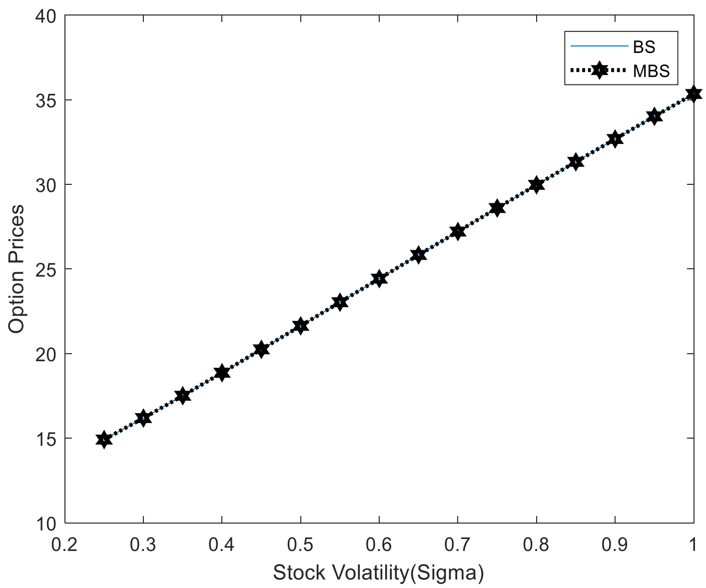

Figure 5: Profiles of BS and MBS for put option when initial stock price is 70.

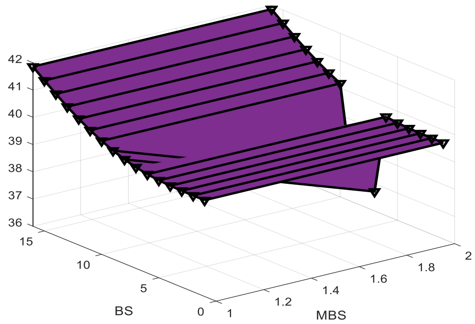

Figure 6: Surface view of BS call option when the initial stock price is 60 with variations of stock volatility (sigma).

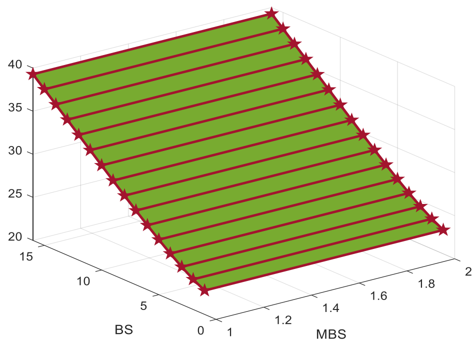

Figure 7: Surface view of BS put option when the initial stock price is 60 with variations of stock volatility (sigma).

Values in Tables 1 and 2 were generated by fixing r=0.2, k=25 $\phi_t = 0.03$ while allowing S_0 and σ vary in (16) - (20) for call and put options such that $S_0 = 60$ and 70 , $\sigma = (0.25, 0.30, ..., 1.00)$ presented in columns 1 are the difference values of σ ,columns 2 and 3 are the exact values of BS and MBS respectively. The 4th columns gives the relative error (RE) of the difference between the estimated prices using BS and MBS pricing schemes .RE is the ratio of absolute difference between BS and MBS to BS such that when this ratio is very small, the performances of both BS and MBS are equivalent.

However, it is clear that increasing stock volatility increases the value of option prices throughout the stipulated trading days. It implies that such trading business is profit maximizing in terms of long and short term investment plans as the future of investment is known against tomorrow. This situation informs investors on the activities of volatility in the capital investment hence it measures the price changes, see Tables 1 and 2 respectively.

Figures 2 and 3 describe the process of trading in respect to call option. The plots moves along sigma axis before it eventually make an upward trend. This price formation informs an investor the best decision to take in order to maximize profit; hence the process of this trading business is curve linear in nature.

As seen in Figures 4 and 5 respectively , the two plots defines changes over short and long term business plans which is linear; this means that there's a linear relationship during the time of trading activities of options. Carefully inspection of the plots shows that volatility increases linearly as option price increases throughout the trading days, with the trend of being 1; which informs an investor for proper decision making. The range of regression is within$1 \leq r \leq -1$; by this formation means that there is total sure of high rate of returns.

Figure 6 shows numerical illustration of different values of option prices. The plane at a point had jump discontinuity in the buying of underlying asset; which causes misrepresentation in stock market throughout the trading days.

In Figure 7, it is evident that there are positive option trajectories as a result of trading continuities. This continuity in selling of commodities is in relation to income price investments. This remark is profit maximizing which may be indexed in millions of naira in life of option trading.

4 Conclusion

The option pricing can be understood properly by the dynamics of Black-Scholes Equation. Consequently this paper, considered the concept of option pricing by means of Black-Scholes equation which governs the growth of option price with esteem to the expiration and cost of the fundamental asset. These equations were modified to assume a probability which measures risk-free interest rate of the underlying asset for Call and Put options. From the simulated results shows as follows:
MBS had comparable results even better than Black-Scholes (BS) exact values.
An increase in stock volatility increases option prices for call and put respectively.
The difference between BS values and MBS values are not significant.

However, we shall be looking at using the same assumption of modification of BS in harnessing the approximate solution of Black-Scholes partial differential equation in the next study.

References

[1] Kwok, Y.K. (2008). Mathematical models of financial derivatives. Springer-Verlag, Singapore.
[2] Hull, J. C. (2012). Option, futures and other derivatives (eighth edition). Prentice Hall, Boston Columbus Indianapolis, New York San Francisco.
[3] Black, F. and Scholes, M. (1973). The pricing of options and corporate liabilities. The Journal of Political Economy, 81: 637-654.
[4] Marcelo, B., Scott, M. and Marco, S. (2014). Implied volatility and the risk-free rate of return in option markets. Preliminary Draft, Comments welcome.
[5] Babasola, O. L., Irakoze, I. and Onoja, A. A. (2008). Valuation of european options within the black-scholes framework using the hermite polynomial. Journal of Scientific and Engineering Research, 5(1): 213-221.
[6] Shin, B. and Kim, H. (2016). The solution of Black-Scholes terminal value problem by means of Laplace transform. Global Journal of Pure And Applied Mathematics, 12: 4153-4158.
[7] Rodrigo, M.R. and Mammon, R.S. (2006). An alternative to solving the Black-Scholes equation with time-varying parameters. Applied Mathematics, 19: 398-402.

[8] Osu, B.O. Okoroafor, A .C and Olunkwa, C. (2009). Stability analysis of stochastic model of stock market price. African Journal of Mathematics and Computer Science Research, 2(6):98-103.
[9] Osu, B.O. (2010). A stochastic model of the variation of the capital market price. International Journal of Trade, Economics and Finance, 1(3):297-302.
[10] Nwobi, F.N., Annorzie, M.N. and Amadi, I.U. (2019). Crank-Nicolson finite difference method in valuation of options. Communications in Mathematical Finance, 8(1):93-122.
[11] Robert, B. (1964). Theories de la Speculative. Gauthier-Villar, Paries.
[12] Westergren, B. and Rade, L. (2003). Mathematics handbook for science and engineering Student literature AB.
[13] Hull, J.C. (2003). Options, futures and other derivatives, (5 Edition). Prentice Hall International, London.
[14] Higham, D.J. (2004). An introduction to financial option valuation: mathematics, statistics and computation. Department of Mathematics, University of Strathclyde, Cambridge University Press.
[15] Wilmott, P., Howison, S. and Dewynne, J. (2008). Mathematics of financial derivatives. Cambridge University Press, New York.

International Journal of Mathematical Analysis and Modelling
Volume 5, Issue 4, November 2022, Pages 14 – 24

Developments in computational optimization techniques of conjugate gradient coefficient, search direction, Broyden-Fletcher-Goldfarb-Shanno, symmetric-rank one and Davidon-Fletcher-Powell quasi-Newton methods.

A. Adams[*†], U.Y. Abubakar[*‡], U. Abubakar[*] and Y. Yakubu[*]

Abstract

In this paper, we propose a modified Conjugate Gradient Coefficient (β) for solving unconstrained minimization problems as well as the Broyden-Fletcher-Goldfarb-Shanno, Davidon-Fletcher-Powell (DFP) and Symmetric-Rank-One (SR1) updates. The modified. It is proved that the resulting Conjugate Gradient Coefficient have global convergence under some mild conditions as well as the search direction(d). It is also proved that the search direction plays a key role in the line search method and the step size approaches mainly guarantee global convergence in general cases. The convergence rate of this method is also investigated. Some numerical results show that the modified Conjugate Gradient Coefficient algorithm is effective in practical computation.

Keywords: unconstrained optimization; quasi-newton method; hybridization; global convergence; symmetric-rank-one (sr1); Davidon-Fletcher-Powell (DFP).

1 Introduction

Quasi-Newton methods are distinguished by their use of approximate Hessian matrices. These approximate matrices are evaluated with respect to some iterative update formula as the algorithm progresses. The update procedure only requires the gradient of the objective function at each iteration. Thus, these methods provide a way of obtaining some curvature information without evaluating the exact Hessian. This is particularly useful when Hessian is very demanding to compute or cannot be computed at all for some reason. Because they are known to be generally more applicable and quite efficient, quasi-Newton methods are still widely used tools of nonlinear programming even after the development of automatic differentiation packages, Nocedal and Wright (2006). There are numerous works on the use of quasi-Newton methods either in line-search or trust-region applications.

[*] Department of Mathematics, Federal University of Technology, Minna, Niger State, Nigeria.
[†] Corresponding Author. Email: adamsayuba90@gmail.com
[‡] Email: abbkruy@yahoo.com

Consider the unconstrained minimization problem

$$\min_{x \in \mathcal{R}^n} f(x), \tag{1}$$

where $f: \mathcal{R}^n \to \mathcal{R}$ is continuously differentiable function, the Conjugate Gradient (CG) methods are the best methods for solving (1), especially when the dimension n is large. The iterates of Conjugate Gradient (CG) methods for solving (1) are obtained as

$$x_{k+1} = x_k + \alpha_k d_k \; ; \qquad k = 0, 1, 2, \dots \dots \dots \tag{2}$$

where x_k is the current iterate point and $\alpha_k > 0$ is the step size. The step size is computed by carrying out some line search, especially the exact line search as given below

$$f(x_k + \alpha_k d_k) = \min_{\alpha \geq 0} f(x_k + \alpha_k d_k) \tag{3}$$

The search direction d_k is defined as

$$d_k = \begin{cases} -g_k & if\ k = 0 \\ -g_k + \beta_k d_{k-1} & if\ k \geq 1 \end{cases} \tag{4}$$

where the Conjugate Gradient Coefficient, $\beta_k \in \mathcal{R}$ is a scalar. Some of the classical formulas for Conjugate Gradient Coefficient (β_k) are the Hestenes Stiefel (HS) in 1952, the Fletcher-Reeves (FR) in 1964, the Polak-Ribiere-Polyak (PRP) in 1969, the Conjugate Descent (CD) method in 1987, the Liu-Storey (LS) in 1992, and the Dai-Yuan (DY) in 2000. The parameters of the β_k are given as follows;

$$\beta_k^{HS} = \frac{g_k^T(g_k - g_{k-1})}{(g_k - g_{k-1})^T d_{k-1}}, \qquad \beta_k^{FR} = \frac{g_k^T g_k}{\|g_{k-1}\|^2}, \qquad \beta_k^{PRP} = \frac{g_k^T(g_k - g_{k-1})}{\|g_{k-1}\|^2}$$

$$\beta_k^{CD} = \frac{-g_k^T g_k}{d_{k-1}^T g_{k-1}}, \qquad \beta_k^{LS} = \frac{g_k^T(g_k - g_{k-1})}{-d_{k-1} g_{k-1}}, \qquad \beta_k^{DY} = \frac{g_k^T g_k}{(g_k - g_{k-1})^T d_{k-1}}$$

where $\|.\|$ is the Euclidean norm of vectors.

In the Conjugate Gradient (CG) methods, many researchers focus on its global convergence properties and descent condition. For the Fletcher-Reeves (FR) method, Zoutendijk (1970) has proved the global convergence properties under the exact line search in (3). Al-Baali (1985) also shows the Fletcher-Reeves (FR) method fulfills global convergence properties under inexact line search. The Conjugate Descent (CD) method generated a descent search direction in each iteration for the parameter $\sigma < 1$ under the strong Wolfe line search, but its global convergence properties are not excellent. The Dai-Yuan (DY) method is a modification of the Fletcher-Reeves (FR) method, under the strong Wolfe line search, the Dai-Yuan (DY) method fulfills the descent condition, but this method has bad numerical results. Under strong Wolfe line search, Yuhong (2002) proved that Polak-Ribiere-Polyak (PRP) method has the global convergence properties and fulfills the descent condition. The (WYL) method is the modification of the Polak-Ribiere-Polyak (PRP) method, this method satisfied both the descent condition and global convergence properties under an exact line search and strong Wolfe line search. The Ibrahim and Rohanin (2020) method is a modification of the Polak-Ribiere-Polyak (PRP) method using an exact line search.

In this paper, the performance of the propose coefficient β_k with the hybridization of Symmetric-Rank One (SR1) and Davidon-Fletcher-Powell (DFP) updates is compared with some classical conjugate gradient methods. The organization of our paper takes the following format. In section 2, a new CG coefficient, hybridization of SR1 and DFP with the general algorithm are presented.

In section 3, the global convergence of β_k is presented. Section 4 covers the numerical experiments and discussions of Tables. Finally, Section 5 deals with conclusion.

2 New CG coefficient, hybridization of SR1-DFP and algorithm

In this section, we propose new β_k defined by:

$$\beta_k^{AMCGC} = \begin{cases} \beta_k^{PRP} & if \left|1 - \frac{g_{k+1}^T g_k}{\|g_k\|^2}\right| \geq \mu, \\ \beta_k^{New} & otherwise. \end{cases} \quad (5)$$

Where

$$\beta_k^{New} = \frac{\mu g_{k+1}^T(g_{k+1} - \lambda g_k)}{\|g_k\|^2}$$

$$\beta_K^{AMCGC} = \frac{\mu\|g_{k+1}\|^2 - \mu\lambda\frac{\|g_{k+1}\|}{\|g_k\|}|g_{k+1}^T g_k|}{\|d_k\|^2} \quad (6)$$

$\mu \geq \frac{\lambda-\sigma}{1-\sigma} > 0, \sigma < \lambda \leq 1.$ Obviously, if $\mu = 1$ and $\lambda = 1$, then $\beta_k^{New} = \beta_k^{PRP}$. If $\mu = 0$, then the method reduces to the steepest descent method. From β_k^{AMCGC}, AMCGC represent Adams Modified Conjugate Gradient Coefficient as defined in (5).

The hybrid conjugate gradient algorithm proposed in Touati-Ahmed and Storey (1990) [16] was a break through which since then, some research work focus on employing hybridization principles to have better algorithms that can handle large scale unconstrained optimization problems such as in [3, 14].

We formulate a new hybridization of SR1 and DFP for solving problem (1) by considering the summation of SR1and DFP quasi-Newton methods as follows:

$$B_{k+1} = B_k + \alpha uu^T + B^* + \theta vv^T + \varphi\omega\omega^T \quad (7)$$

where $\alpha,\ \theta,\ \varphi \neq 0;\ \ u,\ v, \omega \neq 0$

choose $\alpha, \theta, \varphi, u, v$ and ω such that B_{k+1} satisfies Quasi-Newton condition

$$B_{k+1}\gamma_k = \delta_k \quad (8)$$

$$(B_k + uu^T)\gamma_k = \delta_k \quad (9)$$

also

$$(B_k^* + \theta vv^T + \varphi\omega\omega^T)\gamma_k = \delta_k \quad (10)$$

from equation (9), we have

$$B_k\gamma_k + \alpha uu^T\gamma_k = \delta_k$$

$$\alpha u^T\gamma_k u = \delta_k - B_k\gamma_k \quad (11)$$

setting $u = \delta_k - B_k\gamma_k$ (12)

$\therefore \alpha u^T\gamma_k = 1 \Longrightarrow\ \alpha^{-1}(\delta - B_k\gamma_k)^T\gamma_k$ (13)

from equation (10)

$$B_k^*\gamma_k + \theta vv^T\gamma_k + \varphi\omega\omega^T\gamma_k = \delta_k \quad (14)$$

$$\theta vv^T\gamma_k + \varphi\omega\omega^T\gamma_k = \delta_k - B_k^*\gamma_k \quad (15)$$

where

$\theta v^T\gamma_k = \varphi\omega^T\gamma_k = 1$, we have

$$v = \omega = \delta_k - B_k^* \gamma_k \tag{16}$$

also,

$$\theta v^T \gamma_k = 1$$

$$\theta^{-1} = v^T \gamma_k = (\delta_k - B_k^* \gamma_k)^T \gamma_k \tag{17}$$

$$\varphi^{-1} = \omega^T \gamma_k = (\delta_k - B_k^* \gamma_k)^T \gamma_k \tag{18}$$

substitute equations (12), (16), (17) and (18) into (7), we have

$$B_{k+1} = B_k + \frac{1}{(\delta_k - B_k \gamma_k)^T} \times (\delta_k - B_k \gamma_k)(\delta_k - B_k \gamma_k)^T + B_k^T + \frac{1}{\delta_k^T \gamma_k} \times \delta_k \delta_k^T - \frac{1}{\gamma_k^T B_k^* \gamma_k} \times -B_k^* \gamma_k (-B_k \gamma_k^T) \tag{19}$$

where $B_k = B_k^*$

$$B_{k+1}^{AHM} = [2B_k(\delta_k - B_k\gamma_k)^T \gamma_k \delta_k^T \gamma_k^T B_k^* + (\delta_k - B_k\gamma_k)(\delta_k - B_k\gamma_k)^T \delta_k^T \gamma_k^T B_k^* + \delta_k \delta_k^T (\delta_k - B_k\gamma_k)^T \gamma_k^T B_k^* - B_k^* \gamma_k B_k^* \gamma_k^T (\delta_k - B_k\gamma_k)^T \delta_k^T] \div [(\delta_k - B_k\gamma_k)^T \gamma_k \delta_k^T \gamma_k^T B_k^*] \tag{20}$$

Algorithm 2.1

Step 1: $x_o \epsilon \mathcal{R}^n$ and a positive definite matrix $B_o = I_n$.
Choose $\mu \geq 0, \varepsilon > 0$ and set $k \coloneqq 0$.
Step 2: Terminate if $\|g(x_{k+1})\| < \varepsilon$.
If $\|g_k\| \leq \varepsilon$, the algorithm stops. Otherwise, go to step 3.
Step 3: Calculate the search direction by

$$d_k = \begin{cases} -H_k g_k\,; & k = 0 \\ -H_k g_k + \beta_k^{AMCGC} d_{k-1}\,; & k \geq 1. \end{cases}$$

where H_k is the Hybridization Method (AHM) updating matrix
with $\sigma \epsilon (0, 1]$ is chosen to ensure conjugacy.
Step 4: Calculate the step size α_k by

$$f(x_k + \alpha_k d_k) \leq f(x_k) + \mu \alpha_k (g_k^T d_k - \tfrac{1}{2} \alpha_k \eta L_k \|d_k\|^2)$$

where $\mu \epsilon (0, 1), \eta [0, +\infty), \rho \epsilon (0, 1)$ are given constant scalars.
where $L_k = \frac{s_{k-1}^T y_{k-1}}{\|s_{k-1}\|^2}$; for $k > 1$.
Step 5: Compute the difference:
$S_k = x_{k+1} - x_k$ and $y_k = g_{k+1} - g_k$.
Step 6: Update B_k by $B_{k+1}^{AHM} = B_{k+1}^{DFP} + B_{k+1}^{SR1}$ to obtain B_{k+1}^{AHM}.
Step 7: Set $k \coloneqq k + 1$ and go to step 1.

3 Global convergence analysis

In this section, we study the global convergence of β_k^{AMCGC} and start with sufficient descent condition. The sufficient descent condition is defined by

$$g_k^T d_k \leq -c \|g_k\|^2 \quad \forall \quad k \geq 0, \; c > 0. \tag{21}$$

The following theorem shows that AMCGC with the modified exact line search possess the sufficient descent condition.

Theorem 1: Suppose the initial value of x_k and the search direction $d_k$as contain in (2) and (4), while the modified exact line search is used to determine the step size (α_k) then, the condition below holds for all $k \geq 0.$ The theorem helps us to determine the number of iterations.

$g_k^T d_k \leq -c\|g_k\|^2 \quad \forall \quad k \geq 0, \; c > 0.$

Proof:
The proof is by mathematical induction, if $k = 0$ then we have
$$g_0^T d_0 = -c\|g_0\|^2 \tag{22}$$
Hence the condition (21) holds true.

Next, we need to show that it holds for $k = 1$, condition (21), we have
$$g_1^T d_1 = -c\|g_1\|^2 \tag{23}$$
Also, to show that it holds for $k \geq 1$, we multiply equation (4) by g_{k+1}^T then,
$$g_{k+1}^T d_{k+1} = g_{k+1}^T(-g_{k+1} + \beta_{k+1}^{AMCGC} d_k) \tag{24}$$
$$g_{k+1}^T d_{k+1} = -g_{k+1}^T g_{k+1} + \frac{\mu\|g_{k+1}\|^2 - \lambda\frac{\|g_{k+1}\|}{\|g_k\|}|g_{k+1}^T g_k|}{\|d_k\|^2} g_{k+1}^T d_k$$
$$g_{k+1}^T d_{k+1} = -\|g_{k+1}\|^2 + \frac{\mu\|g_{k+1}\|^2 - \lambda\frac{\|g_{k+1}\|}{\|g_k\|}|g_{k+1}^T g_k|}{\|d_k\|^2} g_{k+1}^T d_k$$

For exact line search, we know that $g_{k+1}^T d_k = 0$, thus
$$g_{k+1}^T d_{k+1} = -\|g_{k+1}\|^2 \tag{25}$$
Hence the sufficient condition holds true for $k + 1$.
First, we must prove that our method (β_k^{AMCGC}) are always not less than zero in order to establish the global convergence.
$$\beta_{k+1}^{AMCGC} = \frac{\mu\|g_{k+1}\|^2 - \lambda\frac{\|g_{k+1}\|}{\|g_k\|}|g_{k+1}^T g_k|}{\|d_k\|^2} \geq \frac{\mu\|g_{k+1}\|^2 - \lambda\frac{\|g_{k+1}\|}{\|g_k\|}\|g_{k+1}^T\|\|g_k\|}{\|d_k\|^2} \tag{26}$$
$$\beta_{k+1}^{AMCGC} = \frac{\mu\|g_{k+1}\|^2 - \lambda\frac{\|g_{k+1}\|}{\|g_k\|}|g_{k+1}^T g_k|}{\|d_k\|^2} \leq \frac{\mu\|g_{k+1}\|^2}{\|d_k\|^2} \tag{27}$$

The following are needed to establish the global convergence of our formula;
Assumption 1
The level set $M = \{x \in \mathcal{R}^n; f(x) \leq f(x_0)\}$ is bounded, where x_0 is the starting point.
In some neighborhood N of M, the function is continuously differentiable and its gradient is Lipchitz continuous. That is, there exist a constant $L > 0$ such that
$$\|\nabla f(x) - \nabla f(y)\| \leq L\|x - y\|, \quad \text{for all } x, y \in N. \tag{28}$$
Under this assumption, we have the following Lemma, which was proved by Zoutendijk (1970).
Lemma 1
Suppose Assumption 1 holds and $\{x_k\}$ is generated by (2) and the search direction $\{d_k\}$ satisfies (21) and the step size $\{\alpha_k\}$ satisfies (3), then
$$\sum_{k\geq 1} \frac{(g_k^T d_k)^2}{\|d_k\|^2} < +\infty. \tag{29}$$

From Lemma 1, we have the following theorem.

Theorem 2
Suppose that Assumption 1 holds true. Let $\{x_k\}$ and $\{d_k\}$ be generated by equations (2) and (21) with β_k^{AMCGC} and the sufficient descent condition holds true. Then either
$$\sum_{k\geq 1} \frac{(g_k^T d_k)^2}{\|d_k\|^2} < +\infty \quad \text{or} \quad \lim_{k\to\infty} \|g_k\| = 0 \tag{30}$$

Proof: We proceed by contradiction to prove Theorem 2. Suppose Theorem 2 is not true, then $\exists$ a constant $c > 0$ such that

$$\|g_k\| \geq c \quad \forall \; k \geq 0 \tag{31}$$

Rewriting (4) as

$$d_{k+1} + g_{k+1} = \beta_{k+1} d_k \tag{32}$$

And squaring both sides of the equation above then

$$\|d_{k+1}\|^2 = (\beta_{k+1})^2 \|d_k\|^2 - 2g_{k+1}^T d_{k+1} - \|g_{k+1}\|^2. \tag{33}$$

Dividing both sides of equation (33) by $(g_{k+1}^T d_{k+1})^2$ then,

$$\frac{\|d_{k+1}\|^2}{\left(g_{k+1}^T d_{k+1}\right)^2} = \frac{(\beta_{k+1})^2 \|d_k\|^2}{\left(g_{k+1}^T d_{k+1}\right)^2} - \frac{2}{g_{k+1}^T d_{k+1}} - \frac{\|g_{k+1}\|^2}{\left(g_{k+1}^T d_{k+1}\right)^2}$$

$$\frac{\|d_{k+1}\|^2}{(g_{k+1}^T d_{k+1})^2} = \frac{(\beta_{k+1})^2 \|d_k\|^2}{(g_{k+1}^T d_{k+1})^2} - \left[\frac{1}{\|g_{k+1}\|} + \frac{\|g_{k+1}\|}{g_{k+1}^T d_{k+1}}\right]^2 + \frac{1}{\|g_{k+1}\|^2}$$

$$\frac{\|d_{k+1}\|^2}{\left(g_{k+1}^T d_{k+1}\right)^2} \leq \frac{(\beta_{k+1})^2 \|d_k\|^2}{\left(g_{k+1}^T d_{k+1}\right)^2} + \frac{1}{\|g_{k+1}\|^2}. \tag{34}$$

Applying equation (26) to (34) above we get

$$\frac{\|d_{k+1}\|^2}{\left(g_{k+1}^T d_{k+1}\right)^2} \leq \frac{1}{\|g_{k+1}\|^2}. \tag{35}$$

Hence

$$\frac{\|d_k\|^2}{\left(g_k^T d_k\right)^2} \leq \sum_{i=0}^{k} \frac{1}{\|g_i\|^2}$$

$$\frac{\left(g_k^T d_k\right)^2}{\|d_k\|^2} \geq \frac{c^2}{k}. \tag{36}$$

From equations (36) and (31), it follows that

$$\sum_{k=0}^{\infty} \frac{\left(g_k^T d_k\right)^2}{\|d_k\|^2} = \infty.$$

This contradicts the Zoutendijk condition in Lemma 1.

Theorem 3.3

Suppose that assumption 1 holds, consider any Conjugate Gradient (CG) methods of the form (3) and (4), step size (α_k) is obtained by the exact line search and β_k is obtained using (6), then either $\lim_{k\to\infty} \|g_k\| = 0$ or $\sum_{k=0}^{\infty} \frac{\left(g_k^T\right)^4}{\|d_k\|^2} < \infty$.

Proof:

From (31) and (25)

$$\|d_{k+1}\|^2 = \left(\frac{\|g_{k+1}\|^2}{\|d_k\|^2}\right)^2 \|d_k\|^2 - 2g_{k+1}^T d_{k+1} - \|g_{k+1}\|^2$$

$$\|d_{k+1}\|^2 = \frac{\|g_{k+1}\|^4}{\|d_k\|^2} - 2g_{k+1}^T d_{k+1} - \|g_{k+1}\|^2. \tag{37}$$

We have already proved that sufficient descent condition holds using mathematical induction.

Therefore, we know that

$$g_{k+1}^T d_{k+1} \leq -c\|g_{k+1}\|^2 \tag{38}$$

Hence from (37),

$$\|d_{k+1}\|^2 = \frac{\|g_{k+1}\|^4}{\|d_k\|^2} + 2c\|g_{k+1}\|^2 - \|g_{k+1}\|^2$$

$$\|d_{k+1}\|^2 = \frac{\|g_{k+1}\|^4}{\|d_k\|^2} - \|g_{k+1}\|^2(1-2c). \tag{39}$$

Multiplying both sides of (39) with $\frac{\|g_{k+1}\|^2}{\|d_{k+1}\|^2}$

then,

$$\|d_{k+1}\|^2 \frac{\|g_{k+1}\|^2}{\|d_{k+1}\|^2} = \frac{\|g_{k+1}\|^2}{\|d_{k+1}\|^2}\left[\frac{\|g_{k+1}\|^4}{\|d_k\|^2} - \|g_{k+1}\|^2(1-2c)\right]$$

$$\frac{\|d_{k+1}\|^2\|g_{k+1}\|^2}{\|d_{k+1}\|^2} = \frac{\|g_{k+1}\|^4}{\|d_{k+1}\|^2}\left[(2c-1) + \frac{\|g_{k+1}\|^2}{\|d_k\|^2}\right]$$

$$\frac{\|d_{k+1}\|^2\|g_{k+1}\|^2}{\|d_{k+1}\|^2} \leq \frac{\|g_{k+1}\|^4}{\|d_{k+1}\|^2} \tag{40}$$

Based on theorem 2, we know that $\lim_{k\to\infty} \frac{\left(g_{k+1}^T d_{k+1}\right)^2}{\|d_{k+1}\|^2} < 0.$

This will imply that if theorem (3) is not true, then we have $\lim_{k\to\infty} \frac{\left(g_{k+1}^T d_{k+1}\right)^2}{\|d_{k+1}\|^2} = \infty.$

From (40) we obtain

$$\infty \leq \frac{\|g_{k+1}\|^2}{\|d_{k+1}\|^2}. \tag{41}$$

Hence, theorem 3 holds true for sufficiently large k.

The proof of Theorems 1, 2 and 3 showed that the formulas converge analytically. Next is to validate numerically that the method also converge using Rosenbrock test function. This, we will have in the next section.

4 Numerical results

In this section, experimentation of our proposed method was carried out against some classical methods in the literature, to weigh the significance of our algorithm with $\beta_k = \beta_K^{AMCGC}$. To effect this, Rosenbrock standard test function was considered. The dimension of the function is varied to compare the computational strength against Fletcher-Reeves (FR), Dai-Yuan (DY), (PRP), (FRPRP) which is the hybridization of (FR) and (PRP) and Ibrahim-Rohanin (IR) methods. The modified exact line search condition was used in the computation.

In carrying out the simulation, the number of iterations (NI), the number of function evaluations (NF), CPU time (CT) and the dimension of the standard test problems is 500, 1000, 5000, 10000 and 100000 variables were put into consideration to determine the numerical strength of the proposed algorithms AMCGC with BFGS, DFP and SR1. The choice of values of $\{\mu\}$ and $\{\lambda\}$ must satisfy the conditions $\mu \geq \frac{\lambda-\sigma}{1-\sigma} > 0$ and $\sigma < \lambda \leq 1.$ After numerous experimentation with the randomly selected values for the parameters, the values $\mu = 0.7$ and $\lambda = 1.0$ were taken into consideration to be the best values for the parameters which make our algorithms robust to obtain the results presented.

$\|g_k\| \leq \varepsilon$, where $\varepsilon = 10^{-5}$ is considered as the stopping criterion. The implementation of the algorithm was done using MATLAB R2021 on a window 10 machines with the following specification; processor: Intel Core i7-17050Hcpu@2.6GHz2.59GHz, with RAM of 16GB DDR4 and 1TB SSD storage. Also, comes with a GPU card: 4GB of GDDR5, GDDR6 memory clocked at 8GHz are supplied, altogether it has 128-Bit memory interface that creates a bandwidth of 112.1GB/s. In Tables 1, 2, 3, 4 and 5, we reported the numerical results with different dimension (Dim).

Table 1: Numerical Results of $AMCGC^{SR1}, IR, FR, DY, PRP\ and\ FRPRP$ Methods for Rosenbrock Test Function

Problem	$Dim.$	$AMCGC^{SR1}$			IR			FR			DY			PRP		
		NI	NF	CT	NI	NF	CT	NI	NF	CT	NI	NF	CT	NI	NF	CT
$Rosenbrock$	500	55	57	1.22	56	57	1.73	78	79	1.61	59	60	1.38	56	57	1.21
	1000	53	55	1.37	55	56	1.79	77	78	1.72	58	59	1.50	55	56	1.32
	5000	49	52	2.45	52	53	3.11	74	75	3.53	55	56	2.98	52	53	2.33
	10000	40	41	3.35	40	41	3.48	63	64	5.09	44	45	4.16	40	41	3.03
	100000	12	13	9.15	12	13	10.92	13	14	12.11	13	14	12.81	12	13	11.43

Table 2: Numerical Results of $AMCGC^{DFP}, IR, FR, DY, PRP\ and\ FRPRP$ Methods for Rosenbrock Test Function

$Problem$	$Dim.$	$AMCGC^{DFP}$			IR			FR			DY			PRP			$FRPRP$		
		NI	NF	CT	NI	NF	CT	NI	NF	CT	NI	NF	CT	NI	NF	CT	NI	NF	CT
$Rosenbrock$	500	55	57	1.67	56	57	1.73	78	79	1.61	59	60	1.38	56	57	1.21	55	56	1.26
	1000	54	55	1.75	55	56	1.79	77	78	1.72	58	59	1.50	55	56	1.32	54	55	1.44
	5000	51	52	3.43	52	53	3.11	74	75	3.53	55	56	2.98	52	53	2.33	52	53	2.07
	10000	39	40	3.45	40	41	3.48	63	64	5.09	44	45	4.16	40	41	3.03	40	41	3.39
	100000	12	13	10.32	12	13	10.92	13	14	12.11	13	14	12.81	12	13	11.43	12	13	11.66

Table 3: Numerical Results of $AMCGC^{BFGS}, IR, FR, DY, PRP\ and\ FRPRP$ Methods for Rosenbrock Test Function

$Problem$	$Dim.$	$AMCGC^{BFGS}$			IR			FR			DY			PRP			$FRPRP$		
		NI	NF	CT	NI	NF	CT	NI	NF	CT	NI	NF	CT	NI	NF	CT	NI	NF	CT
$Rosenbrc$	500	54	56	1.24	56	57	1.73	78	79	1.61	59	60	1.38	56	57	1.21	55	56	1.26
	1000	53	54	1.35	55	56	1.79	77	78	1.72	58	59	1.50	55	56	1.32	54	55	1.44
	5000	50	51	2.43	52	53	3.11	74	75	3.53	55	56	2.98	52	53	2.33	52	53	2.07
	10000	40	41	3.37	40	41	3.48	63	64	5.09	44	45	4.16	40	41	3.03	40	41	3.39
	10000	12	13	9.02	12	13	10.92	13	14	12.11	13	14	12.81	12	13	11.43	12	13	11.66

Table 4: Numerical Results of $\boldsymbol{AMCGC^{BFGS}}$,$\boldsymbol{AMCGC^{SR1}}$, $\boldsymbol{AMCGC^{DFP}}$ $\boldsymbol{FRPRP}$ and $\boldsymbol{IR}$ Methods for Rosenbrock Test Function.

$\boldsymbol{Problem}$	$\boldsymbol{Dim}$.	$\boldsymbol{AMCGC^{SR1}}$			$\boldsymbol{AMCGC^{DFP}}$			$\boldsymbol{AMCGC^{BFGS}}$			$\boldsymbol{IR}$			$\boldsymbol{FRPRP}$		
$\boldsymbol{Rosenbrock}$		$\boldsymbol{NI}$	$\boldsymbol{NF}$	$\boldsymbol{CT}$	$\boldsymbol{NI}$	$\boldsymbol{NF}$	$\boldsymbol{CT}$	$\boldsymbol{NI}$	$\boldsymbol{NF}$	$\boldsymbol{CT}$	$\boldsymbol{NI}$	$\boldsymbol{NF}$	$\boldsymbol{CT}$	$\boldsymbol{NI}$	$\boldsymbol{NF}$	$\boldsymbol{CT}$
	500	55	57	1.22	55	57	1.67	54	56	1.24	56	57	1.73	55	56	1.26
	1000	53	55	1.37	54	55	1.75	53	54	1.35	55	56	1.79	54	55	1.44
	5000	49	52	2.45	51	52	3.43	50	51	2.43	52	53	3.11	52	53	2.07
	10000	40	41	3.35	39	40	3.45	40	41	3.37	40	41	3.48	40	41	3.39
	100000	12	13	9.15	12	13	10.32	12	13	9.02	12	13	10.92	12	13	11.66

4.1 Discussion

In Table 1, it is shown that the developed algorithm of AMCGC and the modified exact line search with the SR1 method is promising, because it requires less number of iterations (NI), less number function evaluation (NF) as well as less CPU time (CT) as compare to the existing methods. It is observed that, the (NI) and (NF) increasing down the table with increment in dimension so as the CPU time as well. In Table 2, we also use the CPU time, NI and NF to compare the performance of the AMCGC and the modified exact line search combined with the DFP method. The Table 2 above shown that $AMCGC^{DFP}$ is fastest, then FRPRP, then IR, then PRP, then DY, and FR. These only differ in their choice of the search direction and Conjugate Gradient Coefficient (CGC), then the numerical results show that the proposed method is promising.

In Table 3, it is shown that the results obtained from the modified exact line search and the Conjugate gradient Coefficient (CGC) with the cautious BFGS method indicates that $AMCGC^{BFGS}$ is fastest relative to the less number of iterations (NI) and number of function evaluation (NF), while the CPU time (CT) increased down the table, but relatively low as compare to IR, FR, DY, PRP and FRPRP methods. In Table 4, we also use CPU time (CT), number of iterations (NI) and number of function evaluation (NF) to compare the performance of the $AMCGC^{BFGS}$,$AMCGC^{SR1}$ $AMCGC^{DFP}$ $FRPRP$ and IR algorithms, from the numerical results shown above, $AMCGC^{BFGS}$ is fastest as compare to others for the Rosenbrock standard test function on average with less CPU time (CT), less number of iterations (NI) and less number of function evaluation (NF) as compare to others.

Finally, the effectiveness of our proposed Algorithm AMCGC was shown in Table 4 to be more effective against its counterparts.

5 Conclusion

In this paper, we proposed a new CG coefficient β_k^{AMCGC} with the $HSR1DFP$ methods for the solution of unconstrained optimization problem. The choice of values of μ and λ which must satisfy the conditions $\mu \geq \frac{\lambda-\sigma}{1-\sigma} > 0$ and $\sigma < \lambda \leq 1$. After numerous experimentation with the randomly selected values for the parameters, the values $\mu = 0.7$ and $\lambda = 1.0$ were taken into consideration to be the best values for the parameters which make our algorithms robust to obtain the results presented. This new CG coefficient β_k^{AMCGC} possesses the descent property with exact line search condition. We established the global convergence of the method using Zoutendijk condition given in [10]. The experimentation of the formulas on standard test function showed that our proposed Algorithm AMCGC is efficient and robust.

References

[1] Al-Baali M. (1985). Descent property and global convergence of the fletcher-reeves method with inexact line search. IMA Journal of Numerical Analysis. 5(1):121 – 124.
[2] Al-Baali, M., Narushima, Y. and Yabe, H. (2015). A family of three-term conjugate gradient methods with sufficient descent property for unconstrained optimization. Computational Optimization and Applications. 8(5):1 – 22.
[3] Babaie-Kafaki, S. and Ghanbari, R. (2014a). Two hybrid nonlinear conjugate gradient methods based on a modified secant equation. Optimization. 63(7):1027 – 1042.
[4] Ibrahim A. and Rohanin A. (2020). convergence analysis of a new conjugate gradient method for unconstrained optimization. Applied Mathematical Sciences. 9(140):6969 – 6984.
[5] Liu J and Du S. (2019). Modified three-term conjugate gradient method and its applications. Mathematical Problems in Engineering, https,//doi.org/10.1155/2019/5976595.
[6] Lu J., Li Y. and Pham H. (2020). A modified Dai-Liao conjugate gradient method with a new parameter for solving image restoration problems. Mathematical Problems in Engineering, https,//doi.org/10.1155/2020/6279543.
[7] Lu, Y., Li, W., Zhang, C. and Yang, Y. (2015). A class of new hybrid conjugate gradient method for unconstrained optimization. Journal of Information and Computational Science, 12(5):1941 – 1949.
[8] Touati-Ahmed, D. and Storey, C. (1990). Efficient hybrid conjugate gradient techniques. Journal of Optimization Theory and Applications, 64(2):379 – 397.
[9] Yuhong, D. (2002). A Non-monotone conjugate gradient algorithm for unconstrained optimization. Journal of Systems Science and Complexity, 15(2):139 – 145.
[10] Zoutendijk, G. (1970). Nonlinear programming computational methods. Integer and Nonlinear Programming, 143(1):37 – 86.

International Journal of Mathematical Analysis and Modelling
Volume 5, Issue 4, November 2022, Pages 25 – 37

Modeling the impact of a random perturbation on the yields of tuber crops using a computational approach

B.O. Nwala*†, P. Nwagor*‡, and I.U. Amadi§

Abstract

An application of four dynamical systems of nonlinear first order ordinary differential equations was considered. Therefore, ODE45 was utilized to quantify the impact of a random environmental perturbation on the yields of four competing tuber crops. It was observed that the growth of the four interacting agricultural crops depends on their intra-species coefficients and also on their inter-species coefficient extensively. Hence, the results of this study extensively established that the farmers should endeavor to harvest their crops at harvesting scenario which is vulnerable to biodiversity. Moreover, the analysis of these results also identified that the farmers should cultivate more of cocoyam which produced 760.0240kg, yellow yam 225.4284kg, followed by cassava quantified by 170.7381kg and finally white yam by -66.6667kg. It is therefore recommended that the cultivators should not hesitate to notify the agricultural policy makers for quick intervention immediately they identify the evidence of environmental perturbation on their crops for optimal maximization of profit and adequate food supply in the society.

Keywords: computational; tuber; ode 45; yields; perturbation; biomass.

1 Introduction

The impact of a random perturbation on the food production, ecosystem and human beings is an old environmental global challenge that demands immediate attention to circumvent the issue of food insecurity and lack of food production in the society. [22] reported that "the National Science Academics of G8" including China, Brazil and India affirmed that the impact of a random perturbation is obvious on the ecosystem. To back up this fact, [2] established that the effect of a random perturbation on the earth is a constant process [6, 13,20,3].

The work in [15] revealed that the natural and human activities on the environment such as rain fall, flood, heat, bush boiling, deforestation and diseases are the major well spring of a random perturbation. It is therefore observed that a random perturbation has more influence in African

*Department of Mathematics and Statistics, Ignatius Ajuru University of Education, Port Harcourt, Nigeria
†Corresponding Author. Email: boninwala@gmail.com
‡Email: pnwagor@yahoo.com
§Department of Mathematics/Statistics, Captain Elechi Amadi Polytechnic, Rumuola, Port Harcourt, Nigeria; Email: innocentamadi@portharcourtpoly.edu.ng

regions than any other region [5, 8, 14, 16] etc. In this context, biodiversity loss is a global cost and increasingly endangered through an event of anthropogenic processes [12-23]. Moreover, the increase in a random perturbation affected the agricultural sector globally which threaten all the economy and encouraged raise in food prices [5, 8, 14,23]. In the same vein [8] explained that a computational approach is a calculation conducted using a computer programming that defined a mathematical model for a physical system which is consistent with the research works of [1,4,9] etc.

The work in [18] recently evaluated the impact of a random perturbation on two agricultural species (cassava and yam) using the MATLAB ODE 45 computational approach and his result established that the two crops were vulnerable to biodiversity loss but more vulnerability was captured on yam than the cassava. The study showed that the possibility of having food shortage in the society is certain and this vital prediction is consistent with the research contribution of [3,10 ,17] etc. In the work of [19] investigated numerical and statistical quantifications of biodiversity of two agricultural crops using ODE45 numerical scheme which the result extensively obtained a relative biodiversity loss of the two crops but there was indication of more vulnerability on cassava than yam which could instigate economic downshift in the society which concurred with the contributions of [18].

Having discovered that the previous researchers applied experimental method, theoretical method and two dynamical system of nonlinear first order ordinary differential equations ODE45 to investigate the effect of biodiversity loss in ecosystem which has developed a huge gap in the knowledge base in mathematical modeling. To circumvent this gap, this study has considered the application of four dynamical systems of nonlinear white order ordinary differential equations ODE45 to quantify the impact of random environmental perturbation on the food production of four tuber crops.

The aim of this paper is to simulate the impact of random environmental perturbation on the yields of cassava, white yam, yellow yam and cocoyam respectively considering that the growth of the four agricultural crops depends on their intra-species coefficients and on their inter-species coefficients.

This paper considered the following arrangements. Section 2.1 is mathematical formulations, section 2.2 is considered as materials and methods, the presentation of results is seen in section 3 while discussion of results is located in section 4 and finally, conclusion is seen in section 5.

2.1 Mathematical formulations

For the purpose of this, we shall consider the following four continuous dynamical systems of non-linear white order ordinary differential equations according to [19].

$$\frac{dC}{dt} = \alpha_1 C - \beta_1 C^2 - r_1 C Y_1 - r_2 C Y_2 - r_3 C C_y - \mathrm{r}\psi \mathrm{C}\left(1 - \frac{B}{K}\right), \quad C(0) = C_0 > 0 \qquad 1$$

$$\frac{dY_1}{dt} = \alpha_2 Y_1 - \beta_2 Y_1^2 - r_4 C Y_1 - r_5 Y_1 Y_2 - r_6 Y_1 C_y - \mathrm{r}\psi \mathrm{Y}_1\left(1 - \frac{B}{K}\right), \quad Y_1(0) = Y_{10} > 0 \qquad 2$$

$$\frac{dY_2}{dt} = \alpha_3 Y_2 - \beta_3 Y_2^2 - r_7 C Y_2 - r_8 Y_1 Y_2 - r_9 Y_2 C_y - \mathrm{r}\psi \mathrm{Y}_2\left(1 - \frac{B}{K}\right), \quad Y_2(0) = Y_{20} > 0 \qquad 3$$

$$\frac{dC_y}{dt} = \alpha_4 C_y - \beta_4 {C_y}^2 - r_{10} C_y C - r_{11} C_y Y_1 - r_{12} C_y Y_2 - \mathrm{r}\psi \mathrm{Cy}\left(1 - \frac{B}{K}\right),$$
$$C_y(0) = {C_y}_0 > 0, \qquad 4$$

with the initial conditions, $C(0) = C_0 > 0$, $Y_1(0) = Y_{10} > 0$, $Y_2(0) = Y_{20} > 0$ and $C_y(0) = C_{y0} > 0$.

Let $r\psi C(1 - \frac{B}{K}) = K_1$, $r\psi Y_1(1 - \frac{B}{K}) = K_2$, $r\psi Y_2(1 - \frac{B}{K}) = K_3$, $r\psi C_y(1 - \frac{B}{K}) = K_4$.

For the purpose of this study, this research shall consider the following parameter values and its specifications.

Variable	Interpretation
C(t)	Measures the biomass of cassava at time *t*
$Y_1(t)$	Measures the biomass of white yam at time *t*
$Y_2(t)$	Measures the biomass of yellow yam at time *t*
$C_y(t)$	Measures the biomass of coco-yam at time *t*

Parameter	Interpretation	Value
α_1	measures the intrinsic growth rate of cassava that enhances the growth of cassava.	0.133
β_1	measures the biomass of cassava that interacts with itself to inhibit the growth rate of cassava.	0.0024
r_1	measures the biomass of cassava that interacts with the white yam to inhibit the growth rate of cassava.	0.0018
r_2	measures the biomass of cassava that interacts with the yellow yam to inhibit the growth rate of cassava.	0.0014
r_3	measures the biomass of cassava that interacts with the cocoyam to inhibit the growth rate of cassava.	0.0012
α_2	measure the intrinsic growth rate of white yam that enhances the growth of white yam.	0.132
β_2	measures the biomass of white yam that interacts with itself to inhibit the growth rate of white yam.	0.0018
r_4	measures the biomass of white yam that interacts with the cassava to inhibit the growth rate of white yam.	0.0014
r_5	measures the biomass of white yam that interacts with yellow yam to inhibit the growth rate of white yam.	0.0012
r_6	measures the biomass of white yam that interacts with cocoyam to inhibit the growth rate of white yam.	0.00064
α_3	measures the biomass of yellow yam that enhances the growth rate of yellow yam.	0.132
β_3	measures the biomass of yellow yam that interacts with itself to inhibit the growth rate of yellow yam.	0.0016
r_7	measures the biomass of yellow yam that interacts with cassava to inhibit the growth rate of yellow yam.	0.0014

r_8	measures the biomass of yellow yam that interacts with white yam to inhibit the growth rate of yellow yam.	0.0012
r_9	measures the biomass of yellow yam that interacts with cocoyam to inhibit the growth rate of yellow yam.	0.00048
α_4	measures the biomass of cocoyam that enhances the growth of cocoyam.	0.12
β_4	measures the biomass of cocoyam that interacts with itself to inhibit the growth rate of cocoyam.	0.0015
r_{10}	measures the biomass of cocoyam that interacts with cassava to inhibit the growth rate of coco yam.	0.0013
r_{11}	measures the biomass of cocoyam that interacts with white yam to inhibit the growth rate of cocoyam.	0.0013
r_{12}	measures the biomass of cocoyam that interacts with yellow yam species to inhibit the growth rate of cocoyam.	0.00167
R	Measures the natural depletion rate coefficient of $C0_2$	0.0002
ψ	Measures the rate at which carbon dioxide is used during the photosynthesis process by the green plant for their growth	0.65
B	Measure the biomass density of green plant	12.5
K	Measure the environmental carrying capacity per crop due to a random perturbation	200

Source of arbitrary parameter values (Ekaka-a, 2014)

2.2 Materials and method

In this study, a numerical method is used to quantify the impact of a random perturbation on the yields of four competing tuber crops such as cassava, two species of yam and cocoyam respectively using ordinary differential equations (ODE 45) computational approach.
In this particular section, we prove that the crops growth model is well-posed and this is done by proving that the positively, boundedness, existence and uniqueness of the solutions of the model with non-negative initial data remains non-negative for all time t >0.

Lemma 1: The set $\Omega = \left\{(C, Y_{1,} Y_{2,} Cy)\ \varepsilon R_+^4 : N \ \leq \ \frac{a_1 - K_1}{\beta_1}\right\}$ is positively invariant with respect to the growth model (1) to (4).

Lemma 2: (Positivity) let the set of initial data be $\{(C(0), Y_1(0), Y_2(0), Cy(0)), \varepsilon\ \emptyset\}$. Then, the data set $\{(C(t), Y_1(t), Y_2(t), Cy(t)\}$ of the growth model is non-negative for t > 0.

Proof: Assuming that the set of initial data, $\{(C(0), Y_1(0), Y_2(0), Cy(0))\ \geq\ 0\}$, then equation 1 gives $\frac{dc}{dt} = a_1 C - \beta_1 C^2 - r_1 C Y_1 - r_2 C Y_2 - r_3 C Cy - C K_1$

$$\frac{dc}{dt} = C(a_1 - \beta_1 C - r_1 Y_1 - r_2 Y_2 - r_3 CY - K_1),$$

$$\frac{dc}{C} = (a_1 - \beta_1 - r_1 Y_1 - r_2 Y_2 - r_3 CY - K_1)\, dt,$$

$$\int \frac{dc}{C} \geq \int (a_1 - \beta_1 - r_1 Y_1 - r_2 Y_2 - r_3 CY - K_1)\, dt$$

$$C(t) \geq C(0) e^{(a_1 - \beta_1 C - r_1 Y_1 - r_2 Y_2 - r_3 CY - K_1) \quad \geq 0}.$$

Similarly, the remaining state variables are obtained as:

$Y_1(t) \geq\ Y_1(0)EXP(a_2 -\ \beta_2 -\ r_4C -\ r_5Y_2 -\ r_6Cy - K_2)\ \geq 0,$
$Y_2(t) \geq\ Y_2(0)EXP(a_3 -\ \beta_3 -\ r_7C -\ r_8Y_1 -\ r_9Cy - K_3)\ \geq 0,$
$Cy(t) \geq\ Cy(0)EXP(a_4 -\ \beta_4 -\ r_{10}C -\ r_{11}Y_2 -\ r_{12}Y_2 - K_4)\ \geq 0$ for all t > 0.

Lemma 3: (Boundedness) assuming that the initial condition for growth model (1) to (4) satisfies N(0) $\leq \frac{a_1 - K_1}{\beta_1}$.

Then, whenever the solution exists on an interval 1, it satisfies the property of boundness.
$N(t) \leq \frac{a_1 - K_1}{\beta_1}$.

Proof: Since 1(t) $\geq 0,$

$$\frac{dN}{dt} < \frac{a_1 -\ K_1N}{\beta_1}$$

$N(t) \leq \qquad \frac{a_1 - K_1}{\beta_1}\ +\ N(0) - \left(\frac{a_1 - K_1}{\beta_1}\right)e^{\beta_1 t}\ where\ (0) \leq\ \frac{a_1 - K_1}{\beta_1}, we\ have\ N(t)\ \leq\ \frac{a_1 - K_1}{\beta_1}.$
Consequently, 1(t) $\leq\ \frac{a_1 - K_1}{\beta_1}$.

Lemma 4: Existence and uniqueness
Let $\dot{t}$ > 0, if the initial condition satisfies, $\{(C(0), Y_1(0), Y_2(0), Cy(0)), >\ 0\}$.
Then, $\forall\ t\ \varepsilon\ R,$ the solution set $\{(C(t), Y_1(t), Y_2(t), Cy(t)\}$ exists in R_t^4 and is unique.
Proof: The growth model (1) – (4) could be written as

$$x = \begin{vmatrix} C(t) \\ Y_1(t) \\ Y_2(t) \\ Cy(t) \end{vmatrix}\ and\ F(x) = \begin{vmatrix} C(a_1 -\ \beta_1C -\ r_1Y_1 -\ r_2Y_2 -\ r_3Cy - K_1) \\ Y_1(a_2 -\ \beta_2Y_1 -\ r_4C -\ r_5Y_2 -\ r_6Cy - K_2) \\ Y_2(a_3 -\ \beta_3Y_2 -\ r_7C -\ r_8Y_1 -\ r_9Cy - K_3) \\ Cy(a_4 -\ \beta_4Cy -\ r_{10}C -\ r_{11}Y_1 -\ r_{12}Y_2 - K_4) \end{vmatrix} \qquad 5$$

Therefore, F is continuous and locally satisfies lipschirz condition in R_t^4 using the picart – lindedof theorem and the white – two (1 and 2) lemmas proved the positively and boundedness of the solutions, there exist $\dot{t}$ > 0 such that the solution set of the growth model (1) to (4) exists locally at least on an interval [0, $\dot{t}$] and is unique. Hence, lemma 4 defined the production validity of growth model (1) to (4).

Lemma 5: Therefore, the growth model (1) to (4) is well-posed and valid in the set
$\int \Omega = \int (C(t), Y_1(t), Y_2(t), Cy(t))\ \varepsilon\ R_t^4; N \leq\ \frac{a_1 - K_1}{\beta_1}$.

It is obvious to report that the intrinsic growth rate parameter values undergo more vulnerability than any other parameter value in the event of a random perturbation scenario. To quantify the effect, we considered when the new biomass is higher than the old biomass, that indicated increased in production has been occurred [9], [18] and [19] etc. Therefore, we applied the formula stated below to evaluate the extent of biodiversity gain.

$$EPMY\ (\%) = \left(\frac{New\ crop\ biomass - Old\ crop\ biomass}{Old\ crop\ biomass}\right)(100)$$

Note: EPMY (%) represents the estimated proportion of more in yields in percentage quantification with respect to cassava, yellow yam, and cocoyam respectively.

$$EPMC\ (\%) = \left(\frac{New\ cassava\ biomass - Old\ cassava\ biomass}{Old\ cassava\ biomass}\right)(100)$$
$$= \left(\frac{0.1008 - 0.0533}{0.0533}\right)(100) = (0.8912)(100) = 89.1182\%$$

Similarly,

$$EPMY_2\ (\%) = \left(\frac{New\ yellow\ yam\ biomass - Old\ yellow\ yam\ biomass}{Old\ yellow\ yam\ biomass}\right)(100)$$
$$= \left(\frac{0.1263 - 0.0781}{0.0781}\right)(100) = (0.6172)(100) = 61.7158\%$$

Similarly,

$$EPMY\ Cy(\%) = \left(\frac{New\ cocoyam\ biomass - Old\ cocoyam\ biomass}{Old\ cocoyam\ biomass}\right)(100)$$

$$= \left(\frac{0.0709 - 0.0254}{0.0254}\right)(100) = (1.7914)(100) = 179.1339\%$$

Eventually, when the old biomass is greater than the new biomass which indicated depletion in yields has established [18]. The formula stated below is considered to calculate the effect of biodiversity loss.

$$EPMY\ (\%) = \left(\frac{New\ crop\ biomass - Old\ crop\ biomass}{Old\ crop\ biomass}\right)(100)$$
$$EPMY\ \ Y_1(\%) = \left(\frac{Old\ white\ yam\ biomass - New\ white\ yam\ biomass}{Old\ white\ yam\ biomass}\right)(100)$$
$$= \left(\frac{0.0781 - 0.0749}{0.0781}\right)(100) = (0.04097)(100) = \mathbf{-4.0973}\%$$

3 Results

This section presents the results in the tables which we obtained in section 2.

Note that LGs represents the length of growing season, CB represents the cassava biomass, Y_1B represents the white yam biomass, Y_2 represents the yellow yam biomass while Cy represents the cocoyam biomass.

Table 1: Evaluating a random perturbation impact analysis on the yields of cassava and the white yam using ODE45 computational approach of 0.05 RPV in scenario one

LGS Months	Old CB(kg)	New CB(kg)	Effect 1(%)	Old Y_1B (kg)	New Y_1B (kg)	Effect 2(%)
0	0.0400	0.0400	0.0000	0.0600	0.0200	-66.6667
1	0.0533	0.1008	89.1102	0.0781	0.0749	-4.0973
2	0.0710	0.1696	138.8680	0.1016	0.1381	35.8006
3	0.0946	0.2424	156.2317	0.1322	0.2116	60.1290
4	0.1260	0.3228	156.2317	0.1719	0.2916	69.5812
5	0.1678	0.4273	154.7551	0.2235	0.3850	72.2348
6	0.2231	0.5410	142.4298	0.2905	0.4868	72.2348
7	0.2966	0.6554	120.9411	0.3772	0.5937	57.3550
8	0.3938	0.7688	95.2355	0.4895	0.7087	44.7458
9	0.5222	0.9081	73.9291	0.6346	0.8191	29.0666
10	0.6911	1.0445	51.1423	0.8216	0.9160	11.4817
11	0.9126	1.1523	26.2557	1.6618	1.0293	-3.0673
12	1.2016	1.2563	4.5500	1.3692	1.1262	-17.7662
13	1.5761	1.3324	-15.4648	1.7607	1.2337	-29.9261
14	2.0572	1.3858	-32.6387	2.2557	1.3138	-41.7530
15	2.6689	1.4250	-45.6705	2.8768	1.3615	-52.6731

Table 2: Evaluating a random perturbation impact analysis on the yields of cassava and the white yam using ODE45 computational approach of 0.05 RPV in scenario two

LGS Months	Old CB(kg)	New CB(kg)	Effect 1(%)	Old Y_1B (kg)	New Y_1B (kg)	Effect 2(%)
0	0.0400	0.0400	0.0000	0.0600	0.0200	-66.6667
1	0.0533	0.1015	90.4315	0.0781	0.0755	-3.3291
2	0.0710	0.1722	142.5890	0.1016	0.1429	40.6755
3	0.0946	0.2513	165.5244	0.1322	0.2071	56.6367
4	0.1260	0.3413	170.7381	0.1717	0.3003	74.6956
5	0.1678	0.4417	163.3288	0.2235	0.3900	74.5078
6	0.2231	0.5454	144.4253	0.2905	0.4941	70.1462
7	0.2966	0.6594	122.3392	0.3772	0.6006	59.2167
8	0.3938	0.7743	94.6277	0.4895	0.7218	47.4640
9	0.5222	0.8962	71.6300	0.6346	0.8385	32.1244
10	0.6911	1.0079	45.8396	0.8216	0.9557	16.3396
11	0.9126	1.1170	22.4046	1.0618	1.0725	1.0051
12	1.2016	1.2065	0.4018	1.3692	1.1837	-13.5510
13	1.5761	1.2739	-19.1788	1.7607	1.2829	-27.1354
14	2.0572	1.3256	-35.3635	2.2557	1.3649	-39.4918
15	2.6689	1.3589	-49.0839	2.8768	1.4266	-50.4102

Table 3: Evaluating a random perturbation impact analysis on the yields of cassava and the white yam using ODE45 computational approach of 0.05 RPV in scenario three

LGS Months	Old CB(kg)	New CB(kg)	Effect 1(%)	Old Y_1B(kg)	New Y_1B(kg)	Effect 2(%)
0	0.0400	0.0400	0.0000	0.0600	0.0200	-66.6667
1	0.0533	0.1001	87.8048	0.0781	0.0775	-0.7683
2	0.0710	0.1690	138.0036	0.1016	0.1462	43.8854
3	0.0946	0.2492	163.3939	0.1322	0.2196	66.1281
4	0.1260	0.3300	161.3939	0.1719	0.2943	71.2180
5	0.1678	0.4311	157.0205	0.2235	0.3846	72.0210
6	0.2231	0.5367	140.5158	0.2905	0.4854	67.0822
7	0.2966	0.6580	121.8593	0.3772	0.5957	57.8860
8	0.3938	0.7860	99.5921	0.4895	0.7151	46.0988
9	0.5222	0.9176	75.7313	0.6346	0.8392	32.2470
10	0.6911	1.0395	50.4262	0.8216	0.9474	15.3222
11	0.9126	1.1657	27.7132	1.0618	1.0609	-0.0887
12	1.2016	1.2609	4.9381	1.3692	1.1498	-16.0303
13	1.5761	1.3391	-15.0344	1.7607	1.2487	-29.0780
14	2.0572	1.3853	-32.6656	2.2557	1.3133	-41.7817
15	2.6689	1.4092	-47.1992	2.8768	1.3796	-52.0434

Table 4: Evaluating a random perturbation impact analysis on the yields of yellow yam and the cocoyam using ODE45 computational approach of 0.05 RPV in scenario four

LGS Months	Old Y_2B (kg)	New Y_2B (kg)	Effect 1(%)	Old CyB(kg)	New CyB(kg)	Effect 2(%)
0	0.0400	0.0400	0.0000	0.0600	0.0200	-66.6667
1	0.0781	0.1263	61.7158	0.0254	0.0709	179.1339
2	0.1016	0.2090	105.6828	0.0323	0.1363	322.3292
3	0.1322	0.3181	140.5074	0.0410	0.2216	440.5801
4	0.1720	0.4588	166.7216	0.0521	0.3272	528.6197
5	0.2236	0.6328	182.8988	0.0661	0.4618	598.9561
6	0.2907	0.8591	195.5103	0.0838	0.6323	654.2021
7	0.3776	1.1476	203.8724	0.1063	0.8499	699.2664
8	0.4903	1.5214	210.3103	0.1347	1.1146	727.3113
9	0.6359	1.9937	213.5463	0.1705	1.4418	745.4376
10	0.8239	2.5836	213.5918	0.2156	1.8456	756.0240
11	1.0658	3.3336	212.7919	0.2721	2.3418	760.5048
12	1.3762	4.2646	209.8807	0.3428	2.9382	757.1743
13	1.7726	5.4286	206.2408	0.4307	3.6410	745.4396
14	2.2762	6.8688	201.7681	0.5393	4.4533	725.7746
15	2.9116	8.6162	195.9266	0.6724	5.4252	706.8412

Table 5: Evaluating a random perturbation impact analysis on the yields of yellow yam and the cocoyam using ODE45 computational approach of 0.05 RPV in scenario five

LGS Months	Old Y_2B (kg)	New Y_2B (kg)	Effect 1(%)	Old CyB(kg)	New CyB(kg)	Effect 2(%)
0	0.0400	0.0400	0.0000	0.0600	0.0200	-66.6667
1	0.0781	0.1274	63.1242	0.0254	0.0686	170.0800
2	0.1016	0.2180	114.6634	0.0323	0.1351	318.0853
3	0.1322	0.3323	151.1498	0.0410	0.2221	441.4283
4	0.1720	0.4748	176.0288	0.0521	0.3201	514.7200
5	0.2236	0.6570	193.8313	0.0661	0.4404	566.2292
6	0.2907	0.8949	207.8189	0.0838	0.5999	615.4011
7	0.3776	1.1981	217.2904	0.1063	0.7954	648.0238
8	0.4903	1.5722	220.7148	0.1347	1.0510	680.2166
9	0.6359	2.0618	224.2157	0.1705	1.3750	706.3777
10	0.8239	2.6810	225.4284	0.2156	1.7323	703.5370
11	1.0658	3.4488	223.5954	0.2721	2.1993	708.2060
12	1.3762	4.4139	220.7239	0.3428	2.7222	694.1532
13	1.7726	5.6361	217.9613	0.4307	3.3549	678.9501
14	2.2762	7.1133	212.5058	0.5393	4.1291	665.6573
15	2.9116	8.9428	207.1438	0.6724	5.0122	645.4194

4 Discussion of results

The table 1 result indicated an acceleration of production from one month to fifteen months quantified by 0.1008kg to 1.4250kg respectively with respect to cassava biomass while similar behavior is associated with the white yam biomass from 0.6749kg to 1.3615kg from one month to fifteen months. Although, in the event of the effect, the cassava biomass increased from the yellow months by 89.1102kg to four months by 156.2317kg and thereafter, the biomass of cassava started reducing from 154.7551kg to -45.6705kg whereas the effect of the white yam biomass indicated depletion in yields at one month by -4.0973kg and thereafter, has the evidence of increment from two months by 35.8006kg to five months by 72.2343kg and thereafter, established reduction of yields from six months by 67.6284kg to fifteen months by -52.6731kg. Therefore, the analysis of this table recorded the impact of biodiversity loss and also biodiversity gain. This similar pattern of analysis is associated with the results in table 2 to table 3 but in different dimensions and values.

Table 4 results showed a monotone increased of production from one month by 0.1263kg to fifteen months (8.6162kg) with respect to the yellow yam biomass and similar behaviour is captured to cocoyam biomass from one month (0.0709kg) to 5.4252kg considering fifteen months.

But, in the event of classification of effects, the yellow yam biomass increased monotonically from one month by 61.7155% to ten months by 213.5918% and thereafter, there is an indication of reduction in production from eleven months by 212.7919% to 195.9266% at fifteen months. In this context, similarly behavior is recorded to the cocoyam biomass that associated with 7178.8496% at one month and raised to 760.5048% at eleven months and thereafter, established less production from twelve months by 757.1743% to 706.8412% at fifteen months respectively. Similar behavior is recorded on table 5.

The results also reported more increased on cocoyam biomass in all the months than the yellow yam biomass. Therefore, based on the analysis of this study, the farmers are advised to cultivate more of cocoyam, seconded by yellow yam, followed by cassava and finally, the white yam and also to be harvested at harvesting time to increase the productivity of the crops.

5 Conclusion

The application of a MATLAB ODE45 computational approach to quantify the impact of a random perturbation on the yields of four tuber crops was evaluated which the results showed an evidence that the crops were vulnerable to biodiversity gain and also biodiversity loss based on the simplified assumptions. In this context, this study also established that more vulnerability was captured on white yam by -66.6667kg when compared with other crops. Moreover, this results showed that the highest production was associated with the cocoyam by 760.0240kg followed by yellow yam by 225.4284kg, followed by cassava by 170.7381kg and white yam by -66.6667kg with unequal initial data of 0.0400 and 0.0600 respectively with random perturbation value of 0.05.

References

[1] Abranum, C.M., Omoregbu, O.C. and Ekaka-a, E.N. (2020). Numerical simulation of biodiversity loss: Comparison of numerical method. International Journal of Mathematics Trends and Technology (IJMTT), 66(3):138 – 152.

[2] Arora, N. K. (2019). Impact of a random perturbation on agriculture production and its sustainable solutions. Environmental Sustainability, 2(2):65 – 74.

[3] Atsu, J. U. and Ekaka-a, E. N. (2017). Modeling the policy implications of biodiversity loss: A case study of the Cross River National Park, South-South Nigeria. International Journal of Pure and Applied Science, 10(1):30 – 37.

[4] Atsu, J. U. and Ekaka-a, E. N. (2017). Quantifying the impact of changing intrinsic growth rate on the biodiversity of the forest resources biodiversity: Implications for the cross Rivers State forest resources at the Cross River National Park, South-South, Nigeria. African Scholar Journal of Pure and Applied Science, 7(1):117 – 130.

[5] Brilham, J. (2011). A random perturbation impacts upon crop yields in Kenya. Learning from the Past. Earth Environ, 6(1):1 – 5.

[6] Cardinale, B.J. (2012). Biodiversity loss and its impact on humanity. Nature, 486(74), 59 – 67.

[7] Chandio, A.A., Magsi, H. and Ozturk, I. (2020). Examining the effects of a random perturbation on rice production: Case study of Pakistan. Environmental Science and Pollution Research, 27(8): 7812 – 7822.

[8] Duffy, G.A., Coetzee, B.W.T., Latombe, G., Akermen, A.H., McGeoch, M.A. and Chown, S. L. (2017). Barriers to globally invasive species are weakening across the Antarctic. Diversity and Distributions, 23(9):982 – 996.
[9] Ekaka-a, E.N. (2014). Simulation modeling of the impact of a random perturbation on the interacting legumes, preliminary speaker at the National Mathematics Centre, Abuja.
[10] Ekaka-a, E. N., Osahogulu, D. J., Atsu, J. U. and Isibor, L. A. (2018). Numerical and statistical quantifications of biodiversity: Two-at-a-time equal variations. International Journal of Advanced Engineering, Management and Science, 9(2):67 – 74.
[11] European Environmental Agency (EEA) (2019). A random perturbation adaptation in the agriculture sector in Europe. https://www.europe.eu.publication
[12] Jabbour, J. and Flachsland, C. (2017). 40 years of global environmental assessments: A retrospective analysis. Environmental Science and Policy, 77:193 – 202.
[13] Kilpatrick, A.M., Salkeld, D.J., Titcomb, G. and Hahn, M.B. (2017). Conservation of biodiversity as a strategy for improving human health and well-being. Philosophical Transactions Royal Society Compendium, 4(1).
[14] Lahourari, B. (2015). A random perturbation is hitting African farmers. The Hardest of all NASA Publication.
[15] Michael, A., Obe, G. C., Abanum, C. and Innocent, C. E. (2018). Variational iteration method for 1st and 2nd ordinary differential equation using white kind chebycher polynomials. IJASRE, 4(8):126 – 130.
[16] Njas, W. (2016). Impact of a random perturbation on the food production in Africa. Journal of Life Science, 77(5):71 – 78.
[17] Nwala, B.O. and Nwagor, P. (2021). Computing the effect of varying the intra-species coefficients on the carrying capacity and the biodiversity scenario. International Journal of Mathematics and Educational Review, 3(1):35 – 38.
[18] Nwala, B.O. (2020). Simulation modeling of impact of a random perturbation on the yields of cassava and yam species. Unpublished M.Sc dissertation, Ignatius Ajuru University of Education, Port Harcourt.
[19] Nwala, B.O. (2022). Model study of the impact of a random environmental perturbation on the yields of tuber crops. Unpublished PhD thesis; Ignatius Ajuru University of Education, Port Harcourt.
[20] Pattanayak, S. K., Kramer, R. A. and Vincent, J. R. (2017). Ecosystem change and human health: Implementation economics and policy. Phil. Trans. R. Soc. B., 372:2017 – 2023.
[21] Sara, J.H., Yury, K. and Mark, A.J.C. (2021). Numerical simulations latest research reviews. British Journal of Cancer, 125:1552 – 1560.
[22] United Kingdom Parliamentary Office of Science and Technology (2015). Biodiversity framework: Implementation plan – 2nd Annual report. https://www.hubjncc.govukassets58702.
[23] Wilson, O.E. (2021). Biodiversity conservation: Types, importance, and method. https://www.conserve.energy.future.com.biodiversity.

Mathematical modelling of skilling fishery management for sustainable development of an economy

C. Nkuturum* and I. George†

Abstract

This study considered a non-linear mathematical model of skilling fishery management to understand the dynamics of lives in an aquatic system which involves two zones of unrestricted and restricted fishing zones. The model analysis showcased the existence of equilibrium points in line with the biological and bionomic, dynamical behaviour of equilibrium points and also derived the conditions for stability and instability of the system. The behaviour of this dynamical model of fishery management were illustrated using numerical simulations to establish the analytical results. The findings of this study showed that inadequate knowledge of the resource and ecosystem, lack of interaction between the government and stakeholders, inaccessibility of financial resources to meet specific needs, weak implementation of agricultural policies and programmes, inadequate practical advisory/extension services and lack of monitoring and evaluation of programme/project team led the system to be unstable which implies that the eigen values were greater than zero. This paper identified that management of fisheries is affected by climate change, human actions and population, shortage of food, poverty and lack of policy executions. Amongst all, the study suggested that there should be introduction of environmental impact assessment for fisheries policies to be implemented, skilled or trained fisheries administrators that will monitor and evaluate the policy/programme consistency, against specified goals need to be given more financial resources, and properly staffed and equipped to address effectively all aspects of sustainable fisheries development and management. should be adopted and their efficacy monitored and evaluated against specified goals. There should be better protection to environmental hazards, control of waste disposal and pollution. Finally, government at all levels should recognize its benefit and work towards integrating skilling fisheries management activities, including sharing of expertise and resources for education, research, technology, monitoring, control and surveillance activities and development of the relevant legislative framework.

Keywords: skilling; fishery; zones; management; sustainable development; economy; model

* Corresponding Author. Department of Mathematics, Rivers State University, Port Harcourt, Nigeria; Email: christienkuturum245@gmail.com

† Department of Mathematics/Statistics, Ignatius Ajuru University of Education, Port Harcourt, Nigeria

1 Introduction

The sustainable fisheries development and management is an integration of bio-ecological, technological, environmental, economic and social scopes to bring about and sustainably improve the welfare of all the people engaged directly or indirectly in the fisheries sector as well as the natural productive system. Thus, sustainable development of the fisheries sector in any nation has become of greatest importance to ensure adequate food at affordable prices and as the main source of economic and social progress for the rural poor and the world at large. Sustainable development emphasizes the need to organize and control the dynamics and the complex interactions between man, production activities, and natural resources in order to promote their co-existence and their common evolution. However, this development must integrate the triple nethermost line framework captured in FAO (1995). In Nigeria, there are fisheries laws and policies that brought about in the interim increased fish production. Nevertheless, policy shifts and unsustainable implementation have led to decline of the fisheries sector over the years leaving the target rural economies more vulnerable than ever. Sustainable fisheries development can only be achieved through regulated fishing, which considers fishery management objectives and proper enforcement of regulations.

Nigeria is reasonably endowed with large rivers, small water bodies and some natural springs. It also has an extensive coastline of approximately 900km and an exclusive economic zone of about 217,313 km² (Sea Around Us, 2007). Nigeria has a high demand for fish of about 1.5 million metric tons thus, resulting in a demand-supply gap of about a million metric tons and a per capital consumption of 7.5-8.5kg annually (FDF, 2005). Nkuturum and George (2021) in their work on ecological growth model in marketing dynamics: the role of human actions stated that human action increases the demand-supply of goods in the market.

Thus, fisheries are crucial to the Nigerian economy in contributing about 5.4% of the gross domestic product (FAO, 1995). Although contribution of the fisheries sector is essential to agricultural development in Nigeria to ensure adequate food at affordable prices and as the main source of economic and social progress for the rural poor (Berezansky, et al. 2011). Also, more than half of policies and programmes in agriculture development focus on forest matters while less emphasis is placed on food and animal production requires immediate attention. For fisheries, a useful definition would be the one agreed at FAO in 1988 which states that sustainable development has been defined by the World Commission on Environment and Development (1987) as development that meets the needs of the present generation without compromising the ability of future generations to meet.

Fisheries Management systems in a nation comprises of three methods as the traditional systems: which focuses on operation by the administration of traditional authorities that enforce regulations to control fishing. This pin points on practices such as ban on fishing at certain time of the year or during fish breeding period. The mixed systems: involve the participation of both the traditional and modern government administrations. Finally, the modern systems: includes those operated by the administrations of the central government where fisheries regulations are enforced by agriculture officers of the fisheries departments (Biswas, et al. 2017). Thus, the issues confronting the management of the fisheries are: environmental Change which goes to climatic patterns and man's activities, exogenous factors address human population, poverty and food demand and weak policies and policy implementations.

Efficient skilling and sustainable fisheries management of natural resources, its control measure depends mainly on the essential understanding the mechanisms of their evolution over time where mathematical modelling in terms of non-linear differential equations (ODEs) can play a significant role. Hence, mathematical modelling is broadly used to discuss different types of real phenomena which leads to design better prediction, prevention, management and control strategies. The epitome of this study are the empirical studies done by the following scientists as in Biswas *et al.* (2017) who studied on the potential impacts of global climate change on fish production in Bangladesh. Followed Nkuturum (2021) studied on distortion of ecological systems by human actions: a mathematical model of two coexisting species in a community.

Also, Clark (2016) developed a mathematical model to describe the optimal management of renewable resources. Das, et al. (2009) showed the bioeconomic harvesting of a prey-predator fishery. De Lara and Doyen (2008) discussed on the sustainable management of natural resources: mathematical modelling and methods. Also, Dubey, et al. (2003) carried out a work on a model for fishery resources with reserve area for more knowledge on the applications of mathematical modelling.

Previously, many researchers presented their mathematical models as to optimize the skilling of fish production and management. Mathematical modelling is the use of equations, expressions and mathematics language to translate and proffer solutions to real life situation problems from an application area into traceable mathematical formulation with analytical, theoretical and numerical analysis. Thus, La Salle and Lefschetz, (1961) showed the stability by Lyapunov's direct method with applications. Also, Leung and Wang (1976) presented an analysis of models for commercial fishing covering mathematical and economic aspects. Mesterton-Gibbons, (1996) and Kitabatake, (1982) studied the effects on the optimal policy for combined harvesting of predator-prey and a dynamic predator-prey model for fishery resources in lake Kasumigaura. One of the findings showed that there is irreversibility of capital investment upon optimal exploitation policies for renewable resources stocks. Zhang et al. (2000) proposed and analysed a model to study the stage structured predator-prey model and optimal harvesting policy of the organisms. The study derived necessary and sufficient condition for the coexistence and extinction of species. Song and Chen (2001) carried out a study on the optimal harvesting policy and stability for a two-species competitive system with stage structure, and obtained conditions for the existence of a globally asymptotically stable positive equilibrium and a threshold of harvesting for the mature population and finally proposed a dynamic model for a single-species fishery which depends partially on a logistically growing resource.

The problems identified in skilling fishery management for sustainable development of an economy are as follows: derisory knowledge of the resource and ecosystem, lack of interaction between the government and stakeholders, inaccessibility of financial resources to meet specific needs, weak implementation of agricultural policies and programmes, inadequate practical advisory/extension services and lack of monitoring and evaluation of programme/project team. Based on the above elucidated literatures and challenges enumerated, the researcher deemed it necessary to proposed a mathematical model to optimize the production of fish using system of nonlinear differential equations, discussed the equilibrium points, dynamical behaviour of the points and obtained the conditions of stability and instability of the two zones, ascertained the impact of human effort to both fishing zones and finally, discussed the numerical simulations with graphical representations.

2 Model formulation

This paper considered a fishery resource consisting of two zones: a free fishing zone and a reserved area zone. We study a prey-predator system in a two-patch environment, one accessible to both prey and predators and the other one being a refuge for the prey. Each patch is supposed to be homogenous. The prey refuge constitutes a reserve area of prey and no fishing is permitted in the reserved zone while the unreserved zone area is an open-access fishery zone. It is assumed that the prey migrates between the two patches randomly. It is assumed that, in each zone growth of fish population follows logistic model. Keeping these in view, the model becomes:

$$\frac{dU}{dt} = \beta_1 U\left(1 - \frac{U}{C}\right) - M_1 U + M_2 R - qEU \qquad 1$$

$$\frac{dR}{dt} = \beta_2 R\left(1 - \frac{R}{K}\right) + M_1 U - M_2 R \qquad 2$$

In the equations above, $U(t)$ is the biomass densities of the same population inside the unrestricted area and R(t) is the biomass densities of the same population inside the restricted area respectively at time t. E is the human effort for harvesting the fish population in the unreserved zone and the value of qE is called fishing mortality. Again, a and b are the intrinsic growth rate of fish subpopulation inside the unreserved and reserved area respectively. Let the fish subpopulation of the unreserved area at a rate migrate into reserved area at a rate M_1 and the fish subpopulation of the reserved and migrate into unreserved area at a rate M_2. The carrying capacities of fish species in unreserved and reserved area C and K respectively, q is the catch ability coefficient of fish species in the unreserved area. If there Is no migration of fish population from reserved area to unreserved area (i.e. M_2= 0) and $a - M_1 - qE < 0$ then $\frac{\partial U}{\partial t} < 0.$ similarly, if there I no migration of fish population from unreserved area to restricted area (i.e. $M_1 = 0.$) and $b - M_2 < 0$, then $\frac{dR}{\partial t} < 0.$

3 Model analysis

The non-linear system in equations (1) - (2) has qualitatively analysed in this section so as to find the equilibrium points and the dynamical behaviour of that points as well as test the stability at positivity analysis equilibrium points.
Now we will prove that all the variable in the system model equations (1) and (2) are positive.

Lemma 1. If $U(t) \geq 0,\ R(t) \geq 0,$ then the solution of $U(t)$ and $R(t)$ of the model system of equations (1) and (2) are positive.

Proof: To prove this lemma, we get from the equation (1), $\frac{dU}{dt} = aU\left(1 - \frac{U}{C}\right) - M_1 U + M_2 R - qEU$

Now, $\frac{dU}{dt} + M_1 U + qEU \geq 0 \Rightarrow \frac{dU}{dt} + (M_1 + qE)U \geq 0$ 3
Putting $M_1 - qE = \emptyset$ and the integrating factor, *IF* = $\int e^{\emptyset dt} = e^{\emptyset t}$ 4
Multiplying by *IF* on both sides, we get,

$$U' e^{\emptyset t} + \emptyset U e^{\emptyset t} \geq 0 \Rightarrow (U' + \emptyset U)e^{\emptyset t} \geq 0 \qquad 5$$

$$\frac{dU}{dt} e^{\emptyset t} U \geq 0 \Rightarrow e^{\emptyset t} U \geq A \qquad 6$$

Therefore, $U \geq Ae^{-(M_1 + qE)t}$ 7

where, A is an integrating constant. For the value of A, under the initial conditions, when t = 0, then $U(t) = U(0)$, hence $U(0) \geq$ A. 8

Now putting the value of A in equation (8) gives,
$U(t) \geq U(0)e^{-(\lambda_1 + qE)t}$ 9

Since $U(t) \geq 0$ and $M_1 - qE \geq 0$, hence $U(t) \geq 0$ for all $t \geq 0$.

Similarly, from equation (2) yields,

$$\frac{dR}{dt} = \beta_2 R\left(1 - \frac{R}{K}\right) + M_1 U - M_2 R \geq 0 \Rightarrow \frac{dR}{dt} + M_2 R \geq 0 \qquad 10$$

Using integrating factor $IF = \int e^{M_2 dt} = e^{M_2 t}$ 11

Multiply both sides of equation (10) by equation (11) gives,

$$e^{M_2 t}\frac{dR}{dt} + M_2 R e^{M_2 t} \geq 0 \Rightarrow \frac{d}{dt} e^{M_2 t} R \geq 0 \Rightarrow e^{M_2 t} R \geq B. \qquad 12$$

Thus, $R \geq B e^{-M_2 t}$. 13

where, B is an integrating constant. For the value of B, under the initial conditions, when $t = 0$, then $R(t) = R(0)$, hence $R(0) \geq B$. 14

Now putting the value of B in equation (14) gives,

$R(t) \geq R(0)e^{-M_2 t}$. 15

Since $R(t) \geq 0$ and $M_2 \geq 0$, hence $U(t) \geq 0$ for all $t \geq 0$. Therefore, $U(t)$ and $R(t)$ are positive for all time, $t \geq 0$.

3.1 Existence of equilibrium

The steady states of the two system of equations were obtained by equating the derivatives to zero and resolving it equations analytically. The two possible steady states are given as: S(0, 0) and $S(U^*, R^*)$ respectively. Now, (U^*, R^*) are the positive solutions of equations (1-2).

$$0 = \beta_1 U\left(1 - \frac{U}{C}\right) - M_1 U + M_2 R - qEU \qquad 16$$

$$0 = \beta_2 R\left(1 - \frac{R}{K}\right) + M_1 U - M_2 R \qquad 17$$

Eliminating R from equation (16) yields,

$$R = \frac{\beta_1 U^2 - \beta_1 UC + M_1 CU + CqEU}{CM_2}. \qquad 18$$

Substitute the value of R into equation (18)

$$\beta_2\left(\frac{\beta_1 U^2 - \beta_1 UC + M_1 CU + CqEU}{CM_2}\right)\left(1 - \frac{\beta_1 U^2 - \beta_1 UC + M_1 CU + CqEU}{\frac{CM_2}{K}}\right) + M_1 U - M_2\left(\frac{\beta_1 U^2 - \beta_1 UC + M_1 CU + CqEU}{CM_2}\right) = 0 \qquad 19$$

$$= -\frac{\beta_2 \beta_1^2 U^4}{KC^2 M_2^2} + \frac{\beta_2 \beta_1^2 C U^3}{KC^2 M_2^2} + 2\beta_1\beta_2(\beta_1 - M_1 - qE)U^2 - \left\{\frac{\beta_2(\beta_1 - M_1 - qE)^2}{CM_2^2} - \frac{(\beta_2 - M_2)\beta_1}{CM_2}\right\}U + \frac{(\beta_2 - M_2)}{M_2}(\beta_1 - M_1 - qE) - M_1 = 0 \qquad 20$$

$= aU^4 + bU^3 + cU^2 + dU + y = 0,$ 21

where, $a = -\frac{\beta_2\beta_1^2}{KC^2M_2^2}$, $b = \frac{\beta_2\beta_1^2}{KC^2M_2^2}$, $c = 2\beta_1\beta_2(\beta_1 - M_1 - qE)$, $d = -\left\{\frac{\beta_2(\beta_1-M_1-qE)^2}{CM_2^2} - \frac{(\beta_2-M_2)\beta_1}{CM_2}\right\}$ and $y = \frac{(\beta_2-M_2)}{M_2}(\beta_1 - M_1 - qE) - M_1.$

22

The equation (21) has a unique positive solution $U = U^*$ by satisfying the inequalities below:

$\frac{\beta_2(\beta_1-M_1-qE)^2}{CM_2^2} < \frac{(\beta_2-M_2)\beta_1}{C}, \frac{(\beta_2-M_2)}{M_2}(\beta_1 - M_1 - qE) < M_1M_2.$ 23

Putting the values of U^*, R^* into (16) and for positivity, $U^* > \left(\frac{C}{\beta_1}\right)(\beta_1 - M_1 - qE)$ 24

3.2 Dynamical behaviour of equilibria

The dynamical behaviour of equilibria points can be studied by computing vibrational matrices corresponding to each equilibrium. In equation (1), considering that the trivial equilibrium point p_0 is unstable. Using the Routh-Hurwitz criteria makes it easy to check that all eigenvalues of the vibrational matrix corresponding to p^* have negative real parts. Therefore, $p^*$is locally asymptotically stable in the two-dimensional plane. This indicates that a small circle with centre p^* can be determined such that any solution $U(t), R(t)$ of equation (2) which is inside the circle at time $t = t_1$ will remain inside the circle for all $t \geq t_1$ and will tend to (U^*, R^*) as $t \to \infty$.

Lemma 2. *Let* $Q = \left\{(U,R) \in R_2^2 : p = U + R \leq \frac{\mu}{\emptyset}\right\}$ *be a region of interest for all solutions initiating in the interior of the positive quadrant for* $\emptyset$ *is a positive constant and* $\mu = \frac{C}{4\beta_1}(\beta_1 - \emptyset - eq)^2 + \frac{K}{4\beta_2}(\beta_2 + \emptyset)^2$. This lemma will show that all solutions of model (2) are positive and uniformly bounded.

Proof: Let, $P(t) = U(t) + R(t)$, and $\emptyset > 0$ be a constant. Then,

$\frac{dP}{dt} = -\frac{\beta_1U^2}{C} + (\beta_1 - \emptyset - Eq)^2U^2 - \frac{\beta_2R^2}{K} + (\beta_2 + \emptyset) \leq \frac{K}{4\beta_1}(\beta_1 - \emptyset - Eq)^2 + \frac{K}{4\beta_2}(\beta_2 + \emptyset)^2 = \mu$ 25

Using the theory of differential inequality in Birkhoff and Rota, (1882),

$0 < P(t), U(t), R(t) \leq \frac{\mu}{\emptyset}\left(1 - e^{-\emptyset t}\right) + P(0), U(0), R(0), e^{-\emptyset t},$ 26

when $t \to \infty$ and $0 < P < \frac{\mu}{\emptyset}$

Global stability of equilibrium point ($\boldsymbol{p}^*$).

Theorem 1. The equilibrium point p^* *is globally asymptotically stable.*

Proof: Let us consider the following definite function about p^*

$Q = \left(U - U^*In\frac{U}{U^*}\right) + A\left(R - R^* - R^*In\frac{R}{R^*}\right)$ 27

Upon differentiating Q with respect to time *t*, gives,

$\frac{dQ}{dt} = -\frac{\beta_1}{C}(U - U^*)^2 - \frac{R^*}{U^*}\frac{M_2\beta_2}{M_1\beta_1}(R - R^*)^2 - \frac{M_2}{U^*UR}(UR^* - RU^*) < 0$ 28

This implies that $\frac{dQ}{dt}$ is negative by Liapunov's (1961). Hence, it follows that the positive equilibrium is globally asymptotically stable. Stability analysis reveals that the trivial equilibrium is an unstable system while, the feasible equilibrium is a point whereby both species are existing in the system for the competition, at this point they are stable but the population decrease with time.

3.3 Stability of steady states

Let the two functions W= $W(U,R)=\frac{dU}{dt}$ and V= $V(U,R)=\frac{dR}{dt}$ from the steady state $(U^*,R^*)=(0{,}0)$ for equations (1) and (2). Thus, the Jacobian matrix gives:

$$J(U,R)=\begin{pmatrix}\frac{\partial W}{\partial U} & \frac{\partial W}{\partial R}\\ \frac{\partial V}{\partial U} & \frac{\partial V}{\partial R}\end{pmatrix}=\begin{pmatrix}\beta_1-\frac{2\beta_1 U}{C}-M_1-qE & M_2\\ M_1 & \beta_2-\frac{2\beta_2 R}{K}-M_2\end{pmatrix} \qquad 29$$

Thus, evaluating at the steady state of (0, 0) the Jacobian matrix J is

$$J(0{,}0)=\begin{pmatrix}\beta_1-M_1-qE & M_2\\ M_1 & \beta_2-M_2\end{pmatrix}-\lambda\begin{pmatrix}1&0\\0&1\end{pmatrix}=\begin{pmatrix}\beta_1-M_1-qE-\lambda & 0\\ 0 & \beta_2-M_2-\lambda\end{pmatrix} \qquad 30$$

$\beta_1-M_1-qE-\lambda_1=0$ and $\beta_2-M_2-\lambda_2=0$

Thus, the Eigen values $\boldsymbol{\lambda}$ are:

$\lambda_1=\beta_1-M_1-qE$ and $\lambda_2=\beta_2-M_2$

For $\lambda_1>\lambda_2>0$. Hence, the system is unstable

Here, the eigenvalues $\boldsymbol{\lambda}$ of the matrix "*J*" determine the stability of the states. Depending on $\boldsymbol{\lambda}$, the stability conditions are: 1. If the eigenvalue $\boldsymbol{\lambda}$ <0, then the steady state is stable, 2. If the eigenvalue $\boldsymbol{\lambda}$ >0, then the system is unstable. The findings depicts that the consumption rate of fishes is very high to the extent that at some time, t there should be no matured fish in the zones which in turn causes recurrent skilling on its sustainability. This implies that the biomass density of the two zones or areas are not the same, so also exchange rate in the economy of nations are unstable. This results also showcased that the knowledge of experts about the resource and ecosystem in line with the agricultural policies are not properly implemented. These results conform to Nkuturum (2016, 2017) on the study mathematical model of predator-prey relationship with human disturbance which showed that at time, t one of the species would go extinction while the other recuperate making the system unstable.

4 Numerical simulations and discussion of findings

This section showcases the numerically solved proposed model equations (1-2) and discussion of findings. Already, the existence of equilibrium, positivity analysis and stability of steady states have been discussed above. The model is simulated using the parameter values the total effort applied for harvesting the fish population in the reserve area E = 0.2. The carrying capacities of fish species in unreserved and reserved area respectively C = 110 and K = 200. The intrinsic growth rates of fish sub-population are respectively $\beta_1=0.03$ and $\beta_2=0.04$. The catch ability of fish coefficient q = 0.001. The fish sub-population of unreserved and reserved area are respectively $M_1=M_2=0.05$ and qE denote the fishing mortality rate of the model (1). Then the result is displayed in the Fig. 1. The displayed graph depicts the biomass densities of reserved area unreserved zones or areas where the population increased and decreased within 90 days. Firstly, the Fig. 1 showed that the population of unreserved area and reserved area are same on the 9 days. In 90 days, the population of biomass densities of unreserved area increases above 100. At the same time the population of biomass densities of reserved area increases above 100. Once more, Fig. 2 the population of reserved area increases above 900. At the same time the population of unreserved area increases above 400 and unreserved area are same at 10 days. If the input value of the total effort applied for harvesting the fish population and fish catch ability coefficient increases, then the population decreases. If the population of the total effort applied for harvesting the fish population and fish catch ability coefficient decreases so the population decreases means that human beings have vital roles to play in skilling fisheries management for sustainable development of an economy. Similarly, by changing the values of parameter the shape of graph changed. The Fig. 3 and Fig. 4 are changing the parameter values too, altered the graph in shape. When the parameter values of intrinsic growth rate of unreserved and reserved area are changed by increasing it respectively, then the population are also increasing.

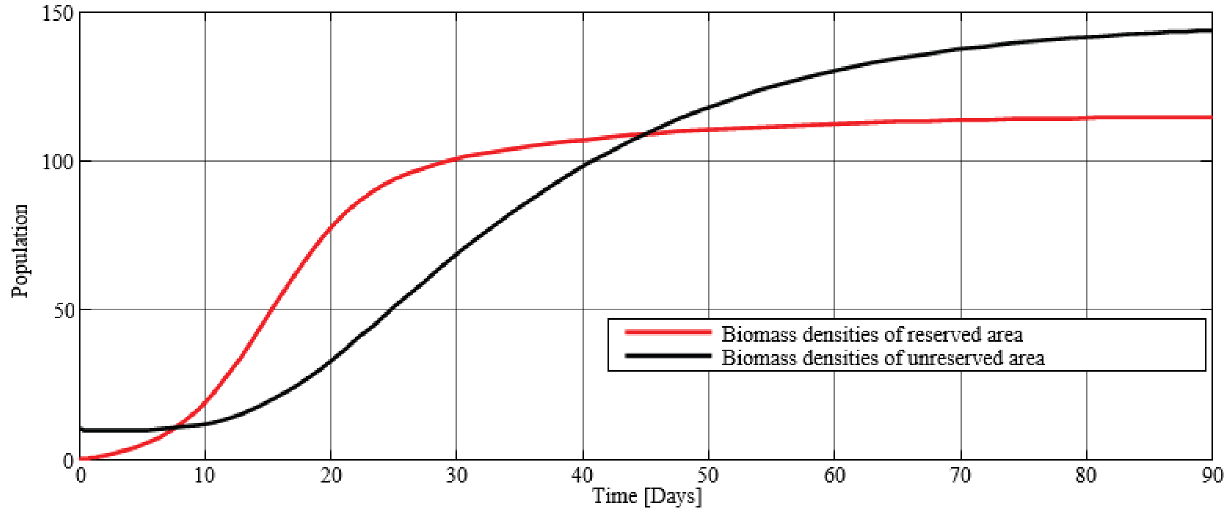

Figure 1. Showing the graph of fishery model of two zones population with time (Days)

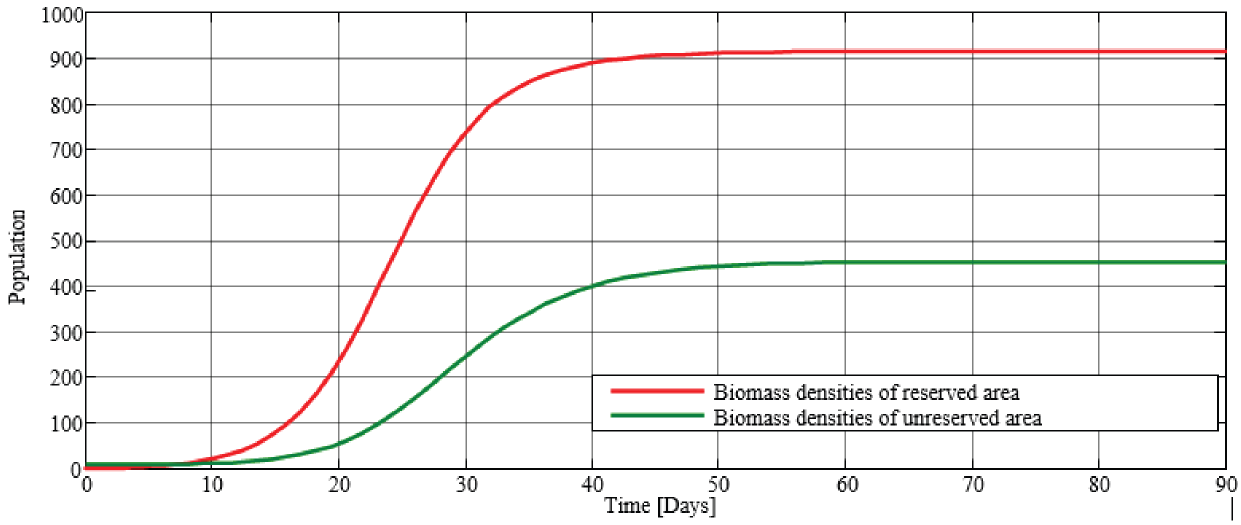

Figure 2. Showing variation of population with time (Days) for E = 0.002, C = 1000, K = 200, $\boldsymbol{\beta_1 = 0.03}$, $\boldsymbol{\beta_2 = 0.04}$ and q = 0.001

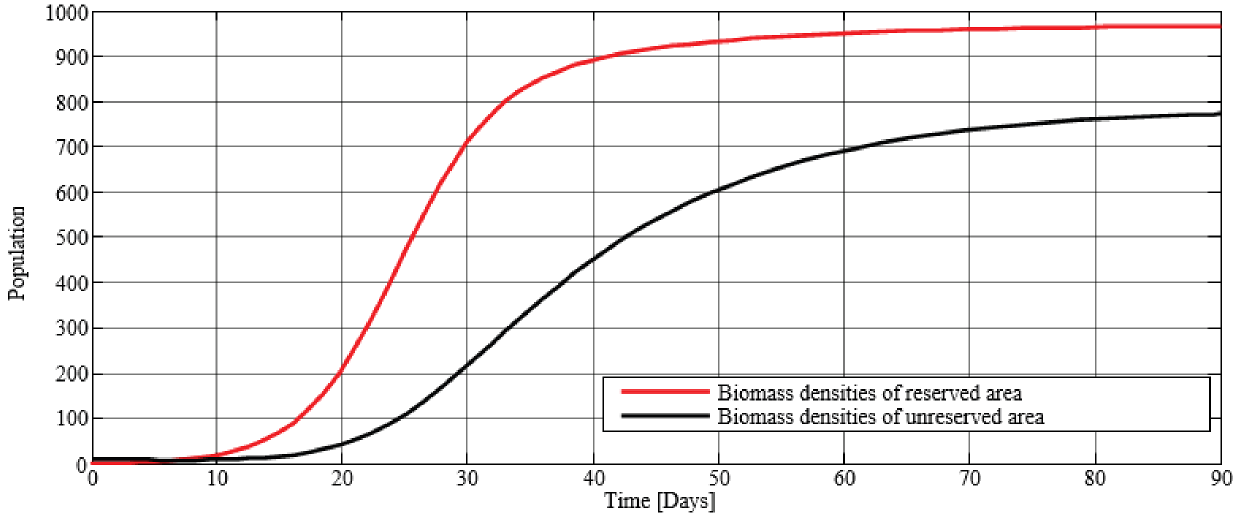

Figure 3. Variation of population with time (Days) for E = 0.002, C = 1000, K = 200, $\boldsymbol{\beta_1 = 0.299}$, $\boldsymbol{\beta_2 = 0.004}$ and q = 0.00001

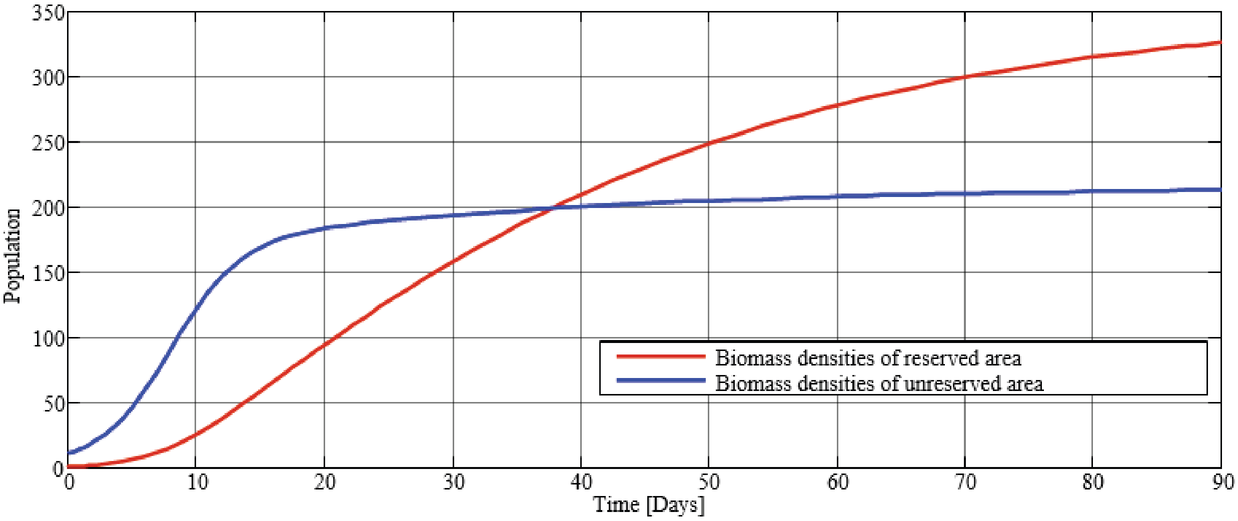

Figure 4. Variation of population with time (Days) for E = 0.002, C = 1000, K = 200, $\boldsymbol{\beta_1 = 0.03}$, $\boldsymbol{\beta_2 = 0.4}$ and q = 0.00001

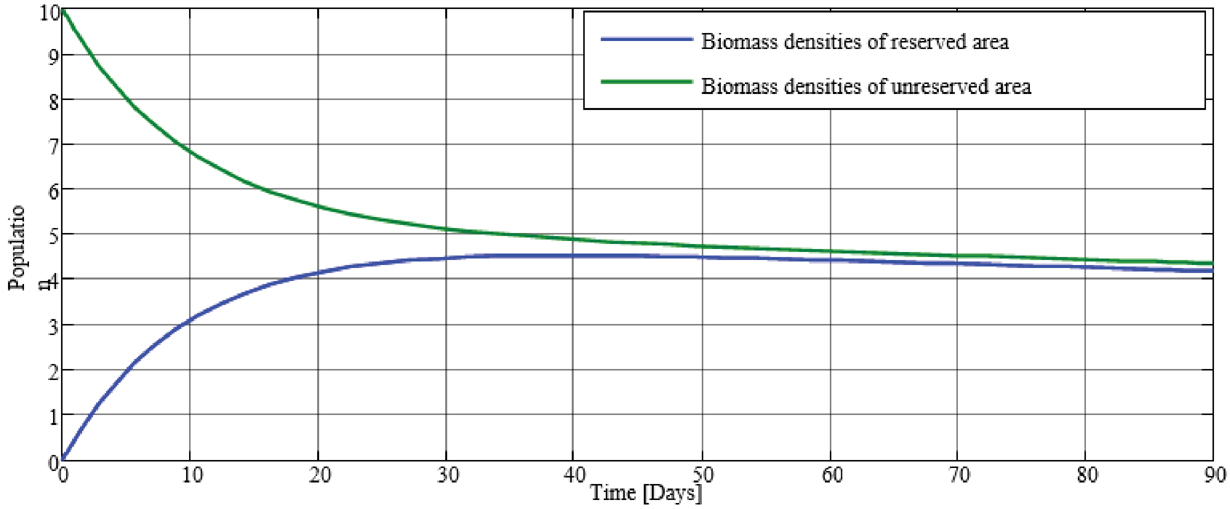

Figure 5. Variation of population with time (Days) for E = 4, C = 1000, K = 200, $\boldsymbol{\beta_1 = 0.03}$, $\boldsymbol{\beta_2 = 0.004}$ and q = 0.1

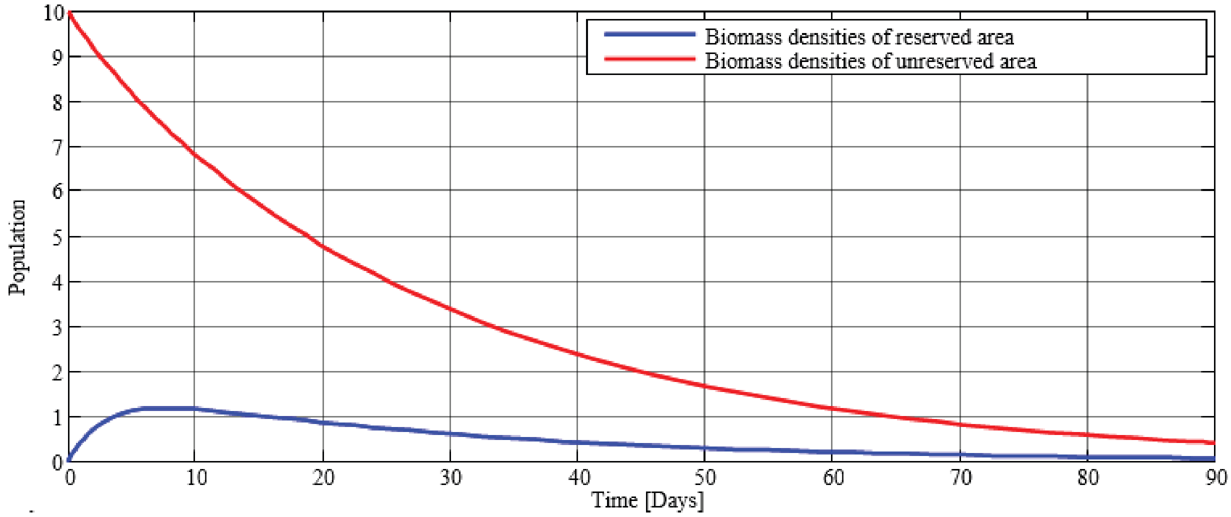

Figure 6. Variation of population with time (Days) for E = 2.8, C = 1000, K = 200, $\boldsymbol{\beta_1 = 0.3}$, $\boldsymbol{\beta_2 = 0.006}$ and q = 0.2

Hence, if the parameter values of carrying capacities of fish spices in the unreserved and reserved area are used for fish production respectively C and K area increasing, then the graph is increasing and by changing the parameter values C and *K* are increasing then, the fish production is increasing. Likewise, the Fig. 5 and Fig. 6 are going below the *X* axis showing that the population decreases with time. The maximum fish production depends on carrying capacities intrinsic growth rate of the unreserved and reserved area and harvesting rate or fishing mortality. In this Figures, it is detected that the harvesting rate of fishing mortality increases as the graph is decreases. Again, the fishing mortality decreases as the graph increases. In these figures, by changing the values of parameter the characteristics figure is changed. So, the model is good for skilling fisheries management for sustainable development of an economy that could lead to minimum and maximum fish production in a reserved and unreserved areas respectively.

The model contains two fixed points: the trivial equilibrium $(U^*, R^*) = (0,0)$ where both populations disappear; when evaluated gives the eigen values as $\lambda_1 = \beta_1 - M_1 - qE$ and $\lambda_2 = \beta_2 - M_2$ depicting unstable system and the feasible equilibrium implies coexistence of both populations. Interestingly, the feasible equilibrium showed abundance of the biomass density in the zones is independent of their own respective growth or death rates but instead it is set by the productivity of the other species in the reserved zone. However, the traditional management system is the most effective especially at the rural community level whereby the village heads have responsibilities of enforcing and regulating the management Systems in their various domains. The mixed system is most prevalent and governments generally lack the logistic support in terms of personnel, funds, field vehicles and so on to enforce fisheries laws and regulations. In general, fisheries management systems in Nigeria can be described as variable and hindered by poor financial support for policy implementation in which the findings of this study rated in percentage gives as mixed system is most common (60%), followed by the traditional type 30% while modern type accounts for only 10%.

5 Conclusion

In this mathematical modelling, the system has been assumed that the two ecosystems; one free fishing zone and the other reserved zone. In this paper, we analysed the catfish production by using many mathematical models. It has been found that the total user's cost of harvest per unit of effort equals to the discounted value of the future marginal profit of the effort at the steady-state level. It has also been noted that if the discounted rate increases, then the economic rent decreases and even may tend to zero if the discounted rate tend to infinity. The possibility that the predator species in this model be itself harvested for commercial purposes, or that its non-use value be an important element in the overall economic value of the marine ecosystem have not been considered in this paper. Their inclusion in the model would surely lead to characterize another set of trade-offs which are bound to be at the centre of marine reserve policies. We have derived existence of equilibrium and globally asymptotically stable and unstable. Finally, skilling fisheries management for sustainable development can be achieved through regulated fishing which considers fishery management objectives that address the status of the resource, human activities, the health of the environment, post-harvest technology and trade, as well as other economic concerns, social benefits, legal and administrative support as observed from graphical representation with different parameter values.

This study can be extended to add noise term, diffusion term and feeding rate of the fishes. This study suggests that there should be introduction of environmental impact assessment for fisheries policies to be implemented, skilled or trained fisheries administrators that will monitor and evaluate the policy/programme consistency, against specified goals need to be given more financial resources, and properly staffed and equipped to address effectively all aspects of sustainable fisheries development and management. should be adopted and their efficacy monitored and evaluated against specified goals. There should be better protection to environmental hazards, control of waste disposal and pollution.

Finally, government at all levels should recognize its benefit and work towards integrating skilling fisheries management activities, including sharing of expertise and resources for education, research, technology, monitoring, control and surveillance activities and development of the relevant legislative framework due to its economic gains.

References

[1] Berezansky, L; Idels, L. and Kipnis, M. (2011). Mathematical model of marine protected areas. IMA J. Appl. Math. 76(1):312-325.

[2] Birkhoff, G. and Rota, G.S. (1882). Ordinary differential equations. Ginn, Boston.

[3] Biswas, Md. H. A.; Hossain, Md. R. and Mondal, M. K. (2017). Mathematical modelling applied to sustainable management of marine resources. ELSEVIER Procedia Engineering, 194(1):337-344

[4] Clark, C. W. (1976). Mathematical Bioeconomics: The optimal management of renewable resources. Wiley, New York.

[5]Das, T. Mukherjee, R.N., and Chaudhuri,K. S. (2009). Bioeconomic harvesting of a prey-Predator fishery. J. Bio. Dyn. 3(1):447-462.

[6] De Lara, M. and Doyen, L. (2008). Sustainable management of natural resources: mathematical models and methods. Springer, Verlag Berlin.

[7] Dubey, B., Chandra, P., and Sinha, P. (2003). A model for fishery resource with reserve area. Nonl. Ana.: Real World Appl., 4(1):625-637.

[8] FAO (1995). The code of conduct for responsible fisheries. FAO: 41

[9] FDF (Federal Department of Fisheries) (2005). Report of presidential committee on fisheries and aquaculture development: Consolidated Report., Vol. 1

[10] Kitabatake, Y. (1982). A dynamic predator-prey model for fishery resources: a case of lake Kasumigaura. Environ. Plan. A, 14(1):225-235.

[11] La Salle, J. and Lefschetz, S. (1961). Stability by Liapunovs direct method with applications. Academic Press, New York.

[12] Leung, A. and Wang, A. (1976). Analysis of models for commercial fishing: mathematical and economical aspects. Econometrica, 44(1):295-303.

[13] Mesterton-Gibbons, M. (1996). On the optimal policy for combined harvesting of predator prey. Nat. Res. Model., 3(1):235-244.

[14] Nkuturum, C. and George, I. (2021). Ecological growth model in marketing dynamics: the role of human actions. Nigeria society of Mathematical Biology (NSMB 5th conference proceedings).

[15] Nkuturum, C. (2021). Distortion of ecological systems by human actions: a mathematical model of two coexisting species in a community. Nigeria society of Mathematical Biology (NSMB 5th conference Proceedings).

[16] Nkuturum, C. (2017). Mathematical model of predator-prey relationship with human disturbance. Department Of Mathematics, University of Nigeria, Nsukka. https://www.repository.unn.edu.ng

[17] Nkuturum, C. (2016). Mathematical model of predator-prey relationship and human disturbance. International Journal of Education Development, 6:183-196.

[18] Sea Around Us (2007). A global database on marine fisheries and ecosystems. www.seaaroundus.org.

[19] Song, X. and Chen, L. (2001). Optimal harvesting and stability for a two-species competitive System with stage structure. Math. Biosci. 170(1):173-186.

[20] Zhang, X., Chen, L. and Neumann, A.U. (2000). The stage structured predator-prey model and optimal harvesting policy. Math. Biosci. 168(1):201-210.

International Journal of Mathematical Analysis and Modelling
Volume 5, Issue 4, November 2022, Pages 50 – 57

Use of a generalized gamma additive model to determine the effect of monetary policy on the Nigerian stock market

O.L. Aako*† and O.A. Agbolade*‡

Abstract

This study looked at how monetary policy affected the Nigerian stock market's performance from 2006 to 2020 using Generalized Additive Model for Location, Scale, and Shape (GAMLSS). The method expands the capabilities of linear, generalized linear and additive models. The All-Share Index was used to gauge the performance of the Nigerian stock market. Money supply, interest rate, exchange rate, and inflation rate were used to gauge monetary policy, which served as the explanatory variable. In order to choose the best fitted model, some selected GAMLSS family distributions in the positive real line, including the Generalized gamma, Gumbel, Weibull, and Log normal distributions, were fitted to the data. The Generalized Gamma (GG) distribution best fits the response variable, according to the AIC and BIC results. In order to ascertain how monetary policy affected the Nigerian Stock Market, GG in GAMLSS was employed. The study's conclusions demonstrate that whereas other variables have negative associations with the All-Share Index, the money supply has a positive link with it. The Nigerian Stock Market All-Share Index is significantly impacted by each of the explanatory variables.

Keywords: all-share index; GAMLSS; generalized gamma distribution; monetary policy; stock market

1 Introduction

The stock market is viewed as the engine of economic growth since it is essential for capital allocation and mobilization to promote economic growth. A sophisticated stock market makes it easier to sterilize significant inflows of capital (Turner, 2002). It is a type of investment that does not necessitate the investor's personal presence or managerial abilities. The rise of the stock market encourages financial integration and development, which boosts economic growth by increasing capital allocation efficiency and facilitating better risk sharing (Laeven, 2014). According to Mishkin (2007), a functioning financial market is essential for fostering long-term economic progress, and underperforming fiscal markets are one of the reasons that many nations around the world continue to live in abject poverty.

* Department of Mathematics and Statistics, Federal Polytechnic, Ilaro, Ogun State, Nigeria
† Corresponding Author. E-mail: olubisi.aako@federalpolyilaro.edu.ng
‡ E-mail: olumuyiwa.agbolade@federalpolyilaro.edu.ng

Financial and monetary economists in Nigeria have been conducting extensive study on the connection between monetary policy and stock market performance since the country's economy was deregulated. Using an error correction model, Maku and Atanda (2010) investigated the factors that affect stock market performance in Nigeria. The results of the empirical investigation demonstrated that macroeconomic factors have effects on the long-term performance of the Nigerian capital market. Okpara (2010) used the Two Stage Least Squares Method to study the influence of monetary policy on the returns on the Nigerian stock market.

Asaolu and Ogunmuyiwa (2011) looked into how macroeconomic factors affected the average share price (ASP) and further explored if shifts in these factors could account for changes in stock prices in Nigeria. Using the OLS, Osisanwo and Atanda (2012) investigated the factors influencing stock market returns in Nigeria. The results showed that the primary factors of stock returns in Nigeria are interest rate, money supply, levels of prior stock returns, and exchange rate. Using the Vector Error Correction Model (VECM), Osamwonyi and Evbayiro-Osagie (2012) examined the association between macroeconomic factors and the Nigerian capital market index. Macroeconomic factors have been discovered to affect the Nigerian stock market index. Nwakoby and Alajekwu (2016) employed price-based monetary policies to look at how monetary policies affected the performance of the Nigerian stock market using three different approaches.

Using the auto-regressive distributed lag (ARDL) model, Anaele and Umeora (2019) investigated the association between monetary policy and the Nigerian capital market. Using the OLS multiple regression technique, Akanbi (2021) investigated the effect of monetary policies on the performance of the stock market in Nigeria.

The majority of the methods used in the literature would be unable to deal with data heterogeneity and model skewness and kurtosis. Thus, using the GAMLSS, this study investigates the effect of the CBN's price-based monetary policy instruments' anchor on stock market performance indicators. The GAMLSS model is a semi-parametric regression model. which can handle data heterogeneity and model skewness and kurtosis. It can also be used to reduce model overdispersion.

2 Materials and methods

2.1 Research design

The data for this study came from past records of data on the All-Share Index, money supply, interest rate, exchange rate, and inflation rate in the Nigerian Stock Market Statistical Bulletin from 2006 to 2020, a period of 15 years. The performance of the Nigerian stock market (proxy as All-share Index) was used as the dependent variable. Monetary policies functioned as explanatory variables. The money supply (MS), yearly interest rate (INT), yearly inflation rate (INF), and exchange rate (EXCH) were used as proxies for monetary policy. The GAMLSS regression model was used to establish a causal effect of independent variables on the dependent variable. The R programming language was used for all analyses.

2.2 Method of data analysis

The LM, GLM, and GAM can all be thought of as extensions of GAMLSS. GAMLSS have two key characteristics. It was predicated that the distribution might be any parametric distribution and that all of its constituent parts—not just its location—may be modeled as smooth or linear functions of the explanatory factors. As a result, the response variable's distribution's position, size, and shape are all subject to vary in response to explanatory variables (Stasinopoulo *et al.*, 2018). GAMLSS are models of the semi-parametric regression variety.

Let $y^T = (y_1, y_2, \ldots, y_n)$ be the response variable of length *n*. Let $g_k(.)$ be a known monotonic link function connecting the distribution parameters to the explanatory variables for k = 1, 2, 3, 4.

$$g_k(\theta_k) = \eta_k = X_k\beta_k + \sum_{j=1}^{J_k} Z_{jk}\gamma_{jk} \quad (1)$$
$$g_1(\mu) = \eta_1 = X_1\beta_1 + \sum_{j=1}^{J_1} Z_{j1}\gamma_{j1} \quad (2)$$
$$g_2(\sigma) = \eta_2 = X_2\beta_2 + \sum_{j=1}^{J_2} Z_{j2}\gamma_{j2} \quad (3)$$
$$g_3(\nu) = \eta_3 = X_3\beta_3 + \sum_{j=1}^{j_3} Z_{j3}\gamma_3, \quad (4)$$
$$g_4(\tau) = \eta_4 = X_4\beta_4 + \sum_{j=1}^{j_4} Z_{j4}\gamma_{j4}, \quad (5)$$

where $\mu, \sigma, \upsilon\ \tau$ and η_k are vectors of length n, $\beta_k^T = \left(\beta_{1k},\ \beta_{2k}, \ldots, \beta_{J_k' k}\right)$ is a parameter vector (Rigby and Stasinopoulos, 2005).

Each distribution parameter can be modelled as a linear function of explanatory variables and/or as a linear function of stochastic variables using the model in (1). In GAMLSS implementation in R packages, there are numerous distributions and additive terms. This study would take into account the generalized gamma, Gumbel, Weibull, and Log normal distributions.

2.3 Model selection criterion

The Akaike Information Criteria (AIC) and the Bayesian Information Criteria (BIC) criterion were used in this study to select the best model in GAMLSS. Let *k* denote the number of parameters, *n* the number of observations in the model and $\hat{L}$ the maximum value of the model's likelihood function.

$$AIC = 2k - 2ln(\hat{L}), \quad (6)$$
$$BIC = kln(n) - 2ln(\hat{L}). \quad (7)$$

The preferred model for a data, out of a set of candidate models, is the one with the lowest AIC and BIC values.

3 Results and discussion

Table 1 displays the minimum, first quartile, median, mean, third quartile, maximum, and skewness values for the ASI, MS, INF, INT and EXCH. ASI, MS, INF, and EXCH are all positively skewed, whereas INT is negatively skewed.

Table 1: Descriptive statistics of variables

	MIN	Q_1	MEDIAN	MEAN	Q_3	MAX	SKEWNESS
ASI	19851.9	25281.9	29692.5	32157.8	37150.9	65652.4	1.1831
MS	2227472.8	9802494.7	7718841.4	18622470	8081470.1	38627352.2	0.2594
INT	11.3	16.0	16.7	16.6	17.2	19.66	-1.0919
INF	5.4	8.8	11.6	11.4	13.2	17.9	0.0997
EXCH	108.3	147.7	155.3	200.0	305.2	379.5	0.7847

Figure 1 presents the correlation matrix of pairs of variables used in this study while table 2 gives the p-values of the correlation matrix. All the variables are negatively correlated All-share index and their p-values are significant.

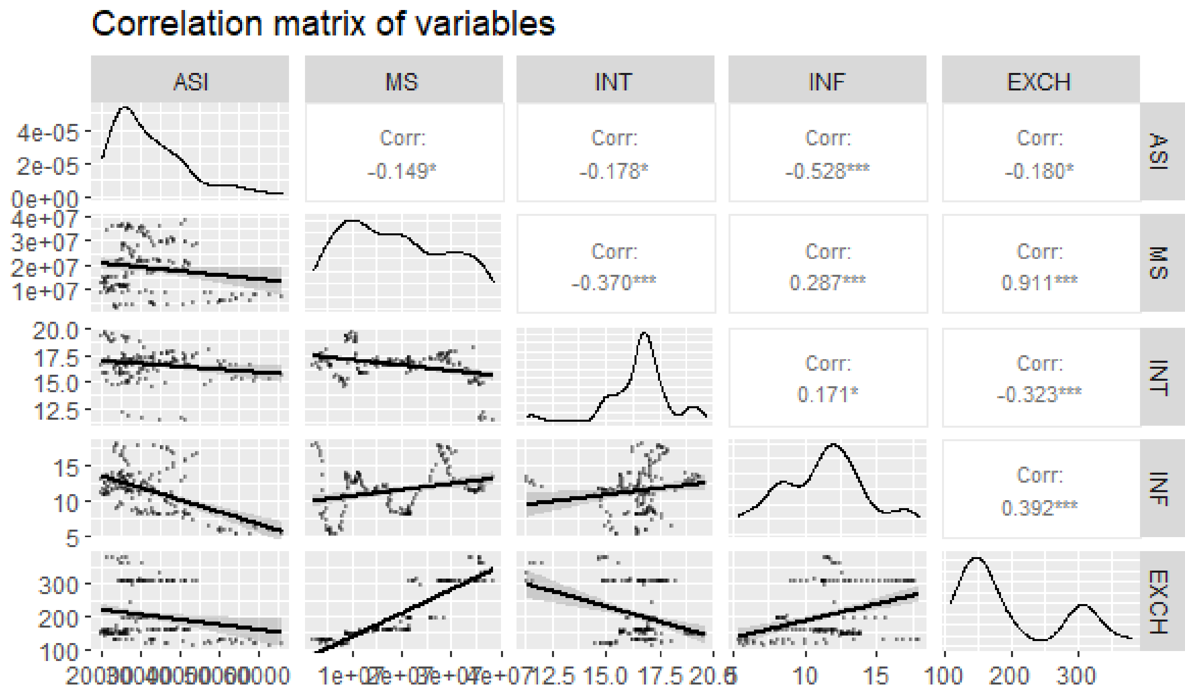

Figure 1: Correlation Matrix of pairs of variables

Table 2: P-values of correlation matrix

	ASI	MS	INT	INF	EXCH
ASI		0.0462	0.0168	0.0000	0.0154
MS	0.0462		0.0000	0.0000	0.0000
INT	0.0168	0.0000		0.0214	0.0000
INF	0.0000	0.0000	0.0214		0.0000
EXCH	0.0154	0.0000	0.0000	0.0000	

We investigate the distribution that corresponds to the response variable. Figure 2 depicts the four most common and appropriate distributions for the response variable. Generalized gamma (GG), Gumbel (GU), Log-normal (LOGNO), and Weibull (WEI) distributions are fitted to the response variable. The generalized gamma distribution has the lowest AIC and BIC and is considered the best fit to the response variable. As a result, the Generalized gamma additive model is used to simulate the impact of monetary policy on the Nigerian stock market.

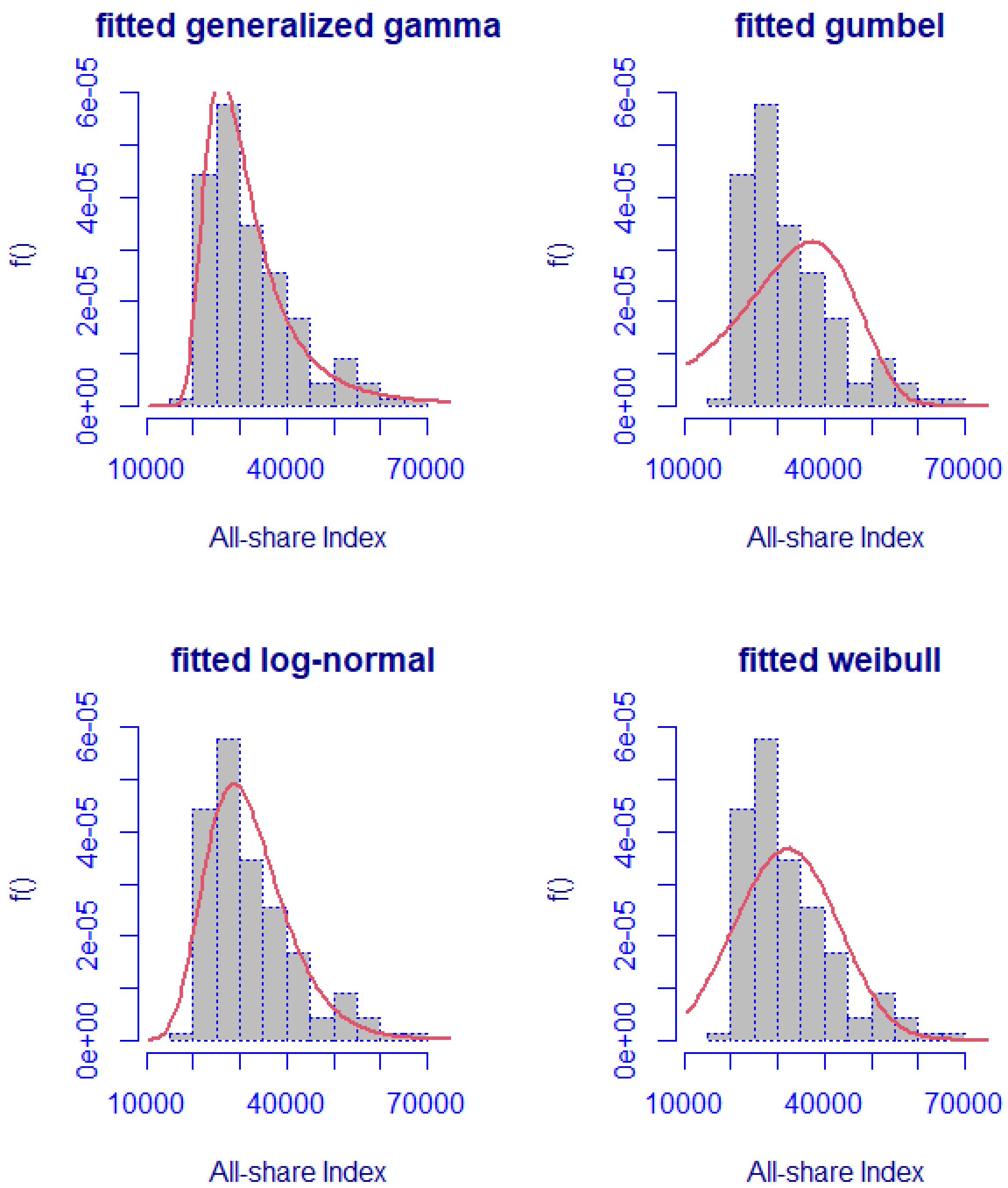

Figure 2: All-share Index and fitted Generalized gamma, Gumbel, Log-normal and Weibull distributions

Table 3: AIC and BIC of some selected distributions

DISTRIBUTION	GG	GU	LOGNO	WEI
AIC	3753.501	3897.999	3768.916	3820.882
BIC	3763.079	3904.385	3775.302	3827.268

We must keep in mind that GG has three distribution parameters. In GAMLSS, model that comprises the GG distribution, smoothing ps() with df = 3 was fitted, scale model modeled MS and shape (υ) model modeled constant (Table 4). MS has a positive impact on the ASI, whereas INT, INF, and EXCH have a negative impact. All of these variables have significant effects. The model's R^2 is 0.6808, indicating that the explanatory variables could only explain approximately 68 percent of the variation in the response variable.

Table 4: Estimate and p-value of generalized gamma additive model for linear scale and shape (RS method)

μ LINK FUNCTION: LOG			
	Estimate	P-value	Status
INTERCEPT	11.57	2×10^{-16}	Significant
PS(MS, DF = 3)	8.626×10^{-9}	1.08×10^{-6}	Significant
INT	-3.598×10^{-2}	5.22×10^{-7}	Significant
INF	-5.261×10^{-2}	2×10^{-16}	Significant
EXCH	-1.373×10^{-3}	1.74×10^{-7}	Significant
σ LINK FUNCTION: LOG			
	Estimate	P-value	Status
INTERCEPT	-2.211	2×10^{-16}	Significant
PB(MS)	1.426$\times 10^{-8}$	0.00508	Significant
ν LINK FUNCTION: IDENTITY			
	Estimate	P-value	Status
INTERCEPT	-2.0175	0.000543	Significant

Thus, the best fitted model can be written in the form:
log (μ) = 11.57+(8.626×10^{-9})ps(MS, df = 3) +(-3.598×10^{-2}) INT +(-5.261×10^{-2}) INF + (-1.373×10^{-3})EXCH
log (σ) = -2.211 + (1.426$\times 10^{-8}$) pb(MS)
$\nu = -2.0175$

4 Conclusion

GAMLSS was used in this study to investigate the effect of monetary policies on stock market activity in Nigeria. AIC and BIC were used to select the model that best fit the response variable from Generalized Gamma, Gumbel, Weibull, and Log-normal. The best model was determined to be Generalized Gamma with the lowest AIC and BIC. As a result, the data was modeled using a generalized gamma additive model. MS, INT, INF, and EXCH could only explain 68 percent of the variation in Nigeria stock exchange market performance, according to the findings. A rise in the MS and a fall in the INT, INF, and EXCH would improve the performance of the Nigerian stock exchange. As a result, monetary policies have a substantial influence on the performance of the Nigerian stock market. In order to keep the Nigerian stock market appealing to investors, the monetary authorities should implement favorable monetary policies.

References

[1] Akanbi, A. (2021). Effect of monetary policy on stock market performance in Nigeria. Journal of Global Economics and Business, 2(5):101-115.

[2] Anaele, S.C. and Umeora, C. E. (2019). Monetary policy and the performance of the Nigerian Capital Market. International Journal of Research in Engineering Science and Management, 2(7):59-72.

[3] Asaolu, T.O. and Ogunmakinwa, M.S. (2011). An econometric analysis of the impact of macroeconomic variables on stock market movement in Nigeria. Asian Journal of Business Management, 3(1):72 – 78.

[4] Laeven, L. (2014). Development of local capital markets: Rationale and challenges. IMF Working Paper: WP/14/234.

[5] Maku, O. E. and Atanda, A. A. (2010). Determinants of stock market performance in Nigeria: Long run analysis. Journal of Management and Organizational Behaviour, 1(3):1-16.

[6] Mishkin, F S. (2007). The Economics of money, banking and financial institutions. (7th ed.). New York: Pearson Publishers.

[7] Nwakoby, C. and Alajekwu, U.B. (2016). Effect of monetary policy on Nigerian stock market performance. International Journal of Scientific Research and Management, 4(9):4530-4442.

[8] Okpara, G. C. (2010). Monetary policy and stock market returns: evidence from Nigeria. Journal of Innovations, 3(4):54-98.

[9] Osamwonyi, I.O. and Evbayiro-Osagie, E.I. (2012). The relationship between macroeconomic variables and stock market index in Nigeria. Journal of Economics, 3(1):55-63.

[10] Osisanwo, B. G. and Atanda, A. A. (2012). Determinants of stock market returns in Nigeria: a time series analysis. African Journal of Scientific Research, 9(1):478 – 496.

[11] Rigby, R.A. and Stasinopoulos, D.M. (2005). Generalized additive models for location, scale and shape (GAMLSS). Appl Statist, 54:507-554.

[12] Stasinopoulos, M.D., Rigby, R.A., and Bastiani, F.D. (2018). GAMLSS: A distributional regression approach. Statistical Modelling, 18(3–4): 1–26.

[13] Turner, P. (2002). Bond markets in emerging economies: An overview of policy issues. BIS Paper, 11:1-12,

International Journal of Mathematical Analysis and Modelling
Volume 5, Issue 4, November 2022, Pages 58 – 71

Tracking oscillating edge-flames: a mathematical approach

R.O. Olayiwola*†, I.B.S. Mohammed‡, J.P. Oyubu*, U. A. Abdullahi*, E. O. Anyanwu§, A. D. Abubakar, and E.M. Yisa††**

Abstract

Accurate simulation of oscillating edge flames is computationally very challenging because of the difficult calculations involved to incorporate most of the physics that is believed to be central to the phenomenon. This paper presents the design of a new simulation tool that can handle among other things the concept of flame speed. The conditions for the existence of unique solutions of energy and species equations are established by the actual solution method and the Lipschitz continuity approach. The analytical solution is obtained via Olayiwola's generalized polynomial approximation method (OGPAM), which shows the influence of the parameters involved on the system. Both the effects of an on-edge and off-edge convective flow, and the effects of a heat sink were examined. The effect of changes in values of parameters such as the Damkohler number and speed with which the flame advances are presented graphically and discussed.

Keywords: convective flow; edge-flame; flames; flame-speed; OGPAM; oscillating edge-flames

1 Introduction

The theory of oscillating edge flames has been investigated in numerous works (see [3], [4[, [5], [6], [18]). An edge flame is a two-dimensional structure in the neighborhood of the edge of a flame sheet (nominally one-dimensional) with an edge [4].

Flames with edges occur in many forms. They are: (i) Flame spreading over a fuel-bed, solid or liquid. (ii) A candle flame burning under microgravity conditions. (iii) A diffusion flame with edge-supported fluxes from a heterogeneous propellant. (iv) A wrinkled torn flame in a turbulent flow. (v) An axisymmetric diffusion flame supported on a tube burner, burning under microgravity conditions. (vi) A diffusion flame sitting on a plate through which fuel is injected. For the configuration of these flames with edges see [3].

* Department of Mathematics, Federal University of Technology, Minna, Nigeria
† Corresponding Author. E-mail: olayiwola.rasaq@futminna.edu.ng
‡ Department of Mathematics, Federal Polytechnic, Bida, Nigeria.
§ Department of Mathematics and Statistics, Federal University, Wukari, Nigeria.
** Department of Mathematics, Federal University, Gashua, Nigeria.
†† Department of Mathematics and Statistics, Niger State Polytechnic, Zungeru, Nigeria.

Oscillating edge flames in which the edge advances and retreats have long been observed in many experimental configurations. For example, when a flame spreads over a liquid fuel bed, Figure 1,

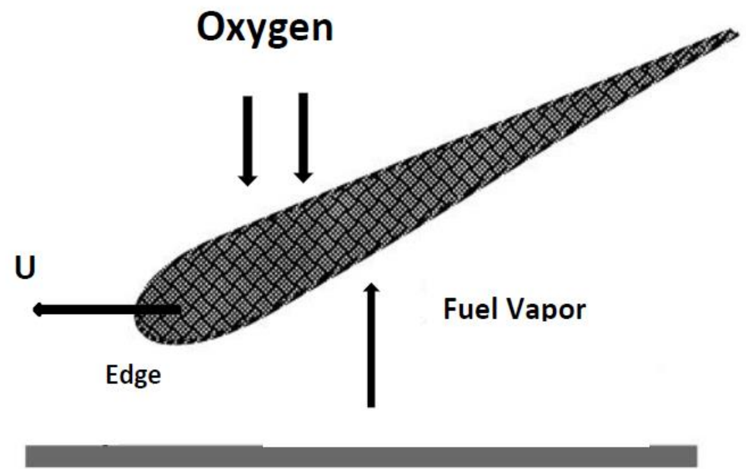

Figure 1: Flame spreading over a liquid pool of fuel

the speed U with which the flame advances is usually a constant, U_0 say. But there are circumstances that U fluctuate with time, viz.
$U = U_0 + U'(t)$
where U' is periodic [15].

In the context of flame spread over liquids, this phenomenon has been captured in numerical simulations, and various explanations have been proposed. One links the oscillations to a gas-phase eddy [10]; the other to Marangoni instabilities [8]. Oscillation instabilities were first predicted for one-dimensional deflagrations by Sivashinsky [16], for large Lewis numbers. Kirkby and Schmitz [11] examined one-dimensional diffusion flames in a theoretical study, and predict oscillating instabilities at near–extinction (blow-off) conditions. These occur only if the Lewis numbers are large, or if there are substantial volumetric heat losses. Joulin and Clavin [9] subsequently showed that volumetric heat losses exacerbate the instability, reducing the Lewis numbers for which they are achieved, and Margolis [12] and Buckmaster [7] showed that conductive heat losses to a burner have a similar effect. Buckmaster *et al.* ([5], [6]) proposed the simple hypothesis, that the edge oscillations are nothing more than a two-dimensional manifestation of the well-known one-dimensional instabilities described earlier. They examined a simple model which incorporates what we believe is the minimum necessary physics, and oscillations are predicted. In another development, Buckmaster *et al.* [4] added new physical ingredients to the model, to test the hypothesis further. They introduced $U\frac{\partial}{\partial x}$, an on-edge convective term and a "cold rectangle", a rectangle of interior mesh points at which the temperature is set equal to the boundary value T_0. They examined both the effects of an on-edge and off-edge convective flow, and the effect of a heat sink, and solutions are found using the method of lines.

This motivates the present analysis where we study oscillating edge flames with a view to providing analytical solutions capable of describing the influence of flame speed on the temperature field.

2 Model formulation

The model configuration consists of an oxygen-supply boundary at $y=-\frac{L}{2}$, $-\infty < x < \infty$, and a fuel-supply boundary at $y=\frac{L}{2}$, $0 < x < \infty$. The remainder of the upper wall ($y=\frac{L}{2}$, $-\infty < x < 0$) supplies neither oxygen nor fuel. The formulation of our model is guided by the following assumptions:

Initially (i.e., at a time $t=0$), the medium is not clean (i.e., the domain is not fuel, oxygen, and temperature free). Let the initial medium temperature, fuel, and oxygen concentrations depend on space variables.

No convection in the $y-$direction.
How the reactants are supplied at the boundaries is of no great consequence, so we impose Dirichlet data at the lower boundary and Neumann data at the upper boundary.
Based on the above description and assumptions, the combustion field within the walls is governed by the two-dimensional equations:

$$\rho\left(\frac{\partial}{\partial t}+U\frac{\partial}{\partial x}\right)\left(X,Y,c_pT\right)=\left(\frac{\partial^2}{\partial x^2}+\frac{\partial^2}{\partial y^2}\right)\left(\rho D_X X,\rho D_X X,kT\right)+\left(-\alpha_X,-\alpha_Y,Q\right)BXYe^{-\frac{E}{RT}} \quad (1)$$

with the initial and boundary conditions:

$$\left.\begin{array}{l} X(x,y,0)=\alpha_X(x+y),\ X\left(-\frac{L}{2},y,t\right)=X_0,\ X\left(x,-\frac{L}{2},t\right)=X_0,\ \left.\frac{\partial X}{\partial x}\right|_{x=\frac{L}{2}}=0,\ \left.\frac{\partial X}{\partial y}\right|_{y=\frac{L}{2}}=0 \\ Y(x,y,0)=\alpha_Y(x+y),\ Y\left(-\frac{L}{2},y,t\right)=0,\ Y\left(x,-\frac{L}{2},t\right)=0,\ \left.\frac{\partial Y}{\partial x}\right|_{x=\frac{L}{2}}=0,\ \left.\frac{\partial Y}{\partial y}\right|_{y=\frac{L}{2}}=0 \\ T(x,y,0)=T_0(\in(x+y)+1),\ T\left(-\frac{L}{2},y,t\right)=T_0,\ T\left(x,-\frac{L}{2},t\right)=T_0,\ \left.\frac{\partial T}{\partial x}\right|_{x=\frac{L}{2}}=0,\ \left.\frac{\partial T}{\partial y}\right|_{y=\frac{L}{2}}=0 \end{array}\right\}, \quad (2)$$

where $U\frac{\partial}{\partial x}$ is an on-edge convective term and U is the speed of an applied convective flow in the x- direction, E is the activation energy, X is the mass fraction of oxidizer, Y is the mass fraction of fuel, T is temperature, x- coordinate parallel to edge-flame travel, y- coordinate perpendicular to edge-flame travel, T_0 is the initial temperature of the medium, X_0 is the initial mass fraction of oxidizer, Y_0 is the initial mass fraction of fuel.

3 Method of solution

3.1 Dimension analysis

Dimensionless variables are been introduced as:

$$\left.\begin{array}{l} x' = \dfrac{x}{L}, \quad y' = \dfrac{y}{L}, \quad t' = \dfrac{kt}{\rho c_p L^2}, \quad U' = \dfrac{\rho c_p LU}{k}, \quad v' = \dfrac{\rho c_p Lv}{k}, \\ \quad \phi = \dfrac{X}{\alpha_X}, \quad \psi = \dfrac{Y}{\alpha_Y}, \quad \theta = \dfrac{E(T - T_0)}{RT_0^2}, \quad \in = \dfrac{RT_0}{E}, \end{array}\right\} \tag{3}$$

Using (3), and after dropping the prime, equations (1) and (2) become

$$\left(\frac{\partial}{\partial t} + U\frac{\partial}{\partial x}\right)(\phi, \psi, \theta) = \left(\frac{\partial^2}{\partial x^2} + \frac{\partial^2}{\partial y^2}\right)\left(\frac{1}{Le_X}\phi, \frac{1}{Le_Y}\psi, \theta\right) + (-\alpha, -\alpha, \sigma)D_a\phi\psi e^{\frac{\theta}{1+\in\theta}} \tag{4}$$

$$\left.\begin{array}{lllll} \phi(x,y,0) = (x+y), & \phi\left(-\dfrac{1}{2}, y, t\right) = \beta, & \phi\left(x, -\dfrac{1}{2}, t\right) = \beta, & \left.\dfrac{\partial \phi}{\partial x}\right|_{x=\frac{1}{2}} = 0, & \left.\dfrac{\partial \phi}{\partial y}\right|_{y=\frac{1}{2}} = 0 \\ \psi(x,y,0) = (x+y), & \psi\left(-\dfrac{1}{2}, y, t\right) = 0, & \psi\left(x, -\dfrac{1}{2}, t\right) = 0, & \left.\dfrac{\partial \psi}{\partial x}\right|_{x=\frac{1}{2}} = 0, & \left.\dfrac{\partial \psi}{\partial y}\right|_{y=\frac{1}{2}} = 0 \\ \theta(x,y,0) = (x+y), & \theta\left(-\dfrac{1}{2}, y, t\right) = 0, & \theta\left(x, -\dfrac{1}{2}, t\right) = 0, & \left.\dfrac{\partial \theta}{\partial x}\right|_{x=\frac{1}{2}} = 0, & \left.\dfrac{\partial \theta}{\partial y}\right|_{y=\frac{1}{2}} = 0 \end{array}\right\}, \tag{5}$$

where

$Le_X = \dfrac{k}{\rho c_p D_X}$ stands for the Lewis number for oxidizer, $Le_Y = \dfrac{k}{\rho c_p D_Y}$ stands for the Lewis number for fuel, $D_a = \dfrac{\alpha_X \alpha_Y BL}{\rho U}$ is the Damkohler number, $\alpha = \dfrac{\rho c_p LU}{k} e^{-\frac{E}{RT_0}}$, $\sigma = \dfrac{\rho LUQ}{k \in T_0} e^{-\frac{E}{RT_0}}$, $\beta = \dfrac{X_0}{\alpha_X}$.

Introducing the following new space variable (Olayiwola [14]):

$$\eta = x + y. \tag{6}$$

Then, equations (4) and (5) can be expressed as

$$\left.\begin{aligned}&\frac{\partial\phi}{\partial t}+U\frac{\partial\phi}{\partial\eta}=\frac{2}{Le_X}\frac{\partial^2\phi}{\partial\eta^2}-\alpha D_a\phi\psi e^{\frac{\theta}{1+\in\theta}}\\&\phi(\eta,0)=\eta,\quad\phi(-1,t)=\beta,\quad\left.\frac{\partial\phi}{\partial\eta}\right|_{\eta=1}=0\end{aligned}\right\}\tag{7}$$

$$\left.\begin{aligned}&\frac{\partial\psi}{\partial t}+U\frac{\partial\psi}{\partial\eta}=\frac{2}{Le_Y}\frac{\partial^2\psi}{\partial\eta^2}-\alpha D_a\phi\psi e^{\frac{\theta}{1+\in\theta}}\\&\psi(\eta,0)=\eta,\quad\psi(-1,t)=0,\quad\left.\frac{\partial\psi}{\partial\eta}\right|_{\eta=1}=0\end{aligned}\right\}\tag{8}$$

$$\left.\begin{aligned}&\frac{\partial\theta}{\partial t}+U\frac{\partial\theta}{\partial\eta}=2\frac{\partial^2\theta}{\partial\eta^2}+\sigma D_a\phi\psi e^{\frac{\theta}{1+\in\theta}}\\&\theta(\eta,0)=\eta,\quad\theta(-1,t)=0,\quad\left.\frac{\partial\theta}{\partial\eta}\right|_{\eta=1}=0\end{aligned}\right\}\tag{9}$$

3.2 Properties of solution

Theorem 1: Let $Le_X = Le_Y = 1$. Then there exists at most one bounded solution of equations (7) – (9).

Proof: Multiply (7) and (8) by σ, (9) by 2α and adding the resulting equations, we obtain

$$\frac{\partial\varphi}{\partial t}+U\frac{\partial\varphi}{\partial\eta}=2\frac{\partial^2\varphi}{\partial\eta^2}\tag{10}$$

$$\varphi(\eta,0)=2(\sigma+\alpha)\eta,\quad\varphi(-1,t)=\sigma\beta,\quad\left.\frac{\partial\varphi}{\partial\eta}\right|_{\eta=1}=0,\tag{11}$$

where

$$\varphi(\eta,t)=\sigma(\psi(\eta,t)+\phi(\eta,t))+2\alpha\theta(\eta,t)$$

Using Olayiwola's generalized polynomial approximation method (OGPAM) (see, [13]), we obtain the solution to the problem (10) and (11) as:

$$\varphi(\eta,t)=\begin{pmatrix}\frac{1}{4}\left(3\left(\frac{\sigma\beta(1+U)}{(2+U)}\left(1-e^{-\frac{3}{2}\left(1+\frac{U}{2}\right)t}\right)+2(\sigma+\alpha)\eta e^{-\frac{3}{2}\left(1+\frac{U}{2}\right)t}\right)+\sigma\beta\right)+\\\frac{1}{2}\left(\left(\frac{\sigma\beta(1+U)}{(2+U)}\left(1-e^{-\frac{3}{2}\left(1+\frac{U}{2}\right)t}\right)+2(\sigma+\alpha)\eta e^{-\frac{3}{2}\left(1+\frac{U}{2}\right)t}\right)-\sigma\beta\right)\eta+\\\frac{1}{4}\left(\sigma\beta-\left(\frac{\sigma\beta(1+U)}{(2+U)}\left(1-e^{-\frac{3}{2}\left(1+\frac{U}{2}\right)t}\right)+2(\sigma+\alpha)\eta e^{-\frac{3}{2}\left(1+\frac{U}{2}\right)t}\right)\right)\eta^2\end{pmatrix}\tag{12}$$

Then, we obtain

$$\phi(\eta,t)=\frac{1}{\sigma}\left(\begin{array}{l}\left(\begin{array}{l}\frac{1}{4}\left(3\left(\frac{\sigma\beta(1+U)}{(2+U)}\left(1-e^{-\frac{3}{2}\left(1+\frac{U}{2}\right)t}\right)+2(\sigma+\alpha)\eta e^{-\frac{3}{2}\left(1+\frac{U}{2}\right)t}\right)+\sigma\beta\right)+\\ \frac{1}{2}\left(\left(\frac{\sigma\beta(1+U)}{(2+U)}\left(1-e^{-\frac{3}{2}\left(1+\frac{U}{2}\right)t}\right)+2(\sigma+\alpha)\eta e^{-\frac{3}{2}\left(1+\frac{U}{2}\right)t}\right)-\sigma\beta\right)\eta+\\ \frac{1}{4}\left(\sigma\beta-\left(\frac{\sigma\beta(1+U)}{(2+U)}\left(1-e^{-\frac{3}{2}\left(1+\frac{U}{2}\right)t}\right)+2(\sigma+\alpha)\eta e^{-\frac{3}{2}\left(1+\frac{U}{2}\right)t}\right)\right)\eta^2\end{array}\right)-\\ (2\alpha\theta(\eta,t)+\sigma\psi(\eta,t))\end{array}\right) \quad (13)$$

$$\psi(\eta,t)=\frac{1}{\sigma}\left(\begin{array}{l}\left(\begin{array}{l}\frac{1}{4}\left(3\left(\frac{\sigma\beta(1+U)}{(2+U)}\left(1-e^{-\frac{3}{2}\left(1+\frac{U}{2}\right)t}\right)+2(\sigma+\alpha)\eta e^{-\frac{3}{2}\left(1+\frac{U}{2}\right)t}\right)+\sigma\beta\right)+\\ \frac{1}{2}\left(\left(\frac{\sigma\beta(1+U)}{(2+U)}\left(1-e^{-\frac{3}{2}\left(1+\frac{U}{2}\right)t}\right)+2(\sigma+\alpha)\eta e^{-\frac{3}{2}\left(1+\frac{U}{2}\right)t}\right)-\sigma\beta\right)\eta+\\ \frac{1}{4}\left(\sigma\beta-\left(\frac{\sigma\beta(1+U)}{(2+U)}\left(1-e^{-\frac{3}{2}\left(1+\frac{U}{2}\right)t}\right)+2(\sigma+\alpha)\eta e^{-\frac{3}{2}\left(1+\frac{U}{2}\right)t}\right)\right)\eta^2\end{array}\right)-\\ (2\alpha\theta(\eta,t)+\sigma\phi(\eta,t))\end{array}\right) \quad (14)$$

$$\theta(\eta,t)=\frac{1}{2\alpha}\left(\begin{array}{l}\left(\begin{array}{l}\frac{1}{4}\left(3\left(\frac{\sigma\beta(1+U)}{(2+U)}\left(1-e^{-\frac{3}{2}\left(1+\frac{U}{2}\right)t}\right)+2(\sigma+\alpha)\eta e^{-\frac{3}{2}\left(1+\frac{U}{2}\right)t}\right)+\sigma\beta\right)+\\ \frac{1}{2}\left(\left(\frac{\sigma\beta(1+U)}{(2+U)}\left(1-e^{-\frac{3}{2}\left(1+\frac{U}{2}\right)t}\right)+2(\sigma+\alpha)\eta e^{-\frac{3}{2}\left(1+\frac{U}{2}\right)t}\right)-\sigma\beta\right)\eta+\\ \frac{1}{4}\left(\sigma\beta-\left(\frac{\sigma\beta(1+U)}{(2+U)}\left(1-e^{-\frac{3}{2}\left(1+\frac{U}{2}\right)t}\right)+2(\sigma+\alpha)\eta e^{-\frac{3}{2}\left(1+\frac{U}{2}\right)t}\right)\right)\eta^2\end{array}\right)-\\ \sigma(\psi(\eta,t)+\phi(\eta,t))\end{array}\right) \quad (15)$$

Hence, there exists a unique solution to the problem (7) – (9). This completes the proof.

Theorem 2: Suppose $f_0(\eta)$, $g_0(\eta)$, and $h_0(\eta)$ are bound for $\eta\in R^n$ and $f(\eta,t,\phi,\psi,\theta)$, $g(\eta,t,\phi,\psi,\theta)$, $h(\eta,t,\phi,\psi,\theta)$ satisfies the uniform Lipschitz condition. Then, there exists a unique solution $\phi(\eta,t)$, $\psi(\eta,t)$, $\theta(\eta,t)$ of equations (7) – (9).

Proof: Let proof as in [2]. We rewrite equations (7) – (9) in the form:

$$\frac{\partial \phi}{\partial t}+U\frac{\partial \phi}{\partial \eta}=\frac{2}{Le_X}\frac{\partial^2 \phi}{\partial \eta^2}+f(\eta,t,\phi,\psi,\theta) \tag{17}$$

$$\frac{\partial \psi}{\partial t}+U\frac{\partial \psi}{\partial \eta}=\frac{2}{Le_Y}\frac{\partial^2 \psi}{\partial \eta^2}+g(\eta,t,\phi,\psi,\theta) \tag{18}$$

$$\frac{\partial \theta}{\partial t}+U\frac{\partial \theta}{\partial \eta}=2\frac{\partial^2 \theta}{\partial \eta^2}+h(\eta,t,\phi,\psi,\theta) \tag{19}$$

$$\phi(\eta,0)=f_0(\eta),\quad \psi(\eta,0)=g_0(\eta),\quad \theta(\eta,0)=h_0(\eta),\quad \eta=(\eta_1,\eta_2,...\eta_n), \tag{20}$$

where

$$f(\eta,t,\phi,\psi,\theta)=-\alpha D_a\phi\psi e^{\frac{\theta}{1+\epsilon\theta}},\ g(\eta,t,\phi,\psi,\theta)=-\alpha D_a\phi\psi e^{\frac{\theta}{1+\epsilon\theta}},\ h(\eta,t,\phi,\psi,\theta)=\sigma D_a\phi\psi e^{\frac{\theta}{1+\epsilon\theta}}.$$

Ignoring the second term at the right-hand side, the fundamental solution of (17) – (19) are (see [17]):

$$F(\eta,t)=\frac{\eta}{2\sqrt{\frac{2\pi}{Le_X}}t^{\frac{3}{2}}}\exp\left(\frac{U}{2\left(\frac{2}{Le_X}\right)}\eta-\frac{U^2}{4\left(\frac{2}{Le_X}\right)}t-\frac{\eta}{4\left(\frac{2}{Le_X}\right)t}\right)$$

$$G(\eta,t)=\frac{\eta}{2\sqrt{\frac{2\pi}{Le_Y}}t^{\frac{3}{2}}}\exp\left(\frac{U}{2\left(\frac{2}{Le_Y}\right)}\eta-\frac{U^2}{4\left(\frac{2}{Le_Y}\right)}t-\frac{\eta}{4\left(\frac{2}{Le_Y}\right)t}\right)$$

$$H(\eta,t)=\frac{\eta}{2\sqrt{2\pi}t^{\frac{3}{2}}}\exp\left(\frac{U}{4}\eta-\frac{U^2}{8}t-\frac{\eta}{8t}\right).$$

Next, it suffices to show that the Lipschitz condition is satisfied. That is if we can show that:

$$|f(\eta,t,\phi_1,\psi_1,\theta_1)-f(\eta,t,\phi_2,\psi_2,\theta_2)|\le k_1(|\phi_1-\phi_2|+|\psi_1-\psi_2|+|\theta_1-\theta_2|) \tag{21}$$

$$|g(\eta,t,\phi_1,\psi_1,\theta_1)-g(\eta,t,\phi_2,\psi_2,\theta_2)|\le k_2(|\phi_1-\phi_2|+|\psi_1-\psi_2|+|\theta_1-\theta_2|) \tag{22}$$

$$|h(\eta,t,\phi_1,\psi_1,\theta_1)-h(\eta,t,\phi_2,\psi_2,\theta_2)|\le k_3(|\phi_1-\phi_2|+|\psi_1-\psi_2|+|\theta_1-\theta_2|) \tag{23}$$

where

$$k_1=\max\left\{\frac{\partial f}{\partial \phi},\frac{\partial f}{\partial \psi},\frac{\partial f}{\partial \theta}\right\},\quad k_2=\max\left\{\frac{\partial g}{\partial \phi},\frac{\partial g}{\partial \psi},\frac{\partial g}{\partial \theta}\right\},\quad k_3=\max\left\{\frac{\partial h}{\partial \phi},\frac{\partial h}{\partial \psi},\frac{\partial h}{\partial \theta}\right\}.$$

Since $\alpha,\ \sigma,\ Da,\ \epsilon>0$, $0\le\phi,\psi\le 1$ and $1\le e^{\frac{\theta}{1+\epsilon\theta}}\le e^{\frac{1}{\epsilon}}\quad\forall\quad 0\le\theta<\infty$.

Hence,

$$k_1=\max\left\{\frac{\partial f}{\partial \phi},\frac{\partial f}{\partial \psi},\frac{\partial f}{\partial \theta}\right\}=0,\ k_2=\max\left\{\frac{\partial g}{\partial \phi},\frac{\partial g}{\partial \psi},\frac{\partial g}{\partial \theta}\right\}=0,\ k_3=\max\left\{\frac{\partial h}{\partial \phi},\frac{\partial h}{\partial \psi},\frac{\partial h}{\partial \theta}\right\}=\sigma Dae^{\frac{1}{\epsilon}}$$

Clearly, $f(\eta,t,\phi,\psi,\theta)$, $g(\eta,t,\phi,\psi,\theta)$, $h(\eta,t,\phi,\psi,\theta)$ are Lipschitz continuous. Hence, the result follows. This completes the proof.

3.3 Analytical solution via Olayiwola's generalized polynomial approximation method

In the limit $\in\to 0$, equations (7) – (9) can be solved analytically using Olayiwola's generalized polynomial approximation method (OGPAM) [13]. Follow the idea in [1], that:

$$\exp(\theta)\approx 1+(e-2)\theta+\theta^2 \tag{24}$$

and let $0<\alpha<<1$, $\sigma=a\alpha$ such that

$$\left.\begin{aligned}\phi(\eta,t)&=\phi_0(\eta,t)+\alpha\phi_1(\eta,t)+\ldots\\ \psi(\eta,t)&=\psi_0(\eta,t)+\alpha\psi_1(\eta,t)+\ldots\\ \theta(\eta,t)&=\theta_0(\eta,t)+\alpha\theta_1(\eta,t)+\ldots\end{aligned}\right\} \tag{25}$$

and using OGPAM in [13], we obtain the solutions to (7) - (9) as:

$$\begin{aligned}\phi(\eta,t)=&\left(\frac{1}{4}\left(3\phi_0|_{\eta=1}+\beta\right)+\frac{1}{2}\left(\phi_0|_{\eta=1}-\beta\right)\eta+\frac{1}{4}\left(\beta-\phi_0|_{\eta=1}\right)\eta^2\right)+\\ &\alpha\left(\frac{3}{4}\phi_1|_{\eta=1}+\frac{1}{2}\phi_1|_{\eta=1}\eta-\frac{1}{4}\phi_1|_{\eta=1}\eta^2\right)\end{aligned} \tag{26}$$

$$\psi(\eta,t)=\left(\frac{3}{4}\psi_0|_{\eta=1}+\frac{1}{2}\psi_0|_{\eta=1}\eta-\frac{1}{4}\psi_0|_{\eta=1}\eta^2\right)+\alpha\left(\frac{3}{4}\psi_1|_{\eta=1}+\frac{1}{2}\psi_1|_{\eta=1}\eta-\frac{1}{4}\psi_1|_{\eta=1}\eta^2\right) \tag{27}$$

$$\theta(\eta,t)=\left(\frac{3}{4}\theta_0|_{\eta=1}+\frac{1}{2}\theta_0|_{\eta=1}\eta-\frac{1}{4}\theta_0|_{\eta=1}\eta^2\right)+\alpha\left(\frac{3}{4}\theta_1|_{\eta=1}+\frac{1}{2}\theta_1|_{\eta=1}\eta-\frac{1}{4}\theta_1|_{\eta=1}\eta^2\right), \tag{28}$$

where

$$\phi_0|_{\eta=1}=m_1+(\eta-m_1)e^{-m_0t},\qquad \psi_0|_{\eta=1}=\eta e^{-m_2t},\qquad \theta_0|_{\eta=1}=\eta e^{-m_3t},$$

$$\phi_1|_{\eta=1}=-\frac{3}{2}\left(\begin{aligned}&\frac{m_4}{m_0-m_2}\eta\left(e^{-m_2t}-e^{-m_0t}\right)-\frac{m_5}{m_2}\eta(\eta-m_1)\left(e^{-(m_0+m_2)t}-e^{-m_0t}\right)+\\ &\frac{m_6}{m_0-m_2-m_3}\eta^2\left(e^{-(m_2+m_3)t}-e^{-m_0t}\right)-\frac{m_7}{m_2+2m_3}\eta^2(\eta-m_1)\left(e^{-(m_0+m_2+2m_3)t}-e^{-m_0t}\right)+\\ &\frac{m_8}{m_0-m_2-2m_3}\eta^3\left(e^{-(m_2+2m_3)t}-e^{-m_0t}\right)-\frac{m_9}{m_2+2m_3}\eta^3(\eta-m_1)\left(e^{-(m_0+m_2+2m_3)t}-e^{-m_0t}\right)\end{aligned}\right),$$

$$\psi_1|_{\eta=1}=-\frac{3}{2}\left(\begin{aligned}&m_4\eta te^{-m_2t}-\frac{m_5}{m_0}\eta(\eta-m_1)\left(e^{-(m_0+m_2)t}-e^{-m_2t}\right)-\frac{m_6}{m_3}\eta^2\left(e^{-(m_2+m_3)t}-e^{-m_2t}\right)-\\ &\frac{m_7}{m_0+m_3}\eta^2(\eta-m_1)\left(e^{-(m_0+m_2+m_3)t}-e^{-m_2t}\right)-\frac{m_8}{2m_3}\eta^3\left(e^{-(m_2+2m_3)t}-e^{-m_2t}\right)-\\ &\frac{m_9}{m_0+2m_3}\eta^3(\eta-m_1)\left(e^{-(m_0+m_2+2m_3)t}-e^{-m_2t}\right)\end{aligned}\right),$$

$$\theta_1\big|_{\eta=1} = \frac{3}{2}a\left(\begin{array}{l} \dfrac{m_4}{m_3-m_2}\eta\left(e^{-m_2 t}-e^{-m_3 t}\right)+\dfrac{m_5}{m_3-m_0-m_2}\eta(\eta-m_1)\left(e^{-(m_0+m_2)t}-e^{-m_3 t}\right)- \\ \dfrac{m_6}{m_2}\eta^2\left(e^{-(m_2+m_3)t}-e^{-m_3 t}\right)-\dfrac{m_7}{m_0+m_2}\eta^2(\eta-m_1)\left(e^{-(m_0+m_2+m_3)t}-e^{-m_3 t}\right)- \\ \dfrac{m_8}{m_2+m_3}\eta^3\left(e^{-(m_2+2m_3)t}-e^{-m_3 t}\right)-\dfrac{m_9}{m_0+m_2+m_3}\eta^3(\eta-m_1)\left(e^{-(m_0+m_2+2m_3)t}-e^{-m_3 t}\right) \end{array}\right),$$

$$m_0 = \frac{3}{2}\left(\frac{2+Le_X U}{2Le_X}\right), \quad m_1 = \beta\left(\frac{1+Le_X U}{2+Le_X U}\right), \quad m_2 = \frac{3}{2}\left(\frac{2+Le_Y U}{2Le_Y}\right), \quad m_3 = \frac{3}{2}\left(\frac{2+U}{2}\right),$$
$$m_4 = \frac{32D_a}{240}(4m_1+\beta), \quad m_5 = \frac{128D_a}{240}, \quad m_6 = \frac{D_a(e-2)}{6720}(2823m_1+512\beta),$$
$$m_7 = \frac{2823D_a(e-2)}{6720}, \quad m_8 = \frac{D_a}{15886080}(22192444m_1+5870600\beta), \quad m_9 = \frac{22192444D_a}{15886080},$$

The computation was done on equations (26) – (28) using the computer symbolic algebraic package MAPLE 2021 version.

4 Results and discussion

The simulation was carried out to show the impact of the model parameters by employing Olayiwola's Generalized Polynomial Approximation Method (OGPAM) on the equations (7) – (9). We are concerned with the nature of the solutions obtained for different values of U and D_a. The computation of equations (26) - (28) was done using the MAPLE 2021 version.

Figure 2 shows the temperature history at $x = 0.75,\ y = 0.08$ for $Le_X = 1.0,\ Le_Y = 1.8,\ U = 0,\ D_a = 12,\ 18,$ and 24. After the first oscillation, the graph displays a rapid transition to a steady solution.

Figure 3 displays the temperature topography for $Le_X = 1.0,\ Le_Y = 1.8,\ D_a = 12,\ 18,\ 24,\ U = 0$, no sink. The graph reveals oscillation solutions.

We turn now to the effects of U, the convective flow in the x direction.

Figures 4 and 5 show the effects of positive U for $Le_X = 1.0,\ Le_Y = 1.8,\ D_a = 12$, for which stable solutions exist and are achieved faster when $U = 1$ than when $U = 0$.

The effects of the negative U are shown in Figures 6 and 7. With the choice $Le_X = 1.0,\ Le_Y = 1.8,\ D_a = 18$, the solutions are stable (the flame stabilizes) and this stability is achieved faster when $U = 0$ than when $U = -1$.

Figure 8 shows that when $U = 0$ and $U = 1$ steady burning solutions are generated faster than when $U = -1$.

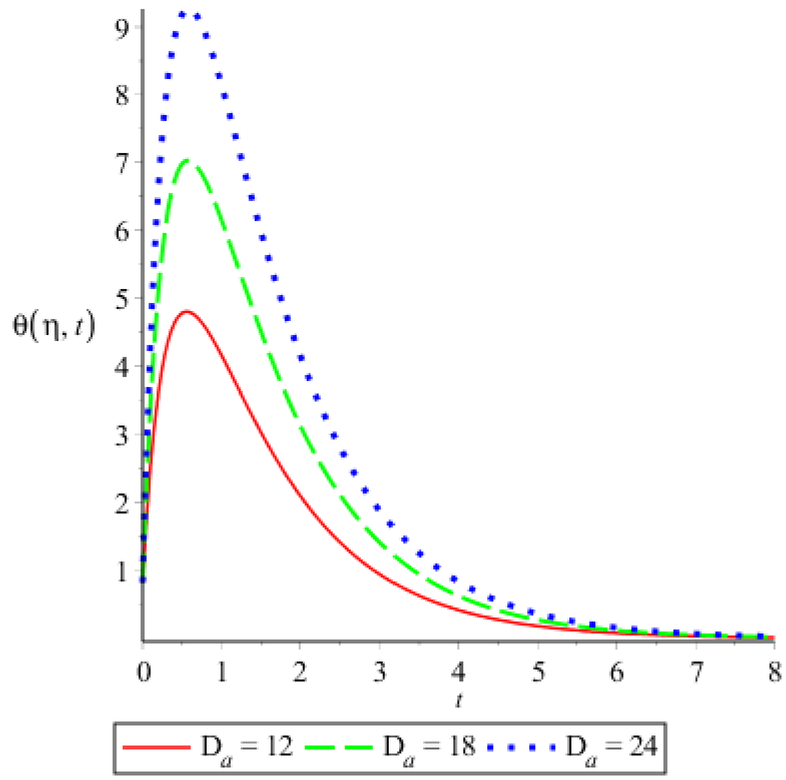

Figure 2: Temperature history at $x = 0.75,\ y = 0.08$ for $Le_X = 1.0,\ Le_Y = 1.8,$ $U = 0,\ D_a = 12, 18, 24$.

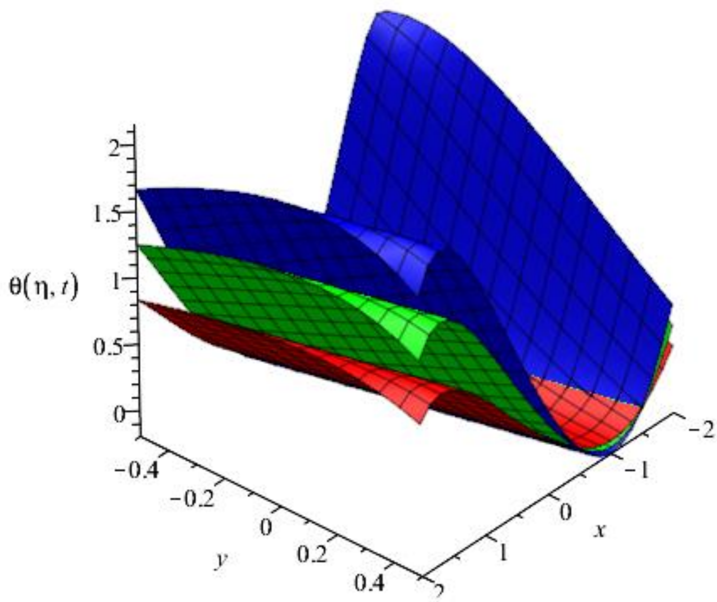

Figure 3: Temperature topography for $Le_X = 1.0,\ Le_Y = 1.8,\ D_a = 12, 18, 24,\ U = 0$, no sink.

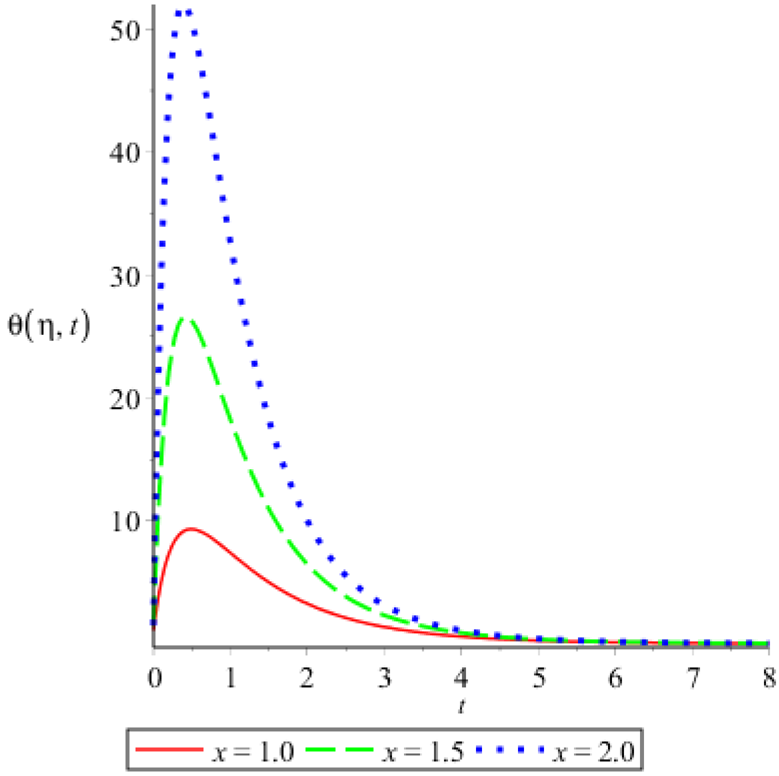

Figure 4: Effects of positive U: temperature history at $x = 1.0, 1.5, 2.0$, $y = 0.08$ for $Le_X = 1.0$, $Le_Y = 1.8$, $U = 0$, $D_a = 12$.

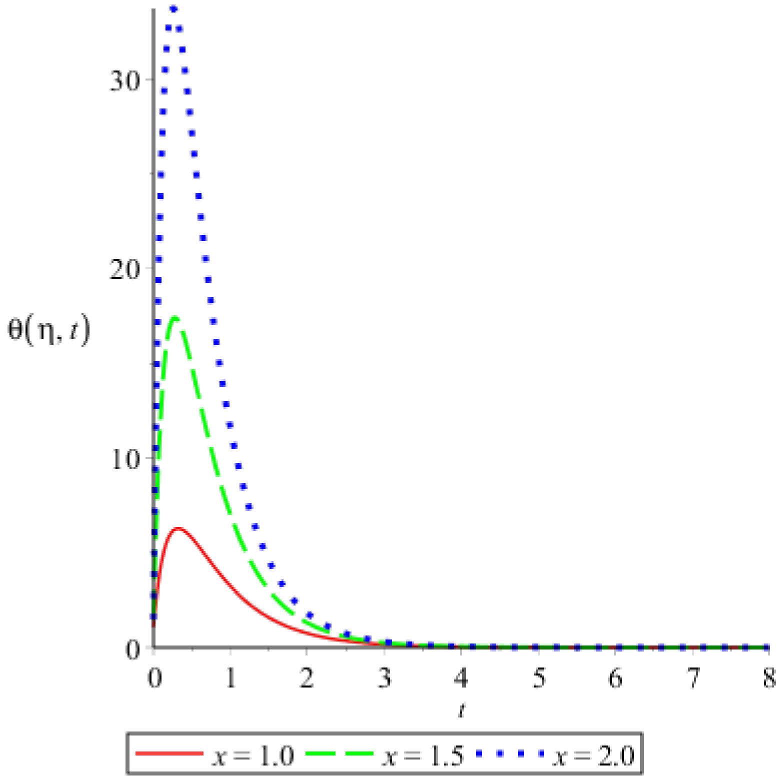

Figure 5: Effects of positive U: temperature history at $x = 1.0, 1.5, 2.0$, $y = 0.08$ for $Le_X = 1.0$, $Le_Y = 1.8$, $U = 1$, $D_a = 12$.

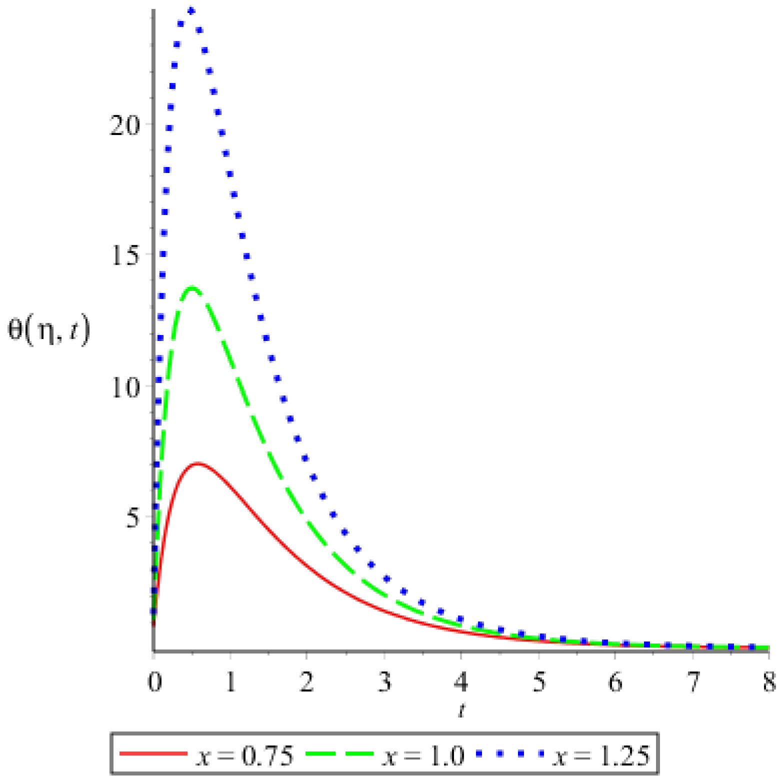

Figure 6: Effects of negative U : temperature history at $x = 0.75, 1.0, 1.25,$ $y = 0.08$ for $Le_X = 1.0,$ $Le_Y = 1.8,$ $U = 0,$ $D_a = 18$.

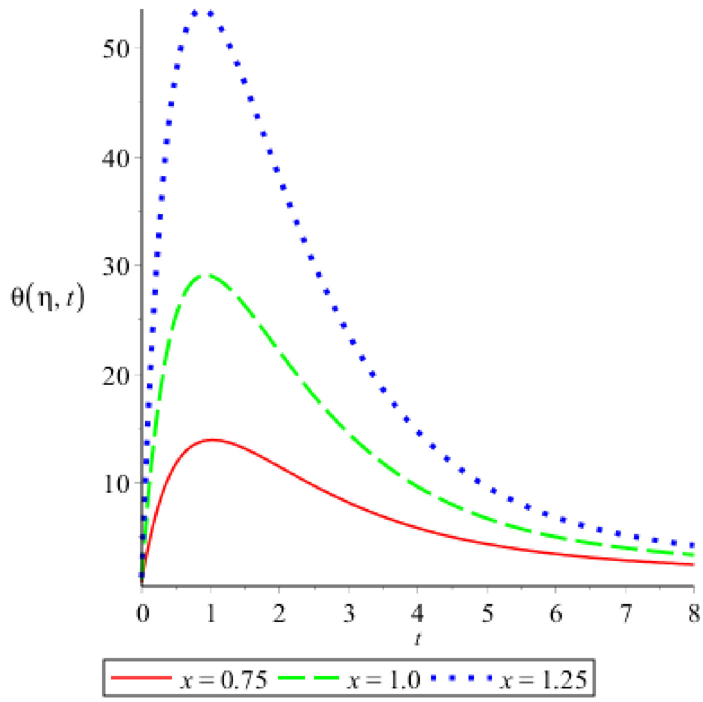

Figure 7: Effects of negative U : temperature history at $x = 0.75, 1.0, 1.25,$ $y = 0.08$ for $Le_X = 1.0,$ $Le_Y = 1.8,$ $U = -1,$ $D_a = 18$.

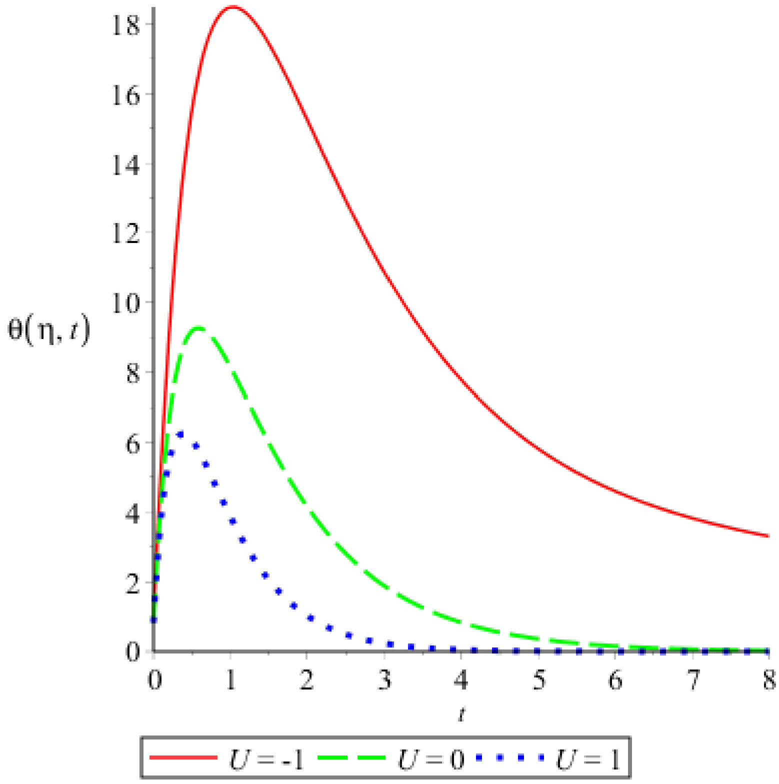

Figure 8: Temperature history at $x = 0.75$, $y = 0.08$ for $Le_X = 1.0$, $Le_Y = 1.8$, $U = -1, 0, 1$, $D_a = 24$.

It is worth pointing out that the effects observed in Figures 2 - 8, are important to guide in controlling the flames.

5 Conclusion

In [6] a universal explanation of edge-flame oscillation is proposed while [4] considered additional physical ingredients (convective flow, heat sink). Here, we have established the conditions for the existence of a unique solution of the model in [4] and provided the approximate analytical solution. The existence of a unique solution to the problem implies that the problem represents a physical situation under specific conditions. The simulation results revealed the impact of the model parameters and the following conclusion can be drawn:

A reduction in the Damkohler number weakens the 2-D edge flame, eventually extinguishing it.
The positive speed ($U > 0$) with which the flame advances weaken the 2-D edge flame.
The negative speed ($U < 0$) enhanced the 2-D edge flame.

References

[1] Ayeni, R. O. (1982). On the explosion of chain-thermal reactions. J. Austral. Math. Soc. (Series B), Vol. 24: 194 – 202.
[2] Ayeni R. O. (1978). Thermal Runway. Ph.D. Thesis. Cornel University USA.
[3] Buckmaster J. (2002). Edge-flames. Progress in Energy and Combustion Science, Vol. 28: 435–475.
[4] Buckmaster J., Hegab A. and Jackson T. L. (2000). More results on oscillating edge-flames. Physics of Fluids, Vol. 12(6): 1592–600.

[5] Buckmaster J. and Zhang Y. (1999). Oscillating edge-flames. Combustion Theory and Modelling, Vol. 3: 547–65.
[6] Buckmaster J. and Zhang Y. (1999). A theory of oscillating edge-flames. Proceedings of the Fifth International Microgravity Combustion Workshop, NASA Conference Publication 1999-208917.
[7] Buckmaster J. (1983). Stability of the porous plug burner flame. SIAM J Appl Math, Vol. 43: 1335–49.
[8] Higuera F. J., Garcia-Ybarra P. L. (1998). Steady and oscillatory flame spread over liquid fuels. Combustion Theory and Modelling, Vol. 2: 43.
[9] Joulin G. and Clavin P. (1979). Linear stability analysis of non-adiabatic flames: diffusional-thermal model. Combust Flame 1979; Vol. 35: 139–53.
[10] Kim I., Schiller D. N. and Sirignano W. A. (1998). Axisymmetric flame spread over propanol pools in normal and zero gravities. Combust Sci Technol, Vol. 139: 249–75.
[11] Kirkby L. L. and Schmitz R. A. (1966). An analytical study of the stability of a laminar diffusion flame. Combust Flame, Vol. 10: 205–20.
[12] Margolis S. B. (1980). Bifurcation phenomena in burner-stabilized premixed flames. Combust Sci Technol, Vol. 22:143–69.
[13] Olayiwola, R. O. (2022). Solving parabolic equations by Olayiwola's generalized polynomial approximation method. International Journal of Mathematical Analysis and Modelling, Vol. 5(3): 24 - 43.
[14] Olayiwola R. O., Jimoh. R. O., Yusuf A. and Abubakar S. (2013). A mathematical study of contaminant transport with first-order decay and time-dependent source concentration in an Aquifer. Universal Journal of Applied Mathematics, Vol. 1(2): 112 –119.
[15] Ross H. D. Ignition of and flame spread over laboratory-scale pools of pure liquid fuels. Prog Energy Combust Sci, Vol. 20: 17–63.
[16] Sivashinsky G. I. (1977). Diffusion-thermal theory of cellular flames. Combust. Sci. Technol., Vol. 15: 137.
[17] Toki C. J. and Tokis J. N. (2007). Exact solutions for the unsteady free convection flow on a porous plate with time-dependent heating. ZAMM Journal of Applied Mathematics and Mechanics, Vol. 87: 4 – 13.
[18] Zhou X., Jackson T. L., Buckmaster J. (2003). Oscillations in propellant flames with edges. Combustion and Flame, Vol. 133: 157–168.

Statistical theories and methods: a panacea for identifying the cause of low political participation among statisticians towards enhanced national development

D.M.O. Omebo[*†], A.Y Emmanuel[‡§], T.D Ailobhio[* **], and A.A. Hassan[††‡‡]

Abstract

The desire of every citizen of a nation is to have overall development. This can only be achieved through implementation of government policies and programmes which are off-shoot of research results. In most cases, persons found on the corridors of power neglect results of this research which is the bedrock of development. This paper made use of statistical theories and methods to ascertain if the claim in some quarters that the poor performance of statistics students in political and social sciences related courses is the cause of the political apathy among statisticians which has paved the way for people who have no regard or importance of research which is the walk path to sustainable development to dominate the political space. An analysis of variance for categorical data (catanova) was used in carrying out the test. The statistical findings were based on the result of GST211 (politics, peace studies and conflict resolution) course of students of department of statistics, computer science and agricultural economics of the Federal University of Lafia, Nasarawa state, Nigeria. It was discovered that students of the department of statistics performed worst among the three departments that took the course thereby justifying the claim that poor performance in political and social science related courses is the cause of political apathy among statisticians. The researchers therefore recommend for aggressive enlightenment by lecturers of the department of statistics among their students on the need to develop high interest in political and social science related courses so as to increase political participation of statisticians in order to bring more statistician to the corridor of power for the implementation of the research results rather than turning out research results that are never implemented.

Keywords: politics; apathy; catanova; performance.

[*] Department of Statistics, Federal University of Lafia, PMB 146, Lafia, Nigeria
[†] Corresponding Author. E-mail: damebo2002@yahoo.co.uk
[‡] Department of Mathematics, Federal University of Lafia, PMB 146, Lafia, Nigeria
[§] E-mail: atanyiemmanuel@gmail.com
[**] E-mail: *ailobhiodorcas@gmail.com*
[††] Department of General Studies, Kogi State College of Health Sciences and Technology, PMB 1037, Idah, Kogi State, Nigeria
[‡‡] E-mail: adajihassan2015@gmail.com

1 Introduction

The aim of any research is to solve a particular problem either for an individual or for a group of people. This therefore means that any research that fails to meet a need is useless. This is the case in most African countries particularly Nigeria. Statisticians and scientist in general are on the field labouring to find solution to many problems of Nigeria, but this usually ends on the shelves of politicians without implementation. Research is the process of arriving at dependable solutions to problem through the planned and systematic collection, analysis and interpretation of data (Chikwe C.K. et al. 2015). After all these processes of getting research results, they are not implemented. This then brings to the fore the question "does it mean that statisticians are not worthy or capable of occupying these political positions"? If they are qualified, then what is the major cause of statisticians not vying for these political offices where they can better be in position to implement the results of this research rather than turning out results that are never implemented? In an attempt to answer these questions, some persons linked the cause of this political apathy among statisticians to poor performance in political related courses taken during their undergraduate studies due to lack of interest and the fact that it is not calculation in nature. In an attempt to ascertain if this claim is true or false, the researchers made use of result of the course G.S. T. 211 (politics, peace studies and conflict resolution) of students of department of statistics, computer science and agricultural economics of the Federal University of Lafia, Nasarawa state, Nigeria for the year 2019/2020 session.

1.1 Aims and objectives of the study

1. To ascertain if performance is dependent on departments
2. To justify the claim that political apathy among statistician is linked to undergraduate programme

1.2 Nature and scope of study

There are 21 departments within the faculties of science, computing and agricultural sciences out of which statistics being the main department of interest was selected from the faculty of science and then, computer science was selected from the faculty of computing and lastly, agricultural economics was taken from the faculty of agricultural sciences. At the end of the examination, successful candidates are classified into five groups – Distinction(A), Good (B), Credit (C), Fair (D) and Pass (E). Similarly, unsuccessful candidates are awarded (F). All findings are based on the analysis of this examination results from the selected departments from the various faculties .

2 Literature review

According to Yusufu A.Y, political apathy manifested itself in the country between 1999 and 2011 in the following forms: one, the decline to register; two, the refusal to vote; three, failure to protest against rigging and four, failure to assist the security agents with useful information. It was discovered that bad governance was responsible for political apathy.

In order to understand political apathy, justice must be done to the term " Democracy" and its link with political apathy. Democracy is popularly conceived as government of the people, for the people and by the people (Hassan, 2003). According to Mikailu and Yaqub (Mikailu and Yaqub, 2003), "Democratic politics is always everywhere built on certain minimum principles. These principles include participation and inclusiveness, responsiveness and accountability, transparency and good governance, regular, free and fair elections, freedom and respect for human rights and the observance of rule of law. Where these principles are in general observed, one can pronounce a government constituted in such a policy as democratic. Thus, from the above, one can see that a democratic government ensures participation and inclusiveness and is also responsive and accountable to its people. Otherwise, there will be apathy in the political system. What then is political apathy? For the purpose of this article, political apathy is the deficiency of love and devotion to a state. It is the indifference on the part of citizens of any state as regards their attitudes towards political activities such as elections, public opinions, and civic responsibilities. Political apathy is therefore absence of interest in, or concern about, socio-political life. Thus, an apathetic person lacks interest in the social and political affairs of his country. The relationship between the Nigerian government and the people between 1999 and 2011 is a continuation of what started at independence in 1960. It was based on the understanding that the government would provide security, justice, liberty and welfare for the people. On the other hand, people would be obedient and discharge their political, economic, social and other responsibilities.

3 Methodological framework

The methodological framework for this study is a two-way analysis of variance for categorical data (CATANOVA).

A two-way CATANOVA with chi-square tests for interaction

Consider a two-way experimental situation with a k-dimensional vector of responses { (n_{ijk}) K, i=1,2,…I, j=1,2,…,J} recorded in frequencies in the (ij)th plot. We assume a multinomial probability model, namely

Pr({n_{ijk}}k/{π_{ijk}} k,n_{ij})= nij !/ $\prod_k \{nijk!\}$ (πijk)$\prod_k$(n^{ijk}
nijk = 0,1,…,n_{ij}
$0 \leq \pi_{ijk} \leq 1$
Nij = $\sum_k nijk$ is held fixed

Nijk, ni$^{/}$ j$^{/}$ k are independent ∀ i≠ i$^{/.}$

The hypothesis to be tested are:
HR: $\prod ijk == \prod jk$, there is no row effect
HC: : $\prod ijk == \prod ik$, there is no column effect
HRC: : $\prod ijk == \prod k$, there is no row x column interaction
The expectation of the sample estimate of : $\prod ijk$ is given by the linear model
E ($\prod^{\wedge}$ ijk) **μ**k + Tik + Bjk + $\boldsymbol{\lambda}$ijk,

where **μ**k, Bjk and $\boldsymbol{\lambda}$ijk assume their usual meaning of constant, row effect, column effect and interaction respectively. The hypothesis, HR, HC, and HRC will be seen to be respectively equivalent to
Hi: Tik = 0 ∀i, HB: Bjk = 0 ∀j and $\boldsymbol{\lambda}$ijk = 0 ∀i,j.

The parameters : $\prod ijk$ may be considered fixed or random with probability density h($\prod ijk$), over [0,1] depending on whether I and J are random or not , C.H. Scheffe (1959). Specially,
g($\prod ijk$) if I and J are random, o≤ $\prod ijk$≤ 1
h($\prod ijk$) = g ($\prod jk$) if I is fixed and J random 0≤ $\prod jk$≤ 1
g($\prod ik$) if I is random and J fixed, 0≤ : $\prod ik$ ≤ 1.

We shall now consider the sum of squares (SS) for {nijk }k. This may be obtained, I.B. Onukogu [1982] also Anderson [1958], as the trace of the sample variance- covariance matrix. That is
SS(nijk) = Σ_k var (nijk)

Upon further simplification, we have that

TSS = n - $\sum_{k}$ n2..k/n , as the total sum of squares
BRSS = n - $\sum_{ik}$ n2i.k/ni , as the between row sum of squares
BCSS = n - $\sum_{jk}$ n2.jk/nj , as the between column sum of squares
WUSS = n - $\sum_{ijk}$ n2ijk/nij, as the within unit sum of squares ,

where
N = $\sum_{i}$ ni = $\sum_{j}$ nj $\sum_{ij}$ ni j
RSS = TSS – BRSS = $\sum_{k}$ n2i.k/ni - $\sum_{k}$ n2..k/n
CSS = TSS – BCSS = = n - $\sum_{jk}$ n2.jk/nj - $\sum_{k}$ n2..k/n
NSS = BRSS + BCSS – TSS – WUSS
= n - $\sum_{ijk}$ n2ijk/nij - $\sum_{ik}$ n2i.k/ni - $\sum_{jk}$ n2.jk/nj + $\sum_{k}$ n2..k/n.

We may reject HR, HC and HRC respectively at specified ἀ-level of error if
$\chi^2_R \geq \chi^2(ἀ)_{(I-1)(J-1)(K-1)}$
where
χ^2_R = (K-1)(n-1)RSS/ TSS
χ^2_C = (K-1)(n-1)css/TSS
χ^2_{NT} = (K-1)(n-1)NSS/TSS

3.1 Materials and methods

Below is the data layout for a two – way analysis of variance for categorical data (CATANOVA).

Table 1: Data layout for two way CATANAVO

	DEPARTM ENTS	COMPUTER SCIENCE							AGRIC ECONOMICS							STATISTICS						
i	responses	A	B	C	D	E	F	T	A	B	C	D	E	F	T	A	B	C	D	E	F	T
	Males	n_{111}	n_{112}	n_{113}	n_{114}	n_{115}	n_{116}	$n_{11.}$	n_{12}	n_{1}	n_{1}	n_{1}	n_{1}	n_{1}	n_{1}	n_{131}	n_{132}	n_{133}	n_{134}	n_{135}	n_{136}	$n_{13.}$
	Females	n211	n212	n213	n214	n215	n216	n21	n2	n22	n23	n24	n25	n26	n2	n23	n232	n233	n234	n235	n236	n23.
	n.jk	n.11	n.12	n.13	n.14	n.15	n.16	n.1	n.2	n.	n.	n.	n.	n.	n.	n.3	n.32	n.33	n.34	n.35	n.36	n.3.

Table 2: Two – way catanova test on performance of male and female students result of G.S. T. 211 (Politics,peace studies and conflict resolution) course of students of department of statistics, computer science and agricultural economics of the Federal University of Lafia, Nasarawa state, Nigeria for the year 2021. DEPARTMENTS

	Computer science							Agric. Econs							Statistics						T							
sex	A	B	C	D	E	F	ni1.	A	B	C	D	E	F	ni2.	A	B	C	D	E	F	ni3.	ni.k						ni..
male	139	62	58	10	55	83	407	71	75	45	24	36	52	303	107	52	53	5	45	75	337	317	189	156	39	136	210	1047
female	80	51	48	11	50	85	325	39	48	29	37	39	51	243	43	20	26	6	30	64	189	162	119	103	54	119	200	757
Total	219	113	106	21	105	168	732	110	123	74	61	75	103	546	150	72	79	11	75	139	526	479	308	259	93	255	410	1804

Total sum of squares (TSS) = n - $\sum_k n2..k/n$
= 1804 - (479^2 + 308^2 + 259^2 + 93^2 + 255^2 +410^2)/ 1804
= 1804 – 633160/1804
= 1804 – 350.9756
TSS = 1453.0244.

Between sex sum of squares (BSSS) = n - $\sum_{ik} n2i.k/n\,i$
= 1804 – (317^2 + 189^2 +156^2 +39^2 +136^2 +210^2)/1047 + (162^2 +119^2 +103^2 +54^2 +119^2 +200^2) / 757
= 1804 - (214.5778 + 142.7886)
= 1804 - 357.3664
BRSS = 1446.6336.

Between departments sum of squares(BDSS) = n - $\sum_{jk} n2.jk/nj$
= 1804 - (219^2 +113^2 + 106^2 + 21^2 +105^2 +168^2)/ 732 + (110^2 + 123^2 +74^2 +11^2 + 75^2 + 139^2)/526
= 1804 - (152.5355 + 96.4469 + 112.1521)
= 1804 - 361.1345
BDSS = 1442.8655.

Row sum of squares (RSS) = TSS – BDSS
= 1453.0244 – 1446.6336
= 6.3908
RSS = 6.3908.

Column sum of squares (CSS) = TSS – BDSS
= 1453.0244 - 1442.8655
= 10.1588.

Table 3: Catanova table

Source of variance	Degree of freedom	Sum of squares
Row or factor levels or sexes	1	6.3908
Departments	2	10.1588
Sex x departments	10	1.3334
Residual	1790	1435.1414
Total	1803	1453.0244

Ho: Performance is independent on the departments.
H1: Performance is dependent on the departments

The test statistic = χ^2_{cal} = k – 1(n-1)CSS/ TSS
= (6-1)1804 – 1) 10.1588/ 1453.0244
= 63.0282,
$\chi^2_{tab} = \chi^{2\,(0.05)}_{(J-1)(K-1)} = \chi^{2\,(0.05)}_{(3-1)(6-1)} = 18.307$.

Decision Rule: Reject Ho if χ^2_{cal} is greater than χ^2_{tab}
Conclusion:
Since $\chi^2_{cal\ = 63.0283} > \chi^2_{tab}$ = 18.307, we reject Ho and conclude that performance depends on the departments.

To determine which of the departments perform best, we compute the proportions of students that passed and failed in each department as follows:

Proportion of pupils in computer science that passed is
$P_{\text{Computer science passed}}$ = nComp science pass/ Ncomp 0.77.

Proportion of students in computer science that failed is
$P_{\text{computer science failed}}$ = nComp Science failed/Ncomp = 168/732 = 0.23.

Proportion of students in Agric Economics that passed is
$P_{\text{Agric Econ passed}}$ = nAgric Econs passed/NAgric Econs = 443/546 = 0.81.

Proportion of students that failed in Agric Econs department is
$P_{\text{Agric Econ failed}}$ = nAgric Econs failed/NAgric Econs = 103/546 = 0.19.

Proportion of students in Statistics department that passed is
$P_{\text{Stat passed}}$ = nStatpassed/NStat = 387/526 = 0.74.

Proportion of students in Statistics department that failed is
$P_{\text{Statfailed}}$ = nStatfailed/NStat = 139/526 = 0.26.

The proportions of students that passed in each department in the decreasing order is as follows:
Agric Econs = 0.81.
Computer Science = 0.77.
Statistics = 0.74.

Similarly, the proportion of pupils that failed in each department in the increasing order is as follows:
Agric Econs = 0.19.
Computer Science = 0.23.
Statistics = 0.26.

4 Conclusion

From the foregoing, it shows that performance depends on the departments. This means that performance of any chosen student depends on which department the student comes from. From the result obtained, students from Agric Economics performed better than the other two departments with the department of statistics having the poorest. It goes to mean that the political apathy among statisticians which has lead to non active participation in political activities is linked to poor performance in political related courses taken during the school. Therefore, efforts should be made to identify the cause of this failure from this early stage.

References

[1] Anderson, T.W. (1958). Catanova for multidimensional contingency tables: Nominal-scale response. 56
[2] Anderson, T.W. (1958). An introduction to multivariate analysis. John Wiley, New York.
[3] Chikwe C.K. et al. (2015). Challenges of Research and Human Capital Development.
[4] Fisher, R.A. (1970). Statistical methods for research workers 14th Edition, 4-6.
[5] Oladele, F. (1972). Performance of boys and girls primary schools Nsukka Educational Zone (Unpublished research)7-9.

[6] Onukogu I.B. (2014). Analysis of variance of categorical data-nested designs. Journal of Statistics: Advances in Theory and Applications, 12:109-116.
[7] Onukogu I.B. (1985). Reasoning by analogy from ANOVA to CATANOVA, Biometrical Journal, 27:839-849.
[8] Onukogu I.B. (1982). One degree of freedom for non-additivity in a contingency table and its multivariate extension. Biometrical Journal, 115-125.
[9] Onukogu I.B. (1981). One degree of freedom for interaction in a two-way classification without replication. Biometrical Journal, 24(8):1-7.
[10] Onukogu I.B (1982). An analysis of variance of nominal data. Biometrical Journal, 7-8.
[11] Peter H.L. (2021). School location and academic performance of pupils in English language in primary schools. Onlineproject.com.ng, 4-5.
[12] Scheffe, H. (1959). The Analysis of Variance. Wiley, New York.
[13] Yusufu A.Y. Democracy and political apathy in Nigeria (1999-2011). European Scientific Journal, 8(20): 2-5.

International Journal of Mathematical Analysis and Modelling
Volume 5, Issue 4, November 2022, Pages 79 – 88

The spread of covid-19 disease and the health of Nigeria

R.T. Abah*

Abstract

COVID-19 is a major cause of death till date, claiming many lives in Nigeria and around the world. Nigeria was classified as one of the countries in Africa that had COVID-19 disease in 2020. February 27,2020, was when the first confirmed case of the novel coronavirus was reported in Nigeria. This was another terrible time when the health of Nigerians was under another serious attack apart from corruption and other economic challenges facing the country. In this study, Mathematical models are the major tools used for studying the transmission dynamics of covid-19. In this journal, we are considering a model on the spread of covid-19 disease and the health of Nigeria and analysed. the equilibrium states of the model which are the disease-free equilibrium states and the endemic equilibrium states were obtained and based on the Routh-Hurwitz criterion, the eigenvalues model equations have negative real parts, that is if and only if all the eigenvalues are negative, then the condition for stability is satisfied.

Keywords: COVID-19; spread; disease; health; Nigeria

1 Introduction

COVID-19 is an infectious disease caused by the SARS-CoV-2 virus. People who are infected with COVID-19 will experience some symptoms and recover without special treatment attention depending on their level of immunity. People with mild symptoms who are healthy can manage their symptoms at home [11].

However, some who become seriously ill require some medical treatment. The virus can spread from an infected person's mouth or nose in small liquid particles when they cough, sneeze, speak, sing or breathe. These particles range from larger respiratory droplets to smaller aerosols. You can be infected by breathing in the virus if you are near someone who has COVID-19, or by touching a contaminated surface and then your eyes, nose or mouth. The virus spreads more easily indoors and in crowded settings [14].

Nigeria was classified as one of the countries in Africa that had Covid-19 disease in 2020 [8]. Meanwhile, February 27, 2020, was when the first confirmed case of the novel coronavirus was reported in Nigeria. It was the case of a 44-yearold Italian citizen who arrived the Murtala Muhammed

* Department of Mathematics, University of Abuja, Abuja, Nigeria; toyin.abah@uniabah.edu.ng

international Airport, Lagos at 10pm on January 24, 2020 aboard Turkish airline from Milan, Italy and proceeded to his company on February 25, 2020 and was presented at the staff clinic in Ogun state on February 26, 2020 and to Lagos because he was suspected with high index by the Managing Physician who later referred and him to the IDH Lagos on 27, 2020 where he was confirmed to have the disease [6]. Since then, the Federal Government has put in place several measures through the Presidential Task Force (PTF-COVID-19) working with the Federal Ministry of Health to curtail the spread and protect the health of Nigerians [8]. From 25th -29th June 2022, 332 new confirmed cases were recorded in Nigeria. Till date, 257290 cases have been confirmed, 250229 cases have been discharged and 3,144 deaths have been recorded in 36 states and the Federal Capital Territory. The 332 new cases are reported from 6 States- Lagos (251), Rivers (50), FCT (21), Kano (7), Delta (2) and Oyo (1) [9]. From 10th to 12th September 2022, 167 new confirmed cases and 1 death was recorded in Nigeria. To date, 264,617 cases have been confirmed, 257,880 cases have been discharged and 3,155 deaths have been recorded in 36 states and the Federal Capital Territory [9]. The 167 new cases are reported from 10 States-Edo (84), Lagos (55), Rivers (11), Kano (5), Cross River (4), Adamawa (3), Delta (2), Ekiti (1), FCT (1) and Kaduna (1). A multi-sectoral national emergency operations center (EOC), activated at Level 2, continues to coordinate the national response activities [9].

Researchers and Scientists have laboured tirelessly to bring some solutions and controls which include the use of facemask, lockdown and other measures employed to curb the COVID-19 rapid spread in Nigeria and around the world.

Mathematical models which help to gain a better insight into real life situations like this COVID-19, have been developed to study the transmission and control of the disease both in Nigeria and around the world by some researchers [4]. Some researchers who have done some major work on the transmission dynamics of COVID-9 Disease to mention but a few among them: Calistus et al. (2020), in their study, "Mathematical assessment of the impact of non-pharmaceutical interventions on curtailing the 2019 novel Coronavirus emphasized the important of social-distancing in curtailing the burden of COVID-19. Also, they found out that an increase in the adherence level of social-distancing protocols, which resulted in dramatic reduction of the burden of the pandemic, and the timely implementation of social-distancing measures in numerous states of the US, which may have averted a catastrophic outcome with respect to the burden of COVID-19. Using face-masks in public (including the low efficacy cloth masks) is very useful in minimizing community transmission and burden of COVID-19, provided their coverage level is high. The masks coverage needed to eliminate COVID-19 decreases if the masks-based intervention is combined with the strict social-distancing strategy [5]. Abba et al (2021) in their journal "A primer on using mathematical COVID-19 dynamics: Modeling, analysis and simulations for understanding the dynamics of COVID-19 [2].

The pandemic has a high mortality rate and currently endemic around the world, having claimed thousands of lives here in Nigeria and other countries [13]. Manuel (2020) in his study, "Modeling behavioural change and COVID-19 containment in Mexico: A trade-off between lockdown and compliance" fitted his model to the available data. The initial phase of the epidemic, from February 17th to March 23rd, 2020, is used to estimate the contact rates, infectious periods and mortality rate using both confirmed cases (by date of symptoms initiation), and daily mortality. Data on deaths after March 23rd, 2020 is used to estimate the mortality rate after the mitigation measures are implemented [7]. Adesoye and Ilyas, on "mathematical model of COVID-19 in Nigeria with optimal control" says that PTF, NCDC, and FMOH can use facemask, hand sanitizers along with social distancing to control the disease [12].

2 Model formulation

A mathematical modelling for the transmission dynamics of COVID-19 disease and the health of Nigeria is considered and formulated in this work. The population is divided into five (5) compartments, namely: Susceptible S(t), Latent L(t), Infected I(t), Quarantined $\mathrm{Q(t)}$ Recovered R(t).

The Total population is

$$\mathrm{N(t) = S(t) + L(t) + I(t) + Q(t) + R(t)} \tag{2.1}$$

This is the schematic diagram describing the model (3.1) - (3.5) below:

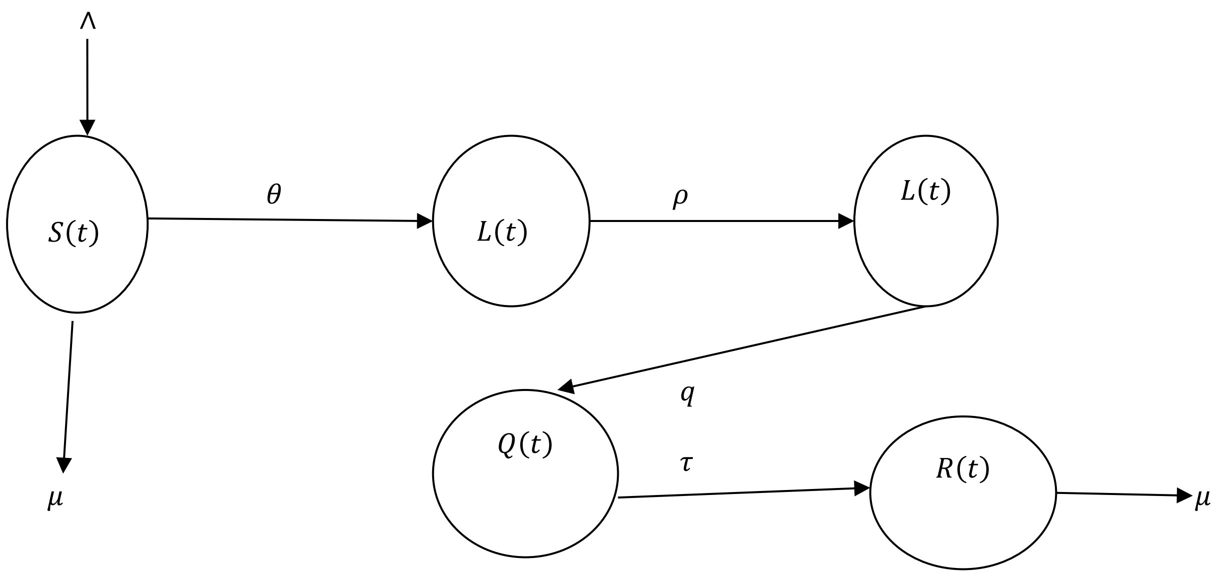

Figure 2.1: Schematic diagram of Covid-19 transmission dynamics model.

The following assumptions were made to formulate the model:

- The mixing of people is homogeneous, meaning that all individuals have equal chance of getting infected if they come in adequate contact with infectious individuals.
- Those in $\mathrm{S(t)}$ get infected through contact with $\mathrm{I(t)}$.
- $\mathrm{L(t)}$ are infected but not yet infectious, since they get infectious, only when they are symptomatic.
- The isolation of $\mathrm{I(t)}$ into $\mathrm{Q(t)}$ cause the spread of covid-19 to be very low at a treatment rate τ.
- $\delta < \sigma$ due to the treatment of $\mathrm{Q(t)}$ at the rate τ .

2.1 Variables and parameter of the model

The variables are defined as follows:

Table 1: Variables

S/N	VARIABLE	DESCRIPTION
1.	$S(t)$	Susceptible class at time t
2.	. $L(t)$	Exposed class at time t
3.	$I(t)$	Infectious class at time t
4.	$Q(t)$	Quarantined class at time t
5.	$R(t)$	Recovered class at time t

The Parameters are defined as follows:

TABLE 2: Parameters

S/N	Parameter	Definition
1	Λ	birth rate
2	μ	death rate
3	δ	disease induced death rate of $I(t)$
4	σ	disease induced death rate of Q(t)
5	$\theta(1-f)$	effective contact rate between $I(t)$ and S(t)
6	p	progression rate from $L(t)$ to $I(t)$
7	q	rate of quarantine
8	τ	treatment rate
9	f	rate of facemask prevention for covid-19

3 Model equations

From the schematic diagram 2.1, the model equations (3.1) – (3.5) are given below

$$\frac{dS(t)}{dt} = \Lambda - \frac{\theta I(t)S(t)(1-f)}{N} - \mu S(t) + fS(t) \tag{3.1}$$

$$\frac{dL(t)}{dt} = \frac{\theta I(t)S(t)(1-f)}{N} - (\rho + \mu - f)L(t) \tag{3.2}$$

$$\frac{dI(t)}{dt} = \rho L(t) - (q + \mu + \delta)I(t) \tag{3.3}$$

$$\frac{dQ(t)}{dt} = qI(t) - (\tau + \mu - f + \sigma)Q(t) \tag{3.4}$$

$$\frac{dR(t)}{dt} = (\tau + f)Q(t) - \mu R(t) \tag{3.5}$$

$$\frac{dN(t)}{dt} = (f + \mu)S(t) + (f - \mu)L(t) - (\mu + \delta)I - (\sigma + \mu)Q(t) + \mu R(t) \tag{3.6}$$

3.1 Positivity of solutions

The model (3.1) to (3.6) is epidemiologically and mathematically well posed in the domain Ω with the initial conditions.

Let $\Omega = (S, \quad L, \ I, \quad Q, \quad R) \in R^5$ (3.7)

$$S + L + I + Q + R \leq N$$

3.1.1 Properties of the Model

To analyze the model (3.1) to (3.6) we consider the following theorem

Theorem 1: The solutions of the model equations (3.1) to (3.6) are positive for all time $t \geq 0$ provided that the initial conditions are positive.

Proof:

Employing the given assumptions, that all initial conditions are positive, i.e.

$$S(0) > 0, \quad L(0) > 0, \quad I(0) > 0, \quad Q(0) > 0, \quad R(0) > 0. \tag{3.8}$$

We have by contradiction that the solutions of (3.1) to (3.5) are positive if we assume for a contradiction that there exists first time,

$$t_1 : S(t_1) = 0$$

and $S(t) > 0, \quad L(t) > 0, \quad I(t) > 0, \quad Q(t) > 0, \quad R(t) > 0$ (3.9)

$$0 < t < t_1$$

or there exists

$$t_2 : L(t_2) = 0$$

and$S(t) > 0, \quad L(t) > 0, \quad I(t) > 0, \quad Q(t) > 0, \quad R(t) > 0$ (3.10)

$$0 < t < t_2$$

or there exists

$$t_3 : I(t_3) = 0$$

and$S(t) > 0, \quad L(t) > 0, \quad I(t) > 0, \quad Q(t) > 0, \quad R(t) > 0$ (3.11)

$$0 < t < t_3$$

or there exists

$$t_4 : Q(t_4) = 0$$

and$S(t) > 0, \quad L(t) > 0, \quad I1(t) > 0, \quad Q(t) > 0, \quad R(t) > 0, \quad I2(t) > 0$ (3.12)

$$0 < t < t_4$$

or there exists

$$t_5 : R(t_5) = 0$$

and $S(t) > 0, \quad L(t) > 0, \quad I(t) > 0, \quad Q(t) > 0, \quad R(t) > 0$ (3.13)

$$0 < t < t_5$$

or there exists

$$t_6 : I(t_6) = 0$$

and $S(t) > 0, \quad L(t) > 0, \quad I(t) > 0, \quad Q(t) > 0, \quad R(t) > 0$ (3.14)

$$0 < t < t_6$$

Now, in the case where

$S(t) = 0$ (3.15)

gives,

$$\frac{dS(t_1)}{dt} = \lim_{t=t_1} \frac{S(t_1)-S(t)}{t_1-t} < 0 \quad (3.16)$$

and similarly, gives

$$\frac{dL(t_2)}{dt} < 0, \quad \frac{dI(t_3)}{dt} < 0, \quad \frac{dQ(t_4)}{dt} < 0, \quad \frac{dR(t_5)}{dt} < 0 \quad (3.17)$$

However, from equations (3.1) to (3.5) gives,

$$\frac{dS(t_1)}{dt} = \Lambda - \frac{\theta I(t)S(t)(1-f)}{N} - \mu S(t) > 0 \quad (3.18)$$

i.e.

$$S^i(t_1) = \Lambda > 0 \quad (3.19)$$

which contradicts (3.17). Therefore, $S(t_1) \neq 0$, and Swill remain positive for all t.

Similarly, for the remaining variables gives

$$L^i(t_2) = \frac{\theta I(t)S(t)(1-f)}{N} + \beta L(t) > 0 \quad (3.20)$$

$$I^i(t_3) = \rho L > 0 \quad (3.21)$$

$$Q^i(t_4) = qI > 0 \quad (3.22)$$

$$R^i(t_5) = (\tau + f)Q > 0 \quad (3.23)$$

$$I^i = \rho L(t) - (q + \mu + \delta)I(t) \quad > 0. \quad (3.24)$$

These are contradictions of what was supposed for each of the variables, meaning that $L(t_2) \neq 0$, , $Q(t_4) \neq 0$, $R(t_5) \neq 0$, and $I(t_6) \neq 0$. Hence, S, L, I, Q, R and remain positive for all t . By this, it is showed that all the solutions of (3.1) to (3.6) are inR^5, provided that the initial conditions are positive. Thus the feasible region is positively- invariant. It is hence, sufficient to consider the dynamics of the model (3.1) to (3.6) in the region Ω.

3.2 Boundedness of solution

The model (3.1) to (3.8) is epidemiologically and mathematically well posed in the domain Ω with the initial conditions.

Let $\quad \Omega = (S, \quad L, \quad I, \quad Q, \quad R, \quad D) \in R^5$

$S \geq 0, \quad L \geq 0, \quad I \geq 0, \quad Q \geq 0, \quad R \geq 0, \quad D \geq 0,$
$S + L + I + Q + R \leq N.$

Theorem 2: All solutions$(S(t), L(t), I(t), R(t), Q(t)$ of Model are bounded

Proof: Model 1
From the five populations we obtain

$$.\frac{d(S+L+I+Q+R)}{dt} = \Lambda - (f+\mu)S(t) + (f-\mu)L(t) - (\mu+\delta)I - (\sigma+\mu)Q(t) + (f+\mu)R(t)$$

.$\frac{d(S+L+I+Q+R)}{dt} = \Lambda - (S+L+R)f + (S+L+I+R)\mu - \delta I - \sigma Q(t)$
$\leq \Lambda - \mu(S+L+I+R)$.

Then $\lim_{t\to\infty}(S+L+I+R) \leq \frac{\Lambda}{\mu}$.

3.3 Existence of Equilibrium States E

Let $E(S(t), L(t), I(t), R(t), Q(t))$ be the equilibrium states of the model system.
At equilibrium state, the rate of change of each variable is equal to zero.

i.e.$\frac{dS}{dt} = \frac{dL}{dt} = \frac{dI1}{dt} = \frac{dQ}{dt} = \frac{dR}{dt} = 0.$ (3.25)

Let

$$\big(S(t), L(t), I\,(t), Q(t), R(t)\big) = (v, w, x, y, z), \quad (3.26)$$
$$N(t) = n \quad (3.27)$$
where
$$n = v + w + x + y + z. \quad (3.28)$$

Hence, equations (3.1) to (3.8) become

$$\Lambda - \frac{\theta vx(1-f)}{n} - \mu v + fv = 0\,, \quad (3.29)$$

$$\frac{\theta vx(1-f)}{n} - (\rho + \mu - f)w = 0, \quad (3.30)$$

$$\rho w - (q + \mu + \delta)x = 0, \quad (3.31)$$

$$qx - (\tau + \mu + \sigma - f)y = 0\,, \quad (3.32)$$

$$(\tau + f)y - \mu z = 0. \quad (3.33)$$

The equilibrium states are then obtained by solving equations (3.30) to (3.36).

3.3.1 Disease-Free Equilibrium E_0

At the disease free equilibrium state E_0, there is absence of infection, thus the infected classes are zero. The whole population comprise of the susceptible class and so we have

$$v = \frac{\Lambda}{\mu} \quad (3.32)$$

Adding equations (3.7) and (3.8) gives

$$w = \frac{\Lambda}{\rho - \mu}. \quad (3.33)$$

Hence all other variables, x, y and z, are given below as:

$$x = \frac{\Lambda\rho}{(\rho-\mu)(q+\mu+\delta)}, \quad (3.34)$$
(3.34)

$$y = \frac{q\,\Lambda\rho}{(\rho-\mu)(q+\mu+\sigma)(\tau+\mu+\sigma)}, \quad (3.35)$$

$$z = \frac{\tau q\,\Lambda\rho}{\mu(\rho-\mu)(q+\mu+\sigma)(\tau+\mu+\sigma}. \quad (3.36)$$

Therefore, the disease-free equilibrium (DFE) state is given by:

$$E_0 = (v, w, x, y, z) = \left(\frac{\Lambda}{\mu}, 0,0,0,0\right). \quad (3.37)$$

3.3.2 Endemic Equilibrium State

From equations (3.32) to (3.36), we have the endemic equilibrium states of the model.

The endemic Equilibrium is given by

$$E_1 = (v, w, x, y, z) = \left(\frac{\Lambda}{\mu}, \frac{\Lambda}{\rho-\mu}, \frac{\Lambda\rho}{(\rho-\mu)(q+\mu+\delta)}, \frac{q\,\Lambda\rho}{(\rho-\mu)(q+\mu+\sigma)(\tau+\mu+\sigma)}, \frac{\tau q\,\Lambda\rho}{\mu(\rho-\mu)(q+\mu+\sigma)(\tau+\mu+\sigma}\right) \quad (3.38)$$

3.3.3 Stability Analysis

From (3.1) to (3.5) we obtained the Jacobian matrix given by,

$$\mathbf{J} = \begin{bmatrix} -\mu - \frac{\theta x(1-f)}{n} & 0 & \frac{\theta v(1-f)}{n} & 0 & 0 \\ \frac{\theta x(1-f)}{n} & -(\rho-\mu) & \frac{\theta v(1-f)}{n} & 0 & 0 \\ 0 & \rho & -(q+\mu+\sigma) & 0 & 0 \\ 0 & 0 & q & -(\tau+\mu+\sigma) & 0 \\ 0 & 0 & 0 & \tau & -\mu \end{bmatrix} = 0 \quad (3.39)$$

3.3.2 Local stability of Disease-Free Equilibrium $\mathbf{E_0}$

We used the Jacobian stability technique of determining the local stability of the system. Consider the Jacobian matrix of (3.39). At disease free equilibrium, E_0 is given by:

$$J = \begin{bmatrix} -\mu & 0 & \frac{\theta v(1-f)}{n} & 0 & 0 \\ \frac{\theta x(1-f)}{n} & -(\rho-\mu) & \frac{\theta v(1-f)}{n} & 0 & 0 \\ 0 & \rho & -(q+\mu+\sigma) & 0 & 0 \\ 0 & 0 & q & -(\tau+\mu+\sigma) & 0 \\ 0 & 0 & 0 & \tau & -\mu \end{bmatrix} = 0 \quad (3.39)$$

Thus from (3.39), the eigenvalues are given by

$\lambda = -\mu < 0$ (3.40)
$\lambda = -(\rho - \mu) < 0$ (3.42)
$\lambda = -(q + \mu + \sigma) < 0$ (3.43)
$\lambda = -(\tau + \mu + \sigma) < 0$ (3.44)
$\lambda = -\mu < 0.$ (3.45)

4 Result

The condition for stability using the Routh Hauwitz criteria is that λ_i where $i = 1,2,3,4,5$ negative real parts. Therefore from (3.41) to (3.45),

λ_1 is negative if $\lambda_1 = -\mu < 0$
λ_2 is negative if $\lambda_2 = -(\rho - \mu) < 0$ implies that $\mu < \rho$
λ_3 is negative since $\lambda_3 - (q + \mu + \sigma) < 0$ which implies that $\mu + \sigma < q$
λ_4 is negative since $\lambda_4 = -(\tau + \mu + \sigma) < 0$ which implies that $\tau > \mu + \sigma$
λ_5 is negative since $\lambda_5 = -\mu < 0$

4.2 Discussion of result

$\tau > \mu + \sigma$ implies that the inequality (3.44) holds and so the condition for stability of the disease free equilibrium state is locally asymptotically stable, which means that the treatment rate τ, is greater than the natural death rate μ and the disease induced death rate [1].

4.3 Conclusion

Covid-19 epidemic has shown that in the absence of a strong public health care delivery system, millions of lives even a rare disease can risk the lives of millions of people. The crux of this epidemic is that a large scale and coordinated international response is the need of the hour to support Nigerians and all who are at-risk, the need for the nation to intensify her response activities and strengthen national capacities.

References

[1] Abah, R. T., Akinwade, N. I., Enagi, I. A., Kuta, A., Abdulrahaman, S., and Somma, S.A. (2015). Stability analysis of the disease free equilibrium state of a mathematical model of ebola fever disease epidemic. International Journal of Innovation in Science and Mathematics, 3(2): 118–123.

[2] Abba B. G, Enahoro A.I., Calistus N. N., and Elamin H.E. (2021). A primer on using mathematical COVID-19 dynamics: Modeling , analysis and simulations. Infectious disease modelling, 6:148-168.

[3] Adesoye I.A., Olumuyiwa, J.P., Hammed. A.O., Oguntolu, F.A., Kayode O., Abdullahi A.I., and Iliyas K. (2021). Mathematical model of COVID-19 in Nigeria with optimal control. Sciencedirect.com/science/article/pii/S2211379721006951.

[4] Akinwande, N.I. (1995). Local stability analysis of equilibrium state of a mathematical model of yellow fever epidemics. J. Nig. Math Soc., 14: 73-79.

[5] Calistus, N.N., Iboi E., and Eikenberry,S., Scotch, M., MacIntyre, C.R., Bonds, M.H., and Gumel, A.B. Mathematical assessment of the impact of non-pharmaceutical interventions on curtailing the 2019 novel Coronavirus. https://doi.org/10.1016/j.mbs.2020.108364

[6] Federal Ministry of Health. https://www.health.gov.ng-/index

[7] Manuel, A.A., Mario S - C , and Velasco-Hernandez, J.X. (2020). Modeling behavioral change and COVID-19 containment in Mexico: A trade-off between lockdown and compliance, Maths. Biosci., 325:1-9.

[8] Nigeria Center for Disease Control (NCDC) https://.covid19.ncdc.gov.ng/advisory/

[9] Public Health Advisory on Covid-19 NCDC 2022

[10] Nigeria Center for Disease Control (NCDC) https://covid19.ncdc.gov.ng

[11] World Health Organisation Coronavirus disease (COVID-19) (2021)- https://www.who.int-health-topic

[12] World Health Organization, Coronavirus disease (COVID-19) technical guidance, WHO (2020) https://www.who.int/emergencies/diseases/novel-coronavirus2019/technical-guidance. (Accessed July 2022)

[13] World Health Organization, Coronavirus disease (COVID-19) technical guidance, WHO (2022) https://www.who.int/emergencies/diseases/novel-coronavirus-2019/situation-reports. (Accessed August 2022)

[14] World Health Organisation WHO Policy Brief: Maintaining Infection Prevention And Control Measures For COVID-19 In Health Care Facilities, WHO 2022.

International Journal of Mathematical Analysis and Modelling
Volume 5, Issue 4, November 2022, Pages 89 – 94

Construction of prior probability distribution using a mollified functional

S.J. Yaga*†, N.P. Dibal*, I.E. Gongsin*, H.R. Bakari*, S.C. Nwaosu‡, and Zara Wudiri§

Abstract

In this paper, we proposed a new class of prior distribution, the Mollified Functional Data Informative Prior using the convolution of standard scaled mollified functional and sampling distribution of the data. We also show that the MFDIP possesses the invariance property to reparameterization and apply the MFDIP to derive the prior for exponential probability distribution.

Keywords: mollifier; mfdip; invariance property; prior probability distribution; parametric functions

1 Introduction

Bayes introduced the notion of inverse probability in doctrine of chances and Laplace did further extensive work. The basic idea in both of their work is that, when there is no prior specified in advance, the uniform prior is use as the prior distribution, but uniform prior has limitations, one of them, is that it does not possess the property of invariance to reparameterization. Kass and Wasserman [1] discussed formal rules of constructing prior distribution, and reference priors [2].

Non-informative prior is formulated in [3], [4]. Structural rules for determining prior distribution as a standard of reference is considered in [5], these rules, use the case when the parameter space is compact. Several modifications were done to this scheme and later, justified the method by looking at the invariance property of the prior under reparameterization. A frequentist approach for constructing prior was discussed in [6] as second order probability matching priors, probability matching equation for parametric function [7], is based on a differential equation that a prior must satisfy if the posterior density is one-sided and the frequentist equalize up to $O(n^{-1})$. Analytic results for Maximal Data Informative Prior (MDIP) densities are described [8], [9], [10], [11], formally adopting calculus of variation. The Summary of past and recent results relating MDIP densities and extensions are found in [12], [13] and an application of MDIP on two-parameter Gamma distribution [14]. [15] Estimate quadratic function of multivariate normal mean and identified the drawbacks of some alternative Bayesian Non-informative priors. The aim of this paper

*Department of Mathematical Sciences, University of Maiduguri, Maiduguri, Nigeria
† Correspondence Author. E-mail: Samailajyaga@unimaid.edu.ng
‡ Department of Statistics, University of Agriculture, Makurdi, Nigeria
§ College of Medical Sciences, Department of Community Medicine, University of Maiduguri, Maiduguri, Nigeria

is to propose a new class prior called mollified functional prior for one-dimensional parametric functions.

2 Mollifier

A mollifier is a family of functions ϕ_d, or non-negative function satisfying the following conditions
$\phi_d(\theta) \geq 0 \; for \; all \; \theta \in \mathbb{R}^n$, for all $d > 0$
$\phi \in C_c^\infty(\mathbb{R}^n)$
$\|\phi\|_1 = 1$ or $\int \phi_d(\theta) d^n \theta = 1$.

A standard mollifier, is given by the function

$$\phi(\theta) = K_v \psi(1 - \|\theta\|^2) = \begin{cases} 0, & for \; \|\theta\| \geq 1 \\ K_\sigma \exp\left(-\frac{1}{1 - \|\theta\|^2}\right), & for \; \|\theta\| < 1 \end{cases} \tag{1}$$

K_v is define such that the integral is normalized. The function can be generalized to multi-dimensional case but we will stick to one-dimension. The function $\phi(\theta)$ is smooth, when we use substitution and differentiate the function. We will scale the mollifier using the function

$$\phi_d(\theta) = \frac{1}{d^v} \phi\left(\frac{\theta}{d}\right). \tag{2}$$

The function in (2) is such a case where the mass is preserved $\|\phi\|_1 = 1$, and concentrate more around the origin like Dirac delta function, where the density is zero everywhere except at point zero, then is an approximate identity. We normalized the mollifier over the region $\mathbb{R}^v$ to get

$$\int \phi_d(\theta) d\theta = \int \frac{1}{d^v} \phi\left(\frac{\theta}{d}\right) d\theta = \int \phi(y) dy = 1. \tag{3}$$

3 Convolution of function by mollifiers

Given a smooth function f, the convolution of f by the mollifier $\phi_d(\theta)$ is

$$f_d(\theta) = (f * \phi_d)(\theta) = \int f(\theta - u) \phi_d(u) du = \int f(u) \phi_d(\theta - u) du, \tag{4}$$

$f_d(\theta)$, is a weighted smoothed average over all the values of, f in the ball $B_d(\theta)$ of radius d and center θ. We illustrate this using the function

$$\psi_d(\theta) = a\big(B_1(0)\big)^{-1} \chi_{B_1(0)}(\theta), \tag{5}$$

ψ_d , satisfies similar properties as ϕ_d except it is not smooth. We define

$$\psi_d(\theta) = \frac{1}{d^v} \psi\left(\frac{\theta}{d}\right). \tag{6}$$

The convolution

$$(f * \psi_d)(\theta) = \int f(u)\psi_d(\theta - u)du = a\big(\mathrm{B}_1(0)\big)^{-1} \int f(u)du, \tag{7}$$

is the average value of f over the ball $\mathrm{B}_d(\theta)$ of radius d and center θ, since $\phi_d \geq 0$ and has integral one over $\mathrm{B}_d(\theta)$. We can consider $(f * \psi_d)(\theta)$ to be weighted average of f over $\mathrm{B}_d(\theta)$.

4 New class of mollified functional priors

In constructing this new class of prior density, we consider a prior that will have the property of invariance and reflect the frequentist density function. First, we will use the standard mollifier

$$\phi(\theta) = K_v\psi(1 - \|\theta\|^2) = K_\sigma \exp\left(-\frac{1}{1 - \|\theta\|^2}\right), for \ \ \|\theta\| < 1, \tag{8}$$

and we scale (8) with (2) to get

$$\phi_d(\theta) = \frac{1}{d^v} k_\sigma \psi\left(1 - \left\|\left(\frac{\theta}{d}\right)^2\right\|\right), for \ \ \|\theta\| < 1. \tag{9}$$

Our prior is a function of the Fisher information since is sensitive to parameter changes.

We define $d = I(\theta)$ and equation (9) becomes

$$\phi_d(\theta) = \frac{1}{|I(\theta)|^v} k_\sigma \psi\left(1 - \left\|\left\{\frac{\theta}{\mathrm{I}(\theta)}\right\}^2\right\|\right), for \ \ \|\theta\| < 1, v = 1,2,3, \ldots, n \tag{10}$$

where v , is the dimension for the parameter of the distribution and for one-dimensional parameter $v = 1$ and when two $v = 2$ etc. hence, the function

$$\psi\left(1 - \left\|\left(\frac{\theta}{|\mathrm{I}(\theta)|}\right)^2\right\|\right) = \exp\left\{-\frac{\mathrm{I}(\theta)}{[\mathrm{I}(\theta)]^2 - \|\theta\|^2}\right\}. \tag{11}$$

Substituting in (10) we have

$$\phi_d(\theta) = \frac{1}{|I(\theta)|^v} k_\sigma \exp\left\{-\frac{\mathrm{I}(\theta)}{[\mathrm{I}(\theta)]^2 - \|\theta\|^2}\right\}. \tag{12}$$

Theorem 1
A density function ϕ_d, (mollifier) with zero mass everywhere except at point zero, and given a smooth function f, without changing the properties of the function, the convolution is the average of the mollifier and the density function.

Proof

Using equation (7) and $\psi_d(\theta) = a\big(B_1(0)\big)^{-1}\chi_{B_1(0)}(\theta)$, where $\chi_{B_1(0)}(\theta)$ is the characteristic function, the convolution

$$(f * \psi_d)(\theta) = \int f(u)\psi_d(\theta - u)du = a\big(\mathrm{B}_1(0)\big)^{-1}\int f(u)du. \tag{13}$$

Using the ball with radius 1 at the center 0, we get the relation $a\big(\mathrm{B}_1(0)\big)^{-1}\int f(u)du = 1$, over a region $\mathbb{R}$. The normalization is because of area of the ball $\psi_d(\theta)$.

Theorem 2

Suppose we have a data model that follows an exponential density function $\psi(x|\theta)$. Under this condition, the prior distribution Mollified Functional Data Informative (MFDIP) Prior denoted by $\phi_d(\theta)$ for the parameter θ, is given by

$$\phi_d = \frac{\theta^2}{n}k_\sigma \exp\left(-\frac{n}{n^2 - \theta^4}\right), \qquad \theta^4 < n^2. \tag{14}$$

Proof

For the proof, we will make use of equation (12) Firstly, we have to evaluate the Fishers Information $\mathrm{I}(\theta)$ for the exponential density, which is obtained after some algebra

$$\frac{d^2}{d\theta^2}\ln L[\psi(x|\theta)] = -\frac{n}{\theta^2}. \tag{15}$$

The Fisher information after substitution becomes

$$\mathrm{I}(\theta) = -E\left(\frac{d^2}{d\theta^2}\ln L[\psi(x|\theta)]\right) = \frac{n}{\theta^2}. \tag{16}$$

Substituting (16) in (12) the MFDIP for the parameter θ is given by

$$\phi_d = \frac{\theta^2}{n}\left[k_\sigma exp\left\{-\frac{n}{n^2 - \theta^4}\right\}\right]. \tag{17}$$

5 Invariance property of MFDIP

Proposition

Consider the Mollified Functional Data Informative Prior (MFDIP) ϕ_d with parameter θ. Let the function $\eta = h(\theta)$ be a smooth reparameterization, the prior density ϕ_d is invariant to change of scale defined as

$$\phi_d(\eta) = \frac{1}{|I(\eta)|^v}\left|\frac{\partial\theta(\eta)}{\partial\eta}\right| k_\sigma \exp\left\{-\frac{\mathrm{I}(\eta)}{[\mathrm{I}(\eta)]^2 - (h^{-1}(\eta))^2}\right\}. \quad (18)$$

Proof

Let $\eta = h(\theta)$ be the smooth reparameterization. We determine the inverse of function for θ and the Jacobian of the transformation, we obtain $\theta = h^{-1}(\eta)$, and the Jacobian is
$\mathcal{J}_{(\theta)} = \left|\frac{\partial\theta(\eta)}{\partial\eta}\right|$.

Since we are able to obtain the Jacobian, the new density function, is derived using the relation

$$\phi_d(\eta) = \left|\frac{\partial\theta(\eta)}{\partial\eta}\right| \phi_d\big((h^{-1}(\eta)\big),$$

to get the density

$$\phi_d(\eta) = \frac{1}{|I(\eta)|^v}\left|\frac{\partial\theta(\eta)}{\partial\eta}\right| k_\sigma \exp\left\{-\frac{\mathrm{I}(\eta)}{[\mathrm{I}(\eta)]^2 - (h^{-1}(\eta))^2}\right\}. \quad (19)$$

6 Summary and discussion

Mollifiers are functions that behave like the Dirac delta function, with zero mass everywhere except at the origin. In this study, we constructed a new class of prior for a v-dimensional parameter density function for the frequentist data model. We constructed the prior using the convolution of the scaled mollifier by preserving normalization to one of the area of the mollifier with the sampling distribution of the data. The new class of prior has the invariance property to smooth reparameterization. We obtain the prior using MFDIP for exponential density. The prior is a function of the Fisher Information.

References

[1] Kass, R and L. Wasserman (1996). The selection of prior distribution by formal rules. Journal of the American Statistical Association 431, 1343-1370
[2] Bernardo, J.M. (1979). Reference posterior distribution for Bayesian inference. Journal of Royal statistical Society Ser B, 41, 113-147
[3] Box, G.E.P, Tiao, G. (1973). Bayesian inference in statistical analysis, John Wiley and Sons.
[4] Bernardo, J.M., Smith, A.F.M (1994). Bayesian theory. New York; John Wiley and Sons, Inc.
[5] Jeffrey, H. (1946). An invariant form of prior probability in estimation problems. Proc. Royal Statistical Society. Ser. A, 186, 453-461.
[6] Mukerjee, R. andGhosh, M. (1997). Second Order probability matching priors. Biometrika, 84, 4:970-975.
[7] Datta, G.S, and Ghosh, J.K. (1994). Probability matching equations for a parametric function. Purdue University, Tech Report, 94-23C.
[8] Good, I.J. (1956). Some terminology and notation in Information theory. Proc of the Institute of Electrical Engineers, C, 103, 200-204.
[9] Lindley, D.V. (1956). On a measure of information provided by an experiment. Annals of Mathematical Statistics, 27, 986-1005.
[10] Shannon, C.E. (1948). A Mathematical theory of communication. Bell System Technical

Journal, 27, 623-659.
[11] Zellner, A. (1977). Maximal data informative prior distribution in new developments in the application of Bayesian methods. Eds. A. Aykac and C. Brumal, Amsterdam North-Holland, 201-215
[12] Zellner, A. (1984). Maximal data informative prior distributions, basic issues in econometrics, The University of Chicago Press, USA.
[13] Tibshirani, R. (1989). Non-informative priors for one parameter of many. Biometrika 3, 604-608
[14] Moala, F. A, Ramos, P.L, Achcar, J.A. (2013). Bayesian inference for two-parameter gamma distribution assuming different non-informative priors. Revista Colombiana de Estadistica, 36, 321-338.
[15] Berger, J.O, Philippe, A., Robert, C.P. (1998). Estimation of quadratic functions: non-informative priors for non-centrality parameters. Statistica Sinica, 8, 358-375.

Thermal explosion with convection in porous media: a mathematical approach

R.O. Olayiwola*†, S.I. Yusuf*, A.D. Abubakar‡, K.J. Audu*, I.B.S. Mohammed§, E.O. Anyanwu, U.A. Abdullahi*, and J.P. Oyubu***

Abstract

This paper studies the interaction between natural convection and thermal explosion in porous media. The model consists of the heat equation with a nonlinear source term describing heat production due to an exothermic chemical reaction coupled with the Darcy law. The conditions for the existence of unique solutions of the energy equation are established by the Lipschitz continuity approach. The analytical solution is obtained via Olayiwola's generalized polynomial approximation method (OGPAM), which shows the influence of the parameters involved on the system. The effect of changes in values of parameters such as the Frank-Kamenetskii number, Rayleigh number, and inverse of Vadasz number are presented graphically and discussed. The results revealed that convection can change the conditions of thermal explosion.

Keywords and Phrases: convection; explosion; first-order reaction; OGPAM; porous medium; thermal explosion; mathematical approach

1 Introduction

An explosion describes the spontaneous development of the rapid rate of heat release by a chemical reaction in an initially nearly homogeneous system. The rate of reaction changes rapidly with temperature. Hence, the temperature may be used to describe the changes within an explosion process [5].

The theory of heat explosion began from the classical works by Semenov [20] and Frank-Kamenetskii [8]. In Semenov's theory, the temperature distribution in the vessel is supposed to be uniform. An average temperature in the vessel is described by the ordinary differential equation

$$\frac{d\theta}{dt} = \exp(\theta) - \lambda\theta \,. \tag{1}$$

* Department of Mathematics, Federal University of Technology, Minna, Nigeria
† Corresponding Author. E-mail.: olayiwola.rasaq@futminna.edu.ng
‡ Department of Mathematics, Federal University Gashua, Nigeria
§ Department of Mathematics, Federal Polytechnic, Bida, Nigeria
** Department of Mathematics and Statistics, Federal University Wukari, Nigeria

The first term on the right-hand side corresponds to heat production due to an exothermic chemical reaction, and the second term to heat loss through the boundary of the vessel. In Frank-Kamenetskii's theory, the spatial temperature distribution is taken into account. The model consists of the reaction-diffusion equation,

$$\frac{d\theta}{dt} = \Delta\theta + F_K \exp(\theta), \tag{2}$$

where the first term on the right-hand side describes heat diffusion, F_K is called the Frank-Kamenetskii parameter. This equation is considered in a bounded domain with the zero boundary condition for the dimensionless temperature.

In both models, heat explosion was treated as an unbounded growth of temperature (blow-up solution). Thus, the problem of heat explosion was reduced to the investigation of the existence, stability, and bifurcations of stationary solutions of differential equations.

The effect of natural convection on heat explosion was first studied in [11, 16]. It was shown that the critical value of the Frank-Kamenetskii parameter increases with the Rayleigh number and explosion can be prevented by vigorous convection. These works were continued by [4, 6, 7, 14] where new stationary and oscillating regimes were found. The authors showed how complex regimes appeared through successive bifurcations leading from a stable stationary temperature distribution without convection to a stationary symmetric convective solution, stationary asymmetric convection, periodic in-time oscillations, and finally periodic oscillations. Oscillating heat explosion, where the temperature grows and oscillates, was discovered. The effects of natural convection and consumption of reactants on heat explosion in a closed spherical vessel were studied in [15]. The influence of stirring on the limit of the thermal explosion was investigated in [10]. Heat explosion with convection in a horizontal cylinder was considered in [19].

All these works study heat explosion in a gaseous or liquid medium with its motion described by the Navier-Stokes equations under the Boussinesq approximation. Thermal ignition in a porous medium is investigated in [13]. The Darcy law in a quasi-stationary form under the Boussinesq approximation is used to describe fluid motion. It is shown that convection decreases the maximal temperature and increases the critical value of the Frank-Kamenetskii parameter. The interaction of free convection and exothermic chemical reaction is studied in [21]. The authors consider zero-order exothermic reactions in a rectangular domain and find the onset of convection by an approximate analytical method. A similar problem with the depletion of reactants is investigated in [9]. The ignition time of heat explosion in a porous medium with convection is found in [22]. Heat explosion in one-dimensional flow in a porous medium is studied in [3].

In this paper, an approximate analytical solution capable of predicting the temperature distribution in a process of thermal explosion with convection in porous media is presented.

2 Model formulation

Here, we consider the first-order reaction,

$$A \xrightarrow{K(T)} B, \tag{3}$$

and the temperature dependence of the reaction rate $K(T)$ given by the Arrhenius law:

$$K(T) = k_0 \exp\left(-\frac{E}{RT}\right), \tag{4}$$

where E is the activation energy, T the temperature, R the universal gas constant, and k_0 the pre-exponential factor.

The system is considered in a $2D$ square domain, $0 \le x \le L$, $0 \le y \le L$. Depletion of reactants in the heat balance equation is neglected. It is a conventional assumption in the theory of heat explosion. The model consists of the $2D$ reaction-diffusion equation with convective terms, continuity, and non-stationary Darcy equations for an incompressible fluid:

$$\frac{\partial u}{\partial x} + \frac{\partial v}{\partial y} = 0, \tag{5}$$

$$\frac{\partial u}{\partial t} + \frac{\mu}{K}u + \frac{\partial p}{\partial x} = 0, \tag{6}$$

$$\frac{\partial v}{\partial t} + \frac{\mu}{K}v + \frac{\partial p}{\partial y} = g\beta\rho(T - T_0), \tag{7}$$

$$\frac{\partial T}{\partial t} + u\frac{\partial T}{\partial x} + v\frac{\partial T}{\partial y} = \frac{k}{\rho c_p}\left(\frac{\partial^2 T}{\partial x^2} + \frac{\partial^2 T}{\partial y^2}\right) + \frac{qk_0}{\rho c_p}\exp\left(-\frac{E}{RT}\right). \tag{8}$$

The initial and boundary conditions are specified as:

$$\left.\begin{array}{c} u(x,y,0) = 0 \\ v(x,y,0) = 0 \\ T(x,y,0) = T_0(\in(x+y)+1), \quad \left.\frac{\partial T}{\partial x}\right|_{x=0} = 0, \quad T(x,0,t) = T_0, \quad \left.\frac{\partial T}{\partial x}\right|_{x=L} = 0, \quad T(x,L,t) = T_0 \end{array}\right\} \tag{9}$$

Here u denotes the fluid velocity along the x-axis, v is the fluid velocity along the y-axis, p is the pressure, k the thermal conductivity, μ the kinematic viscosity, ρ the density, q the heat release, g is the acceleration due to gravity, T_0 the characteristic value of the temperature, U_0 the characteristic value of the velocity, K the permeability.

3 Method of solution

3.1 Dimension analysis

Dimensionless variables are been introduced as:

$$\left.\begin{array}{c} x' = \dfrac{x}{L}, \quad y' = \dfrac{y}{L}, \quad t' = \dfrac{kt}{\rho c_p L^2}, \quad u' = \dfrac{\rho c_p L u}{k}, \quad v' = \dfrac{\rho c_p L v}{k}, \\ p' = \dfrac{\rho c_p K p}{k\mu}, \quad \theta = \dfrac{E(T - T_0)}{RT_0^2}, \quad \in = \dfrac{RT_0}{E}, \end{array}\right\} \tag{10}$$

Using (10), and after dropping the prime, equations (5) - (9) become

$$\frac{\partial u}{\partial x} + \frac{\partial v}{\partial y} = 0, \tag{11}$$

$$\sigma \frac{\partial u}{\partial t} + u + \frac{\partial p}{\partial x} = 0, \tag{12}$$

$$\sigma \frac{\partial v}{\partial t} + v + \frac{\partial p}{\partial y} = R_p \theta, \tag{13}$$

$$\frac{\partial \theta}{\partial t} + u\frac{\partial \theta}{\partial x} + v\frac{\partial \theta}{\partial y} = \left(\frac{\partial^2 \theta}{\partial x^2} + \frac{\partial^2 \theta}{\partial y^2}\right) + \delta \exp\left(\frac{\theta}{1 + \in \theta}\right), \tag{14}$$

$$\left.\begin{array}{c} u(x, y, 0) = 0 \\ v(x, y, 0) = 0 \\ \theta(x, y, 0) = (x + y), \quad \left.\dfrac{\partial \theta}{\partial x}\right|_{x=0} = 0, \quad \theta(x, 0, t) = 0, \quad \left.\dfrac{\partial \theta}{\partial x}\right|_{x=1} = 0, \quad \theta(x, 1, t) = 0 \end{array}\right\} \tag{15}$$

where

$\sigma = \dfrac{kK}{\rho c_p L^2 \mu} = \dfrac{1}{V_a}$ stands for the inverse of the Vadasz number, $V_a = \dfrac{P_r}{D_a}$, $P_r = \dfrac{\rho c_p \mu}{k}$ is the Prandtl number and $D_a = \dfrac{K}{L^2}$ is the Darcy number, $\delta = \dfrac{q k_0 L^2}{k \in T_0} e^{-\frac{E}{RT_0}}$ is the Frank-Kamenetskii parameter, $R_p = \dfrac{g\beta\rho K \rho c_p L \in T_0}{k\mu} = \dfrac{K\rho}{L^2} R_a$, $R_a = \dfrac{g\beta \in T_0 \rho c_p L^3}{k\mu}$ is the Rayleigh number.

Introducing the following new space variable (Olayiwola [18]):

$$z = x + y. \tag{16}$$

Then, equations (11) – (15) reduce to

$$\frac{\partial U}{\partial z} = 0, \tag{17}$$

$$\sigma \frac{\partial U}{\partial t} + U + 2\frac{\partial p}{\partial z} = R_p \theta , \tag{18}$$

$$\frac{\partial \theta}{\partial t} + U\frac{\partial \theta}{\partial z} = 2\frac{\partial^2 \theta}{\partial z^2} + \delta \exp\left(\frac{\theta}{1+\in\theta}\right), \tag{19}$$

$$\left.\begin{array}{c} U(z,0)=0 \\ \theta(z,0)=z, \quad \left.\frac{\partial \theta}{\partial z}\right|_{z=0} + \theta(0,t)=0, \quad \left.\frac{\partial \theta}{\partial z}\right|_{z=2} + \theta(2,t)=0 \end{array}\right\}, \tag{20}$$

where
$U = u + v$.

3.2 Properties of solution

Theorem 1: Then there exists a unique solution $U(z,t),\ \ p(z,t),\ \theta(z,t)$ of (17) – (19) which satisfies (20).

Proof: Clearly $\delta \exp\left(\frac{\theta}{1+\in\theta}\right)$ is Lipschitz continuous. Hence by Ayeni [2], the result follows. This completes the proof.

Theorem 2: Let $\theta(z,t)=\phi(z,t)\exp\left(\frac{U}{4}z-\frac{U^2}{8}t\right),\ \ \eta=\sqrt{2}\,z$. Then $\frac{\partial \phi}{\partial t}\geq 0$.

In the proof, we shall need the following lemma of Kolodner and Pederson [12].

Lemma (Kolodner and Pederson [12]): Let $u(y,t)=O\left(e^{\alpha|y|^2}\right)$ be a solution on $R^n \times [0,t_0)$ of the differential inequality

$$\frac{\partial u}{\partial t} - \Delta u + k(y,t)u \geq 0 \tag{21}$$

where k is bounded from below. If $u(y,0)\geq 0$, then $u(y,t)\geq 0$ for all $(y,t)\in R^n \times [0,t_0)$.

Proof of Theorem 2: Let $\theta(z,t)=\phi(z,t)e^{\left(\frac{U}{4}z-\frac{U^2}{8}t\right)},\ \ \eta=\sqrt{2}\,z,\ \ p=\frac{\partial \phi}{\partial t}$.

Then

$$\frac{\partial p}{\partial t} - \frac{\partial^2 p}{\partial \eta^2} - \frac{\delta}{\left(1+\in\phi(z,t)e^{\left(\frac{U}{4}z-\frac{U^2}{8}t\right)}\right)^2} e^{\frac{\phi(z,t)e^{\left(\frac{U}{4}z-\frac{U^2}{8}t\right)}}{1+\in\phi(z,t)e^{\left(\frac{U}{4}z-\frac{U^2}{8}t\right)}}} p \geq 0$$

$$p(\eta,0)\geq 0.$$

Now

$$-\frac{\delta}{\left(1+\in\phi(z,t)e^{\left(\frac{U}{4}z-\frac{U^2}{8}t\right)}\right)^2}e^{\frac{\phi(z,t)e^{\left(\frac{U}{4}z-\frac{U^2}{8}t\right)}}{1+\in\phi(z,t)e^{\left(\frac{U}{4}z-\frac{U^2}{8}t\right)}}}$$ is bounded.

Hence by Kolodner and Pederson lemma $p(\eta,t)\geq 0$, i.e. $\frac{\partial\phi}{\partial t}\geq 0$. Hence $\phi(z,t)$ is a non-decreasing function of t.

3.3 Analytical solution via Olayiwola's generalized polynomial approximation method

Here, in the limit $\in\to 0$, and by introducing the following new space variable:

$$\eta=\frac{z}{2}. \tag{22}$$

Equations (17) – (20) can be solved analytically using Olayiwola's generalized polynomial approximation method (OGPAM) in [17]. Follow the idea in [1], that:

$$\exp(\theta)\approx 1+(e-2)\theta+\theta^2. \tag{23}$$

Take $\frac{\partial p}{\partial\eta}=b\exp(-\lambda t)$ and let $0<R_p<<1,\ \delta=aR_p$ such that

$$\left.\begin{aligned} U(\eta,t)&=U_0(\eta,t)+R_pU_1(\eta,t)+\ldots\\ \theta(\eta,t)&=\theta_0(\eta,t)+R_p\theta_1(\eta,t)+\ldots\end{aligned}\right\} \tag{24}$$

and using OGPAM in [17], we obtain the solutions to (17) - (20) as:

$$U(\eta,t)=\beta\left(e^{-\frac{1}{\sigma}t}-e^{-\lambda t}\right)+R_p\left(\frac{1}{\sigma}\sqrt{\frac{\pi}{m_0}}\left(3\eta-3\eta^2+\eta^3\right)\begin{pmatrix}erf\left(\frac{m_2}{2\sqrt{m_0}}\right)+\\ erf\left(\frac{2m_0t-m_2}{2\sqrt{m_0}}\right)\end{pmatrix}\right)e^{\left(\frac{m_2^2}{4m_0}-\frac{1}{\sigma}t\right)} \tag{25}$$

$$\theta(\eta,t)=3\theta_0\big|_{\eta=1}-3\theta_0\big|_{\eta=1}\eta+\theta_0\big|_{\eta=1}\eta^2+R_p\left(3\theta_1\big|_{\eta=1}-3\theta_1\big|_{\eta=1}\eta+\theta_1\big|_{\eta=1}\eta^2\right), \tag{26}$$

where

$$\theta_0\big|_{\eta=1}=2\eta e^{-\left(c_0t-m_0t^2-m_1t^3\right)}$$

$$\theta_1\big|_{\eta=1} = e^{-\left(c_0 - m_7 t - m_8 t^2\right)} \left(\begin{array}{l} \frac{a}{2A}\sqrt{\frac{\pi}{m_8}}\left(erf\left(\frac{2m_8 t + m_7}{2\sqrt{m_8}}\right) - erf\left(\frac{m_7}{2\sqrt{m_8}}\right)\right) e^{\frac{4c_0 m_8 + m_7^2}{4m_8}} - \\ \frac{3a(e-2)}{4A}\sqrt{\frac{\pi}{-m_{10}}}\left(erf\left(\frac{2m_{10} t - m_9}{2\sqrt{-m_{10}}}\right) + erf\left(\frac{m_9}{2\sqrt{-m_{10}}}\right)\right) e^{\frac{4c_0 m_{10} - m_9^2}{4m_{10}}} - \\ \frac{36a}{28A}\sqrt{\frac{\pi}{-m_{12}}}\left(erf\left(\frac{2m_{12} t - m_{11}}{2\sqrt{-m_{12}}}\right) + erf\left(\frac{m_{11}}{2\sqrt{-m_{12}}}\right)\right) e^{\frac{4c_0 m_{12} - m_{11}^2}{4m_{12}}} - \\ \frac{86}{240\sigma A}\sqrt{\frac{\pi}{-m_{15} m_0}}\left(erf\left(\frac{2m_0 t - m_2}{2\sqrt{m_0}}\right) + erf\left(\frac{m_2}{2\sqrt{m_0}}\right)\right) \\ \left(erf\left(\frac{2m_{10} t - m_{14}}{2\sqrt{-m_{10}}}\right) + erf\left(\frac{m_{14}}{2\sqrt{-m_{10}}}\right)\right) e^{\frac{4m_{13} m_{10} - m_{14}^2}{4m_{15}}} \end{array} \right),$$

$$A = \frac{11}{6},\ c_0 = \frac{1}{2A},\ \beta = \frac{b}{1-\sigma\lambda},\ c_1 = \frac{\beta}{A}\left(\frac{\sigma\lambda - 1}{\sigma}\right),\ c_2 = \frac{\beta}{A}\left(\frac{1}{2\sigma^2} - \frac{\lambda^2}{2}\right),\ m_0 = \frac{c_1}{2},\ m_1 = \frac{c_2}{3},$$

$$m_2 = \left(\frac{1}{\sigma} - c_0\right),\ m_3 = \beta\left(\frac{\sigma\lambda - 1}{\sigma}\right),\ m_4 = \beta\left(\frac{1}{2\sigma^2} - \frac{\lambda^2}{2}\right),\ m_5 = \frac{m_2^2}{4m_0},\ m_6 = \left(\frac{1}{\sigma} + c_0\right),\ m_7 = \frac{m_3}{A},$$

$$m_8 = \frac{m_4}{A},\ m_9 = (m_7 + c_0),\ m_{10} = (m_0 - m_8),\ m_{11} = (m_7 + 2c_0),\ m_{12} = (2m_0 - m_8),\ m_{13} = (m_5 + c_0),$$
$$m_{14} = (m_7 + m_6)$$

The computation was done on equations (25) and (26) using the computer symbolic algebraic package MAPLE 2021 version.

4 Results and discussion

The simulation was carried out to show the impact of the model parameters by employing Olayiwola's Generalized Polynomial Approximation Method (OGPAM) on the equations (17) – (20). We are concerned with the nature of the solutions obtained for different values of δ, R_p and σ. The computation of equations (25) and (26) was done using the MAPLE 2021 version.

Figure 1 shows the temperature history at $x = 1,\ y = 1$ for $\sigma = 2,\ R_p = 0.1\ \delta = 0.4,\ 0.6,\ 0.8$. The graph displays an increase in maximum temperature with time as the Frank-Kamenetskii number increases. If δ is sufficiently large, the temperature becomes unbounded, which corresponds to the thermal explosion.

Figure 2 displays the temperature topography for $\sigma = 2,\ R_p = 0.1\ \delta = 0.4,\ 0.6,\ 0.8$. The graph reveals a decrease in temperature along the spatial coordinates while this temperature increases as the Frank-Kamenetskii number increases.

Figure 3 shows the temperature history at $x = 1,\ y = 1$ for $\delta = 0.4,\ \sigma = 2\ R_p = 0.1,\ 0.2,\ 0.3$. The graph displays an increase in maximum temperature with time as the Rayleigh number increases.

Figure 4 depicts the velocity history at $x = 1,\ y = 1$ for $\delta = 0.4,\ \sigma = 2\ R_p = 0.1,\ 0.2,\ 0.3$. After the first oscillation, the graph displays a rapid transition to a steady solution. Meanwhile, the graph displays an increase in maximum velocity with time as the Rayleigh number increases.

Figure 5 displays the velocity topography for $\delta = 0.4,\ \sigma = 2\ R_p = 0.1,\ 0.2,\ 0.3$. The graph reveals a steady velocity along the spatial coordinates while this velocity increases as the Rayleigh number increases.

Figure 6 shows the temperature history at $x = 1,\ y = 1$ for $\delta = 0.4,\ R_p = 0.1,\ \sigma = 0.2,\ 2,\ 20$ which an increase in temperature exists when $\sigma \geq 2$. When $2 \leq \sigma < \infty$ (convection), the solution remains bounded (no explosion) but when $\sigma \to 0,\ U(x, y, t) \to \infty$ (convection), however, oscillations are generated (no explosion). It can be stationary or oscillating with convection. When $\sigma \to \infty,\ U(x, y, t) \to 0$ (no convection), then stationary solutions do not exist, and the solution of the evolution problem grows to infinity ($\theta(x, y, t) \to \infty$). This case corresponds to the thermal explosion.

Figure 7 depicts the temperature topography for $\delta = 0.4,\ R_p = 0.1,\ \sigma = 0.2,\ 2,\ 20$. The graph reveals a decrease in temperature along the spatial coordinates while this temperature tends to zero when $\sigma \to \infty$ and it is at maximum value when $\sigma \to 0$.

Figure 8 shows the velocity history at $x = 1,\ y = 1$ for $\delta = 0.4,\ R_p = 0.1,\ \sigma = 0.2,\ 2,\ 20$ which there is a rapid transition to a steady solution when $\sigma = 0.2$ and $\sigma = 2$. Stable solutions exist after oscillation and are achieved faster when $\sigma = 0.2$, $\sigma = 2$ than when $\sigma = 20$.

Figure 9 displays the velocity topography for $\delta = 0.4,\ R_p = 0.1,\ \sigma = 0.2,\ 2,\ 20$. The graph reveals a steady velocity along the spatial coordinates while this velocity tends to zero when $\sigma \to \infty$ and it is at maximum value when $\sigma \to 0$.

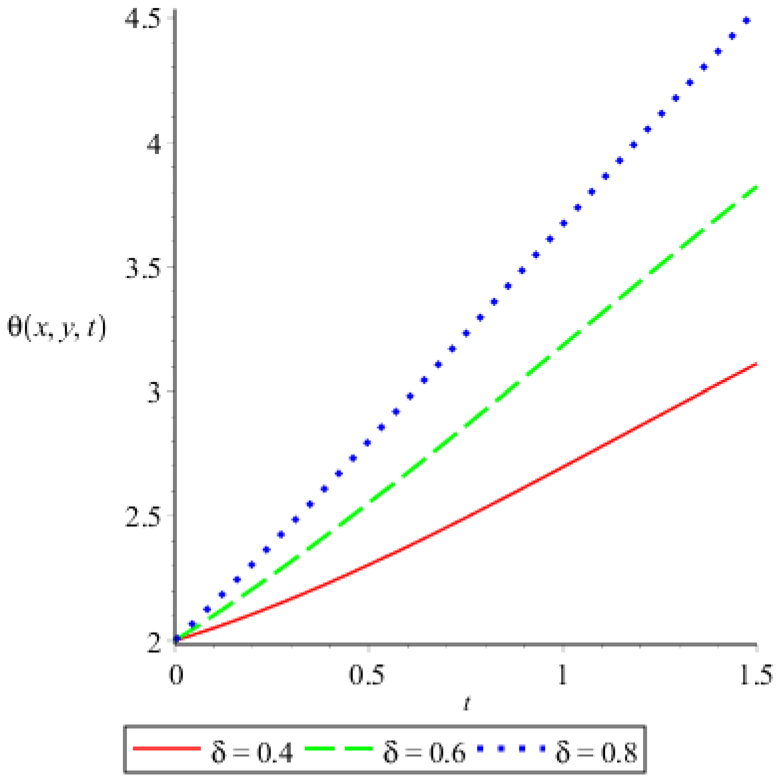

Figure 1: Temperature history at $x = 1,\ y = 1$ for $\sigma = 2.0,\ R_p = 0.1,\ \delta = 0.4,\ 0.6,\ 0.8$.

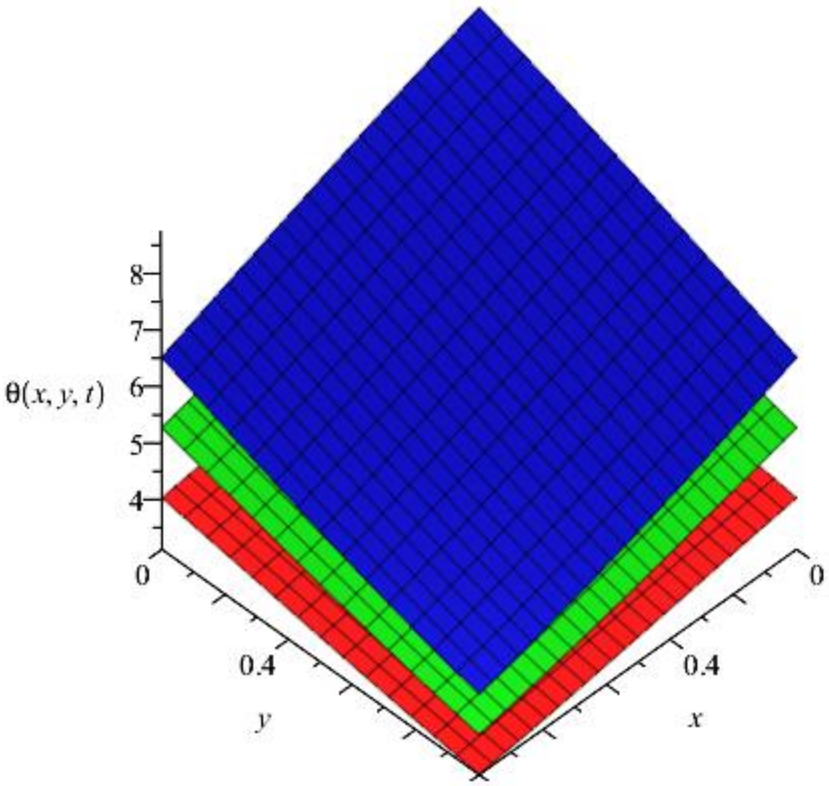

Figure 2: Temperature topography for $\sigma = 2.0,\ R_p = 0.1,\ \delta = 0.4,\ 0.6,\ 0.8$.

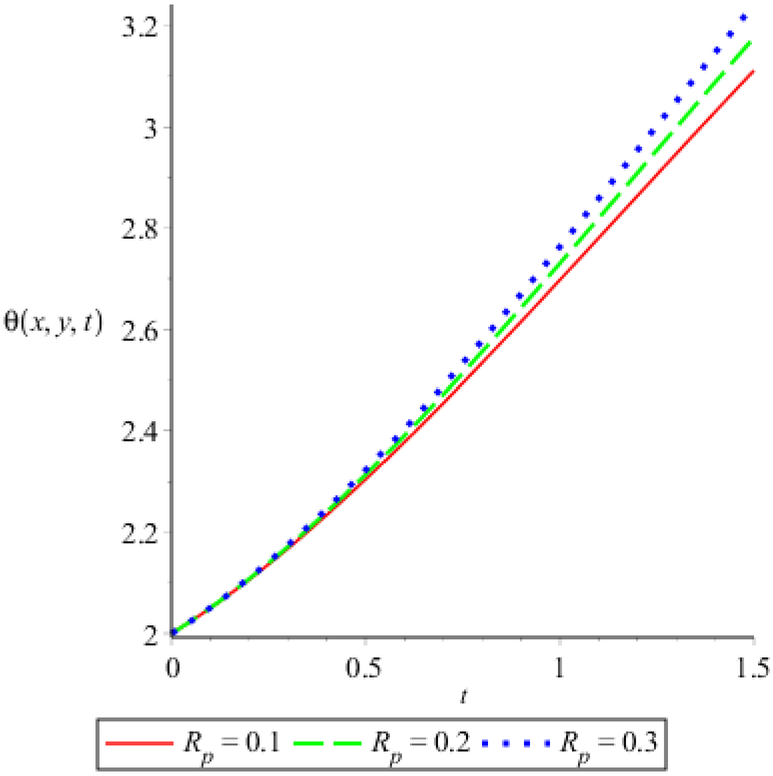

Figure 3: Temperature history at $x = 1,\ y = 1$ for $\sigma = 2.0,\ \delta = 0.4,\ \ R_p = 0.1,\ 0.2,\ 0.3$.

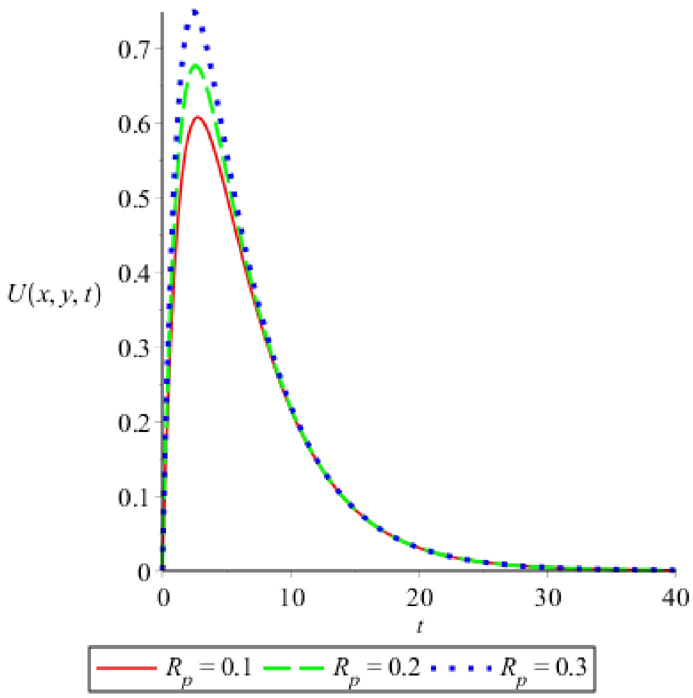

Figure 4: Velocity history at $x = 1,\ y = 1$ for $\sigma = 2.0,\ \delta = 0.4,\ \ R_p = 0.1,\ 0.2,\ 0.3$.

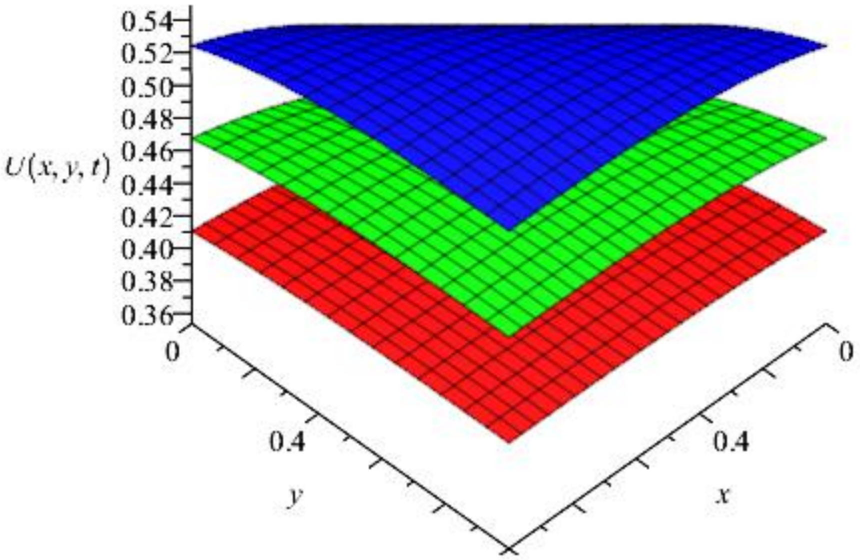

Figure 5: Velocity topography for $\sigma = 2.0$, $\delta = 0.4$, $R_p = 0.1, 0.2, 0.3$.

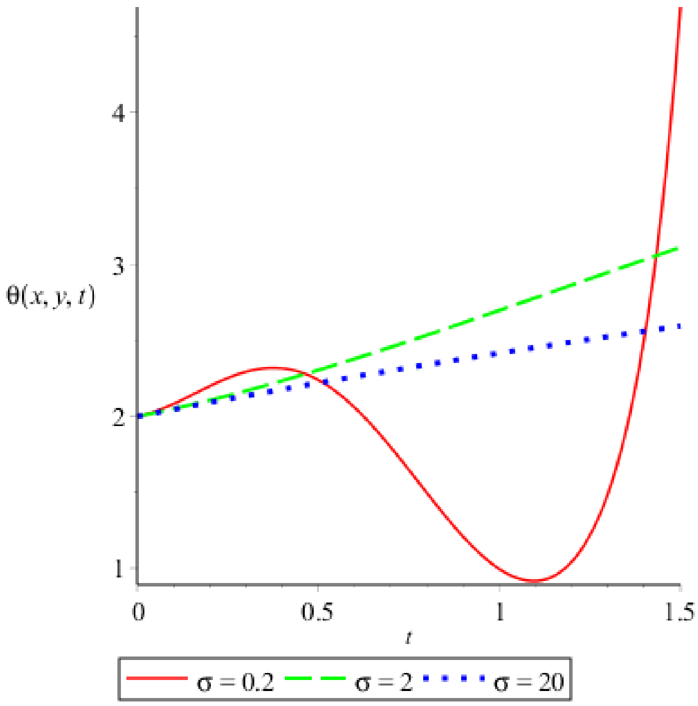

Figure 6: Temperature history at $x = 1$, $y = 1$ for $\delta = 0.4$, $R_p = 0.1$, $\sigma = 0.2, 2, 20$.

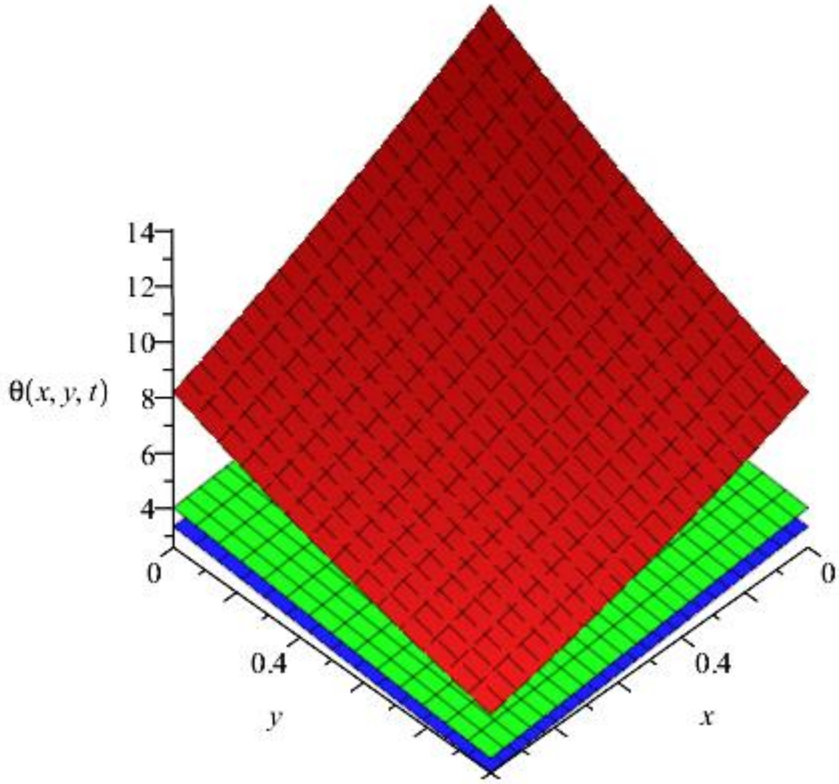

Figure 7: Temperature topography for $\delta = 0.4,\ R_p = 0.1,\ \sigma = 0.2,\ 2,\ 20$.

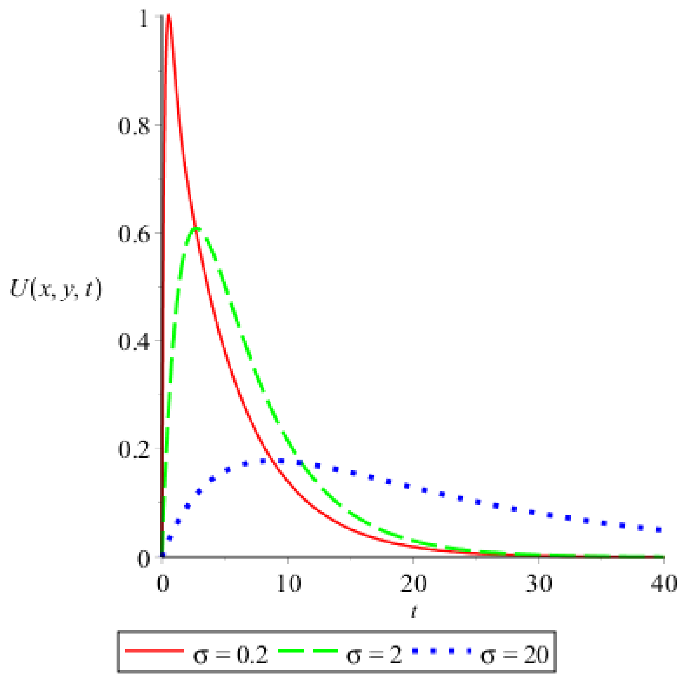

Figure 8: Velocity history at $x = 1,\ y = 1$ for $\delta = 0.4,\ R_p = 0.1,\ \sigma = 0.2,\ 2,\ 20$.

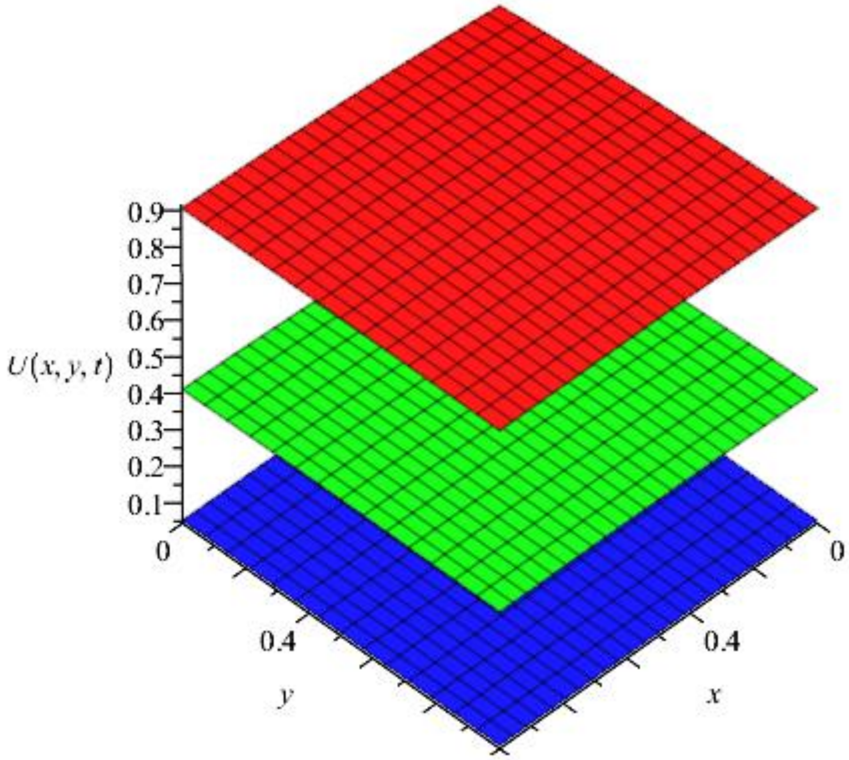

Figure 9: Velocity topography for $\delta = 0.4,\ R_p = 0.1,\ \sigma = 0.2,\ 2,\ 20$.

It is worth pointing out that the effects observed in Figures 1 - 9, are important to guide explosive materials manufacturers to provide safety precautions during storage and usage.

5 Conclusion

Here, we have presented the model describing the interaction between natural convection and thermal explosion in porous media, established the conditions for the existence of a unique solution of the model, and provided the approximate analytical solution. The existence of a unique solution to the problem implies that the problem represents a physical situation under specific conditions. The simulation results revealed the impact of the model parameters and the following conclusion can be drawn:

Temperature is a non-decreasing function of time.
If the Frank-Kamenetskii number is sufficiently large, a thermal explosion can occur.
Convection can change the conditions of a thermal explosion.

Therefore the established conditions and the results obtained are not expected to guide manufacturers of explosive materials but provide safety precautions during storage and usage.

References

[1] Ayeni, R. O. (1982). On the explosion of chain-thermal reactions. J. Austral. Math. Soc. (Series B), Vol. 24: 194 – 202.
[2] Ayeni R. O. (1978). Thermal Runway. Ph.D. Thesis. Cornel University USA.
[3] Balakotaiah V., Pourtalet P. (1990). Natural convection effects on thermal ignition in a

porous medium I. Semenov Model. Proc. R. Soc. Lond. A, Vol. 429: 533–554.

[4] Belk M. and Volpert V. (2004). Modeling of heat explosion with convection. Chaos, Vol. 14: 263–273.

[5] Chan C. Y. and Kong P. C. (1995). A thermal explosion model. Applied Mathematics and Computation, Vol. 71: 201 – 210.

[6] Ducrot A. and Volpert V. (2005). Modelling of convective heat explosion. Journal of Technical Physics, Vol. 46: 129–143.

[7] Dumont T., Genieys S., Massot M., Volpert V. (2002). Interaction of thermal explosion and natural convection: critical conditions and new oscillating regimes. SIAM J. Appl. Math., Vol. 63: 351–372.

[8] Frank-Kamenetskii D. A. (1969). Diffusion and heat transfer in chemical kinetics. Plenum Press, New York.

[9] Gatica J. E., Viljoen H. J., Hlavacek V. (1989). Interaction between chemical reaction and natural convection in porous media. Chemical Eng. Science, Vol. 44(9): 1853-1870.

[10] Kagan L., Berestycki H., Joulin G., Sivashinsky G. (1997). The effect of stirring on the limit of thermal explosion. Combustion Theory and Modelling Vol. 1: 97–111.

[11] Khudyaev S. I., Shtessel E. A., Pribytkova K. V. (1971). Numerical solution of the heat explosion problem with convection. Combustion, Explosion and Shock Waves, (Fizika goreniya i vzryva), Vol. 2: 167–178.

[12] Kolodner J. and Pederson R. H. (1966). Pointwise bounds for solutions of some semi-linear parabolic equations. J. Diff equations, 2(2), 353-364.

[13] Kordilewsky W., Krajewki J. (1984). Convection effects on thermal ignition in porous media. Chemical Eng. Science, Vol. 39 (3): 610–612.

[14] Lazarovici A., Volpert V., Merkin J. H. (2005). Steady states, oscillations and heat explosion in a combustion problem with convection. European Journal of Mechanics B/Fluids, Vol. 24: 189–203.

[15] Liu Ting-Yueh, Campbell Alasdair N., Hayhurst Allan N., Cardoso Silvana S. S. (2010). On the occurrence of thermal explosion in a reacting gas: The effects of natural convection and consumption of reactant. Combustion and Flame, Vol. 157: 230–239.

[16] Merzhanov A. S., Shtessel E. A. (1973). Free convection and thermal explosion in reactive systems. Astronautica Acta, Vol. 18: 191–193.

[17] Olayiwola, R. O. (2022). Solving parabolic equations by Olayiwola's generalized polynomial approximation method. International Journal of Mathematical Analysis and Modelling, Vol. 5(3): 24 - 43.

[18] Olayiwola R. O., Jimoh. R. O., Yusuf A. and Abubakar S. (2013). A mathematical study of contaminant transport with first-order decay and time-dependent source concentration in an Aquifer. Universal Journal of Applied Mathematics, Vol. 1(2): 112 –119.

[19] Osipov A. I., Uvarov A. V. and Roschina N. A. (2007). Influence of natural convection on the parameters of thermal explosion in the horizontal cylinder. Int. J. Heat Mass Transfer, Vol. 50: 5226–5231

[20] Semenov N. N. (1935). Chemical Kinetics and Chain Reactions. Clarendon Press, Oxford.

[21] Viljoen H. J. and Hlavacek V. (1987). Chemically driven convection in a porous medium. AIChE Journal, Vol. 33:1344–1350.

[22] Viljoen H. J., Gatica J. E. and Hlavacek V. (1988). Induction time for thermal explosion and natural convection in porous media. Chemical Eng. Science, Vol. 43 (11): 2951–2956.

International Journal of Mathematical Analysis and Modelling
Volume 5, Issue 4, November 2022, pages 109 - 131

A two-step iterative algorithm for finding common fixed point of Bregman quasi strict pseudo-contraction mappings with applications

E. Ekuma-Okereke*, **F.M. Okoro**†‡, and **C.E. Abhulimen**†§

Abstract

Motivated by some results of authors in this direction, our purpose in this paper is to construct a two-step iterative algorithm with inertial extrapolation term defined with respect to Bregman distance function for approximating common fixed points of a finite family of a closed Bregman quasi strictly pseudo-contraction mappings when the intersection of its set is assumed to be non empty. We prove a strong convergence theorem for it under flexible and relaxed conditions in real reflexive Banach space. Our algorithm is applied in solving finite convex feasibility and equilibrium problems in reflexive Banach space. Furthermore, we demonstrate numerical examples to justify the efficiency and implementability of our algorithms in a finite dimensional real Banach space. Our results improves, generalizes and complements other previously and recently cited results of some authors in the literature of our procedure. It is intended that our procedure complement our motivated result cited in the literature.

Keywords and Phrases: Bregman quasi strict pseudo-contraction mappings; common fixed point; strong convergence theorem; reflexive Banach space; Bregman distance function

1 Introduction

In this paper, all spaces are taking to be real $\mathbb{R}$, with $\mathbb{R}$ as the set of all real numbers and $\mathbb{N}$ the set of natural numbers. The extended real numbers is denoted by $\overline{\mathbb{R}}$. Let X represents reflexive real Banach space with its dual spaces denoted as X^*. Let $||.|| : X \to \mathbb{R}$ represents the norm function. Let $d_h : dom\, h \times int(dom\, h) \to \mathbb{R}^+$ represent a function induced by a convex function $h : X \to (-\infty, +\infty]$. Let $dom\, h := \{u \in X : h(x) < \infty\}$ represents the domain of the convex function h and $int(dom\, h)$ represents the interior domain of h.

A function $h^* : X^* \to (-\infty, +\infty]$ defined by

$$h^*(x^*) = sup\,\{\langle x, x^*\rangle - h(x), x \in X\}$$

is called the conjugate function of h. We see from the conjugate inequality that

$$h(x) \geq \langle x, x^*\rangle - h^*(x^*), \forall x \in X, x^* \in X^*.$$

A function h on X is coercive (see [26]), if the sublevel set of h is bounded, equivalently

$$\lim_{||x||\to\infty} h(x) = +\infty.$$

*Corresponding Author. Department of Mathematics, Federal University of Petroleum Resources, Effurun, P.M.B 1221, Nigeria; E-mail: ekuma.okereke@fupre.edu.ng

†Department of Mathematics, Ambrose Alli University, Ekpoma, Nigeria.

‡E-mail: moibi1@yahoo.com

§Email: cletusabhulimen@yahoo.co.uk

It is said to be strongly coercive (see [26]), if

$$\lim_{\|x\|\to\infty} \frac{h(x)}{\|x\|} = +\infty.$$

If for any $u \in int(dom\, h)$ and $z \in X$, we have the right-hand directional derivative given by

$$h^o(u,z) := \lim_{s\to 0^+} \frac{h(u+sz)-h(u)}{s}.$$

The convex function $h : X \to (-\infty, +\infty]$ is said to be Gâteaux differentiable at a point u if

$$\lim_{s\to 0^+} \frac{h(u+sz)-h(u)}{s}$$

exists for any z element of X. By this definition, $h^o(u,z) := \nabla h(u)$ which is the gradient of a convex function h. The function h is said to be Fréchet differentiable at x if this limit is attained uniformly in $\|y\| = 1$. The convex function h is said to be uniformly Fréchet differentiable on a subset K of X if the limit is attained uniformly for $x \in K$ and $\|y\| = 1$ [25].

Let h be a Gâteaux differentiable function at u, then the bi-function $d_h : domh \times int(domh) \to \mathbb{R}^+$ defined by

$$d_h(z,u) := h(z) - h(u) - \langle \nabla h(u), z-u \rangle \tag{1}$$

is the Bregman distance function induced by the convex function h [25], where $\langle .,. \rangle$ is the duality pairing of X and X^*. It is easy to see that (1) is not symmetric and does not satisfy the well-known triangle inequality associated with classical distance functions, but has the following nice properties (see [7, 10]):

Remark 1.1

$d_h(.,u)$ is convex

P2. $d_h(z,u)$ *is positive if and only if* $z \neq u$

P3. $d_h(z,u) = d_h(z,v) + d_h(v,u) + \langle \nabla h(v), z-v \rangle - \langle \nabla h(u), z-v \rangle$

P4. $d_h(u,v) + d_h(v,u) := \langle \nabla h(u), u-v \rangle - \langle \nabla h(v), u-v \rangle$

P5. $d_h(u,v) \leq ||u||.||\nabla h(u) - \nabla h(v)|| + ||v||.||\nabla h(u) - \nabla h(v)||$

P6. $d_h(u,u) = 0.$

Let K represent a non-void, closed and convex subset of $int(domh)$. Let $T : K \to K$ represent a self-map. The self-map T on K is said to be nonexpansive if $||Tu - Tz|| \leq ||u - z||$, $\forall u \in K$, $z \in K$. Similarly, the self-map T on K is said to be quasi-nonexpansive if $||Tu - z^o|| \leq ||u - z^o||$, $\forall u \in K$, $z^o \in Fix(T)$, where $Fix(T) := \{z^o \in K : Tu = u\}$ is the fixed point set of the self-map T on K. A point u^* is called asymptotic fixed point of a self-map T on K if there exist $u_n \subset K$ which converges weakly to u^* ($u_n \rightharpoonup u^*$) so that $||u_n - Tu_n|| \to 0$ as $n \to \infty$. The asymptotic fixed point (see [11] and the references therein) is represented by $\hat{Fix}(T)$.

A map $T : K \to int(dom\, h)$ with respect to a convex function $h : X \to (-\infty, +\infty]$ is called

1. Bregman relatively nonexpansive (shortly,(BRNE))[26, 24] if the following conditions holds

$$d_h(z^o, Tu) \leq d_h(z^o, u), \forall u \in K, \forall z^o \in Fix(T) = \hat{Fix}(T)$$

2. Bregman quasi nonexpansive (shortly,(BQNE))[34] if the following conditions holds

$$d_h(z^o, Tu) \leq d_h(z^o, u), \forall u \in K, \forall z^o \in Fix(T)$$

3. Bregman quasi strict pseudo-contraction (shortly,(BQSPC))[27] if there exists a constant $\rho \in [0,1)$ and $Fix(T) \neq \emptyset$ such that the following conditions holds

$$d_h(z^o, Tu) \leq d_h(z^o, u) + \rho d_h(u, Tu), \forall u \in K, \forall z^o \in Fix(T) \tag{2}$$

4. T is called closed if for any $\{u_n\} \subset K$ with $u_n \to u$ and $Tu_n \to z \in K$ as $n \to \infty$, then $Tu = z$.

Example 1.1 *(see [28],[29]). Let X be a smooth Banach space, $h(u) := ||u||^2, \forall u \in X$. Let $u_0 \neq 0$ be any element of X, let $T : X \to X$ be defined by*

$$T(u) := \begin{cases} \frac{2^{n+1}+2}{2(2^{n+1})} u_0 & \text{if } u = \frac{2^n+2}{2^{n+1}} u_0 \\ -u & \text{if } u \neq \frac{2^n+2}{2^{n+1}} u_0, \end{cases} \tag{3}$$

$\forall n \geq 1$. *Then T is a Bregman quasi strict pseudo-contraction with $Fix(T) = 0$.*

Example 1.2 *Let $X = \mathbb{R}$, $K = [-1,1]$, $h(u) := \frac{2}{3}u^2, \forall u \in K$. Let $T : K \to K$ be defined by*

$$T(u) := \begin{cases} u^2 + u & \text{if } u \in [-1,0] \\ u & \text{if } u \in (0,1]. \end{cases} \tag{4}$$

Then T is a Bregman quasi-strict pseudo-contraction with $Fix(T) = [0,1]$. Proof. It is obvious from the definition of fixed point set and the mapping above that $Fix(T) := [0,1]$ $\forall u \in [-1,1]$. Next, we prove that T is a BQSPC mapping. From the definition of Bregman function (see 1), we want to show that since $Fix(T) \neq \emptyset$, we can find some constant ρ where $0 \leq \rho < 1$ satisfying (2) Now, if $u \in [-1,0]$, we know that $Fix(T) = 0 = z^o$, and we get

$$\begin{aligned} d_h(0, Tu) &= h(0) - h(u^2+u) - \left\langle \nabla h(u^2+u), 0 - (u^2+u) \right\rangle \\ &= 0 - \frac{2}{3}(u^2+u)^2 + \left\langle \frac{4}{3}(u^2+u), u^2+u \right\rangle \\ &= \frac{2}{3}(u^2+u)^2, && (5) \\ d_h(0, u) &= h(0) - h(u) - \langle \nabla h(u), 0 - u \rangle \\ &= 0 - \frac{2}{3}u^2 + \left\langle \frac{4}{3}(u), u \right\rangle \\ &= \frac{2}{3}u^2, && (6) \\ d_h(u, Tu) &= h(u) - h(u^2+u) - \left\langle \nabla h(u^2+u), u - (u^2+u) \right\rangle \\ &= \frac{2}{3}u^2 - \frac{2}{3}(u^2+u)^2 + \left\langle \frac{4}{3}(u^2+u)u^2 \right\rangle \\ &= \frac{2}{3}u^4. && (7) \end{aligned}$$

Thus,

$$d_h(0, Tu) \leq d_h(0, u) + \rho d_h(u, Tu), \forall u \in [-1,0]. \tag{8}$$

Similarly, if $u \in (0,1]$, *we know* $Fix(T) := (0,1]$, *and for any* $z^o \in (0,1]$ *we arrive at*

$$\begin{aligned} d_h(z^o, Tu) &= h(z^o) - h(u) - \langle \nabla h(u), z^o - u \rangle \\ &= \frac{2}{3}(z^o)^2 - \frac{2}{3}u^2 - \frac{4}{3}z^o u + \frac{4}{3}u^2 \\ &= \frac{2}{3}(u - z^o)^2, \qquad (9) \\ d_h(z^o, u) &= h(z^o) - h(u) - \langle \nabla h(u), z^o - u \rangle \\ &= \frac{2}{3}(z^o)^2 - \frac{2}{3}(u)^2 + \frac{4}{3}z^o u + \frac{4}{3}u^2 \\ &= \frac{2}{3}(u - z^o)^2, \qquad (10) \\ d_h(u, Tu) &= h(u) - h(u^2 + u) - \left\langle \nabla h(u^2+u), u - (u^2+u) \right\rangle \\ &= \frac{2}{3}u^2 - \frac{2}{3}(u^2+u)^2 + \left\langle \frac{4}{3}(u^2+u)u^2 \right\rangle \\ &= \frac{2}{3}u^4. \qquad (11) \end{aligned}$$

Thus,

$$d_h(z^o, Tu) \leq d_h(z^o, u) + \rho d_h(u, Tu), \forall u \in (0,1]. \qquad (12)$$

Therefore, from (8) and (12), we conclude that

$$d_h(z^o, Tu) \leq d_h(z^o, u) + \rho d_h(u, Tu), \forall u \in [-1,1]. \qquad (13)$$

Thus, we have proved that T *is a BQSPC mapping.*

Let $P_K^h : int(dom\ ) \to K$ be a mapping such that $P_K^h(u) \in K$ satisfying

$$d_h(P_K^h(u), u) := inf \left\{ d_h(z,u) : z \in K \right\}, \qquad (14)$$

is the Bregman Projection (see[25]) of $u \in int(dom\, h)$ onto a nonempty closed and convex set $K \subset dom\, h$.

Remark 1.2 *We remark here that, if* X *is a smooth and strictly convex Banach spaces and* $h(u) =: \|u\|^2$, $\forall u \in X$, *then we have that* $\nabla h(u) = 2Ju$, $\forall u \in X$, *where* J *is the normalized duality mapping. Clearly, we obtain that*

$$\begin{aligned} d_h(z,u) &:= h(z) - h(u) - \langle \nabla h(u), z - u \rangle \\ &= \|z\|^2 - \|u\|^2 - 2\langle z, Ju \rangle + 2\|u\|^2 \\ &= \|u\|^2 - 2\langle z, Ju \rangle + \|z\|^2 \\ &= \phi(z,u), \forall u, z \in X, \end{aligned}$$

which is the Lyapunov function introduced by [1] and has extensively been used by various authors (see for example [18, 12] and the references they contain). We clearly see that $P_K^h(u)$ *reduces to the generalized projection [1] given as*

$$\Pi_K(u) := argmin_{z \in K} \phi(z,u).$$

In addition, if X *coincides with* H, *in Hilbert space then* $J = I$ *which is the identity map and*

$$\begin{aligned} d_h(z,u) &:= h(z) - h(u) - \langle \nabla h(u), z - u \rangle \\ &= \|u\|^2 - \|z\|^2 - 2\langle u, z \rangle + 2\|z\|^2 \\ &= \|u\|^2 + \|z\|^2 - 2\langle u, z \rangle \\ &= \|u - z\|^2, \forall u, z \in X. \end{aligned}$$

Hence the Bregman Projection $P_K^h(x)$ *reduces to metric projection of* H *onto* K, $P_K(u)$.

A map $T : K \to K$ is called

1. ϕ relatively nonexpansive if the following conditions holds

$$\phi(z^o, Tu) \leq \phi(z^o, u), \forall u \in K, \forall z^o \in Fix(T) = \hat{Fix}(T)$$

2. ϕ quasi strict pseudo-contraction if there exists a constant $\rho \in [0, 1)$ and $Fix(T) \neq \emptyset$ such that the following conditions holds

$$\phi(z^o, Tu) \leq \phi(z^o, u) + \rho\phi(u, Tu), \forall u \in K, \forall z^o \in Fix(T) \tag{15}$$

The subdifferential of h at x is the convex set defined by

$$\partial h(x) = \{x^* \in X^* : h(x) + \langle x^*, z - x\rangle \leq h(z); \forall z \in X\}. \tag{16}$$

The mapping $J : X \to 2^{X^*}$ called normalized duality mapping is defined by the set

$$J(x) = \left\{x^* \in X^* : \langle x^*, x\rangle = ||x||^2 = ||x^*||^2, \forall x \in X\right\}, \tag{17}$$

A function $h : X \to (-\infty, +\infty]$ is said to be a Legendre function [9], if it satisfies the following two conditions:

1. $int(dom\, h) \neq \emptyset$, h is Gâteaux differentiable on $int(dom\, h)$ and $dom\, f = int(dom\, h)$,
2. $int(dom\, h^*) \neq \emptyset$, h^* is Gâteaux differentiable on $int(dom\, h^*)$ and $dom\, h^* = int(dom\, h^*)$.

Remark 1.3 *(See for e.g [6, 4, 23, 8] Since X is reflexive, then we have that $(\partial h^{-1}) := \partial h^*$ and since h is Legendre, then ∂h is a bijection which satisfies $\nabla h = (\nabla h^*)^{-1}$, $ran\nabla h = dom\nabla h^* = int(dom\, h^*)$ and $ran\nabla h^* = dom\nabla h = int(dom\, h)$. h and h^* are strictly convex on their $int(dom\, h)$. If the subdifferential of h is single valued, it coincides with the gradient of h, that is $\partial h := \nabla h$. Example of a Legendre function is $h(u) := \frac{1}{p}||u||^p$, $(1 < p < \infty)$. If X is smooth and strictly convex Banach spaces, then in this case the gradient ∇h coincides with the generalised duality mapping of X, that is $\nabla h = J_p$. If the space is a Hilbert space, H then $\nabla h = I$, where I is the identity mapping in H. Throughout this paper, we assumed that h is Legendre.*

Let $h : X \to (-\infty, +\infty]$ be a Gâteaux differentiable function. The modulus of total convexity of h at $u \in int(dom\, h)$ is the function $V_h(u, .) : int(dom\, h) \times [0, +\infty) \to [0, +\infty)$ defined by

$$V_h(u, t) := inf\{d_h(z, u) : z \in dom\, h, \|z - u\| = t\}. \tag{18}$$

The function h is called totally convex (see [8] and the references it contains) at u if $V_h(u, t) > 0$ whenever $t > 0$. The function h is called totally convex if it is totally convex at any point $u \in int(dom\, h)$. The function is said to be totally convex on bounded sets if $V_h(B, t) > 0$ for any non-void bounded subset B of X and $t > 0$, where the modulus of total convexity of the function h on the set B is the function $V_h : int(dom\, h) \times [0, +\infty) \to [0, +\infty)$ defined by

$$V_h(B, t) := inf\{V_h(u, t) : u \in B \cap dom\, h\}. \tag{19}$$

Let $V_h : X \times X^* \to [0, +\infty)$ associated with h ([19]) be defined by

$$V_h(u, u^*) := h(u) - \langle u, u^*\rangle + h^*(u^*), \forall u \in X, u^* \in X^*. \tag{20}$$

We see that $V_h(,) \geq 0$ and the relation

$$V_h(u, u^*) := d_h(u, \nabla h^*(u^*)), \tag{21}$$

holds.

Vast research work has been done on construction of effective and implimentable algorithms for finding fixed points of the class of nonexpansive mappings and its natural extensions like pseudo-contraction mappings in the framework of real Hilbert spaces, (see for e.g [18], [33] and the references therein). Outside Hilbert space, some researchers have studied fixed points problems of these important nonlinear mappings. In particular is the great attention given to construction of algorithms for finding fixed points of Bregman nonexpansive-type mappings by the use of Bregman distance techniques (see [2],[3],[15],[16],[19],[30],[20],[35]).

Some well known and used iteration methods abound in the literature (see [21],[33] and the references they contain). Most notably is the Mann iteration method (see [17]) constructed as follows:

$$x_{n+1} = \alpha_n x_n + (1-\alpha_n)Tx_n, \tag{22}$$

for an appropriate chosen value of the scalar $\alpha_n \in [0,1]$. One limitation about this method is that it only guarantees weak convergence to the fixed points of the mapping T when

$$\sum_{n=1}^{\infty} \alpha_n(1-\alpha_n) = \infty. \tag{23}$$

In a bid to establish strong convergence of the generated sequences to the fixed points of the mappings (since strong convergence is better than weak convergence), some authors have over the years successfully modified Mann iteration methods (see for examples, [24],[27],[29] and the references contained in them). In addition to this fact, most of the results obtained in the literature only focused on a one-way iterative methods for the approximation fixed points of various mappings either in Hilbert spaces or general Banach spaces (see for examples [11, 24, 34, 27, 28, 29, 19, 33, 30, 20, 15, 31] and the references therein).

Now, to approximate common fixed points of Bregman quasi strictly pseudo-contraction mappings defined a closed and convex subset K of a reflexive Banach space X, Wang and Wei in [29], formulated and studied the following modified Mann iterative method:

$$\begin{cases} x_0 \in K, \text{ Chosen arbitraily }, \\ C_0^i = K, i = 1, 2, ..., N, \\ C_0 = \cap_{i=1}^N C_o^i, \\ y_n^i = \nabla h^*(b_n \nabla h(x_n) + (1-b_n)\nabla h(T_i)z_n^i), \\ C_{n+1}^i = \{z \in C_n : d_h(z, y_n^i) \leq b_n d_h(z, x_n) + (1-b_n)d_h(z, z_n^i) + \frac{\rho_i}{1-\rho_i}\langle \nabla h(z_n^i) - z, z_n^i - \nabla h(T_i z_n^i)\rangle\}, \\ C_{n+1} = \cap_{i=1}^N C_{n+1}^i, \\ x_{n+1} = P_{C_{n+1}}^h(x_0), n \geq 0, \end{cases} \tag{24}$$

where $z_n^i = x_n + e_n^i$, e_n^i is the sequence of errors in X satisfy $\lim_{n\to\infty} e_n^i = 0$ for each $i = 1, 2, ..., N$ and $b_n \subset [0,1]$ satisfying $\liminf_{n\to\infty}(1-b_n) > 0$ $\rho_i \in [0,1)$. They proved that the sequence $\{x_n\}$ generated by the algorithm (24) converges strongly to the Bregman projection of X onto the common fixed point set.

Very recently in [20], Ogbuisi studied the operator $Res_{\lambda B}^h A_\lambda^h$ which is a composition of the resolvent of a maximal operator B and the anti-resolvent of a Bregman inverse strongly monotone operator A with respect to $\lambda > 0$. They constructed an iterative method for approximating a common solution of a monotone inclusion problem and a fixed point problem involving a Bregman quasi strictly pseudo-contractive mapping in a reflexive Banach space. Below is their algorithm:

$$\begin{cases} x_0 \in K = C_0, \text{ Chosen arbitraily }, \\ y_n = \nabla h^*(\alpha_n \nabla h(x_n) + (1-\alpha_n)[(1-\gamma_n)\nabla h(x_n) + \gamma_n \nabla h(Tx_n)], \\ u_n = \nabla h^*(\beta_n \nabla h(y_n) + (1-\beta_n)\nabla h(Res^h_{\lambda B} A^h_\lambda y_n)), \\ C_{n+1} = \{z \in C_n : d_h(z, y_n) + d_h(z, u_n) \\ \leq \frac{1+\lambda}{1-\lambda}\langle \nabla h(x_n) - \nabla h(Tx_n), x_n - z\rangle + \langle \nabla h(Tx_n) - \nabla h(u_n), x_n - z\rangle\} \\ x_{n+1} = P^h_{C_{n+1}}(x_0), n \geq 0, \end{cases} \tag{25}$$

where $\{\alpha_n\}, \{\beta_n\}$ and $\{\gamma_n\}$ are sequences in $(0,1)$ such that $\liminf_{n\to\infty}(1-\alpha_n)\gamma_n > 0$ and $\liminf_{n\to\infty}(1-\beta_n) > 0$. They proved that the sequence $\{x_n\}$ generated by the algorithm (25)converges strongly to the Bregman projection of K onto the common solution set.

Furthermore, some authors have introduced a two-step iterative method with an inertial extrapolation term to improve the rate of convergence of their introduced algorithms (see [12, 14, 2, 16]). Besides, an inertial modified Krasnoselskii-Mann iteration which is an inexact scheme, was introduced and studied by [21] for approximating nonexpansive mapping in Hilbert space. They assumed that the sum of their positive scalar and control sequences in $(0,1)$ to be less than one, that is $b_n + c_n < 1$. The advantage of this assumption is that it bridges the gap between weak and strong convergence results.

Thus, inspired by the established results of the authors cited above, our purpose in this paper is to construct a two-step iterative algorithm with inertial extrapolation term defined with respect to Bregman distance function for approximating common fixed points of a finite family of a closed Bregman quasi strictly pseudo-contraction mappings when the intersection of its set is assumed to be non empty. We prove a strong convergence theorem for it under flexible and relaxed conditions in real reflexive Banach space. Our algorithm is applied in solving finite convex feasibility and equilibrium problems in reflexive Banach space. Furthermore, we demonstrate numerical examples to justify the efficiency and implementability of our algorithms in a finite dimensional real Banach space. Our results improves, generalizes and complements other previously and recently cited results of some authors in the literature.

The organization of this paper is as follows: section 2 is a collection of basic theoretical framework (lemmas); section 3 is devoted to our main result which involves the analysis of the theoretical convergence properties of the proposed algorithm and some of its consequences; section 4 gives the application of our algorithm with some example; section 5 presents the numerical examples and computations to discuss the convergence of our algorithm and section 6 is the conclusion of our paper.

2 Preliminaries

Lemma 2.1 *[8] The function $h : X \to (-\infty, +\infty]$ is totally convex on bounded sets if and only if given two sequences $\{u_n\}$ and $\{z_n\}$ in X such that either $\{u_n\}$ or $\{z_n\}$ is bounded, then*

$$\lim_{n\to\infty} d_h(z_n, u_n) = 0 \Rightarrow ||z_n - u_n|| = 0$$

Lemma 2.2 *[27] Let $h : X \to (-\infty, +\infty]$ be a Legendre function which is uniformly Fréchet differentiable on bounded subsets of X. Let K be a non-empty, closed and convex subset of X. Let $G : K \to K$ be a Bregman quasi-strict pseudo-contractive mapping with respect to $h : X \to (-\infty, +\infty]$. Then $Fix(T)$ is closed and convex.*

Lemma 2.3 *[32] Let X be a reflexive real Banach space. Let $h : X \to (-\infty, +\infty]$ be a continuous convex function which is super coercive. Then the following assertions are equivalent:*

1. *$h : X \to (-\infty, +\infty]$ is bounded on bounded subsets and uniformly smooth on bounded subsets of X*

2. *$h : X \to (-\infty, +\infty]$ is Fréchet differentiable and ∇h^* is uniformly norm-to-norm continuous on bounded subsets of X^**

3. *dom $h^* = X^*$, h^* is super coercive and uniformly convex on bounded subsets of X^**

Lemma 2.4 *[25] Let $h : X \to (-\infty, +\infty]$ be a differentiable function on int(dom h) such that ∇h^* is bounded on bounded subsets of dom h^*. Let $u_0 \in X$ and $\{u_n\}$ is a sequence in X. If $\{d_h(u_0, u_n)\}$ is bounded, then $\{u_n\}$ is bounded.*

Lemma 2.5 *[27] Let $h : X \to (-\infty, +\infty]$ be a Legendre function which is uniformly Fréchet differentiable on bounded subsets of X. Let K be a non-empty, closed and convex subset of X. Let $T : K \to K$ be a Bregman quasi strict pseudo-contractive mapping with respect to $h : X \to (-\infty, +\infty]$. Then for any $u \in K$, $q \in Fix(T)$ and $\rho \in [0, 1)$, the following hold*

$$d_h(u, Tu) \leq \frac{1}{1-\rho} \langle \nabla h(u) - \nabla h(Tu), u - q \rangle .$$

Lemma 2.6 *[32] Let K be anon-empty, closed and convex subsets of X. Let $h : X \to (-\infty, +\infty]$ be a differentiable and totally convex function and let $u \in X$. Then we have the following equivalent conditions:*

1. *$P^h_K(u) = u_0$ if and only if $\langle \nabla h(u) - \nabla h(u_0), z - u_0 \rangle \leq 0, \forall z \in K$*

2. *$d_h(z, P^h_K(u)) + d_h(P^h_K(u), u) \leq d_h(z, u), \forall z \in K$.*

3 Main results

In this section, we construct and study the following algorithm when $\cap_{i=1}^N Fix(T_i) \neq \emptyset$:

$$\begin{cases} x_0, x_1 \in C_1 = K \\ C_{1,i} = \cap_{i=1}^N C_{1,i}, \\ z_n = x_n + a_n(x_n - x_{n-1}), \\ y_{n,i} = \nabla h^* \left(b_n \nabla h\left(x_n\right) + \left(1 - b_n - c_n\right) \nabla h\left(T_i z_n\right) + c_n \nabla h\left(z_n\right)\right), \\ C_{n+1,i} = \{u \in C_n : d_h\left(u, y_{n,i}\right) \leq d_h\left(u, x_n\right) + d_h\left(x_n, z_n\right) \\ +\langle \nabla h\left(z_n\right) - \nabla h\left(x_n\right), x_n - u\rangle + \frac{\rho_i}{1-\rho_i} \langle \nabla h\left(z_n\right) - \nabla h\left(T_i z_n\right), z_n - u\rangle\}, \\ C_{n+1} = \cap_i^N C_{n+1,i}, \\ x_{n+1} = P^h_{C_{n+1}}(x_0), n \geq 1, \end{cases} \tag{26}$$

where ∇h and ∇h^* are called the gradient functions of h and h^* respectively. Our control sequences: $\{a_n\}$, $\{b_n\}$, and $\{c_n\}$ are all in $(0, 1)$ such that

1. $c_n \in (0, (1 - \rho_i)(1 - b_n) \subset (0, 1)$, $1 \leq i \leq N$,

2. $\liminf_{\to\infty} (1 - b_n - c_n) > 0$.

Theorem 3.1 *Let K be a nonempty, closed and convex subset of X with its dual space X^*. Let $h : X \to (-\infty, +\infty]$ represent a strongly coercive Legendre function which is bounded, uniform Fréchet differentiable and totally convex on bounded subsets of X. Let $T_i : K \to K, \forall 1 \leq i \leq N$ represent finite-family of Bregman quasi strictly pseudo-contraction (BQSPC) maps which is also closed such that $\Omega = \cap_{i=1}^N Fix(T_i) \neq \emptyset$. Then for each choice of $x_1, x_0 \in K$ with $x_1 < x_0$, we have sequences $\{x_n\}$ and $\{z_n\}$ satisfying (26) which converges strongly to $\overline{x} = P^h_\Omega(x_0)$ nearest to x_0, as $n \to \infty$ and where P^h_Ω is known to be Bregman projection map of C_{n+1} onto Ω.*

Proof. This is broken into 6 ways.

Step 1: Show $\Omega = \cap_{i=1}^{N} Fix(T_i)$ to be closed,convex.

It is obvious from Lemma 2.2 that $Fix(T_i)$ is closed,convex for any $1 \leq i \leq N$. Consequently, since the intersection of two or more convex set is convex, we get $\Omega = \cap_{i=1}^{N} Fix(T_i)$ to be closed,convex.

Step 2: Demonstrate the half-set C_n to be closed,convex for each positive integer.

To realize this, note $C_1 = K$ to be closed convex. Again, we demonstrate C_n to be closed convex with $n > 1$. First we demonstrate C_n to be convex for some $n > 1$. We let $u_1, u_2 \in C_{n+1,i}$ be given. Consider $u = \lambda u_1 + (1-\lambda)u_2, \forall \lambda \in [0,1]$. We show that $\lambda u_1 + (1-\lambda)u_2 \in C_{n+1,i} \subset C_n$. From our scheme, $d_h(u, y_{n,i}) \leq d_h(u, x_n) + d_h(x_n, z_n) + \langle \nabla h(z_n) - \nabla h(x_n), x_n - u\rangle + \frac{\rho_i}{1-\rho_i}\langle \nabla h(z_n) - \nabla h(T_i z_n), z_n - u\rangle$ is equivalent to

$h(z_n) - h(y_{n,i}) + \langle \nabla h(x_n), u - x_n\rangle - \langle \nabla h(y_{n,i}), u - y_n\rangle + \langle \nabla h(z_n), x_n - z_n\rangle - \langle \nabla h(z_n), x_n - u\rangle + \langle \nabla h(x_n), x_n - u\rangle - \frac{\rho_i}{\rho_i}\langle \nabla h(z_n), z_n - u\rangle + \frac{\rho_i}{1-\rho_i}\langle \nabla h(T_i z_n), z_n - u\rangle \leq 0.$

Thus, by an easy argument, C_{n+1} and hence C_n is convex with $n > 1$. Secondly, we demonstrate C_n to be closed, $n > 1$. We show that given a sequence $u_n \in C_{n+1}$ such that $u_n \to u$, then $u \in C_{n+1} \subset C_n$ for some $n > 1$. Following the same line of argument above, and taking limits as $n \to \infty$, we have shown C_n to be closed, $n > 1$. Therefore, we have shown C_n to be closed convex.

Step 3: Demonstrate that $\Omega \subset C_{n+1}$, with $n \in N$.

Note $\Omega \subset C_1 = K$. Supposing $\Omega \subset C_n$, $n > 1$ and setting $w_{n,i} = b_n \nabla h(x_n) + (1 - b_n - c_n)\nabla h(T_i z_n) + c_n \nabla h(z_n)$, with $q \in \Omega$, we get using the convexity property of Bregman distance (see Remark4), together with (2) (20) and (21) that

$$\begin{aligned}
d_h(q, y_{n,i}) &= d_h(q, \nabla h^*(w_{n,i})) \\
&= v_h(q, w_{n,i}) \\
&= v_h(q, b_n \nabla h(x_n) + (1 - b_n - c_n)\nabla h(T_i z_n) + c_n \nabla h(z_n)) \\
&= h(q) - \langle q, b_n \nabla h(x_n) + (1 - b_n - c_n)\nabla h(T_i z_n) + c_n \nabla h(z_n)\rangle \\
&+ h^* b_n \nabla h(x_n) + (1 - b_n - c_n)\nabla h(T_i z_n) + c_n \nabla h(z_n) \\
&\leq b_n [h(q) - \langle q, \nabla h(x_n)\rangle + h^* \nabla h(x_n)] + (1 - b_n - c_n) \\
&\times [h(q) - \langle q, \nabla h(T_i z_n)\rangle + h^* \nabla h(T_i z_n)] \\
&+ c_n [h(q) - \langle q, \nabla h(x_n)\rangle + h^* \nabla h(z_n)] \\
&= b_n v_h(q, \nabla h(x_n)) + (1 - b_n - c_n) v_h(q, \nabla h(T_i z_n)) \\
&+ c_n v_h(q, \nabla h(z_n)) \\
&= b_n d_h(q, x_n) + (1 - b_n - c_n) d_h(q, T_i z_n) + c_n d_h(q, z_n) \\
&\leq b_n d_h(q, x_n) + (1 - b_n - c_n)[d_h(q, z_n) + \rho_i d_h(z_n, T_i z_n)] \\
&+ c_n d_h(q, z_n) \\
&= b_n d_h(q, x_n) + (1 - b_n) d_h(q, z_n) + (1 - b_n - c_n)\rho_i d_h(z_n, T_i z_n) \\
&\leq b_n d_h(q, x_n) + (1 - b_n) d_h(q, z_n) + (1 - b_n - c_n) \times \\
&\frac{\rho_i}{1-\rho_i}\langle \nabla h(z_n) - \nabla h(T_i z_n), z_n - q\rangle \\
&\leq b_n d_h(q, x_n) + \frac{\rho_i}{1-\rho_i}\langle \nabla h(z_n) - \nabla h(T_i z_n), z_n - q\rangle \\
&+ (1 - b_n)[d_h(q, x_n) + d_h(x_n, z_n) + \langle \nabla h(z_n) - \nabla h(x_n), x_n - q\rangle] \\
&\leq d_h(q, x_n) + d_h(x_n, z_n) + \langle \nabla h(z_n) - \nabla h(x_n), x_n - q\rangle \\
&+ \frac{\rho_i}{1-\rho_i}\langle \nabla h(z_n) - \nabla h(T_i z_n), z_n - q\rangle . \qquad (27)
\end{aligned}$$

Thus

$$\begin{aligned} d_h(q, y_n) &\leq d_h(q, x_n) + d_h(x_n, z_n) + \langle \nabla h(z_n) - \nabla h(x_n), x_n - q\rangle \\ &+ \frac{\rho_i}{1-\rho_i} \langle \nabla h(z_n) - \nabla h(T_i z_n), z_n - q\rangle . \end{aligned} \tag{28}$$

So $q \in C_{n+1}$ and $C_{n+1} \subset C_n$. By implication, $\Omega \in C_n$ with $n \geq 1$.

Step 4: Demonstrate that all the sequences in (26) are bounded and convergent.

To justify the above claims, notice from our setting in (26), that $x_n = P^h_{C_n}(x_0)$, $x_{n+1} = P^h_{C_{n+1}}(x_0)$. Thus, using Lemma 2.6(2) we arrive at

$$\begin{aligned} d_h(x_n, x_0) &\leq d_h(x_{n+1}, x_0) - d_h(x_{n+1}, x_n) \\ d_h(x_{n+1}, x_0) &\geq d_h(x_n, x_0). \end{aligned} \tag{29}$$

This shows that $\{d_h(x_n, x_0)\}$ is monotone non-decreasing sequence. Again using Lemma 2.6(2), we obtain $\forall n \in N, q \in Fix(T)$ that

$$\begin{aligned} d_h(x_n, x_0) &= d_h(P^h_{C_n}(x_0), x_0) \\ &\leq d_h(q, x_0) - d_h(q, P^h_{C_n}(x_0)) \\ &\leq d_h(q, x_0). \end{aligned} \tag{30}$$

This shows for boundedness of $\{d_h(x_n, x_0)\}$ and through Lemma 2.4, the sequence $\{x_n\}$ becomes bounded. Combining (29) and (30) shows that $\lim_{n\to\infty} d_h(x_n, x_0)$ exist. Now, without loss of generality, let

$$\lim_{n\to\infty} d_h(x_n, x_0) = l. \tag{31}$$

In addition to (31) and Lemma 2.6(b), we get for any positive integer t and as $n \to \infty$, that

$$\begin{aligned} d_h(x_{n+t}, x_n) &= d_h(x_{n+t}, P^h_{C_n}(x_0)) \\ &\leq d_h(x_{n+t}, x_0) - d_h(x_n, x_0) \to 0. \end{aligned} \tag{32}$$

So that $\lim_{n\to\infty} d_h(x_{n+t}, x_n) = 0$. In particular,

$$\lim_{n\to\infty} d_h(x_{n+1}, x_n) = 0. \tag{33}$$

Thus we obtain using Lemma 2.1 that

$$\lim_{n\to\infty} ||x_{n+1} - x_n|| = 0. \tag{34}$$

This shows the sequence $\{x_n\}$ to be Cauchy. Now since ∇h is bounded and going by Lemma 2.3,

$$\lim_{n\to\infty} ||\nabla h(x_{n+1}) - \nabla h(x_n)|| = 0. \tag{35}$$

Furthermore, we obtain from the definition of z_n and together with (34) as $n \to \infty$, that

$$\begin{aligned} ||x_n - z_n|| &= ||x_n - x_n - \alpha_n(x_n - x_{n-1})|| \\ &= ||\alpha_n(x_{n-1} - x_n)|| \\ &\leq ||x_{n-1} - x_n|| \to 0. \end{aligned}$$

We arrive at

$$\lim_{n\to\infty} ||x_n - z_n|| = 0. \tag{36}$$

Consequently,

$$\lim_{n\to\infty} ||\nabla h(x_n) - \nabla h(z_n)|| = 0. \tag{37}$$

By (36), z_n is bounded. Consequent upon the boundedness of ∇h and by (37) $\nabla h(z_n)$ is also bounded. Hence x_n, z_n and y_n are bounded. Moreover, since z_n is bounded we get by (Remark4) that $\lim_{n\to\infty} d_h(x_n, z_n) = 0$. Consequently, since ∇h is bounded we get together with (4) that

$$\begin{aligned} d_h(x_{n+1}, z_n) &= d_h(x_{n+1}, x_n) + d_h(x_n, z_n) + \langle \nabla h(x_n) - \nabla h(z_n), x_{n+1} - x_n \rangle \\ &\leq d_h(x_{n+1}, x_n) + d_h(x_n, z_n) + ||\nabla h(x_n) - \nabla h(z_n)||.||x_{n+1} - x_n||. \end{aligned}$$

Using (33), (34), (37) and the fact that $\lim_{n\to\infty} d_h(x_n, z_n) = 0$, we get

$$\lim_{n\to\infty} d_h(x_{n+1}, z_n) = 0. \tag{38}$$

Using Lemma 2.1,

$$\lim_{n\to\infty} ||x_{n+1} - z_n|| = 0. \tag{39}$$

Since from (26) $x_{n+1} \in C_{n+1} \subset C_n$, it follows from (33),(34),(35),(37),(39) and the boundedness of ∇h that

$$\begin{aligned} d_h(x_{n+1}, y_{n,i}) &\leq d_h(x_{n+1}, x_n) + d_h(x_n, z_n) + \langle \nabla h(z_n) - \nabla h(x_n), x_n - x_{n+1} \rangle \\ &+ \frac{\rho_i}{1-\rho_i} \langle \nabla h(z_n) - \nabla h(T_i z_n), z_n - x_{n+1} \rangle . \\ &\leq d_h(x_{n+1}, x_n) + d_h(x_n, z_n) + ||\nabla h(z_n) - \nabla h(x_n)||.||x_n - x_{n+1}|| \\ &+ \frac{\rho_i}{1-\rho_i} ||\nabla h(z_n) - \nabla h(T_i z_n)||.||z_n - x_{n+1}|| \to 0 \text{ as } n \to \infty. \end{aligned} \tag{40}$$

Hence

$$\lim_{n\to\infty} d_h(x_{n+1}, y_{n,i}) = 0, 1 \leq i \leq N. \tag{41}$$

Thus, by Lemma 2.1 we arrive at

$$\lim_{n\to\infty} ||x_{n+1} - y_{n,i}|| = 0, 1 \leq i \leq N. \tag{42}$$

Since ∇h is bounded and by X^* by Lemma 2.3, we arrive at

$$\lim_{n\to\infty} ||\nabla h(x_{n+1}) - \nabla h(y_{n,i})|| = 0, 1 \leq i \leq N. \tag{43}$$

Consequently,

$$\lim_{n\to\infty} ||x_n - y_{n,i}|| = 0, 1 \leq i \leq N, \tag{44}$$

and

$$\lim_{n\to\infty} ||\nabla h(x_n) - \nabla h(y_{n,i})|| = 0, 1 \leq i \leq N. \tag{45}$$

Using (38), (41), (43) and (39) we also obtain as $n \to \infty$ that

$$\begin{aligned} d_h(z_n, y_{n,i}) &= d_h(z_n, x_{n+1}) + d_h(x_{n+1}, y_{n,i}) + \langle \nabla h(x_{n+1}) - \nabla h(y_{n,i}), z_n - x_{n+1} \rangle \\ &\leq d_h(z_n, x_{n+1}) + d_h(x_{n+1}, y_{n,i}) + ||\nabla h(x_{n+1}) - \nabla h(y_{n,i})||.||z_n - x_{n+1}|| \\ &\to 0. \end{aligned}$$

Hence

$$\lim_{n\to\infty} d_h(z_n, y_{n,i}) = 0, 1 \leq i \leq N. \tag{46}$$

Using Lemma 2.1, we obtain that

$$\lim_{n\to\infty} ||z_n - y_{n,i})|| = 0, 1 \leq i \leq N. \tag{47}$$

Since ∇h is bounded and by Lemma 2.3, we arrive at

$$\lim_{n\to\infty} ||\nabla h(z_n) - \nabla h(y_{n,i})|| = 0, 1 \leq i \leq N. \tag{48}$$

Using (48) and the two point identity of Bregman distance function (see Remark4) we have

$$\begin{aligned} d_h(z_n, y_{n,i}) + d_h(y_{n,i}, z_n) &= \langle \nabla h(z_n) - \nabla h(y_{n,i}), z_n - y_{n,i} \rangle \\ d_h(z_n, y_{n,i}) + d_h(y_{n,i}, z_n) &\leq ||\nabla h(z_n) - \nabla h(y_{n,i})||.||z_n - y_{n,i}|| \\ d_h(z_n, y_{n,i}) &\leq ||\nabla h(z_n) - \nabla h(y_{n,i})||.||z_n - y_{n,i}|| \to 0. \end{aligned} \tag{49}$$

Hence

$$\lim_{n\to\infty} d_h(z_n, y_{n,i}) = 0. \tag{50}$$

Consequently from the definition of $y_{n,i}$ in (26) we have that

$$\begin{aligned} ||\nabla h(z_n) - \nabla h(y_{n,i})|| &= ||\nabla h(z_n) - (\nabla h(\nabla h^*(b_n \nabla h(x_n) \\ &\quad + (1 - b_n - c_n)\nabla h(T_i z_n) + c_n \nabla h(z_n))))|| \\ &\geq (1 - b_n - c_n)\, ||\nabla h(z_n) - \nabla h(T_i z_n)|| \\ &\quad - b_n ||\nabla h(z_n) - \nabla h(x_n)|| + c_n ||z_n - z_n||, \end{aligned} \tag{51}$$

this becomes

$$\begin{aligned} (1 - b_n - c_n)\, ||\nabla h(z_n) - \nabla h(T_i z_n)|| &\leq ||\nabla h(z_n) - \nabla h(y_{n,i})|| \\ &\quad + b_n ||\nabla h(z_n) - \nabla h(x_n)||. \end{aligned} \tag{52}$$

Thus by (37) and (48) as $n \to \infty$ we obtain

$$(1 - b_n - c_n)\, ||\nabla h(z_n) - \nabla h(T_i z_n)|| \to 0. \tag{53}$$

Using our assumption that $\liminf_{n\to\infty}(1 - b_n - c_n) > 0$, we obtain

$$\lim_{n\to\infty} ||\nabla h(z_n) - \nabla h(T_i z_n)|| = 0, i = 1, 2, ..., N. \tag{54}$$

Using Lemma 2.3, we get that

$$\lim_{n\to\infty} ||z_n - T_i z_n|| = 0, i = 1, 2, ..., N. \tag{55}$$

Step 5: Demonstrate that $\overline{x} \in \Omega := \cap_{i=1}^{N} Fix(T_i)$

In view of the sequence x_n being Cauchy and from (39), we have that $z_n \to \overline{x}$ as $n \to \infty$. Following from (55), the fact that $z_n \to \overline{x}$, and by the closedness property of T_i, we arrive at $\overline{x} = T_i \overline{x}$, with $1 \leq i \leq N$.

Step 6: Demonstrate $\overline{x} = P_\Omega^h(x_0)$.

Set $u = P_\Omega^h(x_0)$. In **Step 3**, we demonstrated that $\Omega \subset C_n$. Since $P_\Omega^h(x_0) \in \Omega$, we get that $P_\Omega^h(x_0) \subset C_n$. It then follows from our setting with $x_n = P_{C_n}^h(x_0)$ that

$$d_h(x_n, x_0) \leq d_h(u, x_0). \tag{56}$$

Since $x_n \to \overline{x}$ as $n \to \infty$, we get from (56) that

$$d_h(\overline{x}, x_0) \leq d_h(u, x_0). \tag{57}$$

But by the Property of Bregman Projection mapping in Lemma 2.6, we have for $\forall w \in \Omega$ that

$$d_h(u, x_0) \leq d_h(w, x_0). \tag{58}$$

This implies

$$d_h(u, x_0) \leq d_h(\overline{x}, x_0). \tag{59}$$

Thus by combining (57) and (59) we then arrive at $u = \overline{x}$. Therefore, $\overline{x} = P^h_\Omega(x_0)$. This completes our proof of Theorem 3.1.

Now the following consequences of Theorem 3.1 are gotten.

If $N = 1$, we have an algorithm for a single BQSPC map.

$$\begin{cases} x_0, x_1 \in C_1 = K \\ z_n = x_n + a_n(x_n - x_{n-1}), \\ y_n = \nabla h^* \left(b_n \nabla h\left(x_n\right) + \left(1 - b_n - c_n\right) \nabla h\left(T z_n\right) + c_n \nabla h\left(z_n\right)\right), \\ C_{n+1} = \{u \in C_n : d_h\left(u, y_n\right) \leq d_h\left(u, x_n\right) + d_h\left(x_n, z_n\right) \\ + \langle \nabla h\left(z_n\right) - \nabla h\left(x_n\right), x_n - u\rangle + \frac{\rho}{1-\rho} \langle \nabla h\left(z_n\right) - \nabla h\left(T z_n\right), z_n - u\rangle\}, \\ x_{n+1} = P^h_{C_{n+1}}(x_0), n \geq 1, \end{cases} \tag{60}$$

where ∇h and ∇h^* are called the gradient functions of h and h^* respectively. Our control sequences: $\{a_n\}$, $\{b_n\}$, and $\{c_n\}$ are all in $(0, 1)$ such that

1. $c_n \in (0, (1 - \rho_i)(1 - b_n) \subset (0, 1)\ i = 1,$
2. $\liminf_{\to\infty} (1 - b_n - c_n) > 0.$

Corollary 3.1 *Let K be a nonempty, closed and convex subset of X with its dual space X^*. Let $h : X \to (-\infty, +\infty]$ represent a strongly coercive Legendre function which is bounded, uniform Fréchet differentiable and totally convex on bounded subsets of X. Let $T : K \to K$ represent Bregman quasi strictly pseudo-contraction mapping which is also closed such that $\Omega = Fix(T) \neq \emptyset$. Then for each choice of $x_1, x_0 \in K$ with $x_1 < x_0$, we have sequences $\{x_n\}$ and $\{z_n\}$ satisfying (60) which converges strongly to $\overline{x} = P^h_\Omega(x_0)$ nearest to x_0, as $n \to \infty$, with P^h_Ω as Bregman projection map of C_{n+1} onto Ω.*

If $T_i : K \to K, i = 1, 2, ..., N$ represent finite family of Bregman quasi nonexpansive mappings, we also have this algorithm for it.

$$\begin{cases} x_0, x_1 \in C_1 = K \\ C_{1,i} = \cap_{i=1}^N C_{1,i}, \\ z_n = x_n) + a_n(x_n) - x_{n-1}), \\ y_{n,i} = \nabla h^* \left(b_n \nabla h\left(x_n\right) + \left(1 - b_n - c_n\right) \nabla h\left(T_i z_n\right) + c_n \nabla h\left(z_n\right)\right), \\ C_{n+1,i} = \{u \in C_n : d_h\left(u, y_{n,i}\right) \leq d_h\left(u, x_n\right) + d_h\left(x_n, z_n\right) \\ + \langle \nabla h\left(z_n\right) - \nabla h\left(x_n\right), x_n - u\rangle \\ C_{n+1} = \cap_i^N C_{n+1,i}, \\ x_{n+1} = P^h_{C_{n+1}}(x_0), n \geq 1, \end{cases} \tag{61}$$

where ∇h and ∇h^* are called the gradient functions of h and h^* respectively. Our control sequences: $\{a_n\}$, $\{b_n\}$, and $\{c_n\}$ are all in $(0, 1)$ such that

1. $c_n \in (0, (1 - b_n) \subset (0, 1),$
2. $\liminf_{\to\infty} (1 - b_n - c_n) > 0.$

Corollary 3.2 *Let K be a nonempty, closed and convex subset of X with its dual space X^*. Let $h : X \to (-\infty, +\infty]$ represent a strongly coercive Legendre function which is bounded, uniform Fréchet differentiable and totally convex on bounded subsets of X. Let $T_i : K \to K$ represent* *finite family of closed Bregman quasi nonexpansive mappings such that* $\Omega = \cap_{i=1}^{N} Fix(T_i) \neq \emptyset$*. Then for each choice of* $x_1, x_0 \in K$ *with* $x_1 < x_0$*, we have sequences* $\{x_n\}$ *and* $\{z_n\}$ *satisfying (61) which converges strongly to* $\overline{x} = P_{\Omega}^{h}(x_0)$ *nearest to* x_0*, as* $n \to \infty$*, with* P_{Ω}^{h} *as the Bregman projection mapping of* C_{n+1} *onto* Ω*.*

If $h(x) = \|x\|^2$, then $d_h(x, y) = \phi(x, y)$ (see Remark 1.2). In what follows, we have $T_i : K \to K$ as a finite family of closed quasi-ϕ -strictly pseudo-contraction mappings and the algorithm below for it .

$$\begin{cases} x_0, x_1 \in C_1 = K \\ C_{1,i} = \cap_{i=1}^{N} C_{1,i}, \\ z_n = x_n + a_n(x_n - x_{n-1}), \\ y_{n,i} = J^*\left(b_n J\left(x_n\right) + \left(1 - b_n - c_n\right) J\left(T_i z_n\right) + c_n J\left(z_n\right)\right), \\ C_{n+1,i} = \{u \in C_n : \phi\left(u, y_{n,i}\right) \leq \phi\left(u, x_n\right) + \phi\left(x_n, z_n\right) \\ +\langle J\left(z_n\right) - J\left(x_n\right), x_n - u\rangle + \frac{\rho_i}{1-\rho_i}\langle J\left(z_n\right) - J\left(T_i z_n\right), z_n - u\rangle\}, \\ C_{n+1} = \cap_{i}^{N} C_{n+1,i}, \\ x_{n+1} = \Pi_{C_{n+1}}(x_0), n \geq 1, \end{cases} \tag{62}$$

where J and J^* are called the normalized duality mappings on X and X^* respectively, $\{a_n\} \in (0, 1)$, $\{b_n\} \in (0, 1)$, $\{c_n\} \in (0, 1)$, such that

1. $c_n \in (0, (1 - \rho_i)(1 - b_n) \subset (0, 1)$, $i = 1, 2, ..., N$,
2. $\liminf_{\to\infty} (1 - b_n - c_n) > 0$.

Corollary 3.3 *Let* K *be a nonempty, closed and convex subset a uniformly convex and uniformly smooth real Banach space. Let* $T_i : K \to K$ *represent family of quasi-* ϕ *-strictly pseudo-contraction maps which is closed such that* $\Omega = \cap_{i=1}^{N} Fix(T_i) \neq \emptyset$*. Then for each choice of* $x_1, x_0 \in K$ *with* $x_1 < x_0$*, we have sequences* $\{x_n\}$ *and* $\{z_n\}$ *satisfying (62) which converges strongly to* $\overline{x} = \Pi_{\Omega}(x_0)$ *nearest to* x_0*, as* $n \to \infty$*, with* Π_{Ω} *as the generalized projection mapping of* C_{n+1} *onto* Ω*.*

If $T : K \to K$ represent relatively nonexpansive mapping, we have algorithm for it as follows:

$$\begin{cases} x_0, x_1 \in C_1 = K \\ z_n = x_n + a_n(x_n - x_{n-1}), \\ y_n = J^*\left(b_n J\left(x_n\right) + \left(1 - b_n - c_n\right) J\left(T z_n\right) + c_n J\left(z_n\right)\right), \\ C_{n+1} = \{u \in C_n : \phi\left(u, y_n\right) \leq \phi\left(u, x_n\right) + \phi\left(x_n, z_n\right) \\ +\langle J\left(z_n\right) - J\left(x_n\right), x_n - u\rangle \\ x_{n+1} = \Pi_{C_{n+1}}(x_0), n \geq 1, 8 \end{cases} \tag{63}$$

Corollary 3.4 *Let* K *be a nonempty, closed and convex subset a uniformly convex and uniformly smooth real Banach space. Let* $T : K \to K$ *represent relatively nonexpansive mapping such that* $\Omega = Fix(T) \neq \emptyset$*. Then for each choice of* $x_1, x_0 \in K$ *with* $x_1 < x_0$*, we have sequences* $\{x_n\}$ *and* $\{z_n\}$ *satisfying (63) which converges strongly to* $\overline{x} = \Pi_{\Omega}(x_0)$ *nearest to* x_0*, as* $n \to \infty$*, with* Π_{Ω} *as the generalized projection mapping of* C_{n+1} *onto* Ω*.*

4 Application

In this section we provide some applications of Theorem 3.1 as follows.

4.1. Convex feasibility problems

We let $K_1, K_2, ..., K_N$ represent a closed convex and nonempty sets such that the finite intersection of these sets is not empty. The convex feasibility problem (CFP) is to find a point say $z \in K$. The Bregman Projection onto the i^{th} constraint K_i with respect to a Legendre function h is denoted by $P^h_{K_i}$. It is easy to compute that $Fix(P^h_{K_i}) = K_i, \forall i = 1, 2, ..., N$. If in addition, the Legendre function is necessarily uniform Fréchet differentiable and totally convex on bounded subsets of a real reflexive Banach space X, we get that $P^h_{K_i}$ is in particular a Bregman relatively nonexpansive mappings (see [25]), thus a closed Bregman quasi strictly pseudo-contraction mappings such that $T_i = P^h_{K_i}, \forall i = 1, 2, ..., N$. With this fact, the fixed problem for finite family of closed Bregman quasi strictly pseudo-contraction nonexpansive-type mappings becomes solutions of finite family of convex feasibility problems. From Theorem 3.1, we have a strong convergence results for common solution of convex feasibility problems below:

Theorem 4.1 *Let K be a nonempty, closed and convex subset of X with its dual space X^*. Let $h : X \to (-\infty, +\infty]$ represent a strongly coercive Legendre function which is bounded, uniform Fréchet differentiable and totally convex on bounded subsets of X. Let $K_i, \forall i = 1, 2, ..., N$ represent finite family of closed, nonempty subset of X such that $\Omega = \cap_{i=1}^N Fix(P^h_{K_i}) \neq \emptyset$. Choose $x_0, x_1 \in K$ such that $x_1 < x_0$ and define the sequence $\{x_n\}$ thus:*

$$\begin{cases} x_0, x_1 \in C_1 = K \\ C_{1,i} = \cap_{i=1}^N C_{1,i}, \\ z_n = x_n + a_n(x_n - x_{n-1}), \\ y_{n,i} = \nabla h^* \left(b_n \nabla h(x_n) + (1 - b_n - c_n) \nabla h\left(P^h_{K_i} z_n\right) + c_n \nabla h(z_n)\right), \\ C_{n+1,i} = \{u \in C_n : d_h(u, y_{n,i}) \leq d_h(u, x_n) + d_h(x_n, z_n) \\ + \langle \nabla h(z_n) - \nabla h(x_n), x_n - u\rangle + \frac{\rho_i}{1-\rho_i}\langle \nabla h(z_n) - \nabla h(T_i z_n), z_n - u\rangle\}, \\ C_{n+1} = \cap_i^N C_{n+1,i}, \\ x_{n+1} = P^h_{C_{n+1}}(x_0), n \geq 1, \end{cases} \tag{64}$$

where $\{a_n\} \in (0, 1)$, $\{b_n\} \in (0, 1)$, and $\{c_n\} \in (0, 1)$ such that $c_n \in (0, (1-\rho_i)(1-b_n) \subset (0, 1)$, $i = 1, 2, ..., N$, with $\liminf_{\to\infty}(1 - b_n - c_n) > 0$. Then the sequences $\{x_n\}, \{z_n\}$ in (64) converges strongly to $\overline{x} = P^h_\Omega(x_0)$ nearest to x_0, as $n \to \infty$ and where P^h_Ω is the Bregman projection mapping of C_{n+1} onto Ω.

4.2. Equilibrium problems

A mapping $\Theta : K \times K \to \mathbb{R}$ is called a bifunction so that the equilibrium problem with respect to $\Theta : K \times K \to \mathbb{R}$ is to find $z^0 \in K$ such that

$$\Theta(z^0, z) \geq 0, \forall z \in K. \tag{65}$$

The collection of solution of (65) is represented by

$$EP(K, \Theta) := \left\{z^0 \in K : \Theta(z^0, z) \geq 0, \forall z \in K\right\}.$$

To solve a problem of the form (65) (see [5]), certain conditions are imposed on the bifunction $\Theta : K \times K \to \mathbb{R}$ as follows:
Assumption 1

(A1) $\Theta(z, z) = 0, \forall z \in K$,

(A2) $\Theta : K \times K \to \mathbb{R}$ is monotone, that is $\Theta(z^0, z) + \Theta(z, z^0) \leq 0$,

(A3) $\limsup_{t\downarrow 0} \Theta(\mu x + (1 - \mu)z^0, z) \leq \Theta(z^0, z), \forall x, z, z^0 \in K$,

(A4) The function $z \mapsto \Theta(z^0, z)$ is convex and lsc.

The resolvent of a bifunctions $\Theta : K \times K \to \mathbb{R}$ is the mapping $Res_{\Theta}^{h} : X \to 2^{K}$ defined by

$$Res_{\Theta}^{h}(x) := \left\{z^0 \in K : \Theta(z^0, z) + \left\langle \nabla h(z^0) - \nabla h(x), z - z^0 \right\rangle \geq 0, \forall z \in K \right\}. \tag{66}$$

Lemma 4.1 *[25] Let K be a closed and convex subset of X and let $h : X \to R \cup \{\infty\}$ be a coercive and Gâteaux differentiable function. Let $\Theta : K \times K \to R$ be a bifunction satisfying* ***Assumption 1*** *conditions, then the domain of the resolvent of a bifunctions with respect to h is X (i.e) $dom(Res_{\Theta}^{h}) = X$.*

Lemma 4.2 *[29] Let K be a closed and convex subset of X and let $h : X \to R \cup \{\infty\}$ be a coercive Legendre function. Let $\Theta : K \times K \to R$ be a bifunction satisfying* ***Assumption 1*** *conditions, and let Res_{Θ}^{h} be a resolvent mapping $Res_{\Theta}^{h} : X \to 2^{K}$ defined by (66), then we these conditions are met:*
(a) Res_{Θ}^{h} is single-valued,
(b) $Fix(Res_{\Theta}^{h}) = EP(K, \Theta)$,
(c) $d_h(q, Res_{\Theta}^{h}x) + d_h(Res_{\Theta}^{h}x, x) \leq d_h(q, x), \forall q \in Fix(Res_{\Theta}^{h})$,
(d) Res_{Θ}^{h} is Bregman quasi nonexpansive type mapping.

Theorem 4.2 *Let K be a nonempty, closed and convex subset of X with its dual space X^*. Let $h : X \to (-\infty, +\infty]$ represent a strongly coercive Legendre function which is bounded, uniform Fréchet differentiable and totally convex on bounded subsets of X. Let $\Theta_i : X \times X \to \mathbb{R}, \forall i \in I$ represent finite family of bifunctions which satisfy* ***Assumption 1*** *conditions and let $Res_{\Theta}^{h} : X \to 2^{K}$ be a resolvent mapping such that $\Omega = \cap_{i \in I} Fix(Res_{\Theta_i}^{h}) \neq \emptyset$. Choose $x_0, x_1 \in K$ such that $x_1 < x_0$ and define the sequence $\{x_n\}$ thus:*

$$\begin{cases} x_0, x_1 \in C_1 = K \\ z_n = x_n + a_n(x_n - x_{n-1}), \\ y_n = \nabla h^* \left(b_n \nabla h\left(x_n\right) + (1 - b_n - c_n) \sum_{i \in I} \lambda_n^i \nabla h\left(v_n^i\right) + c_n \nabla h\left(z_n\right)\right), \\ C_{n+1} = \{u \in C_n : d_h\left(u, y_n\right) \leq d_h\left(u, x_n\right) + d_h\left(x_n, z_n\right) \\ + \langle \nabla h\left(z_n\right) - \nabla h\left(x_n\right), x_n - u \rangle\}, \\ x_{n+1} = P_{C_{n+1}}^{h}(x_0), n \geq 1, \end{cases} \tag{67}$$

where $v_n^i := Res_{\Theta_i}^{h}(z_n)$, $\{a_n\} \in (0,1)$, $\{b_n\} \in (0,1)$, $\{c_n\} \in (0,1)$, and $\{\lambda_n^i\} \in (0,1)$ such that (1) $\sum_{i \in I} \lambda_n^i = 1$, (2) $c_n \in (0, (1 - \rho_i)(1 - b_n) \subset (0,1)$ for each $i = 1, 2, ..., N$ and (3) $\liminf_{\to \infty} (1 - b_n - c_n) > 0$. Then the sequences $\{x_n\}, \{z_n\}, \{u_n\}$ in (67) converges strongly to $\overline{x} = P_{\Omega}^{h}(x_0)$ nearest to x_0, with P_{Ω}^{h} as Bregman projection of C_{n+1} onto Ω.

Proof. Following the same approach as demonstrated in the proof of Theorem 3.1, we have

$$\lim_{n \to \infty} ||v_n^i - z_n|| = 0. \tag{68}$$

In view of (68) and the fact that ∇h is uniformly continuous and for each $i \in I$, we obtain

$$\lim_{n \to \infty} ||\nabla h(v_n^i) - \nabla h(z_n)|| = 0. \tag{69}$$

Furthermore,

$$\Theta_i\left(v_n^i, z\right) + \frac{i}{r_n^i} \left\langle z - v_n^i, \nabla h\left(v_n^i\right) - \nabla h\left(z_n\right) \right\rangle \geq 0, z \in K, \forall i \in I. \tag{70}$$

So by the monotocity property $A1$ of the bifunction $\Theta_i : K \times K \to \mathbb{R}$, we get for $n \geq 1$ and for each $i \in I$ that

$$\frac{i}{r_n^i} \left\langle z - v_n^i, \nabla h\left(v_n^i\right) - \nabla h\left(z_n\right) \right\rangle \geq \Theta_i\left(z, v_n^i\right), z \in K. \tag{71}$$

By condition $A4$, (69) and the fact that $v_n^i \to \overline{x}$ for each $i \in I$ and as $n \to \infty$, we get

$$\begin{aligned} 0 &\geq -\Theta_i(\overline{x}, z) \geq \Theta_i(z, \overline{x}) \\ &\geq \Theta_i(z, \overline{x}) + \Theta_i(\overline{x}, z) \\ &\geq \Theta_i(z, \overline{x}), \forall z \in K. \end{aligned}$$

Now consider $z_\mu = \mu z + (1-\mu)\overline{x}$, $\forall \mu \in (0,1)$ and $z \in K$. This shows that $z_\mu \in K$ and so $\Theta_i(z_\mu \overline{x}) \leq 0$. Following from conditions $A1$ and $A4$, we get

$$\begin{aligned} \Theta_i(z_\mu, z_\mu) &= 0 = \Theta_i(z_\mu, \mu z + (1-\mu)\overline{x}) \\ &\leq \mu\Theta_i(z_\mu, z) + (1-\mu)\Theta_i(z_\mu, \overline{x}) \\ &\leq \mu\Theta_i(z_\mu, z). \end{aligned}$$

Since $\mu \in (0,1)$, we get

$$0 \leq \Theta_i(z_\mu, z)$$

for each $i \in I$. Using condition $A3$ we have that

$$0 \leq \Theta_i(z_\mu, z) \leq \Theta_i(\overline{x}, z),$$

$\forall \overline{x}, z \in K$ and for each $i \in I$. This has shown that $\overline{x} \in EP(\Theta_i)$ for each $i \in I$. Hence $\overline{x} \in \cap_{i\in I} EP(\Theta_i)$. Thus, we obtain that $\overline{x} \in \Omega := \cap_{i \in I} EP(\Theta_i))$.

Example 4.1 (as application) *Let $X = R$, $K = [-1,1]$, $h(x) := \frac{2}{3}x^2$. The equilibrium problem with respect to $\Theta : K \times K \to \mathbb{R}$ defined by*

$$\Theta_i(u, z) = z^2 - zu + iuz - iu^2, \forall z \in K, \tag{72}$$

*is to find $u \in K$, for each $i \in I$ (see [22]). It is very obvious that for each $i \in I$, $\Theta_i(u,z)$ satisfies **Assumption 1** conditions. Also using the fact that Res^h_{Θ,r_i} is single valued, we get using*

$$Res^h_{\Theta,r_i}(z_n) := \left\{ v_n^i \in K : \Theta(v_n^i, z) + \frac{1}{r_i}\left\langle \nabla h(v_n^i) - \nabla h(z_n), z - v_n^i \right\rangle \geq 0, \forall z \in K \right\},$$

that

$$v_n^i = Res^h_{\Theta,r_i}(z_n) = \frac{4z_n}{3ir_i + 3r_i + 4}. \tag{73}$$

We see also for each $i \in I$, that $Fix(Res^h_{\Theta_i}) = 0$. Now we set $i \in (1,...10)$, $x_0 = 1.0, x_1 = 0.5$ and $a_n = \frac{1}{(n+10)^2}, b_n = \frac{1}{n+1}, c_n = \frac{1}{4n}$, $r_n^i = \frac{2n}{in+n+i+1}, \lambda_n^i = \frac{1}{2}$, with $\sum_{i\in I} \lambda_n^i = 1$ (see Table and figure below). Thus, our algorithm of Theorem 67 simplifies to

$$\begin{cases} x_0, x_1 \in K, \\ C_1 = K = [-1,1] \\ z_n := \frac{x_n + (x_n - x_{n-1})}{(n+10)^2}, \\ v_n^1 = \cdots v_n^{10} = \frac{2z_n(n+1)}{5n+2}, \\ y_n := \frac{8n^2 z_n + 10nx_n^2 + 11nz_n + 4x_n^2 + 3z_n}{4(n+1)(5n+2)}, \\ C_{n+1} := \left\{ u \in C_n : z \leq \frac{28n^2 z_n + 10nx_n^2 + 39nz_n + 4x_n^2 + 11z_n}{8(n+1)(5n+2)} \right\}, \\ x_{n+1} := P^h_{K_{n+1}}(x_0), n \geq 1. \end{cases} \tag{74}$$

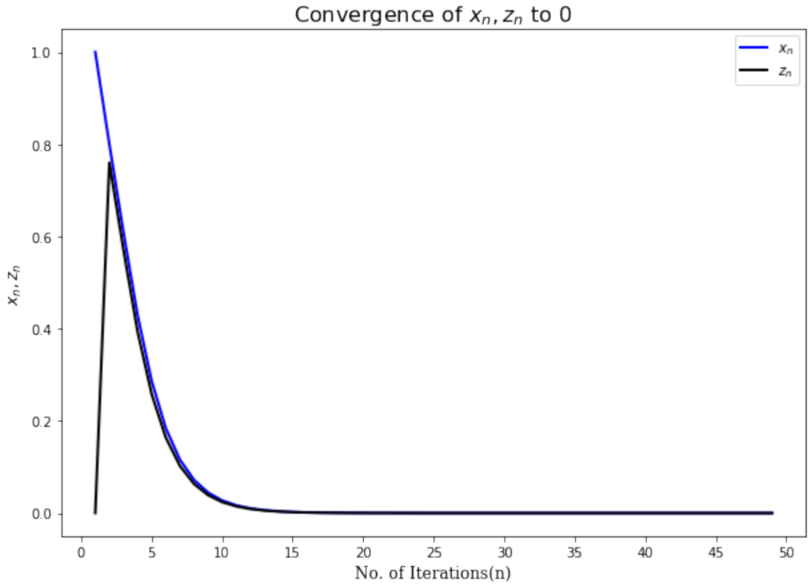

5 Numerical examples and implementation of (26)

In this section we demonstrate the effectiveness, implementation and convergence of our scheme (26) of Theorem 3.1. We do this by considering similar problem of [29]. We also use Python software, run on HP PC with Intel(R)Core(TM)i7-3520M CPU @ 2.90GHz to perform a side by side simulations of our scheme (26) with other similar results of some authors cited in the literature.

Example 5.1 *(cf.[29]) Let* $K = [0, 1]$, $h(x) := x^2$. *Let* $T_1, T_2 : K \to K$ *be defined by* $T_1(x) = sinx$ *and* $T_2(x) = sin(\frac{1}{2}x)$ *respectively. Then it is easy to see that both* T_1 *and* T_2 *are Bregman quasi strictly pseudo-contraction mappings with* $Fix(T_i) = \{0\}$, *and* $\rho_i = 0.5$ *for each* $i = 1, 2$.

Now, with two different sets of scalar sequences as follows: ***(a)*** $a_n = 0.6$, $b_n = \frac{5}{10}$, $c_n = \frac{1}{4} \in (0, (1-\rho_i)(1-b_n)) \subset (0, 1)$ *used in Table 1 and Figure 1, and* ***(b)*** $a_n = 0.4$, $b_n = \frac{1}{2n}$, $c_n = \frac{2n-1}{4n} \in (0, (1-\rho_i)(1-b_n)) \subset (0, 1)$ *used in Table 2 and Figure 2, then our assumptions in Theorem 3.1 are all satisfied. In addition, our scheme (26) is simplified thus:*

$$\begin{cases} x_0, x_1 \in K, \\ C_{1,i} = K = [0,1], i = 1, 2, \\ z_n := x_n + a_n(x_n - x_{n-1}), \\ y_{n,1} := b_n x_n + (1 - b_n - c_n) sin z_n + c_n z_n, \\ y_{n,2} := b_n x_n + (1 - b_n - c_n) sin \frac{1}{2} z_n + c_n z_n, \\ C_{n+1,1} := \{u \in C_n : u \leq \frac{(2\rho_1 sin(z_n) z_n - \rho_1 y_{n,1}^2 - \rho_1 z_n^2 + y_{n,1}^2 - z_n^2)}{2(\rho_1 sin(z_n) - \rho_1 y_{n,1} + y_{n,1} - z_n)}\}, \\ C_{n+1,2} := \{u \in C_n : u \leq \frac{(2\rho_2 sin(\frac{1}{2} z_n) z_n - \rho_2 y_{n,2}^2 - \rho_2 z_n^2 + y_{n,2}^2 - z_n^2)}{2(\rho_2 sin(\frac{1}{2} z_n) - \rho_2 y_{n,2} + y_{n,2} - z_n)}\}, \\ C_{n+1} := C_{n+1,1} \cap C_{n+1,2}, \\ x_{n+1} := P^h_{C_{n+1}}(x_0), n \geq 1. \end{cases} \tag{75}$$

Figure 1: Sequence values versus number of iterations showing comparison of our scheme (26) (indicated with Pink & Purple) and that of (24) (indicated with Black) respectively.

Table 1: Selected values of the sequences $\{x_n\}, \{z_n\}$ in our scheme (26) and $\{x2_n\}$ for that of (24) with the following cases.

Case 1 Take $x_0 = 1.0, x_1 = 0.8, z_0 = 0.0; x2_0 = 1.0, \rho_1 = \rho_2 = 0.5$

n	0	50	100	200	300	400	450	500
x_n	1.000000	0.054787	0.033168	0.012157	0.004456	0.001633	0.000989	0.000605
z_n	0.000000	0.054345	0.032900	0.012059	0.004420	0.001620	0.000981	0.000600
$x2_n$	1.000000	0.888736	0.790539	0.626695	0.497675	0.395650	0.352870	0.315479

Case 2 $x_0 = 1.0, x_1 = 1.0, z_0 = 0.0; x2_0 = 1.0, \rho_1 = \rho_2 = 0.5$

n	0	50	100	200	300	400	450	500
x_n	1.000000	0.871373	0.749156	0.555358	0.412674	0.307051	0.264935	0.229301
z_n	0.000000	0.869254	0.747349	0.554033	0.411695	0.306324	0.264309	0.228760
$x2_n$	1.000000	0.888736	0.790539	0.626695	0.497675	0.395650	0.352870	0.315479

Case 3 $x_0 = 0.5, x_1 = 0.3, z_0 = 0.0; x2_0 = 0.5, \rho_1 = \rho_2 = 0.5$

n	0	50	100	200	300	400	450	500
x_n	0.500000	0.097475	0.038147	0.005845	0.000896	0.00137	0.000054	0.000021
z_n	0.000000	0.095997	0.037569	0.005756	0.000882	0.000135	0.000053	0.000021
$x2_n$	0.500000	0.393700	0.310231	0.192864	0.119991	0.074674	0.058912	0.046698

Figure 2: Sequence values versus number of iterations showing comparison of our scheme (26) (indicated with Pink & Purple) and that of (24) (indicated with Black) respectively.

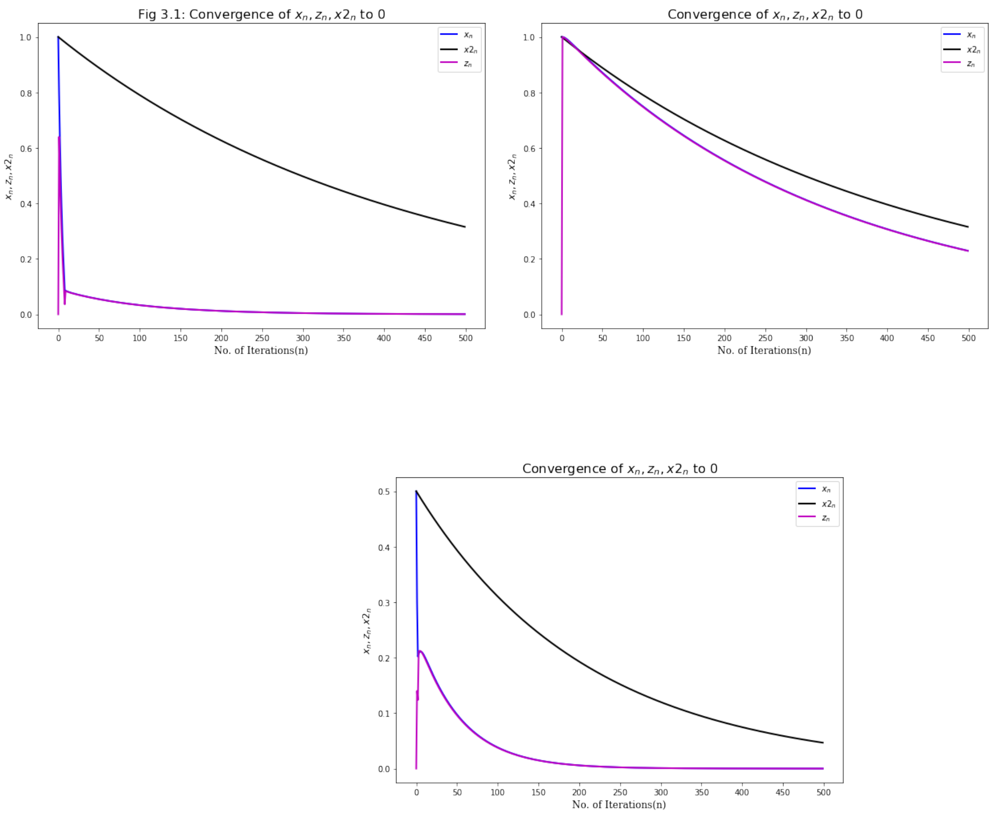

Table 2: Selected values of the sequences $\{x_n\}$ and $\{z_n\}$ in our scheme (26) and $\{x2_n\}$ with the following cases.

Case 1 Take $x_0 = 1.0, x_1 = 0.8, z_0 = 0.0; x2_0 = 1.0, \rho_1 = \rho_2 = 0.5$

n	0	5	10	20	30	40	45	50
x_n	1.000000	0.501570	0.199426	0.021442	0.001968	0.000170	0.000049	0.000018
z_n	0.000000	0.470859	0.181492	0.019192	0.001753	0.000151	0.000041	0.000016
$x2_n$	1.000000	0.741965	0.431008	0.129957	0.037177	0.010388	0.005462	0.003260

Case 2 $x_0 = 1.0, x_1 = 1.0, z_0 = 0.0; x2_0 = 1.0, \rho_1 = \rho_2 = 0.8$

n	0	5	10	20	30	40	45	50
x_n	1.000000	0.897273	0.642592	0.291564	0.126819	0.054203	0.035294	0.025005
z_n	0.000000	0.879106	0.623060	0.281636	0.122361	0.052267	0.034027	0.024104
$x2_n$	1.000000	0.899435	0.733148	0.463565	0.287177	0.176368	0.137932	0.113223

Case 3 $x_0 = 0.5, x_1 = 0.3, z_0 = 0.0; x2_0 = 0.5, \rho_1 = \rho_2 = 0.3$

n	0	5	10	20	30	40	45	50
x_n	0.500000	0.102363	0.024258	0.000694	0.000014	0.00000	0.000000	0.000000
z_n	0.000000	0.091246	0.020658	0.000567	0.000011	0.000000	0.000000	0.000000
$x2_n$	0.500000	0.319823	0.145020	0.025390	0.004134	0.000653	0.000258	0.000122

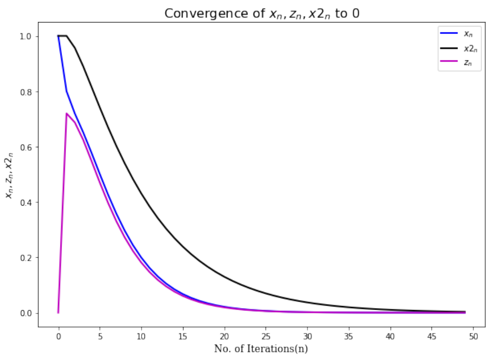

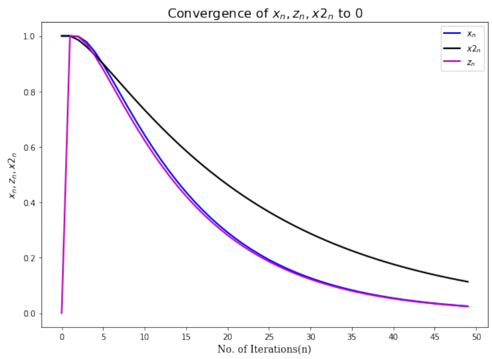

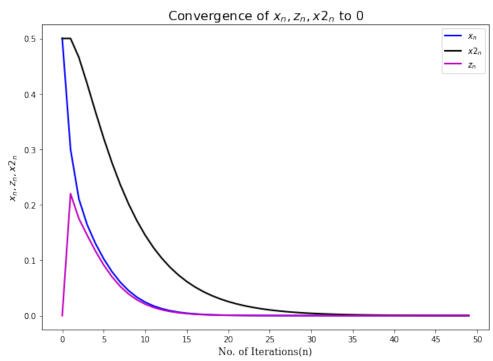

We observe a better performance of our scheme when compared with an existing result for finite family of Bregman quasi-strict pseudocontarction mappings.

6 Conclusion

In this paper, we constructed a two-step iterative algorithm with inertial extrapolation term defined with respect to Bregman distance function which approximated common fixed points of the finite family of a closed Bregman quasi strictly pseudo-contraction mappings when the intersection of its set is assumed to be non empty. The inertial extrapolation term has a flexible relaxed condition on the initial iterates x_n and x_{n-1}. We proved a strong convergence theorem for it. Through the use of Python program, we obtained that the sequences generated by our algorithm showed faster convergence results as displayed in the tables and figures above. Thus, our result improves, generalizes and complements other previously and recently cited results of some authors in the literature.

References

[1] Alber, Y.I. (1996). Metric and generalized projection operators in Banach Spaces Properties and Applications, Lecture Notes in Pure and Applied Mathematics; 15–50.

[2] Ali, B., Ezeora, J.N., and Lawan, M. S. (2019). Inertial algorithm for solving fixed point and generalized mixed equilibrium problems in Banach spaces. PanAmerican Mathematical Journal, 29(3):64–83.

[3] Ali, B., and Lawan, M.S. (2021). A forward-backward splitting algorithm for quasi-Bregman non-expansive mapping, equilibrium problems and accretive operators. Journal of the Nigerian Mathematical Society, 40(1):31–46.

[4] Bauschke, H.H., Borwein, J.M., and Combettes, P.L.(2001). Essential smoothness, essential strict convexity, and Legendre functions in Banach spaces. Communications in Contemporary Mathematics,3(4):615–647

[5] Blum, E., and Oettli, W. (1994). From optimization and variational inequalities to equilibrium problems. Mathematical Studies, 63:123-145.

[6] Bonnas, J.F., and Shapiro, A. (2000). Perturbation Analysis of Optimization Problems, Springer, New York.

[7] Bregman, L.M. (1967). The relaxation method for finding the common point of convex sets and its application to the solution of problems in convex programming. USSR Computational Mathematics and Mathematical Physics, 7(3):200–217.

[8] Butnariu, D., and Iusem, A.N. (2000). Totally convex functions for fixed points computation and infinite dimensional optimization. Kluwer Academic, Dordrecht, 40.

[9] Butnariu, D., and Resmerita, E. (2006). Bregman distances, totally convex functions and a method for solving operator equations in Banach spaces. Abstract and Applied Analysis, 1–39.

[10] Censor, Y. (1981). A. Lent, An iterative row-action method for interval convex programming. J. Optim. Theory Appl., 34:321–353.

[11] Chen, J., Wan, Z., Yuan, L., and Zheng, Y. (2011). Approximation of fixed points of weak Bregman relatively nonexpansive mappings in Banach spaces. International Journal of Mathematics and Mathematical Sciences, 420192.

[12] Chidume, C. E., Ikechukwu, S. I., and Adamu, A. (2018). Inertial algorithm for approximating a common fixed point for a countable family of relatively nonexpansive maps. Fixed Point Theory and Applications, 9.

[13] Dong, Q.L., and Lu, Y.Y.(2015). A new hybrid algorithm for a nonexpansive mapping. Fixed Point Theory Appl., 37.

[14] Dong, Q. L., Cho, Y. J., and Rassias, Th. M. (2016). General Inertial Mann Algorithms and their convergence analysis for nonexpansive mappings. Applications of Nonlinear Analysis, Springer Optimization and its Applications, 134.

[15] Ekuma-Okereke, E., and Oladipo, A. T.(2020). A Stong convergence theorem for finite families of Bregman quasi-nonexpansive and monotone mappings in Banach spaces. Fixed Point Theory, 21(1):167–180.

[16] Ekuma-Okereke, E., and Okoro, F.M. (2020). Common solution for nonlinear operators in Banach spaces. GUJ Sci. 33(3):737–749.

[17] Mann, W.R. (1953). Mean value methods in iteration. Proc. Am. Math. Soc., 4:506–510.

[18] Matsushita, S., and Takahashi, W.A. (2005). strong convergence theorem for relatively nonexpansive mappings in a Banach space. J. Approx. Theory, 134:257–266.

[19] Naraghirad, E., and Yao, J.C. (2013). Bregman weak relatively nonexpansive mappings in Banach spaces, Fixed Point Theory and Applications, 141.

[20] Ogbuisi, F.U. (2019). On common solution of a monotone variational inclusion for two mappings and a fixed point problem. U.P.B. Sci. Bull., Series A, 81(1):111–122.

[21] Padcharoen, A., Kuman, P., Chaipunya, P., and Shehu, Y. (2020). Convergence of inertial modified Krasnoselskii-Mann iteration with application to image recovery. Thai Journal of Mathematics, 18(1):126–142.

[22] Payvand, M. A., and Jahedi, S. (2016). System of generalized mixed equilibrium problems, variational inequality, and fixed point problems. Fixed Point Theory and Applications, DOI 10.1186/s13663-016-0583-7.

[23] Phelps, R. P. (1993). Convex Functions, Monotone Operators and Differentiability, Springer, Berlin, 1364.

[24] Reich, S., and Sabach, S. (2009). A strong convergence theorem for a proximal-type algorithm in reflexive Banach spaces. Journal of Nonlinear Convex Analysis, 10(3):471–485.

[25] Reich, S. and Sabach, S. (2010). Two strong convergence theorems for Bregman strongly nonexpansive operators in reflexive Banach spaces. Nonlinear Anal., 73:122–135.

[26] Rockafellar, R.T. (1970). Convex Analysis, Princeto University Press, Princeton.

[27] Ugwunnadi, G. C., Ali, B., Minjibir, M. S., and Idris, I. (2014). Strong convergence theorem for quasi-Bregman strictly pseudocontractive mappings and equilibrium problems in reflexive Banach spaces. Fixed Point Theory Appl., 231:1–16.

[28] Wang, Z.-M. (2015). Strong convergence theorems for Bregman quasi-strict pseudo-contractions in reflexive Banach spaces with applications. Fixed Point Theory Appl.

[29] Wang, Z.-M., and Wei, A. (2017). Some results on a finite family of Bregman quasi-strict pseudo-contractions. J. Nonlinear Sci. Appl., 10:975–989.

[30] Yongfu, S., and Yongchun, X. (2015). New hybrid shrinking projection algorithm for common fixed points of a family of countable quasi-Bregman strictly pseudocontractive mappings with equilibrium and variational inequality and optimization problems. Fixed Point Theory and Appl., 95.

[31] Yousuf, S. (2019). Iterative methods for some classes of equilibrium problems and fixed point problems, Ph.D thesis, Aligarh Muslim University, India.

[32] Zalinescu, C. (2002). Convex analysis in general vector spaces, World Scientific, River Edge, NJ, USA.

[33] Zegeye, H., and Shahzad, N. (2013). An algorithm for a common fixed point of a family of pseudocontractive mappings. Fixed Point Theory and Applications, 234(1).

[34] Zegeye, H., and Shahzad, N. (2014). Strong convergence theorems for a common fixed point of a finite family of Bregman weak relativity nonexpansive mappings in reflexive Banach spaces. The Scientific World Journal, Article ID 493450, 8 pages.

[35] Zegeye, S. B., Zegeye, H., Sangagoa, M. G., and Boikanyo, O. A. (2022). A convergence theorem for a common solution of f-fixed point, variational inequality and generalized mixed equilibrium problems in Banach spaces, Int. J. Nonlinear Anal. Appl., 1–19, http://dx.doi.org/10.22075/ijnaa.2022.25363.2995.

International Journal of Mathematical Analysis and Modelling
Volume 5, Issue 4, November 2022, Pages 132 – 163

Mathematical analysis of Ebola virus population dynamics

J. Andrawus*†, S. Abdulrahman†‡, R.V.K. Singh†, and S.S. Manga§

Abstract

In this paper, a non-linear mathematical model for the population dynamics of Ebola virus disease in existence of vaccination was developed and analyzed. Existence of equilibrium point was carried out, which shows us that the model consists of two equilibrium point. Local stability analyses of DFE have been carried out, it was found that the DFE is locally asymptotically stable if the threshold called reproduction number can be brought to a number less than unity. Comparison theorem was used to access the globally Stability of DFE, it was found that the DFE is globally asymptotically stable if the reproduction number can be brought to a number less than unity. LAS of endemic equilibrium point was done using Centre manifold theorem, it was established that the endemic equilibrium point is locally asymptotically stable if the reproduction number is greater than one. We were able to prove the global stability of endemic equilibrium point using Lyapunov function of Goh-Volterra type, it shows us that the endemic equilibrium point is globally asymptotically stable if the reproduction number is less than one. The numerical simulation shows that vaccinating a good number of people in a society can mitigate the Ebola virus disease (EVD).

Keywords and Phrases: Ebola virus; mathematical model; population dynamics; mathematical; population.

1 Introduction

EVD is a serious infection which is referred to as deadly, harmful and infectious disease which claimed numerous humans and other mammals' lives that causes huge damages economically in the West African Countries. A river in DRC was the main origin of EBV and it was named after the

*Corresponding Author. Department of Mathematics, Federal University Dutse, Jigawa State, Nigeria
†Department of Mathematics, Kebbi State University of Science and Technology Aliero, Kebbi State, Nigeria
‡Department of Mathematics, Federal University Birnin Kebbi, Kebbi State, Nigeria
§Department of Biological Sciences, Kebbi State University of Science and Technology Aliero, Kebbi State, Nigeria

DRC (Democratic Republic of Congo) river and it was in the year 1976 Ebola virus disease was discovered which can also harm primates and humans (Abdulrahman, 2016; Deepaa, 2015 and Tae and Lee, 2016).

The virus transmits into human population through blood contacts, secretions, other bodily fluids of infected animals or organs (Herick *et al.,*2020). Characterization of EBV is by flu which quickly progress to vomiting, diarrhea, rash, internal and external bleeding (Birmingham and Cooney, 2002; Eric *et al.*, 2020 and WHO, 2014). It is said that, Ebola virus can transmit from human to human, bats (fruit bats) to human and from other animals such as Monkeys, Gorillas and Chimpanzees etc (Amenoghawan and Aboubakary, 2015 and Ustun and Ozguller, 2004).

The recent 2018 to 2020 outbreak in Democratic republic of Congo was very multifaceted due to lack of security which affected the public health workers badly rejoinder activities, sequencing of samples suggests that cases in this outbreak are connected to cases in the area throughout the year 2018 to 2020 outbreak and possibly resulted from continual infection in a survivor that led to either a reversion or sexual transmission of the virus (CDC, 2019; Eric, *et al.,* 2020 and WHO, 2019).

Recent researches in mathematical modeling of Ebola virus (EBV) suggest that, tracing of infected /exposed individuals must be efficiently done in order to quarantine/isolate the affected population and educate community on the various ways in which the disease transmit, symptoms and preventive measures in order to minimize human to human transmissions (Herick *et al.*, 2020; Hussain *et al.,*2017 and Rachah and Torres, 2015).

Bats as a main reservoir of numerous viral infections are widely accepted (Pourrut *et al.*, 2009; Leroy *et al.*, 2005; Hayman, 2016 and Zineb *et al.*, 2018). Hayman (2016) think that the disease can be contracted by eating of contaminated fruits that is touched by bodily fluids of infectious bats (Zineb *et al.*, 2018). Over quite some years ago, there were several models which were developed mathematically to understand the dynamics of Ebola virus disease (EVD) (Azuaba *et al.,* 2017; Berge *et al.,* 2018; Eric, *et al.,* 2020 Espinoza *et al.,* 2015; Herick *et al.*, 2020; Kalu *et al.,* 2016; Nourridine, 2020; Lekone and Finkenstadt, 2006 and Murtaza *et al.,* 2016). Though, the said systems have normally considered the spread of the disease in human populace, only (Berge *et al.,* 2018 and Zineb *et al.*, 2018) considered bats population. In addition, they do not take into account the vaccinated humans and natural recovery due to immune response. For these precise and biological considerations, we propose a universal deterministic model for EVD.

2 Model formulation and fundamental properties

We build a model in a mathematical form of an Ebola virus dynamics by considering natural recovery and vaccination. We subdivided the system compartmentally in nine places, namely: Susceptible individuals (S_h), Latently infected individuals (L_h), Infectious individuals (I_h), Isolated individuals (J_h), Removed persons as a result of permanent recovery from the disease (R_h), Dead bodies of humans induced by Ebola virus disease before burial (D_h), environmental virus (V), Non-Carrier bats (N_b), Carrier-bats (C_b), humans Total population (T_h) and bats Total population (T_b). Figure 1 is the schematized representation of the model.

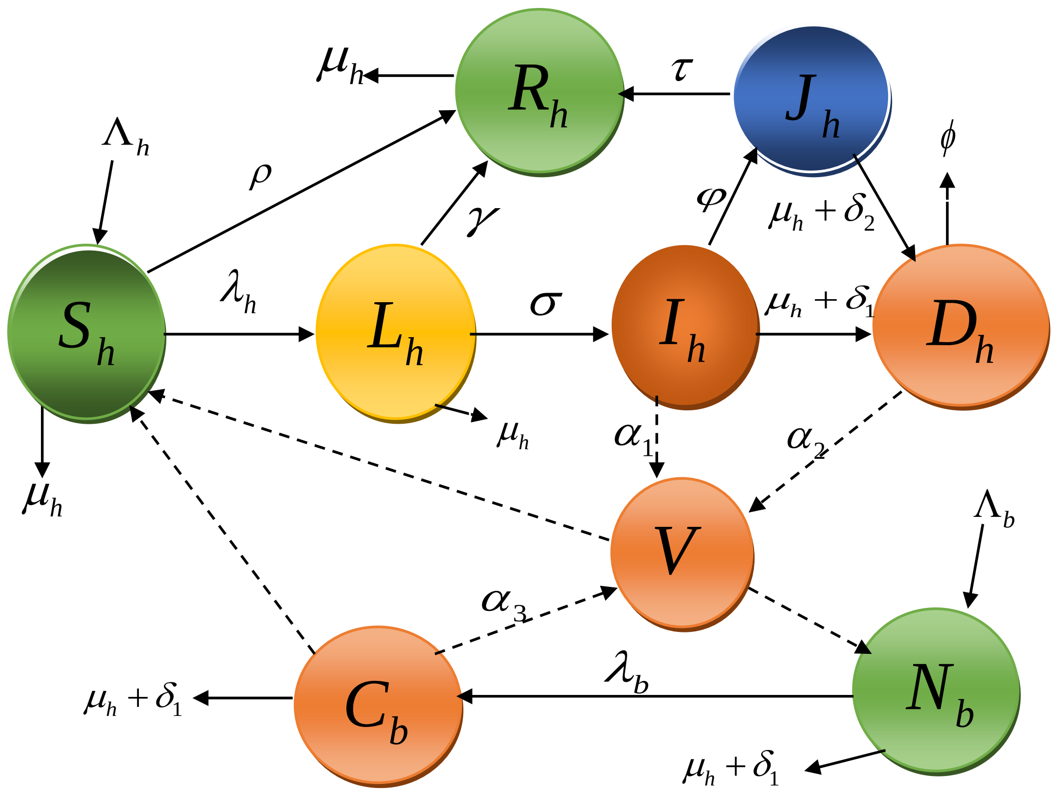

Figure 1. Schematized EVD transmission dynamics diagram

The S_h compartment is a representation of humans that are prone to the disease. This class are increased as a result of daily recruitment due to birth/immigration at the rate Λ_h. They get infected and transfer to L_h class by intermingling with those humans in the I_h and D_h compartments, virus in the environment and bats in the C_b compartment given by the term $\lambda_h = \frac{\beta_1(1-\varepsilon)(I_h+\eta D_h)+\beta_2(1-\varepsilon)V+\beta_3(1-\varepsilon)C_b}{T_h}$. The parameters β_1, β_2 and β_3 are the effective contact rate of human to human, virus in the environment to human and bats to humans respectively, η is the modification parameters which is tight to reduced contacts with the human dead body compare to humans who are infectious, the term $(1-\varepsilon)$ is the enhancement of public enlightenment on personal hygiene in respect of the transmission of the disease; $0<\varepsilon<1$. The class decreases due to people that have been vaccination at rate ρ.

$$\frac{dS_h}{dt} = \Lambda_h - (\lambda_1+\lambda_2+\lambda_3)S_h - (\rho+\mu_h)S_h \quad (1)$$

The L_h class represents the already infected persons with the virus but the clinical symptoms of Ebola not yet developed and are not capable of infecting others. L_h class is increased by effective/actual contact between S_h with I_h, D_h , V and C_b given by the term $\lambda_h = \frac{\beta_1(1-\varepsilon)(I_h+\eta D_h)+\beta_2(1-\varepsilon)V+\beta_3(1-\varepsilon)C_b}{T_h}$ as earlier explained. They decrease at the rates γ and σ due to natural recovery and disease progression respectively.

$$\frac{dL_h}{dt} = \left(\lambda_1+\lambda_2+\lambda_3\right)S_h - \left(\sigma+\gamma+q+\mu_h\right)L_h \tag{2}$$

I_h class is a representation of individuals who are symptomatic, infected as well as infectious. I_h class are increased at the rate σ from the L_h class as a result of clinical symptoms of Ebola developed by those in the L_h class. The I_h class diminishes at rates φ and δ_1 due to isolation and disease induced dead respectively.

$$\frac{dI_h}{dt} = \sigma L_h - \left(\varphi+\delta_1+\mu_h\right)I_h \tag{3}$$

The J_h class is a representation of humans who clinical symptoms are developed and have been isolated for treatment. The compartment is generated from I_h at the rate φ due to isolation. The class diminishes at the rates τ and δ_2 due to treatment and disease-induced death.

$$\frac{dJ_h}{dt} = \varphi I_h - \left(\tau+\delta_2+\mu_h\right)J_h \tag{4}$$

The removed humans' compartment, R_h represents humans that are effectively vaccinated as well as those that recovered from the disease and they possess lasting immunity against EVD as assumed. R_h class is increased from L_h, J_h and S_h classes at the rates γ, τ and ρ due to natural recovery of individuals in latent class, recovery due to effective treatment of individuals in J_h class and effective vaccination of individuals in S_h class respectively.

$$\frac{dR_h}{dt} = \rho S_h + \gamma L_h + \tau J_h - \mu_h R_h \tag{5}$$

The D_h class is a representation of human dead bodies of those that die due to Ebola virus from both J_h and I_h classes. The compartment decreases due to proper burial at the rate ϕ. The human's natural mortality can take place in all the existing humans' classes (in exception of D_h) at the rate μ_h.

$$\frac{dD_h}{dt} = \left(\delta_1+\mu_h\right)I_h + \left(\delta_2+\mu_h\right)J_h - \phi D_h \tag{6}$$

The V class is a representation of the virus in the environment. The class is generated as a result of the virus shade by I_h, D_h and C_b in the environment denoted by α_1, α_2 and α_3 respectively. The compartment diminishes due to natural death of virus ξ.

$$\frac{dV}{dt} = \alpha_1 I_h + \alpha_2 D_h + \alpha_3 C_b - \xi V \tag{7}$$

The N_b class is a representation of non-career bats. The class is increased as a result of constants recruitment at the rate Λ_b. They got infected and moved to C_b class by getting contacts with carrier bats in the C_b compartment and virus in the environment, given by the term $\lambda_b = \frac{\beta_4 C_b}{T_b} + \frac{\beta_5 V}{T_b}$ where β_4 and β_5 is rate of effective mingling of bats and environment to bats respectively.

$$\frac{dN_b}{dt} = \Lambda_b - (\lambda_4 + \lambda_5) N_b - (\delta_b + \mu_b) N_b \tag{8}$$

The C_b class is a representation of the Carrier bats who are capable of getting others infected. The class is increased by effective contact between N_b with C_b and V given by the term $\lambda_b = \frac{\beta_4 C_b}{T_b} + \frac{\beta_5 V}{T_b}$ as earlier explained. Both N_b and C_b classes diminish at the rates δ_b and μ_b due to human activities such as hunting and natural death respectively.

$$\frac{dC_b}{dt} = (\lambda_4 + \lambda_5) N_b - (\delta_b + \mu_b) C_b \tag{9}$$

The following assumptions and conditions are considered during the development of the system:

- Personal hygiene is enhancing by public enlightenment.
- Effective vaccinated and recovered individuals are permanently immune from the Ebola virus.

In synopsis the model consists of the following structure of nonlinear (deterministic) differential equations.

$$
\begin{aligned}
\dot{S}_h &= \Lambda_h - \lambda_h S_h - (\rho + \mu_h) S_h \\
\dot{L}_h &= \lambda_h S_h - (\sigma + \gamma + q + \mu_h) L_h \\
\dot{I}_h &= \sigma L_h - (\varphi + \delta_1 + \mu_h) I_h \\
\dot{J}_h &= \varphi I_h - (\tau + \delta_2 + \mu_h) J_h \\
\dot{R}_h &= \rho S_h + \gamma L_h + \tau J_h - \mu_h R_h \\
\dot{D}_h &= (\delta_1 + \mu_h) I_h + (\delta_2 + \mu_h) J_h - \phi D_h \\
\dot{V} &= \alpha_1 I_h + \alpha_2 D_h + \alpha_3 C_b - \xi V \\
\dot{N}_b &= \Lambda_b - \lambda_b N_b - (\delta_b + \mu_b) N_b \\
\dot{C}_b &= \lambda_b N_b - (\delta_b + \mu_b) C_b .
\end{aligned}
\tag{10}
$$

where

$$T_h = S_h + L_h + I_h + J_h + R_h + D_h,$$

and

$$T_b = N_b + C_b .$$

3 Basic analysis of the model (10)

The total population of human T_h is giving by adding the first six equations of the model (10) gives $\frac{dT_h}{dt} = \Lambda_h - \mu_h (T_h - I_h - J_h) - \phi D_h$, so that $T_h \to \frac{\Lambda_h}{\mu_h}$ as $t \to \infty$. Thus, $\frac{\Lambda_h}{\mu_h}$ is an upper bound of $T_h(t)$ provided that $T_h(0) \le \frac{\Lambda_h}{\mu_h}$. Furthermore, if $T_h(0) > \frac{\Lambda_h}{\mu_h}$, then $T_h(t)$ will decrease to this level. Similarly, calculation for the bats equations shows that $T_b \to \frac{\Lambda_b}{\mu_b}$ as $t \to \infty$.

Thus, the following feasible region:

$$\Pi = \left\{ (S_h, \mathrm{L}_h, \mathrm{Q}_h, \mathrm{I}_h, \mathrm{J}_h, \mathrm{D}_h, \mathrm{R}_h, \mathrm{N}_b, \mathrm{C}_b) \in \mathrm{R}_+^9 : T_h \le \frac{\Lambda_h}{\mu_h}, T_b \le \frac{\Lambda_b}{K_8} \right\}$$

is positively invariant set under the flow described in (1). Hence, no solution path leaves through and boundary of Π. Also, since solution paths cannot leave Π, solutions remain non-negative for non-negative initial conditions. Solutions exist for all time t. In this region, the model (10) is said to be well posed mathematically and epidemiologically.

3.1 Existence of equilibria (E^*)

At any giving equilibrium state the rate of change of each variable is equal to zero. That is

$$\frac{dS_h}{dt}=\frac{dL_h}{dt}=\frac{dI_h}{dt}=\frac{dJ_h}{dt}=\frac{dR_h}{dt}=\frac{dD_h}{dt}=\frac{dV}{dt}=\frac{dN_b}{dt}=\frac{dC_b}{dt}=0. \tag{11}$$

At any arbitrary equilibrium state, let

$$\left(S_h^*,L_h^*,I_h^*,J_h^*,R_h^*,D_h^*,V^*,N_b^*,C_b^*\right)=\left(S_h,L_h,I_h,J_h,R_h,D_h,V,N_b,C_b\right). \tag{12}$$

Thus, the state variables give

$$S_h^*=\frac{\Lambda_h}{\lambda_1^*+\lambda_2^*+\lambda_3^*+K_1},\ L_h^*=\frac{\left(\lambda_1^*+\lambda_2^*+\lambda_3^*\right)\Lambda_h}{K_2(\lambda_1^*+\lambda_2^*+\lambda_3^*+K_1)},\ I_h^*=\frac{\sigma\left(\lambda_1^*+\lambda_2^*+\lambda_3^*\right)\Lambda_h}{K_2\,\mathrm{K}_3\left(\lambda_1^*+\lambda_2^*+\lambda_3^*+K_1\right)}$$

$$J_h^*=\frac{\sigma\varphi\left(\lambda_1^*+\lambda_2^*+\lambda_3^*\right)\Lambda_h}{K_2\,\mathrm{K}_3\,K_4\left(\lambda_1^*+\lambda_2^*+\lambda_3^*+K_1\right)},$$

$$R_h^*=\frac{K_2K_3K_4\rho\Lambda_h+K_3K_4\gamma\Lambda_h\left(\lambda_1^*+\lambda_2^*+\lambda_3^*\right)+\tau\sigma\varphi\Lambda_h\left(\lambda_1^*+\lambda_2^*+\lambda_3^*\right)}{\mu_hK_2K_3K_4\left(\left(\lambda_1^*+\lambda_2^*+\lambda_3^*\right)+K_1\right)}$$

$$D_h^*=\frac{\sigma K_3K_5\Lambda_h\left(\lambda_1^*+\lambda_2^*+\lambda_3^*\right)+\sigma\varphi K_6\Lambda_h\left(\lambda_1^*+\lambda_2^*+\lambda_3^*\right)}{\phi K_2K_3K_4\left(\lambda_1^*+\lambda_2^*+\lambda_3^*+K_1\right)},\quad N_b^*=\frac{\Lambda_b}{\left(\lambda_4^*+\lambda_5^*+K_7\right)}$$

$$C_b^*=\frac{\left(\lambda_4^*+\lambda_5^*\right)\Lambda_b}{K_7\left(\lambda_4^*+\lambda_5^*+K_7\right)},\quad V^*=\frac{\begin{pmatrix}\sigma K_7\Lambda_h\left(\lambda_1^*+\lambda_2^*+\lambda_3^*\right)\left(\lambda_4^*+\lambda_5^*+K_7\right)\left(\alpha_1\phi K_4+\alpha_2\left(K_3K_5+\varphi K_6\right)\right)\\+\alpha_3\phi K_2K_3K_4\Lambda_b\left(\lambda_1^*+\lambda_2^*+\lambda_3^*+K_1\right)\left(\lambda_4^*+\lambda_5^*\right)\end{pmatrix}}{\xi\phi K_2K_3K_4K_7\left(\lambda_1^*+\lambda_2^*+\lambda_3^*+K_1\right)\left(\lambda_4^*+\lambda_5^*+K_7\right)}$$

where

$$\lambda_2^*=\frac{\beta_2\left(1-\varepsilon\right)V^*}{T_h^*} \tag{14}$$

$$\lambda_3^*=\frac{\beta_3\left(1-\varepsilon\right)C_b^*}{T_h^*} \tag{15}$$

$$\lambda_4^*=\frac{\beta_4C_b^*}{T_b^*} \tag{16}$$

$$\lambda_5^* = \frac{\beta_5 V^*}{T_b^*} \tag{17}$$

substituting the state variable concern in (13), we have

$$\lambda_1^* = \frac{\dfrac{\sigma\beta_1(1-\varepsilon)\Lambda_h\left(\lambda_1^*+\lambda_2^*+\lambda_3^*\right)}{K_2 K_3\left(\lambda_1^*+\lambda_2^*+\lambda_3^*+K_1\right)} + \dfrac{\sigma\eta\beta_1(1-\varepsilon)\Lambda_h\left(K_3K_5+\varphi K_6\right)\left(\lambda_1^*+\lambda_2^*+\lambda_3^*\right)}{\phi K_2K_3K_4\left(\lambda_1^*+\lambda_2^*+\lambda_3^*+K_1\right)}}{T_h^*} \tag{18}$$

simplifying (18), gives

$$\left(P_3\lambda_1^*+P_3\lambda_2^*+P_3\lambda_3^*+P_3K_1-\left(P_1+P_2\right)\right)\lambda_1^*-\left(P_1+P_2\right)\lambda_2^*-\left(P_1+P_2\right)\lambda_3^*=0 \tag{19}$$

where $P_1=\sigma\beta_1(1-\varepsilon)\Lambda_h\phi K_4, P_2=\sigma\eta\beta_1(1-\varepsilon)\Lambda_h\left(K_3K_5+\varphi K_6\right), P_3=\phi K_2K_3K_4T_h^*$.

Substituting the state variable concern in (14), gives

$$\lambda_2^* = \frac{\begin{pmatrix}\sigma\beta_2(1-\varepsilon)K_7\Lambda_h\left(\lambda_1^*+\lambda_2^*+\lambda_3^*\right)\left(\lambda_4^*+\lambda_5^*+K_7\right)\left(\alpha_1\phi K_4+\alpha_2\left(K_3K_5+\varphi K_6\right)\right)\\ +\beta_2(1-\varepsilon)\alpha_3\phi K_2K_3K_4\Lambda_b\left(\lambda_1^*+\lambda_2^*+\lambda_3^*+K_1\right)\left(\lambda_4^*+\lambda_5^*\right)\end{pmatrix}}{\xi\phi K_2K_3K_4K_7\left(\lambda_1^*+\lambda_2^*+\lambda_3^*+K_1\right)\left(\lambda_4^*+\lambda_5^*+K_7\right)}. \tag{20}$$

Simplifying (20), we have

$$\left(P_6\lambda_2^*+P_6\lambda_1^*+P_6\lambda_3^*+P_6K_1-\left(P_4+P_5\right)\right)\lambda_2^*-\left(P_4+P_5\right)\lambda_1^*-\left(P_4+P_5\right)\lambda_3^*-P_5K_1=0, \tag{21}$$

where

$$\begin{array}{l}P_4=\sigma\beta_2(1-\varepsilon)K_7\Lambda_h\left(\lambda_4^*+\lambda_5^*+K_7\right)\left(\alpha_1\phi K_4+\alpha_2\left(K_3K_5+\varphi K_6\right)\right)\\ P_5=\beta_2(1-\varepsilon)\alpha_3\phi K_2K_3K_4\Lambda_b\left(\lambda_4^*+\lambda_5^*\right),\ P_6=\xi\phi K_2K_3K_4K_7\left(\lambda_4^*+\lambda_5^*+K_7\right)\end{array}.$$

Substituting the state variable concern in (15), gives

$$\lambda_3^* = \frac{\beta_3(1-\varepsilon)\left(\lambda_4^*+\lambda_5^*\right)\Lambda_b}{T_h^*K_7\left(\lambda_4^*+\lambda_5^*+K_7\right)}. \tag{22}$$

Substituting the state variable concern in (16), we have

$$\lambda_4^* = \frac{\beta_4\left(\lambda_4^* + \lambda_5^*\right)\Lambda_b}{T_b^* K_7\left(\lambda_4^* + \lambda_5^* + K_7\right)}. \tag{23}$$

Simplifying (23), gives

$$\left(T_b^* K_7 \lambda_4^* + T_b^* K_7 \lambda_5^* + T_b^* K_7 K_7 - \beta_4 \Lambda_b\right)\lambda_4^* - \beta_4 \Lambda_b \lambda_5^* = 0 \tag{24}$$

Substituting the state variables concern into (17), we have

$$\lambda_5^* = \frac{\beta_5\begin{pmatrix}\sigma K_7 \Lambda_h\left(\lambda_1^* + \lambda_2^* + \lambda_3^*\right)\left(\lambda_4^* + \lambda_5^* + K_7\right)\left(\alpha_1 \phi K_4 + \alpha_2\left(K_3 K_5 + \varphi K_6\right)\right)\\ +\alpha_3 \phi K_2 K_3 K_4 \Lambda_b\left(\lambda_1^* + \lambda_2^* + \lambda_3^* + K_1\right)\left(\lambda_4^* + \lambda_5^*\right)\end{pmatrix}}{\xi \phi K_2 K_3 K_4 K_7 T_b^*\left(\lambda_1^* + \lambda_2^* + \lambda_3^* + K_1\right)\left(\lambda_4^* + \lambda_5^* + K_7\right)}. \tag{25}$$

Simplifying (25), we have

$$\lambda_5^* = \frac{\left(P_7 + P_8\right)\lambda_4^* + \left(P_7 + P_8\right)\lambda_5^* + P_7 K_7}{P_9 \lambda_4^* + P_9 \lambda_5^* + P_9 K_7} \tag{26}$$

$$\left(P_9 \lambda_4^* + P_9 \lambda_5^* + P_9 K_7 - \left(P_7 + P_8\right)\right)\lambda_5^* - \left(P_7 + P_8\right)\lambda_4^* - P_7 K_7 = 0, \tag{27}$$

where

$$P_7 = \sigma \beta_5 K_7 \Lambda_h\left(\lambda_1^* + \lambda_2^* + \lambda_3^*\right)\left(\alpha_1 \phi K_4 + \alpha_2\left(K_3 K_5 + \varphi K_6\right)\right),$$
$$P_8 = \beta_5 \alpha_3 \phi K_2 K_3 K_4 \Lambda_b\left(\lambda_1^* + \lambda_2^* + \lambda_3^* + K_1\right),\ P_9 = \xi \phi K_2 K_3 K_4 K_7 T_b^*\left(\lambda_1^* + \lambda_2^* + \lambda_3^* + K_1\right)$$

Consider a scenario where $\lambda_1^*, \lambda_2^*, \lambda_3^*, \lambda_4^*, \lambda_5^* > 0$, at endemic all the force of infection are positive. Also, consider

$$\lambda_5^* = 0. \tag{28}$$

Substituting (28) into (24), gives

$$\left(T_b^* K_7 \lambda_4^* + T_b^* K_7 K_7 - \beta_4 \Lambda_b\right)\lambda_4^* = 0. \tag{29}$$

Equation (29) gives

$$\lambda_4^* = 0 \tag{30}$$

or

$$T_b^* K_7 \lambda_4^* + T_b^* K_7 K_7 - \beta_4 \Lambda_b = 0. \tag{31}$$

Simplifying (31), we have

$$\lambda_4^* = \frac{\beta_4\Lambda_b - T_b^* K_7 K_7}{T_b^* K_7} \tag{32}$$

Considering the last model equation in system (1), it is easy to deduce that $K_7 < 1$, therefore K_7K_7 will become smaller, which makes $\lambda_4^* > 0$.

$$\lambda_4^* > 0 \tag{33}$$

Substituting (28) and (30), into (22), gives

$$\lambda_3^* = 0 \tag{34}$$

Substituting (28) while $\lambda_5^* > 1$ into (22), we have

$$\lambda_3^* > 0 \tag{35}$$

if

$$\lambda_1^* = 0 \tag{36}$$

Substituting (28), (30), (34) and (36) into (21), gives

$$\left(P_6\lambda_2^* + P_6K_1 - \left(P_4 + P_5\right)\right)\lambda_2^* = 0 \tag{37}$$

either

$$\lambda_2^* = 0 \tag{38}$$

or

$$\lambda_2^* = \frac{\left(P_4 + P_5\right) - P_6K_1}{P_6} \tag{39}$$

For λ_2^* to be greater than zero ($\lambda_2^* > 0$) it is very important to compare the values of P_4, P_5 and P_6 within mind that multiplication of numbers less than zero is smaller.

$$P_4 + P_5 - P_6K_1 = P_4 = \sigma\beta_2\left(1-\varepsilon\right)K_7K_7\Lambda_h\left(\alpha_1\phi K_4 + \alpha_2\left(K_3K_5 + \varphi K_6\right)\right) - \xi\phi K_1K_2K_3K_4K_7K_7 > 0 \tag{40}$$

with the above reason clearly $\lambda_2^* > 0$, therefore

$$\lambda_2^* > 0 \tag{41}$$

Substituting (28), (30), (34), (36) and (39) into (19),
we have

$$\left(P_3\lambda_1^* + P_3K_1 - \left(P_1 + P_2\right)\right)\lambda_1^* = 0 \tag{42}$$

either

$$\lambda_1^* = 0 \tag{43}$$

or

$$P_3\lambda_1^* + P_3K_1 - \left(P_1 + P_2\right) = 0 \tag{44}$$

Simplifying (44), gives

$$\lambda_1^* = \frac{(P_1 + P_2) - P_3K_1}{P_3} \tag{45}$$

For λ_1^* to be greater than zero ($\lambda_1^* > 0$) it is very important to compare the values of P_1, P_2 and P_3 within mind that multiplication of numbers less than zero is smaller.

$$P_1 + P_2 - P_3 = \sigma\beta_1(1-\varepsilon)\Lambda_h\phi K_4 + \sigma\eta\beta_1(1-\varepsilon)\Lambda_h(K_3K_5 + \varphi K_6) - \phi K_2K_3K_4T_h^* \tag{46}$$

Therefore, based on the explanation above, is greater than zero. Thus

$$\lambda_1^* > 0. \tag{47}$$

Substituting (30), (34), (36), (39) and (43) into (27), gives

$$\left(P_9\lambda_5^* + P_9K_7 - P_8\right)\lambda_5^* = 0 \tag{48}$$

either

$$\lambda_5^* = 0$$

or

$$P_9\lambda_5^* + P_9K_7 - P_8 \tag{49}$$

Simplifying (49), we have

$$\lambda_5^* = \frac{\beta_5\alpha_3\phi K_1K_2K_3K_4\Lambda_b - \xi\phi K_1K_2K_3K_4K_7K_7T_b^*}{P_3} \tag{50}$$

for λ_5^* to be greater than zero, it is very important to consider the numerator of (50), ξK_7K_7 is far less than one because all the three parameters are less than one. Therefore,

$$\beta_5\alpha_3\phi K_1K_2K_3K_4\Lambda_b - \xi\phi K_1K_2K_3K_4K_7K_7T_b^* > 0 \tag{51}$$

Thus, we have

$$\lambda_5^* > 0 \tag{52}$$

Hence, considering (28), (30), (34), (36) and (39) the exist DFE, also considering (33), (35), (41), (47) and (52) there exist EEP.

3.2 Local stability of disease-free equilibrium (DFE)

There is no infection at disease-free equilibrium. Therefore, all the disease classes are zero at this point and population will reduced to non-Career bats and vaccinated individuals. The DFE of system (10) obtained by setting the right-hand side of the system (10) to zero is given by $E^0 = (S_h, L_h, I_h, J_h, R_h, D_h, V, N_b, C_b, T_h, T_b) = \left(\frac{\Lambda_h}{K_1}, 0, 0, 0, \frac{\rho\Lambda_h}{\mu_h K_1}, 0, 0, \frac{\Lambda_b}{K_8}, 0, \frac{\Lambda_h}{\mu_h}, \frac{\Lambda_b}{K_8}\right)$. Next generation operator method has been to prove the local stability of DFE (E^0) of system (10). Considering only infected classes $(L_h, I_h, J_h, D_h, V, C_b)$ at DFE and taking into consideration the notation in Van den Driessche and Watmough (2002) the F and V matrices for those who are newly infected and those remaining terms that are transferred from the infected compartments respectively, are respectively given as

$$F=\begin{pmatrix} 0 & \frac{\beta_1(1-\varepsilon)\mu_h}{K_1} & 0 & \frac{\eta\beta_1(1-\varepsilon)\mu_h}{K_1} & \frac{\beta_2(1-\varepsilon)\mu_h}{K_1} & \frac{\beta_3(1-\varepsilon)\mu_h}{K_1} \\ 0&0&0&0&0&0\\ 0&0&0&0&0&0\\ 0&0&0&0&0&0\\ 0&0&0&0&0&0\\ 0&0&0&0&\beta_5&\beta_4 \end{pmatrix} \tag{53}$$

and

$$V=\begin{pmatrix} K_2&0&0&0&0&0\\ -\sigma&K_3&0&0&0&0\\ 0&-\varphi&K_4&0&0&0\\ 0&-K_5&-K_6&\phi&0&0\\ 0&-\alpha_1&0&-\alpha_2&\xi&-\alpha_3\\ 0&0&0&0&0&K_7 \end{pmatrix} \tag{54}$$

where $K_1=\rho+\mu_h$, $K_2=\sigma+\gamma+\mu_h$, $K_3=\varphi+\delta_1+\mu_h$, $K_4=\tau+\delta_2+\mu_h$, $K_5=\delta_1+\mu_h$ $K_6=\delta_2+\mu_h$, $K_7=\delta_b+\mu_b$

the product of (FV^{-1}), gives

$$FV^{-1}=\begin{pmatrix} R_0^{hhv1}&R_0^{hhv2}&R_0^{hhv3}&R_0^{hhv4}&R_0^{hv}&R_0^{hvb}\\ 0&0&0&0&0&0\\ 0&0&0&0&0&0\\ 0&0&0&0&0&0\\ 0&0&0&0&0&0\\ R_0^{bv1}&R_0^{bv2}&R_0^{bv3}&R_0^{bv4}&R_0^{bv5}&R_0^{bbv} \end{pmatrix} \tag{55}$$

where $R_0^{hhv1}=\frac{\sigma\beta_1(1-\varepsilon)\mu_h}{K_1K_2K_3}+\frac{\sigma\eta\beta_1(1-\varepsilon)\mu_h\left(\varphi K_6+K_4K_5\right)}{\phi K_1K_2K_3K_4}+\frac{\sigma\beta_2(1-\varepsilon)\mu_h\left(\phi\alpha_1K_4+\varphi\alpha_2K_6+\alpha_2K_4K_5\right)}{\phi\xi K_1K_2K_3K_4}$,

$$R_0^{hhv2}=\frac{\sigma\beta_1(1-\varepsilon)\mu_h}{K_1K_3}+\frac{\eta\beta_1(1-\varepsilon)\mu_h\left(\varphi K_6+K_4K_5\right)}{\phi K_1K_3K_4}+\frac{\beta_2(1-\varepsilon)\mu_h\left(\phi\alpha_1K_4+\varphi\alpha_2K_6+\alpha_2K_4K_5\right)}{\phi\xi K_1K_3K_4}$$

$$R_0^{hhv3}=\frac{\eta\beta_1(1-\varepsilon)\mu_h K_6}{\phi K_1 K_4}+\frac{\beta_2(1-\varepsilon)\mu_h\alpha_2 K_6}{\phi\xi K_1 K_4},\quad R_0^{hhv4}=\frac{\eta\beta_1(1-\varepsilon)\mu_h}{\phi K_1}+\frac{\beta_2(1-\varepsilon)\mu_h\alpha_2}{\phi\xi K_1},\qquad R_0^{hv}=\frac{\beta_2(1-\varepsilon)\mu_h}{\xi K_1},$$

$$R_0^{hvb}=\frac{\beta_2(1-\varepsilon)\mu_h\alpha_3}{\xi K_1 K_7}+\frac{\beta_3(1-\varepsilon)\mu_h}{K_1 K_7},\ R_0^{bv1}=\frac{\sigma\beta_5\left(\phi\alpha_1 K_4+\varphi\alpha_2 K_6+\alpha_2 K_4 K_5\right)}{\phi\xi K_2 K_3 K_4},$$

$$R_0^{bv2}=\frac{\beta_5\left(\phi\alpha_1 K_4+\varphi\alpha_2 K_6+\alpha_2 K_4 K_5\right)}{\phi\xi K_3 K_4},\ R_0^{bv1}=\frac{\beta_5\alpha_2 K_6}{\phi\xi K_4},\ R_0^{bv4}=\frac{\beta_5\alpha_2}{\phi\xi},\ R_0^{bv5}=\frac{\beta_5}{\xi}\ \text{and}\ R_0^{bbv}=\frac{\beta_5\alpha_3}{\xi K_7}+\frac{\beta_4}{K_7}.$$

Then the spectral radius is given by

$$\rho\left(FV^{-1}\right)=max\left\{\frac{R_0^{bbv}+R_0^{hhv1}+\sqrt{\left(R_0^{bbv}-R_0^{hhv1}\right)^2+4R_0^{bv1}R_0^{hvb}}}{2},\frac{R_0^{bbv}+R_0^{hhv1}-\sqrt{\left(R_0^{bbv}-R_0^{hhv1}\right)^2+4R_0^{bv1}R_0^{hvb}}}{2}\right\} \tag{56}$$

$$R_c=\frac{R_0^{bbv}+R_0^{hhv1}+\sqrt{\left(R_0^{bbv}-R_0^{hhv1}\right)^2+4R_0^{bv1}R_0^{hvb}}}{2} \tag{57}$$

The following result is established using Theorem 2 in Van den Driessche and Watmough (2002).
Lemma 1: The DFE of the system (10) is locally asymptotically stable if $R_c<1$ and unstable if R_c > 1.

The epidemiological threshold R_c gives the average number of Ebola virus cases generated by the infected individual into an entirely susceptible population (Agusto *et al.,* 2017; Anderson and May, 1991; Andrawus *et al.,* 2017; Hethcot, 2000 and Van den Driessche and Watmough, 2002). The value called the threshold quantity R_c is the effective reproduction number for the model (10). The significance of Lemma 1 epidemiologically is that if R_c is less than unity, a small inflow of infected persons into the population would produce large outbreaks, and the disease dies out in time. However, the disease-free equilibrium might not be globally asymptotically stable even if R_c < 1 in the case of when backward bifurcation exists. That is, there is an existence of a stable EEP co-existing with the DFE.

3.3 GAS of DFE of model (10)

The stability of DFE at global level of the model (10) will be established. We claim the following result.

Theorem 1. The disease-free state of the model (10) is GAS whenever $R_c < 1$.

Proof: To prove the global stability of the disease-free equilibrium of model (10), we need to follow the approach in Castillo Chavez *et al*. (2002) that the two conditions (G1) and (G2) must be mate for $R_c < 1$. Let $X = (S_h, R_h, N_b)$ and $Y = (L_h, I_h, J_h, D_h, V, C_b)$ and separate model (10) into:

$$\frac{dX}{dt} = F(X, Y) \tag{58}$$

$$\frac{dY}{dt} = G(X, Y);\ G(X, 0) = 0 \tag{59}$$

with the components of $X \in R^3$ representing the uninfected compartment and the components $Y \in R^6$ representing the infected compartment.

The disease-free equilibrium is now represented as

$$E^0 = (X^*, 0) \tag{60}$$

where

$$X^* = (T_h^0 / T_b^0, 0) \tag{61}$$

Considering the first condition, that is global stability of X^*, gives

$$\frac{dX_1}{dt} = F(\mathrm{X}_1, 0) = \begin{bmatrix} \Lambda_h - K_1 S_h{}^0 \\ \rho S_h{}^0 - \mu_h R_h{}^0 \\ \Lambda_b - \mu_b N_b{}^0 \end{bmatrix} \tag{62}$$

Now, using integrating factor (I.F)

$$S_h{}^0(t) = \frac{\Lambda_h}{K_1} - \frac{\Lambda_h}{K_1} e^{-K_1 t} + S_h{}^0(0) e^{-K_1 t} \tag{63}$$

$$R_h{}^0(t) = \frac{\rho S_h{}^0}{\mu_h} - \frac{\rho S_h{}^0}{\mu_h} e^{-\mu_h t} + R_h{}^0(0) e^{-\mu_h t} \tag{64}$$

$$N_b{}^0(t) = \frac{\Lambda_b}{\mu_b} - \frac{\Lambda_b}{\mu_b} e^{-\mu_b t} + N_b{}^0(0) e^{-\mu_b t}. \tag{65}$$

Now, obviously $S_h{}^0(t) + R_h{}^0(t) \to T_h{}^0(t)$ and $N_b{}^0 \to T_b{}^0$ as $t \to \infty$ regardless of the value of $S_h{}^0(0)$, $R_h{}^0(0)$ and $N_b{}^0(0)$. Thus, $X^* = (T_h^0 / T_b^0, 0)$ is a GAS.

Further, for the other criterion that is $\overline{G}(X,Y)=BY-G(X,Y)$ gives

$$B=\begin{pmatrix} -K_2 & \frac{\beta_1(1-\varepsilon)S_h{}^0}{T_h{}^0} & 0 & \frac{\eta\beta_1(1-\varepsilon)S_h{}^0}{T_h{}^0} & \frac{\beta_2(1-\varepsilon)S_h{}^0}{T_h{}^0} & \frac{\beta_3(1-\varepsilon)S_h{}^0}{T_h{}^0} \\ \sigma & -K_3 & 0 & 0 & 0 & 0 \\ 0 & \varphi & -K_4 & 0 & 0 & 0 \\ 0 & K_5 & K_6 & -\phi & 0 & 0 \\ 0 & \alpha_1 & 0 & \alpha_2 & -\xi & \alpha_3 \\ 0 & 0 & 0 & 0 & \frac{\beta_5 N_b{}^0}{T_b{}^0} & -K_7+\frac{\beta_4 N_b{}^0}{T_b{}^0} \end{pmatrix} \tag{66}$$

The matrix (66) is M- matrix clearly (the off-diagonal element of B are non-negative).

$$\overline{G}(X,Y)=\begin{bmatrix} (\lambda_1+\lambda_2+\lambda_3)S_h{}^0-K_2L_h{}^0 \\ \sigma L_h{}^0-K_3I_h{}^0 \\ \varphi I_h{}^0-K_4J_h{}^0 \\ K_5I_h{}^0+K_6J_h{}^0-\phi D_h{}^0 \\ \alpha_1I_h{}^0+\alpha_2D_h{}^0+\alpha_3C_b{}^0-\xi V^0 \\ (\lambda_4+\lambda_5)N_b{}^0-K_7C_b{}^0 \end{bmatrix} \tag{67}$$

then,

$$\overline{G}(X,Y)=[0,0,0,0,0,0]^T. \tag{68}$$

It is thus clearly that $\overline{G}(X,Y)=0$. Hence, the proof is complete.

Consider scenario where the endemic equilibrium exists.

3.4 Stability of endemic equilibrium at local level of model (10)

Theorem 2: The EEP of system (10) is LAS if the control reproduction number, $R_c>1$.

Proof: Because of the high dimension of the system, standard linearization around the endemic equilibrium cannot be used. Therefore, the theory of Centre manifold which is clearly explained in Castillo-Chavez and Song (2004) for LAS analysis have been used in this work, in order to apply the theorem. Therefore, it is very important to make the following changes of variables. Let

$$(x_1,x_2,x_3,x_4,x_5,x_6,x_7,x_8,x_9)=(S_h,L_h,I_h,J_h,R_h,D_h,\mathrm{V},N_b,C_b) \tag{69}$$

Furthermore, using the vector notation

$$X = (x_1, x_2, x_3, x_4, x_5, x_6, x_7, x_8, x_9)^T \tag{70}$$

The system (10) can be written in the form

$$\frac{dX}{dt} = F = (f_1, f_2, f_3, f_4, f_5, f_6, f_7, f_8, f_9)^T \tag{71}$$

such that

$$\begin{aligned}
\dot{x}_1 &= \Lambda - \frac{\beta_1(1-\varepsilon)(x_3+\eta x_6)}{T_h}x_1 - \frac{\beta_2(1-\varepsilon)x_7}{T_h}x_1 - \frac{\beta_3(1-\varepsilon)x_9}{T_h}x_1 - K_1x_1 = f_1\\
\dot{x}_2 &= \frac{\beta_1(1-\varepsilon)(x_3+\eta x_6)}{T_h}x_1 + \frac{\beta_2(1-\varepsilon)x_7}{T_h}x_1 + \frac{\beta_3(1-\varepsilon)x_9}{T_h}x_1 - K_2x_2 = f_2\\
\dot{x}_3 &= \sigma x_2 - K_3x_3 = f_3\\
\dot{x}_4 &= \varphi x_3 - K_4x_4 = f_4\\
\dot{x}_5 &= \gamma x_2 + \rho x_1 + \tau x_4 - \mu_h x_5 = f_5\\
\dot{x}_6 &= K_5x_3 + K_6x_4 - \phi x_6 = f_6\\
\dot{x}_7 &= \alpha_1x_3 + \alpha_2x_6 + \alpha_3x_9 - \xi x_7 = f_7\\
\dot{x}_8 &= \Lambda_b - \frac{\beta_4x_9}{T_b}x_8 - \frac{\beta_5x_7}{T_b}x_8 - K_7x_8 = f_8\\
\dot{x}_9 &= \frac{\beta_4x_9}{T_b}x_8 + \frac{\beta_5x_7}{T_b}x_8 - K_8x_9 = f_9.
\end{aligned} \tag{72}$$

The Jacobian evaluated at DFE for the system (72) above is given by the Jacobian (73) as

$$J(E^0) = \begin{pmatrix}
-K_1 & 0 & -\frac{\beta_1(1-\varepsilon)x_1^0}{T_h^0} & 0 & 0 & -\frac{\beta_1\eta(1-\varepsilon)x_1^0}{T_h^0} & -\frac{\beta_2(1-\varepsilon)x_1^0}{T_h^0} & 0 & -\frac{\beta_3(1-\varepsilon)x_1^0}{T_h^0}\\
0 & -K_2 & \frac{\beta_1(1-\varepsilon)x_1^0}{T_h^0} & 0 & 0 & \frac{\beta_1\eta(1-\varepsilon)x_1^0}{T_h^0} & \frac{\beta_2(1-\varepsilon)x_1^0}{T_h^0} & 0 & \frac{\beta_3(1-\varepsilon)x_1^0}{T_h^0}\\
0 & \sigma & -K_3 & 0 & 0 & 0 & 0 & 0 & 0\\
0 & 0 & \varphi & -K_4 & 0 & 0 & 0 & 0 & 0\\
\rho & \gamma & 0 & \tau & -\mu_h & 0 & 0 & 0 & 0\\
0 & 0 & K_5 & K_6 & 0 & -\phi & 0 & 0 & 0\\
0 & 0 & \alpha_1 & 0 & 0 & \alpha_2 & -\xi & 0 & \alpha_3\\
0 & 0 & 0 & 0 & 0 & 0 & -\beta_5 & -K_7 & -\beta_4\\
0 & 0 & 0 & 0 & 0 & 0 & \beta_5 & 0 & -K_7+\beta_4
\end{pmatrix} \tag{73}$$

Suppose $\beta_5 = \beta_5^*$ is chosen as a bifurcation parameter at $R_c = 1$, we have that

$$\beta_5^{\ *} = \frac{\phi\xi K_4\left[\left(2-\left(R_0^{bbv}+R_0^{hhv1}\right)\right)^2-\left(R_0^{bbv}-R_0^{hhv1}\right)^2\right]}{4\alpha_2 K_6 R_0^{hvb}}. \tag{74}$$

Eigenvectors $J(E^0)_{\beta_5=\beta_5^*}$

Given W and V as a right and left eigenvectors associated with the zero eigenvalues of the Jacobian $J(E^0)_{\beta_5=\beta_5^*}$ (denoted by $J_{\beta_5^*}$) chosen such that $VJ(E^0)=0$ and $J(E^0)\mathrm{W}=0$ with $VW=1$ where $V=\left[v_1,v_2,v_3,v_4,v_5,v_6,v_7,v_8,v_9\right]$ and $W=\left[w_1,w_2,w_3,w_4,w_5,w_6,w_7,w_8,w_9\right]^T$. Thus,

$$v_1=v_6=v_8=0,\ v_2=v_4>0,\ v_3=\frac{\beta_1(1-\varepsilon)x_1^{\ 0}}{T_h^{\ 0}}v_2+\varphi v_2+\frac{\beta_2(1-\varepsilon)x_1^{\ 0}}{T_h^{\ 0}}v_2+\frac{\beta_3\beta_5(1-\varepsilon)x_1^{\ 0}}{(K_7-\beta_4)T_h^{\ 0}}v_2$$

$$v_5=\frac{K_4}{\tau}v_2,\ v_7=\frac{\beta_2(1-\varepsilon)x_1^{\ 0}}{T_h^{\ 0}}v_2+\frac{\beta_3\beta_5(1-\varepsilon)x_1^{\ 0}}{(K_7-\beta_4)T_h^{\ 0}}v_2,\ v_9=\frac{\beta_3\beta_5(1-\varepsilon)x_1^{\ 0}}{(K_7-\beta_4)T_h^{\ 0}}v_2,$$

and

$$w_2=w_2>0,\ w_3=\frac{\sigma}{K_3}w_2,\ w_4=\frac{\varphi\sigma}{K_3K_4}w_2,$$

$$w_1=-\left\{\begin{array}{l}\dfrac{\sigma\beta_1(1-\varepsilon)x_1^{\ 0}}{K_1K_3T_1^0}+\dfrac{\sigma\beta_1\eta(1-\varepsilon)x_1^{\ 0}\left(K_4K_5+K_6\varphi\right)}{K_1K_3K_4T_1^0}\\ +\dfrac{\beta_2(1-\varepsilon)x_1^{\ 0}\xi(K_7-\beta_4)}{K_1T_1^0\left(\xi(K_7-\beta_4)-\alpha_3\beta_5\right)}\left(\dfrac{\alpha_1\sigma}{\xi K_3}+\dfrac{\alpha_2K_5\sigma}{\xi\phi K_3}+\dfrac{\alpha_2K_6\varphi\sigma}{\xi\phi K_3K_4}\right)\\ +\dfrac{\beta_2(1-\varepsilon)x_1^{\ 0}\beta_5}{K_1T_1^0\left(\xi(K_7-\beta_4)-\alpha_3\beta_5\right)}\left(\dfrac{\alpha_1\sigma}{\xi K_3}+\dfrac{\alpha_2K_5\sigma}{\xi\phi K_3}+\dfrac{\alpha_2K_6\varphi\sigma}{\xi\phi K_3K_4}\right)\end{array}\right\}w_2,$$

$$w_5=-\frac{\rho}{\mu_h}\left\{\begin{array}{l}\dfrac{\sigma\beta_1(1-\varepsilon)x_1^{\ 0}}{K_1K_3T_1^0}+\dfrac{\sigma\beta_1\eta(1-\varepsilon)x_1^{\ 0}\left(K_4K_5+K_6\varphi\right)}{K_1K_3K_4T_1^0}\\ +\dfrac{\beta_2(1-\varepsilon)x_1^{\ 0}\xi(K_7-\beta_4)}{K_1T_1^0\left(\xi(K_7-\beta_4)-\alpha_3\beta_5\right)}\left(\dfrac{\alpha_1\sigma}{\xi K_3}+\dfrac{\alpha_2K_5\sigma}{\xi\phi K_3}+\dfrac{\alpha_2K_6\varphi\sigma}{\xi\phi K_3K_4}\right)\\ +\dfrac{\beta_2(1-\varepsilon)x_1^{\ 0}\beta_5}{K_1T_1^0\left(\xi(K_7-\beta_4)-\alpha_3\beta_5\right)}\left(\dfrac{\alpha_1\sigma}{\xi K_3}+\dfrac{\alpha_2K_5\sigma}{\xi\phi K_3}+\dfrac{\alpha_2K_6\varphi\sigma}{\xi\phi K_3K_4}\right)\end{array}\right\}w_2+\frac{\gamma}{\mu_h}w_2+\frac{\tau\varphi\sigma}{\mu_hK_3K_4}w_2,$$

$$w_6 = \frac{\sigma\left(K_4K_5 + \varphi K_6\right)}{\phi K_3 K_4} w_2,\; w_7 = \frac{\xi\left(K_7 - \beta_4\right)}{\left(\xi\left(K_7 - \beta_4\right) - \alpha_3\beta_5\right)}\left(\frac{\alpha_1\sigma}{\xi K_3} + \frac{\alpha_2 K_5\sigma}{\xi\phi K_3} + \frac{\alpha_2 K_6\varphi\sigma}{\xi\phi K_3 K_4}\right) w_2$$

$$w_8 = -\frac{\xi\left(K_7 - \beta_4\right)}{\left(\xi\left(K_7 - \beta_4\right) - \alpha_3\beta_5\right)}\left(\frac{\beta_5}{K_7} + \frac{\beta_4\beta_5}{K_7\left(K_7 - \beta_4\right)}\right)\left(\frac{\alpha_1\sigma}{\xi K_3} + \frac{\alpha_2 K_5\sigma}{\xi\phi K_3} + \frac{\alpha_2 K_6\varphi\sigma}{\xi\phi K_3 K_4}\right) w_2$$

$$w_9 = \frac{\beta_5}{\left(\xi\left(K_7 - \beta_4\right) - \alpha_3\beta_5\right)}\left(\frac{\beta_5}{K_7} + \frac{\beta_4\beta_5}{K_7\left(K_7 - \beta_4\right)}\right)\left(\frac{\alpha_1\sigma}{\xi K_3} + \frac{\alpha_2 K_5\sigma}{\xi\phi K_3} + \frac{\alpha_2 K_6\varphi\sigma}{\xi\phi K_3 K_4}\right) w_2$$

a and b computations.

For a, gives

$$a = \sum_{k,i,j=1}^{n} v_k w_i w_j \frac{\partial^2 f_k}{\partial x_i \partial x_j}(0,0). \tag{75}$$

For the system, gives $n = 9$ and for $k = 1,6,8$. $v_1 = v_6 = v_8 = 0 \Rightarrow a_1 = a_6 = a_8 = 0$, we therefore compute the associated non-zero partial derivatives of F at the DFE for f_2, f_3, f_4, f_5, f_7 and f_9.

$$\frac{\partial^2 f_2}{\partial x_1^* \partial x_3^*}(0,0) = \frac{\partial^2 f_2}{\partial x_3^* \partial x_1^*}(0,0) = \frac{\beta_1^*(1-\varepsilon)}{T_h^0},\; \frac{\partial^2 f_2}{\partial x_1^* \partial x_6^*}(0,0) = \frac{\partial^2 f_2}{\partial x_6^* \partial x_1^*}(0,0) = \frac{\eta\beta_1^*(1-\varepsilon)}{T_h^0}$$
$$\frac{\partial^2 f_2}{\partial x_1^* \partial x_7^*}(0,0) = \frac{\partial^2 f_2}{\partial x_7^* \partial x_1^*}(0,0) = \frac{\beta_2^*(1-\varepsilon)}{T_h^0},\; \frac{\partial^2 f_2}{\partial x_1^* \partial x_9^*}(0,0) = \frac{\partial^2 f_2}{\partial x_9^* \partial x_1^*}(0,0) = \frac{\beta_3^*(1-\varepsilon)}{T_h^0},$$
$$\frac{\partial^2 f_9}{\partial x_7^* \partial x_8^*}(0,0) + \frac{\partial^2 f_9}{\partial x_8^* \partial x_7^*}(0,0) = \frac{\beta_4}{T_b^0},\; \frac{\partial^2 f_9}{\partial x_8^* \partial x_9^*}(0,0) = \frac{\partial^2 f_9}{\partial x_9^* \partial x_8^*}(0,0) = \frac{\beta_5}{T_b^0}.$$

Now, considering $v's, w's$ and the partial derivative above, one can be able to show that

$$a_1 = a_3 = a_4 = a_5 = a_6 = a_7 = a_8 = a_9 = 0 \tag{76}$$

$$a = a_1 + a_2 + a_3 + a_4 + a_5 + a_6 + a_7 + a_8 + a_9 = -\left(\Pi_1\Pi_2 + P_1P_2\right) < 0 \tag{77}$$

where

$$\Pi_1=\begin{pmatrix}\dfrac{\sigma\beta_1(1-\varepsilon)x_1^{\ 0}}{K_1K_3T_1^0}+\dfrac{\sigma\beta_1\eta(1-\varepsilon)x_1^{\ 0}(K_4K_5+K_6\varphi)}{K_1K_3K_4T_1^0}\\+\dfrac{\beta_2(1-\varepsilon)x_1^{\ 0}\xi(K_7-\beta_4)}{K_1T_1^0(\xi(K_7-\beta_4)-\alpha_3\beta_5)}\left(\dfrac{\alpha_1\sigma}{\xi K_3}+\dfrac{\alpha_2K_5\sigma}{\xi\phi K_3}+\dfrac{\alpha_2K_6\varphi\sigma}{\xi\phi K_3K_4}\right)\\+\dfrac{\beta_2(1-\varepsilon)x_1^{\ 0}\beta_5}{K_1T_1^0(\xi(K_7-\beta_4)-\alpha_3\beta_5)}\left(\dfrac{\alpha_1\sigma}{\xi K_3}+\dfrac{\alpha_2K_5\sigma}{\xi\phi K_3}+\dfrac{\alpha_2K_6\varphi\sigma}{\xi\phi K_3K_4}\right)\end{pmatrix} \tag{78}$$

$$\Pi_2=\begin{pmatrix}\dfrac{2\varphi\sigma\beta_1(1-\varepsilon)}{K_3K_4T_h^0}+\dfrac{2\sigma(K_4K_5+\varphi K_6)\eta\beta_1(1-\varepsilon)}{\phi K_3K_4T_h^0}\\+\dfrac{2\xi(K_7-\beta_4)\beta_2(1-\varepsilon)}{(\xi(K_7-\beta_4)-\alpha_3\beta_5)T_1^0}\left(\dfrac{\alpha_1\sigma}{\xi K_3}+\dfrac{\alpha_2K_5\sigma}{\xi\phi K_3}+\dfrac{\alpha_2K_6\varphi\sigma}{\xi\phi K_3K_4}\right)\\+\dfrac{\beta_5\beta_1(1-\varepsilon)}{(\xi(K_7-\beta_4)-\alpha_3\beta_5)T_h^0}\left(\dfrac{\beta_5}{K_7}+\dfrac{\beta_4\beta_5}{K_7(K_7-\beta_4)}\right)\left(\dfrac{\alpha_1\sigma}{\xi K_3}+\dfrac{\alpha_2K_5\sigma}{\xi\phi K_3}+\dfrac{\alpha_2K_6\varphi\sigma}{\xi\phi K_3K_4}\right)\end{pmatrix} \tag{79}$$

$$P_1=\frac{2\beta_3\beta_5(1-\varepsilon)x_1^{\ 0}}{(K_7-\beta_4)T_h^{\ 0}}\frac{\xi(K_7-\beta_4)\beta_4}{T_b^0(\xi(K_7-\beta_4)-\alpha_3\beta_5)}\left(\frac{\beta_5}{K_7}+\frac{\beta_4\beta_5}{K_7(K_7-\beta_4)}\right)\left(\frac{\alpha_1\sigma}{\xi K_3}+\frac{\alpha_2K_5\sigma}{\xi\phi K_3}+\frac{\alpha_2K_6\varphi\sigma}{\xi\phi K_3K_4}\right)v_2w_2 \tag{80}$$

and

$$P_2=\begin{pmatrix}\dfrac{\xi(K_7-\beta_4)}{(\xi(K_7-\beta_4)-\alpha_3\beta_5)}\left(\dfrac{\alpha_1\sigma}{\xi K_3}+\dfrac{\alpha_2K_5\sigma}{\xi\phi K_3}+\dfrac{\alpha_2K_6\varphi\sigma}{\xi\phi K_3K_4}\right)\\+\dfrac{\beta_5}{(\xi(K_7-\beta_4)-\alpha_3\beta_5)}\left(\dfrac{\beta_5}{K_7}+\dfrac{\beta_4\beta_5}{K_7(K_7-\beta_4)}\right)\left(\dfrac{\alpha_1\sigma}{\xi K_3}+\dfrac{\alpha_2K_5\sigma}{\xi\phi K_3}+\dfrac{\alpha_2K_6\varphi\sigma}{\xi\phi K_3K_4}\right)\end{pmatrix} \tag{81}$$

equation (77) holds, since $v_2>0,\ w_2>0$ and all the parameters in the model are positive. Now, it is easy to conclude that parameter $a<0$.

Similarly, for b given

$$b=\sum_{k,i,=1}^{n}v_kw_i\frac{\partial^2 f_k}{\partial x_i\partial\beta_1^*}(0,0) \tag{82}$$

for $k=1,6,8$. $v_1=v_6=v_8=0\Rightarrow b_1=b_6=b_8=0$, we therefore compute the associated non-zero partial derivatives of F at the DFE for f_2, f_3, f_4, f_5, f_7 and f_9 where $\beta_5=\beta_5^*$.

$$\frac{\partial^2 f_9}{\partial x_7\partial\beta_5^*}(0,0)=1 \tag{83}$$

Now, considering $v's, w's$ and the partial derivative above, one can also be able to show that (84) is equal to zero.

$$b_1 = b_2 = b_3 = b_4 = b_5 = b_6 = b_7 = b_8 = 0 \tag{84}$$

$$b_9 = v_9 w_7 \frac{\partial^2 f_2}{\partial x_7 \partial \beta_5^*}(0,0) \tag{85}$$

Substituting the values of $v's, w's$ and the partial derivative concerned, we have

$$b_9 = \frac{\beta_3\beta_5(1-\varepsilon)x_1^0}{(K_7-\beta_4)T_h^0}\frac{\xi(K_7-\beta_4)}{(\xi(K_7-\beta_4)-\alpha_3\beta_5)}\left(\frac{\alpha_1\sigma}{\xi K_3}+\frac{\alpha_2K_5\sigma}{\xi\phi K_3}+\frac{\alpha_2K_6\varphi\sigma}{\xi\phi K_3K_4}\right)w_2v_2. \tag{86}$$

Therefore

$$\begin{aligned} b &= b_1 + b_2 + b_3 + b_4 + b_5 + b_6 + b_7 + b_8 + b_9 \\ &= \frac{\beta_3\beta_5(1-\varepsilon)x_1^0}{(K_7-\beta_4)T_h^0}\frac{\xi(K_7-\beta_4)}{(\xi(K_7-\beta_4)-\alpha_3\beta_5)}\left(\frac{\alpha_1\sigma}{\xi K_3}+\frac{\alpha_2K_5\sigma}{\xi\phi K_3}+\frac{\alpha_2K_6\varphi\sigma}{\xi\phi K_3K_4}\right)w_2v_2 > 0. \end{aligned} \tag{87}$$

Therefore, $a<0$ and $b>0$. So, by Theorem 2 of Castillo-Chavez and Song (2004) the following result is established. The EEP of the model (10) is LAS when $R_c > 1$.

3.5 Global stability of E^{**}

Let $D_3 = \{(S_h, L_h, I_h, J_h, R_h, D_h, V, N_b, C_b) \in \Omega\}$ (88)

be the stable manifold of the E^{**}.

Theorem 3: The endemic equilibrium of the model (10) is GAS in D_3 with $\delta_1 = \delta_2 = \rho = \gamma = 0$ whenever $R_c > 1$.

Proof: Suppose $R_c > 1$ and $\delta_1 = \delta_2 = \rho = \gamma = 0$ then the existence of the endemic equilibrium point is assured. Also, let the non-linear Lyapunov function (of the Goh-Volterra type) be

$$\begin{aligned} F &= \left(S_h - S_h^{**} - S_h^{**}\ln\frac{S_h}{S_h^{**}}\right) + \left(L_h - L_h^{**} - L_h^{**}\ln\frac{L_h}{L_h^{**}}\right) + \frac{(\sigma+\mu_h)}{\sigma}\left(I_h - I_h^{**} - I_h^{**}\ln\frac{I_h}{I_h^{**}}\right) \\ &+ \frac{(\sigma+\mu_h)(\varphi+\mu_h)}{\sigma\varphi}\left(J_h - J_h^{**} - J_h^{**}\ln\frac{J_h}{J_h^{**}}\right) + \frac{(\sigma+\mu_h)(\varphi+\mu_h)(\tau+\mu_h)}{\sigma\varphi\tau}\left(R_h - R_h^{**} - R_h^{**}\ln\frac{R_h}{R_h^{**}}\right) \\ &+ \left(N_b - N_b^{**} - N_b^{**}\ln\frac{N_b}{N_b^{**}}\right) + \left(C_b - C_b^{**} - C_b^{**}\ln\frac{C_b}{C_b^{**}}\right) \end{aligned} \tag{89}$$

Taking the time derivative of (89)

$$\dot{F}=\left(\dot{S}_h-\frac{S_h^{**}}{S_h}\dot{S}_h\right)+\left(\dot{L}_h-\frac{L_h^{**}}{L_h}\dot{L}_h\right)+\frac{(\sigma+\mu_h)}{\sigma}\left(\dot{I}_h-\frac{I_h^{**}}{I_h}\dot{I}_h\right)+\frac{(\sigma+\mu_h)(\varphi+\mu_h)}{\sigma\varphi}\left(\dot{J}_h-\frac{J_h^{**}}{J_h}\dot{J}_h\right)$$
$$+\frac{(\sigma+\mu_h)(\varphi+\mu_h)(\tau+\mu_h)}{\sigma\varphi\tau}\left(\dot{R}_h-\frac{R_h^{**}}{R_h}\dot{R}_h\right)+\left(\dot{N}_b-\frac{N_b^{**}}{N_b}\dot{N}_b\right)+\left(\dot{C}_b-\frac{C_b^{**}}{C_b}\dot{C}_b\right) \quad (90)$$

with $T_h=\dfrac{\Lambda_h}{\mu_h}$, $\quad \lambda_h=\dfrac{\beta_1(1-\in)\left(\mathrm{I}_h+\eta D_h\right)}{T_h}+\dfrac{\beta_2(1-\in)V}{T_h}+\dfrac{\beta_3(1-\in)C_b}{T_h}$

becomes

$$\tilde{\lambda}_h=\beta_1(1-\in)\frac{\Lambda_h}{\mu_h}\left(\mathrm{I}_h+\eta D_h\right)+\beta_2(1-\varepsilon)\frac{\Lambda_h}{\mu_h}V+\beta_3(1-\varepsilon)\frac{\Lambda_h}{\mu_h}C_b$$
$$=\tilde{\beta}_1(1-\in)\left(\mathrm{I}_h+\eta D_h\right)+\tilde{\beta}_2(1-\varepsilon)V+\tilde{\beta}_3(1-\varepsilon)C_b$$

where $\tilde{\beta}_1=\beta_1\dfrac{\Lambda_h}{\mu_h}$, $\tilde{\beta}_2=\beta_2\dfrac{\Lambda_h}{\mu_h}$, $\tilde{\beta}_3=\beta_3\dfrac{\Lambda_h}{\mu_h}$

and

$$\tilde{\lambda}_b=\beta_4\frac{\Lambda_b}{\mu_b}C_b+\beta_5\frac{\Lambda_b}{\mu_b}V=\tilde{\beta}_4C_b+\tilde{\beta}_5C_b$$

where

$$\tilde{\beta}_4=\beta_4\frac{\Lambda_b}{\mu_b},\ \tilde{\beta}_5=\beta_5\frac{\Lambda_b}{\mu_b}.$$

Substituting (10) in (49), we have

$$\dot{F}=\Lambda_h-\tilde{\lambda}_hS_h-\mu_hS_h-\frac{S_h^{**}}{S_h}\left(\Lambda_h-\tilde{\lambda}_hS_h-\mu_hS_h\right)+\tilde{\lambda}_hS_h-(\sigma+\mu_h)L_h$$
$$-\frac{L_h^{**}}{L_h}\left(\tilde{\lambda}_hS_h-(\sigma+\mu_h)L_h\right)+\frac{(\sigma+\mu_h)}{\sigma}\left(\sigma L_h-(\varphi+\mu_h)I_h\right)-\frac{(\sigma+\mu_h)}{\sigma}\frac{I_h^{**}}{I_h}\left(\sigma L_h-(\varphi+\mu_h)I_h\right)$$
$$+\frac{(\sigma+\mu_h)(\varphi+\mu_h)}{\sigma\varphi}\left(\varphi I_h-(\tau+\mu_h)J_h\right)-\frac{(\sigma+\mu_h)(\varphi+\mu_h)}{\sigma\varphi}\frac{J_h^{**}}{J_h}\left(\varphi I_h-(\tau+\mu_h)J_h\right) \quad (91)$$
$$+\frac{(\sigma+\mu_h)(\varphi+\mu_h)(\tau+\mu_h)}{\sigma\varphi\tau}\left(\tau J_h-\mu_hR_h\right)-\frac{(\sigma+\mu_h)(\varphi+\mu_h)(\tau+\mu_h)}{\sigma\varphi\tau}\frac{R_h^{**}}{R_h}\left(\tau J_h-\mu_hR_h\right)$$
$$+\Lambda_b-\tilde{\lambda}_bN_b-(\delta_b+\mu_b)N_b-\frac{N_b^{**}}{N_b}\left(\Lambda_b-\tilde{\lambda}_bN_b-(\delta_b+\mu_b)N_b\right)$$
$$+\tilde{\lambda}_bN_b-(\delta_b+\mu_b)C_b-\frac{C_b^{**}}{C_b}\left(\tilde{\lambda}_bN_b-(\delta_b+\mu_b)C_b\right)$$

$$\Lambda_h=\tilde{\lambda}_hS_h^{**}+\mu_hS_h^{**} \quad (92)$$

$$\left.\begin{array}{l}(\sigma+\mu_h)L_h^{**}=\tilde{\lambda}_h S_h^{**}\\(\varphi+\mu_h)I_h^{**}=\sigma L_h^{**}\\(\tau+\mu_h)J_h^{**}=\varphi I_h^{**}\\\mu_h R_h^{**}=\tau J_h^{**}\end{array}\right\}\quad(93)$$

$$\tilde{\lambda}_b N_b=(\delta_b+\mu_b)C_b^{**}\quad(94)$$

$$\Lambda_b=\tilde{\lambda}_b N_b^{**}+(\delta_b+\mu_b)N_b^{**}\quad(95)$$

Substituting the relation in (92), (93), (94) and (95) into (91), we have

$$\begin{aligned}\dot{F}\leq{}&\mu_h S_h^{**}\left[2-\frac{S_h}{S_h^{**}}-\frac{S_h^{**}}{S_h}\right]+(\sigma+\mu_h)L_h^{**}\left[6-\frac{S_h^{**}}{S_h}-\frac{S_hL_h^{**}}{S_h^{**}L_h}-\frac{L_hI_h^{**}}{L_h^{**}I_h}-\frac{I_hJ_h^{**}}{I_h^{**}J_h}-\frac{J_hR_h^{**}}{J_h^{**}R_h}-\frac{R_h}{R_h^{**}}\right]\\&+\delta_b+\mu_b)N_b^{**}\left[2-\frac{N_b}{N_b^{**}}-\frac{N_b^{**}}{N_b}\right]+(\delta_b+\mu_b)C_b^{**}\left[3-\frac{N_b^{**}}{N_b}-\frac{N_bC_b^{**}}{N_b^{**}C_b}-\frac{C_b}{C_b^{**}}\right]\end{aligned}\quad(96)$$

Since geometric mean is less than arithmetic mean, we have that

$$\left[2-\frac{S_h}{S_h^{**}}-\frac{S_h^{**}}{S_h}\right]\leq 0,\ \left[6-\frac{S_h^{**}}{S_h}-\frac{S_hL_h^{**}}{S_h^{**}L_h}-\frac{L_hI_h^{**}}{L_h^{**}I_h}-\frac{I_hJ_h^{**}}{I_h^{**}J_h}-\frac{J_hR_h^{**}}{J_h^{**}R_h}-\frac{R_h}{R_h^{**}}\right]\leq 0\quad(97)$$

$$\left[2-\frac{N_b}{N_b^{**}}-\frac{N_b^{**}}{N_b}\right]\leq 0,\ \left[3-\frac{N_b^{**}}{N_b}-\frac{N_bC_b^{**}}{N_b^{**}C_b}-\frac{C_b}{C_b^{**}}\right]\leq 0\quad(98)$$

Thus, we have that $\dot{F}\leq 0$ for $\delta_1=\delta_2=\rho=\gamma=0$, $R_c>1$. Since the relevant variable in the equations for L_h, I_h, J_h, D_h, V and R_h are at endemic steady state, it follows that this can be substituted into the equations for L_h, I_h, J_h, D_h, V and R_h so that

$$\lim_{t\to\infty}\left(L_h(\mathrm{t}), I_h(\mathrm{t}), J_h(\mathrm{t}), D_h(\mathrm{t}), V(t), R_h(\mathrm{t})\right)\to\left(L_h^{**}, I_h^{**}J_h^{**}, D_h^{**}, V^{**}, R_h^{**}\right).\quad(99)$$

Therefore, from Lasalle's invariant principle Lassalle, (1976), it implies that the endemic equilibrium E^{**} is globally asymptotically stable in Ω whenever $R_c>1$ Hence, F is a Lyapunov function in Ω. The epidemiological implication of the result above is that, in the absence of vaccination and natural recovery $\rho=\gamma=0$, Ebola virus cannot be eliminated from the society if the basic reproduction number is greater than unity.

4 Numerical Simulations

Simulations are performed in this section under maple software and MATLAB ODE 45 to know the sensitive parameters by numerical illustration and to detect the impact on the dynamics of EVD in the long-run. We will use the baseline parameters in Table (1) to simulate the system.

Table 1. Parameter values of system (1)

Parameters	Values (per day)	Sources
$\beta_1, \beta_2, \beta_3$	0.9,0.7,0.8	Abdulrahman, 2016
β_4, β_5	0.5,0.6	Berge *et al.*,2018
δ_1, δ_2	0.04227, 0.027855	Chowell *et al.*, (2004); Leung *et al.*, (2004); Safi and Gumel, 2011
δ_b	0.00014	Chowell *et al.*, (2004);
γ	0.03521	Leung *et al.*, (2004)
φ	(0,1)	variable
σ	0.1	Gumel *et al.,* 2014
τ	(0,1)	variable
η	0.25	Leung *et al.*, (2004)
ε	(0,1)	variable
$\alpha_1, \alpha_2, \alpha_3$	0.11, 0.21, 0.25	Assumed
ρ	(0,1)	variable
ϕ	(0,1)	variable
Λ_h	136	Safi and Gumel, 2011
Λ_b	10	Berge *et al.*,2018
μ_h	0.0000351	Safi and Gumel, 2011
μ_b	0.0011	Berge *et al.*,2018

Global asymptotic stability of equilibria

The global asymptotic stability of the disease-free equilibrium and endemic equilibrium of model (10) were analytically proved in Theorems 1 and 3, respectively. Hence, they are supported by Fig. 2 and Fig. 3 numerically, which are plotted for β_1=0.9, ϕ=0.04 (Fig. 2) and β_1=0.2, ϕ=0.08 (Fig.3). Specifically, Fig. 2 shows that when R_c=0.4213, EVD is wiped out after some days, while Fig.3 shows that for R_c =3 .2521, EVD persists and becomes endemic in a society.

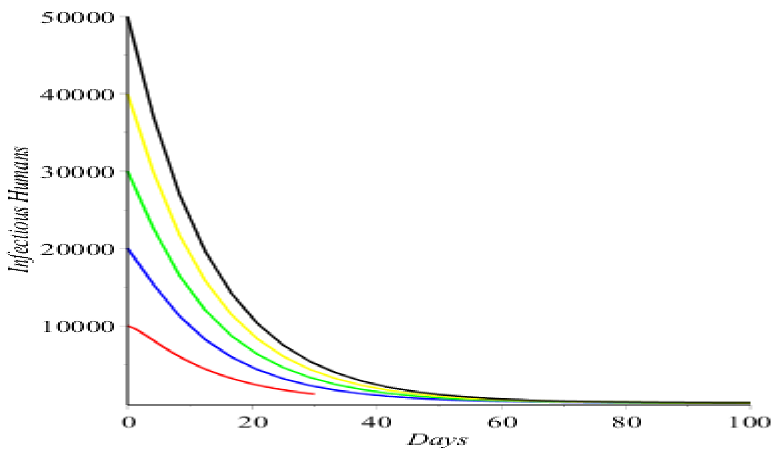

Figure 2. GAS of the disease-free equilibrium when R_c=0.4213< 1. The solution curves are plotted with β_1=0.9, ϕ=0.04, with different initial population of infectious humans and the remaining parameters are as in Table 1.

Figure 2 shows the GAS of the DFE, the solution curves are plotted with R_c=0.4213< 1 and β_1 =0.9, ϕ=0.04. With different initial condition of Infectious human, no matter how large is the initial Infectious humans introduced into society whenever both the control reproduction numbers are less than unity the disease can be mitigated.

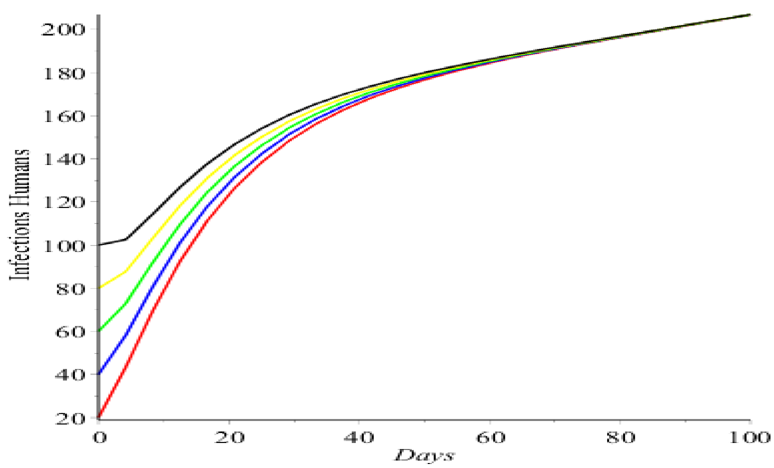

Figure 3. GAS of endemic equilibrium point when R_c=3.2521>1. The solution curves are plotted with β_1=0.2, ϕ=0.08 and the remaining parameters are as in Table 1.

Figure 3 shows the global asymptotic stability of endemic equilibrium point, the solution curves are plotted with β_1=0.2, ϕ=0.08 so that R_c=3.2521>1. With different initial condition of Infectious human no matter how small is initial population of Infectious humans introduced into society whenever both the control reproduction numbers are greater than unity the disease cannot be mitigated in a society.

4.2 Assessing the impact of proper burial

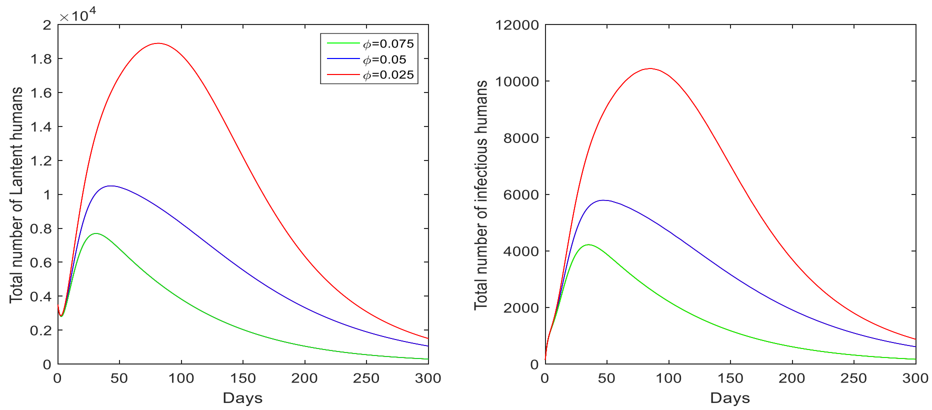

Figure 4. Assessing the impact of proper burial: The latent humans and infectious humans (non-hospitalized) as a function of proper burial rate.

Figure 4 shows that latent humans (E_h) and infectious humans (I_h) (non-hospitalized) are decreasing function of proper burial. Specifically, when the proper burial implementation is low, during the first forty days, the latent humans and infectious humans (non-hospitalized) increase very fast. After fifty days, the latent humans and infectious humans (non-hospitalized) decreases but the disease persist in the society (Note that $R_c = 1.0502$ in this case). If the proper burial is boosted to 75% ($\phi = 0.75$), then the disease drops down in short period of time but not totally wiped out: This shows that proper burial alone cannot mitigate the infection in the society.

4.3 Impact of personal hygiene

Figure 5 shows that latent humans (E_h) and infectious humans (I_h) (non-hospitalized) are decreasing function of personal hygiene. More precisely, when the personal hygiene implementation is low, during the first thirty days, the latent humans and infectious humans (non-hospitalized) increase very fast. After fifty days, the latent humans and infectious humans (non-hospitalized) numbers decreases but the disease continues in the society (Note that $R_c = 1.0502$ in this case). If the personal hygiene is boosted to 75% ($\varepsilon = 0.75$), then the disease diminishes in short period of time but not totally wiped out: This shows that personal hygiene alone cannot control the infection in the society but it can help.

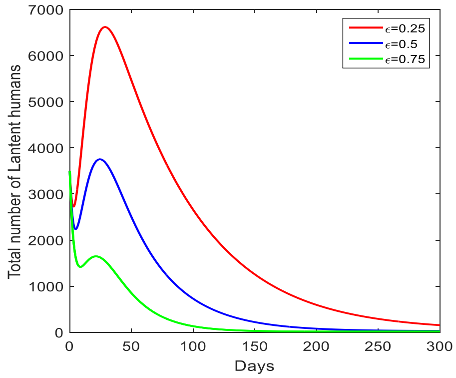

Figure 5. Impact of personal hygiene: The latent humans and infectious humans (non-hospitalized) as a function of personal hygiene.

4.4 Impact of isolation

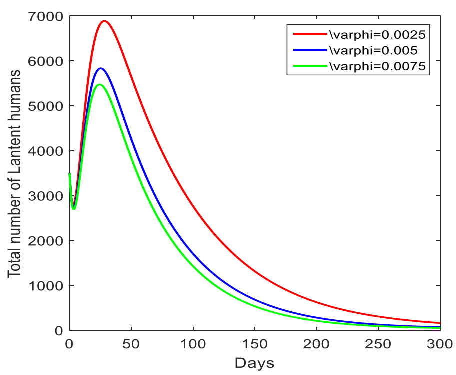

Figure 6. Impact of Isolation: The latent humans and infectious humans (non-hospitalized) as a function of Isolation rate.

Figure 6 show that isolation also can help in reducing the disease in a society but it cannot remove the disease completely from the society. The graph shows us that if the isolation rate is low the disease increases immensely in first fifty days but if it is high the disease decreases within short period of time.

4.5 Assessing the efficacy of vaccine

Without the loss of generality, we assumed the vaccination as parameter in this work. Figure 7 shows that the latent humans and infectious humans (non-hospitalized) are decreasing function of the vaccination parameter (ρ). To be specific, when the vaccination rate is minimal, the daily cases in both the two classes increases immensely in first twenty days. After fifty days, the number of infected ones decreases but EVD persists in the population (Note that $R_c = 1.0502$ in this case). If the vaccination rate is boosted up to 0.75% of the population daily ($\rho = 0.0075$), then the disease will drop down and goes to extinction. So, a high rate of vaccination, that is vaccinating 0.75% of the population daily can mitigate the infection in the society.

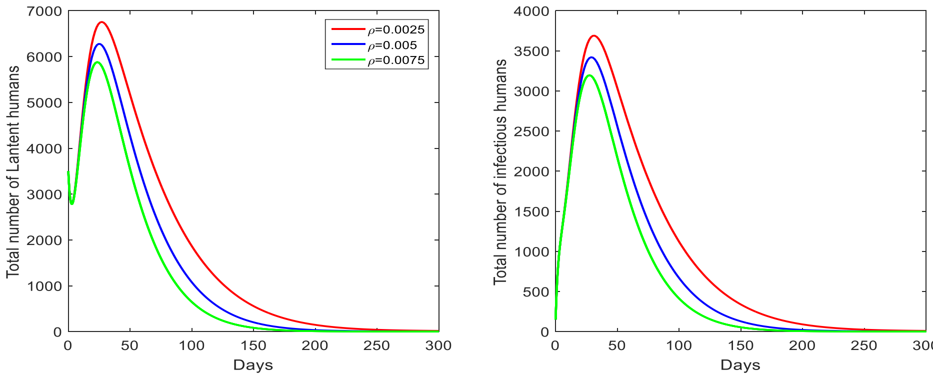

Figure 7. Assessing the efficacy of vaccine: The latent humans and infectious humans (non-hospitalized) as a function of vaccination rate.

4.6 Cumulative incidence varying different control parameters

In this sub-section we will consider variation of control parameter one after the other. Note that all the parameter values used in this sub-section are in Table 1 above with $R_c = 1.0502$.

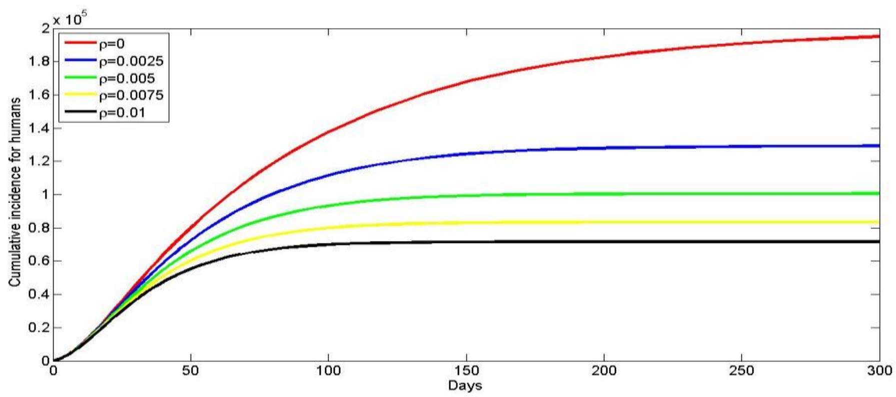

Figure 8. Cumulative incidence for humans varying vaccination rate.

Figure 8 is showing the cumulative incidence for humans varying vaccination rate, the graph reveals that when there is no vaccine the disease can escalate but if some certain percent of the population are vaccinated per day it will help to control the Ebola virus in the society.

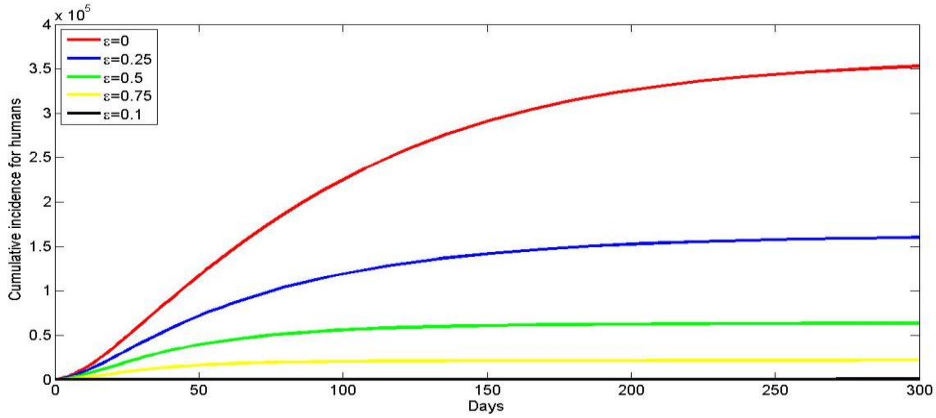

Figure 9. Cumulative incidence for humans varying personal hygiene.

Figure 9 is showing the cumulative incidence for humans varying personal hygiene rate, the graph reveals that when there is no personal hygiene control the disease can escalate within short period but if personal hygiene is adopted as a control strategy in the population, then the disease can be mitigated in a society.

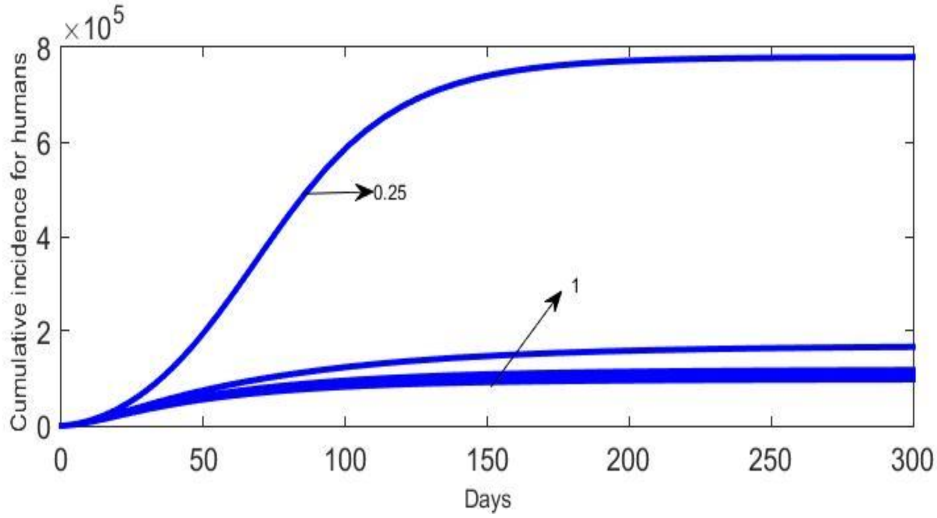

Figure 10. Cumulative incidence for humans varying isolation rate.

Figure 10 is showing the cumulative incidence for humans varying isolation rate, the graph reveals that when there is no isolation control in Infectious humans the disease can escalate within short period of time but if isolation is adopted as a control strategy in the population of infectious humans, then the disease can be mitigated in a society.

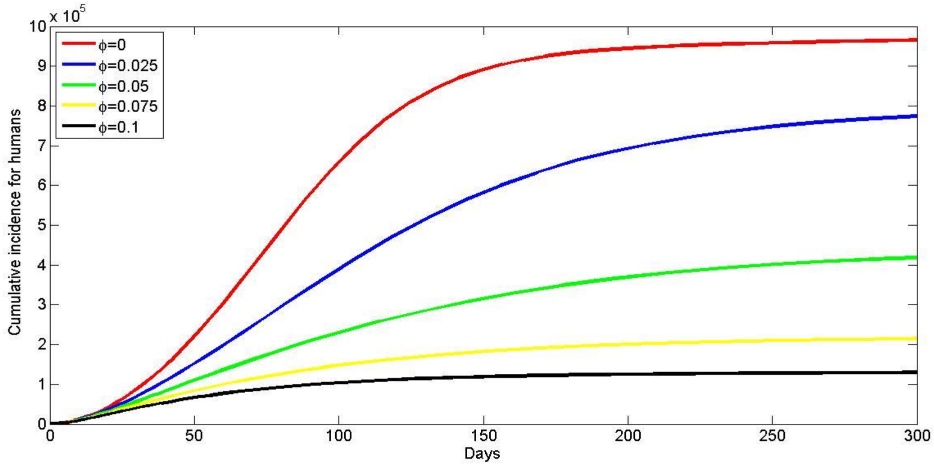

Figure 11. Cumulative incidence for humans varying proper burial rate.

Figure 11 is showing the cumulative incidence for humans varying proper burial rate, the graph reveals that when there is no proper burial control of deceased Infected humans the disease can escalate within short period of time but if proper burial is adopted as a control strategy in the population of humans, varying the proper burial rate shows significant changes and it also helps in controlling the disease in a society.

5 Summary and Conclusion

Over many years ago, series of EVD models were constructed and analyzed to investigate how the disease spread in human and between animals and humans, but only some few Authors considered vaccine and its influence on the EVD control. Again, only some few Authors considered bat to bat transmission. This article mainly concentrates on these strategies (which implies vaccination, personal hygiene, isolation and proper burial of EVD deceased humans), with in mind that hundred percent vaccination is not possible. In addition, (i) Some in latently infected humans L_h are assumed to recover naturally due to strong immune system, (ii) vaccinated are assumed to have permanent immunity from the Ebola virus, (iii) the efficacy of the vaccine is assumed to be almost hundred percent, (iv) the dead humans who are infected could transmit infection during funerals. In this case, the main results obtain are point out below.

1. However, this model considered threshold quantity very important, when the corresponding reproduction number is less than unity, the disease-free is a GAS. The meaning of this epidemiologically, no matter how few or large is the initial number of infectious individuals, if the reproduction number is less than unity, the disease will asymptotically drive to extinction. on the other hand, when the reproduction number is greater than unity, the DFE becomes unstable, the disease continuous and a GAS of EEP occurs.
2. Numerically, it was shown that: (1) the disease can be trash out if one percent of the population can be vaccinated daily. (2) the infected humans decrease in number as

vaccination rate increases. (3) Combining personal hygiene and proper burial leads to less infected individual.

The afore-mentioned imaginary and numerical results shows that: (a) vaccination alone is not capable of driving out the EVD to death. (b) Personal hygiene alone cannot be enough to drive out EV D in a society. Therefore, it is recommended to develop a model that will take into account the inherent to vaccine, though this will lead to delay differential equations, which can be more realistic but less mathematical tractable.

References

[1] Abdulrahman, S. (2016). On the Modelling of Ebola: A Case Study Nigeria: Abacus, 43(2): 1-13.

[2] Amenoghawan, C.O., Aboubakary, D. (2015). Modelling the transmission Dynamics of Ebola Virus. Applied and Computational Mathematics, 4(4): 313-320.

[3] Anderson, R.M. and May, R.M. (1982). Population Biology of Infectious Diseases. New York, Springer-Veily.

[4] Anderson, R.M. and May, R.M. (1991). Infectious Diseases of Humans: Dynamics and Control, Oxford, England: Oxford University Press.

[5] Andrawus, J., Nwankwo, A. and Okuonghae, D. (2017). Bifurcation Analysis of the mathematical model for TB-Dengue co-infection. Nigeria Research Journal of Engineering and Environmental Sciences, 2(2): 390-407.

[6] Azuaba, E., Akinwande, N.I., Abdulrahman, S. and Kuta, F.A. (2017). Existance of equilibrium points of the mathematical model of ebola virus disease dynamics incorporating infection age structure in the quarantined compartment with treatment. 13(4): 58-69.

[7] Berge, T., Chapwanya, J., Lubuma, M.S. and Terefe, Y.A. (2018). A mathematical model for Ebola epidemic with self-protection measures. Journal of Biological Systems, 26(1): 107 - 131.

[8] Birmingham, K. and Cooney, S. (2002), Ebola: Small but real progress (News feature)), Nature med, 8(4): 313.

[9] Castillo-Chavez, C. x Espinoza, C., Moreno, V., Bichara. D. (2004) Assessing the efficiency of condom sanitive as a control strategy Ebola. xiv:150:07415vi.

[10] Castillo-Chavez, C., Feng, Z., and Huang, W. (2004). On the computation of R_0 and its role on global stability. Mathematical approaches for emerging and re-emerging infectious diseases. An Introduction. The IMA Volumes in Mathematics and its applications. New York: Springer-Verlag 125: 229-250

[11] Centres for Disease Control. (2019) West Africa Outbreak. Retrieved from http://www.cdc.gov.vhf/Ebola/outbreak/2019-westafrica/previous-updates.html

[12] Chowell, G., Castillo-Chavez, C. , P. Fenimore, C. Kribs-Zaleta, L. Arriola, J. Hyman, (2004) Model parameters and outbreak control for SARS, Emerg. Infect. Dis., 10:1258–1263

[13] Eric Okyere, Johnson De-Graft Ankamah, Anthony Kodzo Hunkpe, and Dorcas Mensah, (2020. Deterministic Epidemic Models for Ebola Infection with Time-Dependent Controls, Hindawi Discrete Dynamics in Nature and Society. https://doi.org/10.1155/2020/2823816.

[14] Espinoza, B., Moreno, V., Bichara, D. and Castillo-Chavez, C. (2015). Assessing the Efficiency of Condom Sanitive as a Control Strategy Ebola. xiv:150:07415vi.

[15] Deepaa, O.S., Sravanthi Nallamallib, L. Nikitha, Singh Naikc, GopiVenkata and Sai Tejad,

(2015., Mathematical Model for Transmission of Ebola, Science Direct, Elsevier. Procedia Computer Science, 48: 741–745.
[16] Gumel, A.B. et al., (2014) Modelling strategies for controlling SARS outbreaks. Proc. R. Soc.Ser. B271: 2223–2232
[17] Hayman, D.T.S. (2016). "Bats as Viral Reservoirs", Annual Review of Virology, 3:77–99.
[18] Herick L.K., Estomih S.M., Makinde D.O., and Immanuel, L.E. (2020). Modelling and optimal control of Ebola virus disease in the presence of treatment and quarantine of infectives, International Journal of Systems Science and Applied Mathematics, 5(4): 43 - 53.
[19] Hethcot, H.W. (2000). The Mathematics of Infectious Diseases. Society for Industrial and Applied Mathematics Review. 42(4): 599-653.
[20] Hussain H., Ali, A., Chaudary A., Jarral F., Yasmeen T., and Chaudary, F. (2017). Numerical solution for mathematical model of Ebola virus. M Int. J. Adv. Res., 5(3): 15321538.
[21] Kalu, A.U., Agbonyim, A.N. and Agwu, A. (2016). A mathematical model for the control of the spread of Ebola virus disease in west Africa- a disease free equilibrium approach. British Journal of Mathematics and Computer Science, 12(5): 1-9.
[22] La Salle, J. (1976). The stability of Dynamical systems. In Proceedings of the CBMS-NSF Regional Conference Series in Applied Mathematics 25, SIAM, Philadelphia, Pa, USA.
[23]Lekone, P.E. and Finkenstadt, B.F. (2006). Statistical inference in stochastic epidemic seir model with control intervention: Ebola as a case study. Biometrics. 62: 1170-1177.
[24] Leroy, E.M. B. Kumulungui, X. Pourrut, et al., (2005). Fruit bats as reservoirs of Ebola virus. Nature. 438(7068): 575-576.
[25] Leung, G., et al. (2004). The epidemiology of severe acute respiratory syndrome in the 2003 Hong Kong epidemic: analysis of all 1755 patients. Ann. Intern. Med., 9: 662–673.
[26] Murtaza, M., Yusof, I.M., Kassim, M., Jeffree, M. S., Ellzam, E.M. and Shariffa, A.M. (2016). Ebola virus disease, management and prevention. 15(4): 142-148.
[27] Nourridine S., Bradford G., and Fefferman N.H. (2020). Mathematical model of the role of asymptomatic infection in outbreaks of some. emerging pathogens. Tropical Medicine and Infectious Disease. Trop. Med. Infect. Dis. 71: 185.
[28] Okuonghae, D. and Ikhimwin, B.O. (2016). Dynamics of mathematical model for tuberculosis with variability in susceptibility and disease progressions due to difference in awareness level. Front. Micro. Biol., 6:1530-1538.
[29] Okuonghae, D. and Omosigho, S.E. (2011). Analysis of mathematical model for tuberculosis: what could be done to increase case detection. Journal of Theoretical Biology, 269:31-45.
[30] Pourrut, X., Souris, M., Towner, J.S. et al. (2009). Large serological survey showing cocirculation of Ebola and Marburg viruses in Gabonese bat populations, and a high seroprevalence of both viruses in Rousettusa egyptiacus. BMC Infectious Disease 9: 1659.
[31] Rachah, A. and Torres, F.M. (2017). Analysis simulation and optimal control of a SEIR model for Ebola virus with demographic effects. Comm. Fac. Uni. Ank. Ser. A1 Maths. Stat. xiv:1705.01079v1[q-bioPE]
[32] Safi, M. and Gumel A.B. (2011). Mathematical analysis of a disease transmission model with quarantine, isolation and an imperfect vaccine. Computer and Mathematics Application, 61:3044–3070.
[33] Tae Sug Do and Young S.L. (2016). Modeling the spread of Ebola. Osong Public Health Res Perspect., 71:43-48.
[34] Tsanou, B., Samuel, B., Jean, L. and Martins, L.M.M. (2018). Modelling Ebola virus disease transmissions in a complex virus life ecology. Mathematical Biosciences and Engineering,

15(5): 21-56.
[35] Ustun, C. and Ozguller O. (2015). Ebola: As an infectious disease and as a potential bioterrorism agent. Turk J Med Sci. and Applications, 35: 1-4.
[36] van den Driessche, P., and Watmough, J. (2002). Reproduction number and sub threshold Endemic Equilibrium for compartmental models of disease transmission. Mathematical Biosciences, 180:29-48.
[37] World Health Organization (WHO) (2014). International Travel on Health. Ebola Virus Disease outbreak in West Africa.Travel and transport Risk Assessments: Recommendations for Public Heath Authorities and Transport Sector. Available at: http://www.who.int/ith/update/2014042/en/.
[38] World Health Organization (WHO) (2019). Fact sheet general information on Ebola virus disease. Controlling the Infection WHO response. Htts://www.who.int>ebola.
[39] World Health Organization. (2019). Facts Sheet General Information on Ebola Virus, Geneva World Health Organization. Geneva. http://www.who.int/wtersanitationhealth/publication/technotes/en/.
[40] Zineb E.L., Rhoubari, Hajar B., Khalid H., and Noura Y. (2018). Mathematical modeling of Ebola virus disease in bat population. Hindawi Discrete Dynamics in Nature and Society, Article ID 5104524.

International Journal of Mathematical Analysis and Modelling
Volume 5, Issue 4, November 2022, Pages 164 – 174

Particle characteristics in a multi-phase Newtonian flow

F.E. Nzerem[*†] and H.C. Ugorji[*]

Abstract

The flow pattern associated with a multi-phase fluid is the fluid-mediated inter-particle collision, or the exertion of forces on the fluid by the colliding particles. The solid phase is reasonably dispersed but admits collision as a result of either some fluid behaviour or some spatial consideration or both. For some applicable purposes, there may be the need to track a particle's instantaneous position as it is being buffeted during flow. The knowledge of the position, together with a collision history, is critical to predictions concerning the general behaviour of motion. The uncertainty in determining such leads to the recourse to the stochastic differential equation that governs the random stochastic dynamic system - the stable Ornstein-Uhlenbeck process (OUP). A given flow path characterized by the OUP is amenable to the dynamical equation that furnishes the instantaneous position of a particle that is being acted upon by surface forces. Therefore, this work relied on the provision of the equation, whose explicit solution relies on the Fokker-Plank equation that governs the evolution of the space-time probability current.

Keywords and phrases: particles; collision; drag; Weiner process; Markov process

1 Introduction

The flow pattern associated with a single-component fluid is not characterized by fluid-mediated inter-particle collisions or the exertion of forces on the fluid by the colliding particles. This is so because there is no relative motion between the particles and the fluid in the event of flow. When flow is composed of multiple components involving a solid phase and a liquid phase, the associated complexities are so irksome that they require a cautious analysis. There is the convention of modelling the solid-phase as a continuum in keeping with the Eulerian mode of flow regimes. This mode was adopted by Berselli *et al.* [4] wherein the particle-particle interactions were not considered consequential. The use of the Eulerian mode presupposed the minuteness of Stokes' number. In multi-component flow, the fluid is treated as the carrier while the solid-in-motion is treated as the dispersed phase. In Eulerian mode both are treated as interpenetrating fluid media, and therefore both the

[*] Department of Mathematics and Statistics, University of Port Harcourt, Choba, Nigeria
[†] Corresponding author; E-mail: frankjournals@yahoo.com

particulate solid-phase and fluid-phase characteristics are represented as a continuous field. In Marble [13] the *Stokes time* was considered small, and the number of particles was assumed reasonably large that the Eulerian approach was seen to be more applicable than Lagrangian mode. Away from Eulerian consideration, there are cases in which the solid-phase is reasonably dispersed but admit collision as a result of either some fluid behaviour or some spatial consideration or both. Mulin [16] discussed the behavior of flows in some spatial configuration, albeit a homogeneous flow. Numerous Lagrangian simulations based on the instantaneous tracking of numerous particles have been conducted. Such may be found in Tanaka *et al.* [21] and in Berlemont *et al.* [3]. Berlemont and Achim [2], adopted the Lagrangian approach in dealing with fluid/solid and solid/solid correlated motion for colliding solid. The importance of inter-particle collision was underscored by Sommerfeld [19] as was earlier indicated by Oesterle´ and Petitjean [17]. Expectedly, inter-particle collisions induce disordered motion, especially a Brownian type (when the size of each particle is considered minute) or when Stokes time is in favour of particle velocity with respect to the surrounding fluid. The spatiotemporal location of a given particle in the milieu of inter-particle collisions is rather stochastic than deterministic. In effect, stochastic differential equations may be used in modelling the behavior of the solid phase when it is subjected to some random excitation. Holmes *et al.* [11] treated an aspect of random process in dealing with coherent structures being mediated by turbulence. Stochastic models for dispersion of flowing particles have been widely used as discussed by Pai and Subramaniam [18] and some references therein. The issue of much importance is the interactions between the dispersed and carrier phases. This engaged the attention of Wells and Stock [24], Liu [12], and Groszmann, and Rogers [10].

Here the surface effect on a two-component fluid is treated. The flow under consideration is laminar. The work sought a stochastic differential equation that governs the random stochastic dynamic system - the stable Ornstein-Uhlenbeck process (OUP) to provide the instantaneous position of a particle that is being acted upon by surface forces. The explicit solution to the equation is dependent upon the provision of the Fokker-Plank equation, which governs the evolution of the space-time probability.

2 The two-component flow model

A multi-component flow model consisting of many disperse (solid) phases and the multi-fluid phase is a regular occurrence in both nature and man-mediated phenomena. The limiting case, which involves a two-component flow is, by far, an easier task to analyze albeit its inherent cumbersomeness. This type of flow is hereunder discussed.

2.1 Transport equation

A generic transport equation is of the form

$$\frac{\partial\varphi}{\partial t}+\frac{\partial(\varphi u_j)}{\partial x_j}+R+\frac{\partial S_j}{\partial x_j}+D+Q=0, \tag{1}$$

where R encodes the radiation effect, D is the dissipation of φ within a volume, V, Q is the production of φ within V and S_j encodes the surface effect.

Assume, first, that the fluid is a single-component one and replace the scalar function φ with the fluid density ϱ. If no relativistic effects prevail, then $D = Q = 0$, and suppose that $R = 0$. The continuity equation reads

$$\frac{\partial \rho}{\partial t}+\frac{\partial}{\partial x_j}(u_j \rho)=0 \cdot \tag{2}$$

Equation (2) above can be used in developing the transport equation of a two-component flow. Denote the two components by ξ (solid) and η (fluid). Then, introduce the mean flow velocity of the components, u^{ξ}_{j}, and u^{η}_{j} respectively, together with their mass concentrations, c^{ξ} and c^{η}. For a two-component flow in which there is no interchange of mass, the continuity equations are of the form

$$\begin{aligned} &\frac{\partial}{dt}(\lambda^{\xi} c^{\xi})+\frac{\partial}{dx_j}(\lambda^{\xi} c^{\xi} u_j^{\xi})=0, \\ &\frac{\partial \lambda^{\eta} c^{\eta}}{dt}+\frac{\partial}{dx_j}(\lambda^{\eta} u_j^{\eta} c^{\eta})=0. \end{aligned} \tag{3}$$

In a multi-component flow D and Q in (1) are nonzero. Therefore, the drag force takes the form

$$(D^{\xi\eta}+Q^{\xi\eta})_i = F_i^{\xi\eta} \tag{4}$$

The drag force $F^{\xi\eta}_i$ depends on an ensemble of factors. Its dependence on the slip velocity $u_i^{\xi\eta}$, and some other parametric characteristics of the forces exerted on the individual solids in motion is given by

$$F_i^{\xi\eta} = \rho (u_j^{\xi\eta})^2 n_s c_{Di}, \tag{5}$$

where c_{Di} encodes the non-dimensional drag coefficient of the fluid relative to the solids. The numerical value of c_{Di} depends on the dimensionless group applicable, i.e. $c_{Di} = f$ (Re, Fr, We, Ma). In the present case, $c_{Di} = f$(Re). For spherical solids, the numerical value is [6]

$$c_{Di}=\frac{24}{\mathrm{Re}_{\xi}}\left(1+0.15\mathrm{Re}_{\xi}^{0.687}\right) \quad \text{for } \mathrm{Re}_{\xi}<1000. \tag{6}$$

It is noteworthy to emphasize that the solids considered here are without cavitation. Sometimes would suffice to write the drag force in the form

$$F_i^{\xi\eta}=\frac{\rho^{\xi\eta} u_i^{\xi\eta}}{u_j^{\xi}} g \lambda^{\xi} \lambda_{\eta}^{1-n}, \tag{7}$$

where $u_i^{\xi\eta} = (u^{\xi}_i - u^{\eta}_i)$ encodes the local relative velocity of the components, $\rho^{\xi\eta}=(\rho^{\xi}-\rho^{\eta})$; u_j^{ξ} is the final velocity of a single particle in a static fluid and it may be evaluated as

$$u_j^{\xi}=\frac{d_{\xi}^2 \rho^{\xi\eta}}{k\mu_{\eta}} g. \tag{8}$$

The expression above serves as a reference for non-uniform-sized particles. The drag force is dependent on the magnitude of the individual particle's relative velocity u^{ξ}_i acting in opposite direction and ordered by the particle's Reynold's number

$$\mathrm{Re}_{\xi}=\frac{\rho^{\eta}\left|u_j^{\xi}\right| d^{\xi}}{\mu^{\eta}}, \tag{9}$$

where μ^{η} encodes the viscosity coefficient of the fluid. It is noteworthy that the index n in (7) depends on the particle Reynold number; it decreases as the Reynold number increases (see Glasser *et al.* [8]

and Wallis [22]). The presence of Reynold number (equation (9)) supposes the dominance of the surface forces, especially pressure and viscous stress.

We now suppose the existence of a body force, in which the term *R* in equation (1) is nonzero. If this force acts on the solid component, then

$$R_j = c^{\xi}\frac{\partial \psi}{\partial x_i}, \tag{10}$$

where ψ encodes the gravitational potential. The surface forces as mentioned may be denoted by $S_{ij}^{\xi\xi}$ and $S_{ij}^{\xi\eta}$. $S_{ij}^{\xi\xi}$ is the effect of inter-particle collisions on the surface and the force exerted by the fluid on the particles is denoted by $S_{ij}^{\xi\eta}$. With these, the momentum equations, for *R, D, Q* ≠ 0 each, read

$$\begin{aligned}
&\frac{\partial}{\partial t}(\lambda^{\xi}c^{\xi}u_j^{\xi})+\frac{\partial}{\partial x_j}\{\lambda^{\xi}c^{\xi}(u_j^{\xi})^2\}+\frac{\partial \psi}{\partial x_j}+c^{\xi}\frac{\partial}{\partial x_j}(S^{\Sigma}{}_{ij})=-\lambda^{\xi}c^{\xi}g+F_i^{\xi\eta}, \qquad (a)\\
&\frac{\partial}{\partial t}(\lambda^{\eta}c^{\eta}u_j^{\eta})+\frac{\partial}{\partial x_j}\{\lambda^{\eta}c^{\eta}(u_j^{\eta})^2\}+\frac{\partial \psi}{\partial x_j}+c^{\eta}\frac{\partial}{\partial x_j}(S_{ij}^{\eta\eta}+S_{ij}^{\eta\xi})=-\lambda^{\eta}c^{\eta}g-F_i^{\xi\eta}, \qquad (b)
\end{aligned} \tag{11a,b}$$

where λ^{ξ} and λ^{η} are the volume fractions of the solid and the fluid, respectively, *g* encodes gravity-induced acceleration.

3 Collision effects

Non-constrained particles in flow are amenable to collision largely due to some fluid characteristics and the particles' parameters. The incidence of collision may be on both phases, inducing stress on the disperse phase and an augmented strain rate on the fluid.

3.1 Particle in a stream

In this subsection, the particle(s) being considered are assumed spherical, for ease of analysis. Consider a uniform stream with a stream function $\frac{1}{2}Ur^2\sin^2\theta$. When a spherical particle, with $r = a$ is inserted into the stream, the stream function reads

$$\psi = \frac{1}{2}Ur^2\sin^2\theta\left(1-\frac{a^3}{r^3}\right), \tag{12}$$

and the velocity potential takes the form

$$\varphi = U\left(r\cos\theta+\frac{a^3\cos\theta}{2r^2}\right). \tag{13}$$

If the fluid is at rest at infinity and the sphere moves with the velocity *U*, then the velocity potential and stream function are [15]

$$\varphi = \frac{1}{2}Ua^3\frac{\cos\theta}{r^2}, \qquad \psi = -\frac{1}{2}Ua^3\frac{\sin^2\theta}{r}. \tag{14}$$

The total kinetic energy of the system fluid and solid) is

$$E_K = \frac{1}{2}(M+\frac{1}{2}M')U^2 \tag{15}$$

where *M* is the mass of the spherical particle and M' is the mass of the fluid displaced by the particle.

The pressure on the surface of the moving spherical particle reads

$$\frac{p-\Xi}{\rho}=\frac{1}{2}a\mathbf{f}+\frac{1}{8}U^2\left(9\cos^2\theta-5\right),\quad r=a(\text{on the sphere})\text{,} \tag{16}$$

where: $\frac{\Xi}{\rho}=\frac{p}{\rho}-\frac{1}{2}\frac{a^3}{r^3}r\mathbf{f}+\frac{1}{8}\frac{U^2a^8}{r^6}\left(3\cos^2\theta+1\right)-\frac{1}{2}\frac{U^2a^3}{r^3}\left(3\cos^2\theta+1\right)$,

$\mathbf{f}=\partial\boldsymbol{U}/\partial t$ (being the acceleration of the centre of the spherical particle).

3.1.2 Solid-phase collisions

An elastic collision is conservatively a compression process that is accompanied by a restitution phase. Upon interaction, the solid deforms and a part of the kinetic energy is stored as strain energy. Then, some remnant of the kinetic energy propagates into the body with compression, shear, or surface Rayleigh waves. For ease of analysis, but without loss of generalization, we shall consider two-particle classes whose diameters are d_1 and d_2 and radii r_1 and r_2 respectively. It is presupposed that the particles are elastic and isotropic. Two scenarios come into play- the case in which the particles are sufficiently close to each other and the case in which the particles are sufficiently isolated. In the first case $S_{ij}^{\xi\xi}$ dominates. Let the instantaneous velocities $\boldsymbol{V}_i^1$ and $\boldsymbol{V}_i^2$, and the number of particles per unit of volume N_{p1} and N_{p2}. The collision frequency with which particle 1 collides with particle 2 is in the form [2]

$$freq_{coll}=\frac{\pi}{4}(d_1+d_2)^2N_{p2}\int\int_{-\infty}^{\infty}\left|\boldsymbol{V}_{j,rel}\right|f_{\xi}^2d\boldsymbol{u}_1d\boldsymbol{u}_2\text{ ,} \tag{17}$$

where $\left|\boldsymbol{V}_{rel}\right|=\left|\boldsymbol{V}_2-\boldsymbol{V}_1\right|$ and f_{ξ}^2 encodes the interparticle pair distribution function. Under molecular chaos assumption in which the colliding particle velocities are assumed Independent, each particle velocity assumes a Gaussian distribution of the form

$$f_{\xi}^{(1)}=\frac{1}{\left(2\pi\bar{u}_{\xi}^2\right)^{3/2}}\exp\left(-\frac{\boldsymbol{V}_{\xi}^2}{2\bar{u}_{\xi}^2}\right), \tag{18}$$

wherein the interparticle pair distribution function is the product of the two distribution functions.

When the particles collide, the stress and the rate of strain in the solid bodies reads

$$S_{ij}^{\xi\xi}=\lambda\delta_{ij}e_{kk}+2\mu e_{ij}\ , \tag{19}$$

where the constant μ is the coefficient of rigidity of the solid and λ relates with μ to some parameters.

The collision frequency of the particles is described by Gourdel *et al.* [9] as

$$\mathrm{f}_{\mathrm{coll}}=\frac{\pi}{4}(d_1+d_2)^2N_{\xi 2}\left\|\boldsymbol{V}_{rel}\right\|H(z), \tag{20}$$

where

$$\mathrm{H(z)}=\frac{e^{-z}}{\sqrt{\pi z}}+\mathrm{erf}(\sqrt{z})\left(1+\frac{1}{2z}\right),\quad z=\frac{1}{2}\frac{\left\|\boldsymbol{V}_{\mathrm{rel}}\right\|^2}{\overline{u_1^2}+\overline{u_2^2}}. \tag{21}$$

There are two asymptotic behaviors for large values of z and small values of z. The first case amounts to a high drift between particles, therefore $H(z)$ tends toward unity. Thus, equation (20) reduces to

$$\mathrm{f}_{\mathrm{coll}}=\frac{\pi}{4}(d_1+d_2)^2N_{\xi 2}\left\|\boldsymbol{V}_{rel}\right\|\ . \tag{22}$$

Therefore, the collision frequency largely depends on particle mean relative velocity. The second case amounts to a small drift between particles. The application of Taylor expansion for $H(z)$, gives [3]

$$\mathrm{f}_{\mathrm{coll}} = \frac{2^{3/2}\pi^{1/2}}{4} N_{\xi 2}(d_1+d_2)^2\sqrt{\overline{u_1^2}+\overline{u_2^2}}, \tag{23}$$

which indicates that the collision frequency largely depends on the particle agitation.

If the distance between the particles each time admits frequent collision, then the length of time of application of stress and strain has to be considered. The stress has to be expressed in terms of a memory function (t), which weighs the effect of any previous strain history. Thus,

$$S_{ij}^{\xi\xi}(t) \cong \int_{-\infty}^{t} \beta(t-s)e_{ij}(s)ds. \tag{24}$$

The concern about the motion of any particle with memory may be explained by a generic Langevin equation (see Wang *et al.* [23])

$$\begin{cases} \dot{x} = u & (a) \\ \dot{u} = -\int_0^t \beta(t-t')\gamma(u)udt' - \nabla U(x) + W(u)\zeta(t) & (b) \end{cases}, \tag{25}$$

where x and u represent a displacement and velocity of the particle, correspondingly. $\beta(t)$ represents the memory function. In (25), $\gamma(u)$ encodes the non-linear damping function, which may be carefully chosen as the procedure suggested by Rayleigh-Helmholtz, $\gamma(u) = u^2 - a$, where a is a positive constant which splits the velocity space into two regions, the positive damping region and the negative driving one. $U(x)$ denotes a generalized potential, taken as $\frac{\omega^2}{2}x^2$ as well as linear -gradient force $\nabla U(x) = \omega_0^2 x$. $W(u)\xi(t)$ encodes random quantity related to the Langevin force induced by fluctuation. $W(u)$ is the strength of noise and $\zeta(t)$ the Gaussian white noise that is categorized by zero mean value, $\langle\zeta(t)\rangle = 0$. $W(u)\ \zeta(t)$ comprises the additive noise $\zeta(t)$ and multiplicative $w(u)\varsigma(t)$($w(u)$ is the strength of multiplicative noise, which may be carefully chosen as the linear function of velocity u). The time correlation function between the memory and the damping term is

$$S_{ij}^{\xi\xi}(t) = \int_0^t [\beta(t-s)e_{ij}(s)]\gamma(u(s))u(s)ds\cdot \tag{26}$$

Wang et al. [19] showed that the memory function in a general form can be written as

$$\beta(t,s) = \frac{\gamma_0}{\Gamma(u)}(t-s)^u \tag{27}$$

where γ_0 encodes the damping coefficient, $u \in (-1,0)$ the power-law exponent, and $\Gamma(u)$ denotes the Gamma function.

3.2 Fluid rate of strain

Tangential stress does not apply on the surface of the fluid at rest on a macroscopic scale. Only the normal stress, $-p\delta_{ij}$, which is thermodynamic in origin, and is sustained by molecular collisions applies. When the fluid is in relative motion on the continuum scale an additional stress τ_{ij} applies (see Mei [14] for elementary theory). The resulting total stress is

$$\sigma_{ij} = -p\delta_{ij} + \tau_{ij} \tag{28}$$

The viscous stress τ_{ij} must depend on velocity gradients,

$$\frac{\partial q_i}{\partial x_j}, \frac{\partial^2 q_i}{\partial x_j \partial x_k}, \ldots \tag{29}$$

The gradient $\frac{\partial q_i}{\partial x_j}$ consists of two parts,

$$\frac{\partial q_i}{\partial x_j} = \frac{1}{2}\left(\frac{\partial q_i}{\partial x_j} + \frac{\partial q_j}{\partial x_i}\right) + \frac{1}{2}\left(\frac{\partial q_i}{\partial x_j} - \frac{\partial q_j}{\partial x_i}\right), \tag{30}$$

with the rate of strain tensor and the vorticity tensor given by

$$e_{ij} = \frac{1}{2}\left(\frac{\partial q_i}{\partial x_j} + \frac{\partial q_i}{\partial x_i}\right) \quad \text{and} \quad \Omega_{ij} = \frac{1}{2}\left(\frac{\partial q_i}{\partial x_j} - \frac{\partial q_i}{\partial x_i}\right) \tag{31}$$

respectively. We note that fluid incompressibility requires that $\nabla.\boldsymbol{q} = 0$, and with the viscous stress tensor

$\tau_{ij} = \mu\left(\frac{\partial q_i}{\partial x_j} + \frac{\partial q_i}{\partial x_i}\right)$, the total stress is

$$\sigma_{ij} = -p\delta_{ij} + \mu\left(\frac{\partial q_i}{\partial x_j} + \frac{\partial q_i}{\partial x_i}\right). \tag{32}$$

In the fluid/fluid interaction regime the surface effect $S_{ij}^{\eta\eta}$ may be determined in terms of the rate of strain in the fluid as

$$S_{ij}^{\eta\eta} \equiv e_{ij} = \frac{1}{2}\left(\frac{\partial u_i}{\partial x_j} + \frac{\partial u_j}{\partial x_i}\right). \tag{33}$$

3.3 Infinitely large surface effect

We consider flows wherein the disperse-phase is a bit close-packed. In the absence of the fluid, the particle phase may be modeled as a coarse flow based on the kinetic theory description. By the presence of the fluid phase, the particle momentum is modified through a drag term in the kinetic equation. Suppose two spherical particles in flow whose radii are a and b, and are of distance c units apart are sufficiently dispersed. The surface stress $S_{ij}^{\xi\eta}$ dominates. Assume that the particles sustain their fixed position and undergo oscillatory motion about their fixed position. Then the mean value of the force acting on each of the particles is [15]

$$S_{ij}^{\xi\eta} = 3\pi\rho\left(\frac{a^3b^3}{c^4}\right)kk'p^2\cos\varepsilon, \tag{34}$$

where k, k' are the amplitudes of oscillation, $\frac{2\pi}{\rho}$ the period, and ε the phase difference. When the particle behind is released, and it moves closer to the one in front, the distance c decreases. This decrease is progressive as the behind particle gets closer. Thus,

$$\lim_{c\to 0} S_{ij}^{\xi\eta} = \infty. \tag{35}$$

The above explains an infinitely large surface effect occasioned by particle collision as described. It is of note that hydrodynamic coupling, through the drag term, induces particle clustering and cluster-induced turbulence [5] in the fluid–particle flow. Within the same flow field, therefore a turbulent fluid–particle flow has time-dependent regions wherein the particle phase is almost in clusters. Depending on the fluid rheological characteristics, the cluster may be separated by regions wherein the particle–particle collisions are absent.

4 Statistical ensemble

Let us consider particles that are being buffeted during flow, whose temporal location may be determined amid great uncertainty. In the face of such difficulty, a recourse to a stochastic differential equation that governs a random stochastic dynamic system may lead the way. The stable Ornstein-Uhlenbeck process (OUP), is of the form

$$\dot{x} = \upsilon\left(\gamma - x_t\right) + \varepsilon\varphi(t), \tag{36}$$

where υ is a parametric, x_t is the particles' temporal location, and $\varphi(t)$ (the white noise) is the formal derivative of a non-zero mean Weiner process (W_t) (see Holmes and Berzook [11]). It holds well for the motion of a particle in a quadratic potential well subject to first-order dynamics and random excitation (see Arnold [1]). In Einstein's idealization, the description of Brownian motion indicates that increments of a particle's position over disjoint time intervals are independent random quantities. Wiener process describes a probabilistic model in which a random trajectory, although continuous, is nowhere differentiable. Since W_t is nowhere differentiable, $\varphi(t)$ is a distribution rather than a function. $x(t)$ may be represented unconditionally as a scaled time transformed Weiner process in the form

$$h_s(x) = \sqrt{\frac{\theta}{\pi\sigma^2}} e^{-\theta(x-\mu)^2/\sigma^2} \tag{37}$$

or conditionally (given x_0)

$$x_t = x_o e^{-\theta t} + \mu(1 - e^{-\theta t}) + \frac{\sigma}{\sqrt{2\theta}} W(e^{2\theta t}) e^{-\theta t} \cdot \tag{38}$$

In a section of flow where a particle obeys the model (36), a probabilistic description of its temporal location may be given as a conditional probability density function (pdf) of the form

$$h\left(x, t \mid x_0\right) \in \left(-\infty, +\infty\right) \times \left[0, +\infty\right), \qquad x_0 = x(0). \qquad (h \text{ is a pdf}) \tag{39}$$

In equation (39) the first term on the right-hand side encodes the *drift*; if $\upsilon < 0$, the particle drifts along the vector field, and if $\varepsilon \neq 0$ the particle is buffeted by a random force. The explicit solution of equation (36) may be found by recourse to the Fokker-Plank equation

$$\frac{\partial h}{\partial t} = \frac{\partial}{\partial x}\left[\upsilon(x-\mu)p\right] + \frac{\varepsilon^2}{2}\frac{\partial^2 h}{\partial x^2} \cdot \tag{40}$$

The terms on the right-hand side of (40) above are associated with surface effects, with the first encoding the drift and the second the diffusion. The solution is [1]

$$h(x, t \mid x_0) = \sqrt{x_0 e^{\upsilon t}, \frac{\varepsilon^2}{2\upsilon}\left(e^{2\upsilon t} - 1\right)} \quad , \qquad x(0) = x_0 \qquad , \tag{41}$$

with $\sqrt{(\mu, \sigma^2)} = \frac{1}{\sqrt{2\pi\sigma^2}} e^{-(x-\mu)^2/2\sigma^2}$ as the normal distribution with mean μ and σ the variance. The stationary solution is a Gau-ssian distribution given by

$$h_s(x) = \sqrt{\frac{\theta}{\pi\sigma^2}} e^{-\theta(x-\mu)^2/\sigma^2} \tag{42}$$

4.2 Particle collision history

The history of collision is a *sine-qua-non* to the making of predictions regarding the general behaviour of motion. In some dynamic phenomena, such as the one being considered, an existing state may be influenced by former states. Specifically, the sequence of previous collisions between two flowing particles, say, may give a clue to the possibility of the existence of some memory, which will in effect ease predictions.

If the present state depends on the former states, there is a describing linear memory equation of the form [20]

$$\dot{u}(t) = -au + K * u = -au + \int_0^t K(t-s)u(s)ds, \quad u(0) = u_0 \tag{43}$$

where u: $[0, \infty) \to \mathbb{R}$ is a scalar state variable, $u_0 \in \mathbb{R}_{\geq 0}$ and K: $\mathbb{R}_{\geq 0} \to \mathbb{R}_{\geq 0}$ is a positive real kernel. It is observed from the above equation that the second member of the right-hand side (which encodes the prevalence of the previous states) halts the speedy decay of the system.

4.2.1 Collision and Markov process

Definition (1). Suppose $\boldsymbol{\varsigma}$ is a σ-algebra, $\boldsymbol{\varsigma} \subseteq U$, then $P(A \mid \boldsymbol{\varsigma}) := E(\boldsymbol{\chi}_A \mid \boldsymbol{\varsigma})$ for $A \in U$. Thus, $P(A \mid \boldsymbol{\varsigma})$ is the conditional probability of A, given $\boldsymbol{\varsigma}$, and a random variable.
Given a stochastic process X(.), the σ-algebra

$$U(s) := U(X(l) \mid 0 \leq l \leq s \tag{44}$$

is termed the *history of the process* up to and including time s (see Evans [7]). Thus, in the stochastic collision episode, $U(s)$ tracks the statistics accessible from observing $X(l)$ for all times $0 \leq l \leq s$.

Definition (2) [7]. An R^n-valued stochastic process X(·) is called a Markov process if

$$P(X(t) \in B \mid U(s)) = P(X(t) \in B \mid X(s)) \text{ a.s.} \tag{45}$$

for all $0 \leq s \leq t$ and all Borel subset B of R^n.
Suppose the collision process is denominated at present value $X(s)$, the probabilities of future values of $X(t)$ may be predicted in a way similar to the possible knowledge of the total history of the process before time s. Thus, the process only recognizes its value at time s and does not remember how it got there. Markov property, therefore somewhat explains the non-differentiability of particle paths in Brownian motion.

5 Summary and conclusion

In the flow of a single-component fluid, there are no fluid-mediated inter-particle collisions and no exertion of forces on the fluid by colliding particles. Flows involving a solid phase and a liquid phase present associated complexities that are so irksome that they entail a rigorous analysis. The thrust of this work is the examination of surface forces on a two-phase flow. The flow consists of the liquid phase, which is considered a carrier and the disperse phase, whose motion is in the direction of the flowing fluid and whose content (the particles) is in a mutual state of collision. The uncertainty in determining the temporal location of a flowing particle that is being buffeted leads to the recourse to the stochastic differential equation that governs a random stochastic dynamic system - the stable Ornstein-Uhlenbeck process whose equation furnishes the "white noise", term which is the formal derivative of a non-zero mean Weiner process (W_t).

Collision history is a *sine-qua-non* to predictions concerning the general behaviour of motion. Since an existing state may be influenced by former states, the sequence of previous collisions between two flowing particles, say, may give a clue to the possibility of the existence of some memory, thereby aiding predictions. When a given flow path is characterized by the OUP, the equation (41) furnishes the instantaneous position of a particle that is being acted upon by surface forces.

References

[1] Arnold, L. (1974). Stochastic Differential Equations, John Wiley, NY.
[2] Berlemont, A. and Achim, P. (1999). On the fluid/particle and particle/particle correlated motion for colliding particles in Lagrangian approach, 3rd ASME/JSME Joint Fluids Engineering Conference, (FEDSM99-7859, 1999), 1-5.
[3] Berlemont, A., Chang, Z. and Gouesbet, G. (1998). Particle Lagrangian tracking with hydrodynamic interactions and collisions, Flow Turbul. Combust. 60 (1): 1-18.
[4] Berselli, L.C., Cerminara, M.,and Iliescu,T. (2015). Disperse two-phase flows, with applications to geophysical problems, Pure and Applied Geophysics, 172 (1): 181-196, doi:10.1007/s00024-014-0889-5
[5] Capecelatro, J., Desjardins, O., and Fox, R.O. (2016). Strongly coupled fluid–particle flows in vertical channels. I. Reynolds-averaged two-phase turbulence statistics. Physics of Fluids, 28(3) DOI:10.1063/1.4943234
[6] Dietzel, M., Ernst, M., Sommerfeld, M. (2016). Application of the Lattice-Boltzmann method for particle-laden Flows: Point-particles and fully resolved particles. Flow Turbulence Combust., 97:539–570.
[7] Evans, L. C. (2013). An Introduction to Stochastic Differential equations, American Mathematical Society.
[8] Glasser, B.J., Kevrekidis, I., and Sundraesan, G. S. (1997). Fully developed travelling wave solutions and bubble formation in fluidized beds. Journal of Fluid Mechanics, 334: 157-188.
[9] Gourdel, Simonin, C.O., and Brunier, E. (1999). Two-Maxwellian equilibrium distribution function for the modeling of a binary mixture of particles, Proceedings of the 6th International Conference on Circulating Fluidized Beds, (edited by J. Werther ~DECHEMA, (1999)), Frankfurt am Main, Germany, 205–210.
[10] Groszmann, D.E. and Rogers, C.B. (2004). Turbulent scales of dilute particle-laden flows in microgravity. Phys. Fluids, 16 (12:) 4671–4684.
[11] Holmes, P., Lumley, J.L., and Berkooz, G. (1996). Turbulence, Coherenet structures, dynamical systems and symmetry, Cambridge University Press.
[12] Liu, D. (1993). Fluid dynamics of Two-phase systems (in Chinese), Higher Educ. Press (Beijing).
[13] Marble, F. (1970). Dynamics of dusty gases. Annu. Rev. Fluid Mech., 3: 397-446.
[14] Mei, C.C. Relations between stress and rate-of-strain tensors. http://web.mit.edu›Lec-notes›chap1_basics ›
[15] Milne-Thomson, L.M., (1968). Theoretical hydrodynamics (5th ed.), New York: Dover Publications.
[16] Mullin, T. (1993). Disordered fluid motion in a small closed system. Physica D, 62: 192-201.
[17] Oesterle´, B. and Petitjean, A. (1993). Simulation of particle-to-particle interactions in gas–solid flows, Int. J. Multiphase Flow 19: 199-211.
[18] Pai, M. G. and Subramaniam, S. (2012), Two-way coupled stochastic model for dispersion of

inertial particles in turbulence J. Fluid Mech., 700: 1-34.
[19] Sommerfeld, M. (1995). The importance of inter-particle collisions in horizontal gas–solid channel flows, Gas–particle flows, ASME Fluids Engineering Conference, Hilton Head, (FED 228, (335).
[20] Stephan, A. and Stephan, H. (2019). Memory equations as reduced Markov processes, Discrete & Continuous Dynamical Systems, 39(4): 2133-2155.
[21] Tanaka, T. and Tsuji, Y. (1991). Numerical simulation of gas–solid two-phase flow in a vertical pipe: On the effect of inter-particle collision, Gas–Solid Flows, ASME Fluids Engineering Conference, Portland (FED1991), 121: 123-128.
[22] Wallis, G. B. (1969). One-Dimensional Two-Phase Flow, McGraw-Hill, New York.
[23] Wang, P., Huo, J., and Wang, X-M. (2019). Diffusion and memory effect in a stochastic process and the correspondence to an information propagation in a social system, arXiv:1909.04220v1 [physics.soc-ph].
[24] Wells, M.R. and Stock, D.E. (1983), The effects of crossing trajectories on the dispersion of particles in a turbulent flow, J. Fluid Mech., 136: 31–62.

International Journal of Mathematical Analysis and Modelling
Volume 5, Issue 4, November 2022, Pages 175 – 187

Flow propensities in biological vessels and valves

F.E. Nzerem*† and H.C. Ugorji*

Abstract

Flows through the vascular appurtenances and biological valves are in a deep sense analogous to those obtained in other pipes and valves of similar configuration. However, the pulsatile nature of the cardiovascular flow, and the intrinsic coherent perturbation associated with the physiological and anatomical complications that reside in the biological structures, precisely the arteries and veins, and the heart valves, strike a remarkable distinction between them. The flow through the vascular structures was treated as a cylindrical pipe flow with characteristic coherent perturbation; the sound associated with or resulting from flow was considered, and the relationship between pressure and flow in open heart valves was treated, all of which were presented with the relevant equations. The equation involving the open heart valves is as good as furnishing the volume of blood in a physiological transmitral flow.

Keywords and phrases: circulatory system; acoustic wave; turbulence; coherent perturbation; boundary conditions

1 Introduction

Blood vessels are conduits through which blood circulates, and valves are structures in a hollow organ, such as the heart, each with a flap to insure a unidirectional flow of fluid (blood) through it. In describing the flow of blood in a vessel, the driving pressure is the pressure difference between any two chosen points along a specified length of the vessel. However, this does not define the flow of blood in an organ in which the pressure difference is expressed as the variation between arterial pressure (P_A) and venous pressure (P_V). In the kidney, the renal artery pressure, renal vein pressure, and renal vascular resistance determine the flow of blood. Pressure difference at points along the vessel or across a heart valve is crucial in determining the pathophysiology of an organ and the cardiovascular parameters. For example, a pressure difference of at least 30mmHg is a baseline for turbulent flow between heart chambers [7]. The circulatory system is virtually marked by laminar blood flow, with concentric layers of blood flowing in parallel down the length of a blood vessel. However, the laminar flow may be disrupted and become turbulent under conditions of high flow velocity such that the critical Reynolds number (Re) is exceeded. When this occurs, blood does not flow linearly and smoothly in adjacent layers instead, the flow can be described as being chaotic. In the ascending aorta, laminar flow may transit to turbulent in the event of extremely high flow velocity [12]. Flow in the vicinity of the valve resembles a pulsed jet through a nonaxisymmetric orifice, as pulsatile cardiac blood flow causes the heart valve leaflets to open and close, inducing a dynamically changing area. In effect, shear layers, regions of recirculation, and flow instabilities that could eventually lead to a

* Department of Mathematics and Statistics, University of Port Harcourt, Choba, Nigeria
† Corresponding author; E-mail: frankjournals@yahoo.com

transition to turbulence develop. Heart valves serve as governors or control devices and are the major sources of noise in piping systems. They perform the following essential functions: (a) modulating or throttling flow, (b) regulating pressure, (c) getting rid of excess pressure, and (d) preventing backflow. The complex flow patterns are intrinsically valve-and-patient-specific [22]. Sabbah and Stein [20] corroborated studies in humans that show that turbulent flow occurs above the aortic valve under some conditions in normal humans, and it occurs characteristically in the presence of aortic valvular disease. They disclosed that intra-arterial ejection murmurs were at all times associated with turbulent or highly disturbed flow in the ascending aorta. The vibrating cardio-vascular structures, distressed regions of turbulent flow, mixing of flows of diverse temperatures, and their similitudes generate pressure fluctuations that are communicated through a fluid as *sound*. This sound is the progression of compressions and rarefactions propagated away from the acoustic source vicinity. In the vasculature as well as the cardiac chambers, murmurs are generated by turbulent flow. Heart murmurs are well described concerning the site on the thoracic cage, pitch and volume, and phase of the cardiac cycle [23]. Vascular bruit turbulence outside the heart can be located along the carotid artery, which supplies blood to the brain. Jung and Rajat [10] were of the view that the primary source of arterial bruits is perturbation initiated by vortex flow in the near post-stenotic region. Turbulence has its mixed blessings; Wei *et al.* [25] suggested that flow turbulization is a major way of heat transfer enhancement; accordingly, special tubulising elements can be placed into tubes and channels to enhance heat transfer. Turbulence may create some physiological cardiac murmurs, but murmurs are most often considered pathologic [10, 21]. In their work, Farzad *et al.* [4] sought to evaluate the performance of modern acoustic detection of murmurs by acoustic signals taken from patients undergoing coronary angiography. According to them, acoustic signal patterns may identify intracoronary murmurs generated by hemodynamically substantial coronary artery stenosis in all major vessels.

A large amount of investigation has been carried out about flows with free boundaries that include [9, 14]. The question of where turbulence develops and how the concomitant acoustic wave propagates through the arterial vessels requires elucidation. Laufer [13] was driven to investigate the structure of turbulent flow in fully developed pipe flow. Elsewhere [17] the noise generated by turbulent pipe flow was studied. Both cases [9, 14] are tenable in arterial flow [20] and therefore may use used for investigating such flow in arteries and valves.

2 Flow in pipes

In what follows, attention is given to a cylindrical pipe in line with the arterial/venous structure.

2.1 Reynolds equation of pipe flow

Consider a section of the artery with incompressible mean flow. The continuity equation and Reynolds equation in cylindrical polar coordinates read:

$$\frac{\partial U}{\partial x}+\frac{1}{r}\left(\frac{\partial_r V}{\partial r}+\frac{\partial W}{\partial \varphi}\right)=0 \tag{1}$$

$$\left.\begin{aligned}
&U\frac{\partial U}{\partial x}+V\frac{\partial U}{\partial r}+\frac{W}{r}\frac{\partial U}{\partial \varphi}=-\frac{1}{\rho}\frac{\partial P}{\partial x}-\left(\frac{\partial}{\partial x}\overline{u^2}+\frac{1}{r}\frac{\partial}{\partial r}r\overline{uv}+\frac{1}{r}\frac{\partial}{\partial \varphi}\overline{uw}\right)+\upsilon\nabla^2 U\\
&U\frac{\partial V}{\partial x}+V\frac{\partial V}{\partial r}+\frac{W}{r}\frac{\partial V}{\partial \varphi}-\frac{W^2}{r}=-\frac{1}{\rho}\frac{\partial P}{\partial r}-\left(\frac{\partial}{\partial x}\overline{uv}+\frac{1}{r}\frac{\partial}{\partial r}r\overline{v^2}+\frac{1}{r}\frac{\partial}{\partial \varphi}\overline{vw}-\frac{\overline{W^2}}{r}\right)+\upsilon\left(\nabla^2 V-\frac{V}{r^3}-\frac{2}{r^2}\frac{1}{r}\frac{\partial W}{\partial \varphi}\right)\\
&U\frac{\partial W}{\partial x}+V\frac{\partial W}{\partial r}+\frac{W}{r}\frac{\partial W}{\partial \varphi}+\frac{VW}{r}=-\frac{1}{\rho r}\frac{\partial P}{\partial \varphi}-\left(\frac{\partial}{\partial x}\overline{uw}+\frac{\partial}{\partial r}\overline{vw}+\frac{1}{r}\frac{\partial}{\partial \varphi}\overline{w^2}-\frac{2\overline{vw}}{r}\right)+\upsilon\left(\nabla^2 W-\frac{2}{r^2}\frac{\partial W}{\partial \varphi}-\frac{W}{r^2}\right)
\end{aligned}\right\} \tag{2.a, b, c.}$$

where $\nabla^2 = \frac{\partial^2}{\partial x^2} + \frac{\partial^2}{\partial r^2} + \frac{1}{r}\frac{\partial}{\partial r} + \frac{1}{r^2}\frac{\partial^2}{\partial \varphi^2}$, and U and P encode the mean velocity and pressure respectively that are measured at any point in the artery or valve; *u, v, w* represent the instantaneous velocity fluctuations in x (axial), r (radial), and φ (azimuthal) directions respectively; $\overline{u}, \overline{v}, \overline{w}$ are the average velocity in x, r and φ directions respectively; V and W are the mean velocities in radial and azimuthal directions respectively, **ν** is the viscosity, and ρ, density. As a consequence of a fully developed flow, the mean velocities in radial and azimuthal directions vanish. The least velocity (V= 0) is observed along the vessel wall. We find $V = W = 0$; since pipe flow is homogeneous in the axial and azimuthal directions, $\frac{\partial}{\partial \varphi} = 0$, and $\frac{\partial}{\partial x} = 0$ except at total pressure. Moreover, the velocity field does not depend on the axial coordinate, x. With these, equation (2) reads

$$\left.\begin{aligned} \frac{1}{\rho}\frac{\partial P}{\partial x} &= -\frac{1}{r}\frac{d}{dr} r\overline{uv} + \nu\left(\frac{d^2}{dr^2} + \frac{1}{r}\frac{dU}{dr}\right) \\ \frac{1}{\rho}\frac{\partial P}{\partial r} &= -\frac{1}{r}\frac{d}{dr} r\overline{v^2} + \frac{\overline{w^2}}{r} \\ -\frac{d}{dr}\overline{vw} - \frac{2\overline{vw}}{r} &= 0 \end{aligned}\right\} \quad . \qquad (3.\text{ a, b, c})$$

Applying the boundary condition $\overline{vw} = 0$ at $r = r_I$ shows that $\overline{vw} = 0$ for each value of r. Therefore the turbulent pipe flow is

$$\left.\begin{aligned} \frac{1}{\rho}\frac{\partial P}{\partial x} &= -\frac{1}{r}\frac{d}{dr} r + \left(\overline{uv} - \nu\frac{dU}{dr}\right) \\ \frac{1}{\rho}\frac{\partial P}{\partial r} &= -\frac{1}{r}\frac{d}{dr} r\overline{v^2} + \frac{\overline{w^2}}{r} \end{aligned}\right\} \qquad (4.\text{ a, b})$$

Note that, $\overline{vw}$ must be zero everywhere save at the pipe centre; but if it is continuously dependent on r, then it will vanish at the pipe centre. With suitable radial boundary conditions the shearing stress, $\overline{uv}$, is given in terms of the mean velocity by

$$\overline{uv} = \nu\frac{dU}{dr} + \frac{r}{r_1}U_*^2 \ , \qquad (5)$$

and the normal stresses $\overline{v^2}$ and $\overline{w^2}$ relate to mean pressure by

$$\overline{v^2} + \int_{r_1}^{r} \frac{\overline{v^2} - \overline{w^2}}{r}\, dr = -\frac{P}{\rho} - \frac{2}{r_1}U_*^2 x. \qquad (6)$$

where r_I is pipe radius, U_* is friction velocity. The above equation, excluding the second term on the right hand side, may be rewritten as

$$\frac{1}{\rho}\int\left(\frac{\partial P}{\partial r}\right) dr = -\int d\overline{v^2} + \int \frac{\overline{w^2} - \overline{v^2}}{r} dr \qquad (7)$$

Carrying out the indicated integration between the limits r_1 and r and noting at $r = r_1$, $\overline{v^2} = 0$ one gets

$$\frac{P_{r,x}-P_{r_1,x}}{\rho}=-\overline{v^2}+\int_{r_1}^{r}\frac{\overline{w^2}-\overline{v^2}}{r}dr \tag{8}$$

where, $P_{r,x}$ = mean pressure at r, x; $P_{r1,x}$ = mean pressure at r_1, x. At an arbitrary point, x_1 one finds

$$\frac{P_{r,x}-P_{r,x_1}}{\rho}=-\frac{2U_*^2 x}{r_1}\,. \tag{9}$$

Thus, adding (9) to (8) gives

$$\frac{P_{r,x}-P_{r_1,x_1}}{\rho}=-\overline{v^2}+\int_{r_1}^{r}\frac{\overline{w^2}-\overline{v^2}}{r}dr-\frac{2U_*^2 x}{r_1}\,. \tag{10}$$

The equations so far are given in terms of the radial coordinate of the vessel, r. The energy equation takes the form, (see Laufer [13] for the derivation):

$$\overline{uv}\frac{dU}{dr}+\frac{1}{r}\frac{d}{dr}r\overline{v\left(\frac{u^2+v^2+w^2}{2}+\frac{p}{\rho}\right)}-\frac{\nu}{r}\frac{d}{dr}r\frac{d}{dr}\overline{\left(\frac{u^2+v^2+w^2}{2}\right)}+\nu\overline{\left(\frac{\partial u_i}{\partial x_j}\right)\left(\frac{\partial u_i}{\partial x_j}\right)}=0\,. \tag{11}$$

In the equation above, the first term encodes the rate of production of turbulent energy due to shearing stresses. The second term is the diffusion term, the third term may represent a gradient form of energy diffusion which is of interest near the wall. The fourth term indicates viscosity-induced energy dissipation into heat.

2.2 Perturbation equations in cylindrical coordinates

The fundamental Navier-Stokes equations that govern flow include the continuity equation, the momentum equations, and the energy equation. The continuity equation reads:

$$\frac{\partial\tilde{\rho}}{\partial t}+\bar{u}_i\frac{\partial\tilde{\rho}}{\partial x_i}+\rho_0\frac{\partial\tilde{u}_i}{\partial x_i}=0, \tag{12}$$

where ρ is the fluid density, and u_i is the velocity.

The momentum equation for the coherent **perturbations reads:**

$$\left(\frac{\partial\tilde{u}_i}{\partial t}+\tilde{u}_j\frac{\partial\bar{u}_i}{\partial x_j}+\bar{u}_j\frac{\partial\tilde{u}_i}{\partial x_j}+\frac{\tilde{\rho}\bar{u}_j}{\rho_0}\frac{\partial\bar{u}_i}{\partial x_j}\right)=-\frac{1}{\rho_0}\frac{\partial\tilde{p}}{\partial x_i}+\nu\left[\frac{\partial^2\tilde{u}_i}{\partial x_j\partial x_j}+\left(\frac{1}{3}+\frac{\mu_B}{\mu}\right)\frac{\partial^2\tilde{u}_j}{\partial x_j\partial x_i}\right]-\frac{\partial\tilde{r}_{ij}}{\partial x_j}, \tag{13}$$

where μ is the dynamic viscosity, and μ_B is the bulk viscosity (see **Pierce** [16]) which is assumed constant here. The perturbation Reynolds stress reads

$$\tilde{r}_{ij}\equiv\left\langle u_i'u_j'\right\rangle-\overline{u_i'u_j'}. \tag{14}$$

The quantity $-\tilde{r}_{ij}$ may be construed as the oscillation of the background Reynolds stress as a result of the passage of the coherent perturbations [2]. Equations (13, 14) govern the motion of a Newtonian fluid, together with the motion of coherent perturbations, such as sound wave propagation. In cardiovascular flows it is often advisable to examine the flow and the coherent perturbation quantities separately, essentially by some splitting technique (see Morfey [15]). The following decomposition ensues:

$$H(\mathrm{x},t) = \bar{H}(\mathrm{x}) + \tilde{H}(\mathrm{x},t) + \hat{H}(\mathrm{x},t), \tag{15}$$

where $\bar{H}$ encodes the mean (time-averaged) contribution, $\tilde{H}$ is the coherent perturbation (periodic wave) driven by the pulsatile structure of flow, and $\hat{H}$ represents to the turbulent fluctuation. Here H denotes any one of the variables: ρ, u_i, T, or p, as the case may be. The time-averaged mean defined as

$$\bar{H}(\mathrm{x,t}) = \lim_{\varepsilon\to\infty} \frac{1}{\varepsilon}\int_t^{t+\varepsilon} H(\mathrm{x,t'})\mathrm{dt'}, \tag{16}$$

and the phase average is

$$\langle H(\mathrm{x},t)\rangle = \lim_{N\to\infty} \frac{1}{N_p}\sum_{\xi=0}^{N_p} H\left(\mathrm{x},\, t+\frac{\xi}{f}\right), \tag{17}$$

where f is the frequency of the coherent perturbation.

In a fully developed turbulent pipe flow, the there is a homogeneous stream-wise mean flow, whose velocity is $\bar{\boldsymbol{u}} = [\bar{u}_x(r),\, 0,\, 0]$. The mean flow is locally parallel in fully developed turbulent pipe flows, therefore the mean flow velocity $\bar{\boldsymbol{u}} = [\bar{u}_x(r),\, 0,\, 0]$ is parallel to the x-axis and fluctuating in the radial direction r. The perturbation equations in cylindrical coordinates are:

$$\left(\frac{\partial}{\partial t} + \bar{\varsigma}\right)\frac{\tilde{\rho}}{\rho_0} + \left(\frac{\partial \tilde{u}_r}{\partial r} + \frac{\tilde{u}_r}{r} + \frac{1}{r}\frac{\partial \tilde{u}_\theta}{\partial \theta} + \frac{\partial \tilde{u}_x}{\partial x}\right) = 0 \qquad \text{(continuity equation)} \tag{18}$$

$$\begin{aligned}
\left(\frac{\partial}{\partial t} + \bar{\varsigma}\right)\tilde{u}_x + \frac{\tilde{\rho}}{\rho_0}\bar{\varsigma}\bar{u}_x = &-\frac{1}{\rho_0}\frac{\partial \tilde{\rho}}{\partial x} + \nu\left(\frac{\partial^2 \tilde{u}_x}{\partial r^2} + \frac{1}{r}\frac{\partial \tilde{u}_x}{\partial r} + \frac{1}{r^2}\frac{\partial^2 \tilde{u}_x}{\partial \theta^2} + \frac{\partial^2 \tilde{u}_x}{\partial x^2}\right) \\
&+\nu\left(\frac{1}{3} + \frac{\mu_B}{\mu}\right)\left(\frac{\partial^2 \tilde{u}_r}{\partial x \partial r} + \frac{1}{r}\frac{\partial^2 \tilde{u}_\theta}{\partial x \partial \theta} + \frac{1}{r}\frac{\partial^2 \tilde{u}_r}{\partial x} + \frac{\partial^2 \tilde{u}_x}{\partial x^2}\right) \\
&-\left[\frac{\partial \tilde{r}_{rx}}{\partial r} + \frac{1}{r}\left(\frac{\partial \tilde{r}_{\theta x}}{\partial \theta} + \tilde{r}_{rx}\right) + \frac{\partial \tilde{r}_{xx}}{\partial x}\right]
\end{aligned} \qquad \text{(x}-\text{momentum equation)} \tag{19}$$

$$\begin{aligned}
\left(\frac{\partial}{\partial t} + \bar{\varsigma}\right)\tilde{u}_r + \frac{\tilde{\rho}}{\rho_0}\bar{\varsigma}\bar{u}_r - 2\frac{\bar{u}_\theta \tilde{u}_\theta}{r} = &-\frac{1}{\rho_0}\frac{\partial \tilde{\rho}}{\partial r} + \nu\left(\frac{\partial^2 \tilde{u}_r}{\partial r^2} + \frac{1}{r^2}\frac{\partial^2 \tilde{u}_r}{\partial \theta^2} + \frac{1}{r}\frac{\partial \tilde{u}_r}{\partial r} - \frac{\tilde{u}_r}{r^2} - \frac{2}{r^2}\frac{\partial \tilde{u}_\theta}{\partial \theta} + \frac{\partial^2 \tilde{u}_r}{\partial x^2}\right) \\
&+\nu\left(\frac{1}{3} + \frac{\mu_B}{\mu}\right)\left(\frac{\partial^2 \tilde{u}_r}{\partial r^2} + \frac{1}{r}\frac{\partial^2 \tilde{u}_\theta}{\partial \theta \partial r} + \frac{1}{r}\frac{\partial^2 \tilde{u}_r}{\partial r} - \frac{1}{r^2}\frac{\partial \tilde{u}_\theta}{\partial \theta} - \frac{\tilde{u}_r}{r^2} + \frac{\partial^2 \tilde{u}_x}{\partial r \partial x}\right) \\
&-\left[\frac{\partial \tilde{r}_{rr}}{\partial r} + \frac{1}{r}\left(\frac{\partial \tilde{r}_{\theta x}}{\partial \theta} + (\tilde{r}_{rr} - \tilde{r}_{\theta\theta})\right) + \frac{\partial \tilde{r}_{xr}}{\partial x}\right]
\end{aligned} \qquad \text{(r}-\text{momentum equation)} \tag{20}$$

$$\begin{aligned}
\left(\frac{\partial}{\partial t} + \bar{\varsigma} + \frac{\bar{u}_r}{r}\right)\tilde{u}_\theta + \left(\frac{\tilde{\rho}}{\rho_0}\bar{\varsigma} + \frac{\tilde{u}_r}{r}\right)\bar{u}_\theta = &-\frac{1}{\rho_0 r}\frac{\partial \tilde{\rho}}{\partial \theta} + \nu\left(\frac{\partial^2 \tilde{u}_\theta}{\partial r^2} + \frac{1}{r}\frac{\partial \tilde{u}_\theta}{\partial r} - \frac{\tilde{u}_\theta}{r^2} + \frac{1}{r^2}\frac{\partial}{\partial \theta}\left(\frac{\partial \tilde{u}_\theta}{\partial \theta} + 2\tilde{u}_r\right) + \frac{\partial^2 \tilde{u}_\theta}{\partial x^2}\right) \\
&+\nu\left(\frac{1}{3} + \frac{\mu_B}{\mu}\right)\left(\frac{1}{r}\frac{\partial^2 \tilde{u}_r}{\partial \theta \partial r} + \frac{1}{r^2}\frac{\partial}{\partial \theta}\left(\tilde{u}_r + \frac{\partial \tilde{u}_\theta}{\partial \theta}\right) + \frac{1}{r}\frac{\partial^2 \tilde{u}_x}{\partial x \partial \theta}\right) \\
&-\left[\frac{\partial \tilde{r}_{r\theta}}{\partial r} + \frac{1}{r}\left(\frac{\partial \tilde{r}_{\theta\theta}}{\partial \theta} + (\tilde{r}_{r\theta} - \tilde{r}_{\theta r})\right) + \frac{\partial \tilde{r}_{x\theta}}{\partial x}\right]
\end{aligned} \qquad (\theta-\text{momentum equation}) \tag{21}$$

$$\left(\frac{\partial}{\partial t}+\bar{\varsigma}\right)\tilde{T}+\frac{\tilde{\rho}}{\rho_0}\bar{\varsigma}\bar{T}=\frac{1}{c_{p\rho_0}}\left[\left(\frac{\partial}{\partial t}+\bar{\varsigma}\right)\tilde{p}+\tilde{\zeta}\bar{p}\right]+\lambda\left(\frac{\partial^2\tilde{T}}{\partial r^2}+\frac{1}{r}\frac{\partial\tilde{T}}{\partial r}+\frac{1}{r^2}\frac{\partial^2\tilde{T}}{\partial\theta^2}+\frac{\partial^2\tilde{T}}{\partial x^2}\right), \quad \textit{The energy equation,} \tag{22}$$
$$-\left[\frac{\partial\tilde{q}_r}{\partial r}+\frac{1}{r}\left(\frac{\partial\tilde{q}_\theta}{\partial\theta}+\tilde{q}_r\right)+\frac{\partial\tilde{q}_x}{\partial x}\right]+\frac{2\nu}{c_p}(\alpha+\beta)$$

where,

$$\bar{\varsigma}=\bar{u}_x\frac{\partial}{\partial x} \text{ and } \tilde{\zeta}=\tilde{u}_x\frac{\partial}{\partial x}, \quad \text{and} \quad \alpha=\frac{\partial\bar{u}_x}{\partial r}\frac{\partial\tilde{u}_x}{\partial r}, \ \beta=\frac{\partial\bar{u}_x}{\partial r}\frac{\partial\tilde{u}_r}{\partial x}.$$

3 Acoustic analogy and noise generation

Noise is inviolable component of turbulence. It is created by the Reynolds stresses. Velocity and pressure fluctuations do result in the development of acoustic sources which radiate sound with intensities and directionality that are typical of the particular nature and magnitude of the sources and the acoustic features of the surrounding media. Pressure is a parameter of much interest in the wave equation in the sense that ears and the auscultation devices, such as the stethoscope for measuring sound within the body, are sensitive to pressure fluctuations. Turbulent fluctuating pressures which are related to acoustical pressure are termed *sound pressure* or *sound*, and fluctuations of pressures which are related to sound are frequently referred to as *intra-arterial sound* [5]. Aerodynamically generated noise is essentially based on density fluctuations, which are frequently converted to pressure variations by means of a linear relationship. A good relationship is found between pressure and velocity because the acoustic velocity is frequently used as a boundary condition in calculations involving solid bodies. Acoustic velocity is the usual fluid dynamic boundary condition that must be satisfied [16]. Morfey and Wright [15] improved on the pioneering work of Lighthill [14] on acoustic analogy. Their formulation for bounded domains enables the application of pressure-based options to the fluid density as a wave variable.

Consider the windowed equations of motion for a fluid occupying a region *R*. The expressions for conservation of mass and momentum are

$$\underline{\frac{\partial}{\partial t}(\rho-\rho_0)}+\underline{\frac{\partial}{\partial x_i}(\rho u_i)}=0, \qquad \underline{\frac{\partial}{\partial t}(\rho u_i)}+\underline{\frac{\partial}{\partial t}(\rho u_i u_j+p_{ij})}=\underline{B_i}. \tag{23}$$

In the above, and subsequently, an underscored quantity or variable means that it is multiplied by some Heaviside functions G and Ξ. Thus, it is windowed in space and time; u_i is the fluid velocity in the x_i direction; $p_{ij}=P_{ij}-P_0\delta_{ij}$ where P is absolute pressure and P_{ij} is the compressive stress in the fluid; δ_{ij} is the Kronecker delta and B_i is an applied body force per unit volume. The Heaviside functions G and Ξ are such that:

$$G(\boldsymbol{n})=\begin{cases}1 & \text{in } \mathcal{R} \text{ and on } S\\ 0 & \text{in } \mathcal{R}' \text{ (prime indicates complement);}\end{cases} \tag{24}$$

$$\Xi(t)=\begin{cases}1 & \text{for } t\geq 0\\ 0 & \text{for } t<0\end{cases}, \tag{25}$$

In (24), **n** is a local normal coordinate defined for points in the neighbourhood of S; $\boldsymbol{n}=f$.**S** is a moving closed surface in an appropriate dimension, assumed smooth and $|\nabla f|$ is single-valued. The following derivatives apply from the property of the Heaviside function:

$$\frac{\partial \Xi}{\partial t} = \delta(t), \quad \frac{\partial \Xi}{\partial x_i} = 0, \quad \frac{\partial G}{\partial n} = \delta(n), \quad \frac{\partial G}{\partial x_i} = \mathbf{n}_i \delta(n), \tag{26}$$

where $\delta(.)$ is the Dirac delta function and $\boldsymbol{n}_i = \partial n / \partial x_i$ is the unit normal to S. For any field variable η,

$$\frac{\overline{\partial \eta}}{\partial x_i} - \frac{\partial \eta}{\partial x_i} = -\eta \mathbf{n}_i \delta(n)\Xi, \qquad \frac{\overline{\partial \eta}}{\partial t} - \frac{\partial \eta}{\partial t} = \eta\left[v_i \mathbf{n}_i \delta(n)\Xi - G\delta(t)\right] \tag{27}$$

where $v_i = v\boldsymbol{n}_i$, v is the normal velocity of the surface S directed into $\mathscr{R}$. The application of equation (27) to equation (23) yields

$$\underline{\frac{\partial}{\partial t}(\rho - \rho_0)} + \frac{\partial}{\partial x_i}\left(\underline{\rho u_i}\right) = (\rho - \rho_0)G\delta(t) + \left[\rho u_i - (\rho - \rho_0)v_i\right]\mathbf{n}_i \delta(n)\Xi \tag{28}$$

and

$$\frac{\partial}{\partial t}\left(\underline{\rho u_i}\right) + \frac{\partial}{\partial x_i}\left(\underline{\rho u_i u_j + p_{ij}}\right) = \underline{B_i} + \rho u_i G\delta(t) + \left[\rho u_i\left(u_j - v_j\right) + p_{ij}\right]\mathbf{n}_j \delta(n)\Xi. \tag{29}$$

The second time derivative of the perturbed density valid for all (x_i, t) may be obtained by eliminating $\underline{\rho u_i}$ from (28) and (29). Thus,

$$\begin{aligned}\frac{\partial^2}{\partial t^2}\left(\underline{\rho - \rho_0}\right) &= \frac{\partial}{\partial t}[(\rho - \rho_0)G\delta(t)] - \frac{\partial}{\partial x_i}[\rho u_i G\delta(t)] + \frac{\partial}{\partial t}\left[\left[\rho u_i - (\rho - \rho_0)v_i\right]\mathbf{n}_i \delta(n)\Xi\right] \\ &\quad - \frac{\partial}{\partial x_i}\left[\left[\rho u_i\left(u_j - v_j\right) + p_{ij}\right]\mathbf{n}_j \delta(n)\Xi\right] - \frac{\partial \underline{B_i}}{\partial x_i} + \frac{\partial}{\partial x_i \partial x_j}\left(\underline{\rho u_i u_j + p_{ij}}\right) \quad .\end{aligned} \tag{30}$$

The density form of the acoustic analogy is in the form (see Morfey and Wright [15])

$$\begin{aligned}\left(\frac{1}{c_0^2}\frac{\partial^2}{\partial t^2} - \nabla^2\right)\left[c_0^2\left(\underline{\rho - \rho_0}\right)\right] &= \frac{\partial}{\partial t}[(\rho - \rho_0)G\delta(t)] - \frac{\partial}{\partial x_i}[\rho u_i G\delta(t)] + \frac{\partial}{\partial t}\left[J_i \boldsymbol{n}_i \delta(n)\Xi\right] \\ &\quad - \frac{\partial}{\partial x_i}\left[L_{ij}\boldsymbol{n}_j \delta(n)\Xi\right] - \frac{\partial B_i}{\partial t} + \frac{\partial^2 T_{ij}}{\partial x_i \partial x_j}\end{aligned} \tag{31}$$

T_{ij}, J_i and L_{ij} on the right of (31) encode: the Lighthill stress tensor

$$T_{ij} = \rho u_i u_j + p_{ij} - c_0^2\left(\rho - \rho_0\right)\delta_{ij}, \tag{33}$$

the surface mass flux vector

$$J_i = \rho u_i - \left(\rho - \rho_0\right)v_i \equiv \rho\left(u_i - v_i\right) + \rho_0 v_i, \tag{34}$$

and the surface momentum flux tensor

$$L_{ij} = \rho u_i\left(u_i - v_i\right) + p_{ij}. \tag{35}$$

The right members of (31) are the sources that represent the physical properties of the acoustic wave. The first two members encode the aggregate impulsive mass and momentum required to drive flow from its original reference state; the second and third members contain the so called Ffowcs Williams & Hawkings (FWH) formulation [5] of surface monopoles and dipoles, evinced by Ξ, and subsequently the volume source terms, with the body force B_i and the stress tensor T_{ij} encoded spatially and temporally by $G\,\Xi$. Reethuf [17] suggested that mass-flow fluctuations may be associated with monopole sources as compact fluctuating forces, momenta, or pressures in a flow field relate with dipole sources; and fluctuating shear stresses relate with quadrupole sources. The FWH equation (31) with no initial source terms furnishes an extrapolative bridge between the simulation domain and the acoustic far field. Using [18], the replacement of the local density ϱ by a new variable ϱ^* related to ϱ together with some arithmetic operations give the equation for $\partial^2\left(\underline{\rho^* - \rho_0}\right)/\partial t^2$ in the form

$$\frac{\partial^2\left(\underline{\rho-\rho_0}\right)}{\partial t^2} = \frac{\partial}{\partial t}[\left(\rho^* - \rho_0\right)G\delta(t)] - \frac{\partial}{\partial x_i}\left[\rho^* u_i G\delta(t)\right] + \frac{\partial}{\partial t}\left[\mathrm{J}_i^* \mathbf{n}_i \delta(n)\Xi\right]$$
$$-\frac{\partial}{\partial x_i}\left[L_{ij}^* \mathbf{n}_j \delta(n)\Xi\right] + \frac{\partial \underline{\underline{\Psi^*}}}{\partial x_i} - \frac{\partial}{\partial x_i}\left[\underline{\Psi^* u_i - (\rho - \rho^*)\frac{Du_i}{Dt} + B_i}\right] + \frac{\partial}{\partial x_i \partial x_j}\left(\underline{\rho^* u_i u_j + p_{ij}}\right) \quad ,$$

(36)

Where J_i^* and L_{ij}^* are similar to Ji and Lij when ρ^* replaces ϱ and

$$\Psi^* = \frac{D\rho^*}{Dt} + \rho^* \Delta \ . \tag{37}$$

Now, a general acoustic analogy may be written in the form

$$\left(\frac{1}{c_0^2}\frac{\partial^2}{\partial t^2} - \nabla^2\right)\left[c_0^2\left(\underline{\rho^* - \rho_0}\right)\right] = \frac{\partial}{\partial t}\left[(\rho^* - \rho_0)G\delta(t)\right] - \frac{\partial}{\partial x_i}\left[\rho^* u_i G\delta(t)\right] + \frac{\partial}{\partial t}\left[J_i{}^* \boldsymbol{n}_i \delta(n)\Xi\right]$$
$$-\frac{\partial}{\partial x_i}\left[L_{ij}\boldsymbol{n}_j \delta(n)\Xi\right] + \frac{\partial \underline{\underline{\Psi^*}}}{\partial t} - \frac{\partial}{\partial x_i}\left(\underline{\Psi^* u_i + \frac{\rho^*}{\rho}B_i + \frac{\rho - \rho^*}{\rho}\frac{\partial p_{ij}}{\partial x_j}}\right) + \frac{\partial^2 \underline{\underline{T_i^*{}_j}}}{\partial x_i \partial x_j} \tag{38}$$

where the penultimate term is gotten by setting the equation of conservation as

$$\frac{Du_i}{Dt} = \frac{B_i}{\rho} - \frac{1}{\rho}\frac{\partial p_{ij}}{\partial x_j}, \tag{39}$$

and T_{ij}^* is defined in the same way as T_{ij} when ρ^* replaces ϱ

3.1 Propagation of sound inside pipes (vessels) with flow

Turbulent noise sources are typically contained in rigid walled vessels, which are acoustically reflecting. Some vessel walls are not acoustically rigid and impermeable; they therefore permit the absorption of some of the incident sound and in so doing progressively reduce the propagated and radiated sound power. In arteriosclerosis the induration (pathological hardening or thickening) of the arterial wall may cause the vasculature to be treated as rigid walled vessels. Therefore such vascular tissues will be acoustically reflecting. Non-acoustically rigid (compliant) blood vessels reduce the propagated and radiated sound power by permitting the absorption of some of the incident sound. The compliance or capacitance is a measure of changes in volume in response to changes in pressure. If it is assumed that vessel length does not alter with transmural pressure, the arterial cross-sectional compliance C_c (see [18]) could be estimated by

$$C_c = \frac{dA}{dp} \ , \tag{36}$$

where A is the vessel's cross-sectional area. The vessel's distensibility D_v is given in terms of its compliance by

$$D_v = \frac{1}{A}\frac{dA}{dp} = \frac{1}{A}C_c \ . \tag{37}$$

Suppose the perturbation fields $\tilde{H}$ (see Eq. (15)) in the pipe can be characterised by modal solutions, and each mode can be written in cylindrical coordinate in the form

$$\tilde{H}(x,r,\theta,t) = \left[\hat{H}_+(r)e^{(-ik_+x)} + \hat{H}_-(r)e^{(ik_-x)}\right]e^{(i\omega t + im\theta)}, \tag{36}$$

where subscripts + and − indicate the downstream and upstream propagating waves corresponding to the mean flow, $\omega = 2\pi f$ is the angular frequency, and $k\pm$ are the corresponding wavenumbers. The phase shift and the attenuation of the sound waves can be determined from the wave number $k\pm$ when the modes which represent the sound waves are known. The dimensionless wavenumber

$$\Gamma_\pm = \frac{k_\pm}{k_0} \tag{37}$$

may be used to described the propagation, with $k_0 = \omega/c_0$ the wavenumber in free space. Γ consists of the real part, which specifies the phase shift of the waves within one reference wavelength $\lambda_0 = 2\pi c_0/\omega$, and the imaginary part which specifies the decay of the wave amplitudes within λ_0. The value of $\Gamma_\pm$ is largely affected by mean flow convection and refraction, viscothermal effects within the acoustic boundary layer, turbulent absorption, among other factors.

We consider a plane wave regime associated with acoustic waveguide theory [16]. Assume an inviscid and adiabatic fluid, and assume further that the mean velocity profile (MVP) is uniform over the pipe cross-section, then, by indication [1] the acoustic pressure in the pipe is

$$\tilde{p}_m = \hat{p}_m(r)e^{(i\omega t - ik_m x + im\theta)}, \tag{38}$$

where,

$$\hat{p}_m(r) = BJ_m(\Re_m), \qquad B \text{ is a constant,} \tag{39}$$

and

$$\Re_m = \sqrt{(k_0 - Mk_m)^2 - k_m^2} \tag{40}$$

represents the radial wavenumber, represents the azimuthal wavenumber, $k_0 = \omega/c_0$ is the wavenumber in free space, J_m is the m-th order Bessel function of the first kind, and M is the Mach number. The boundary condition is such that the wall-normal velocity $\hat{u}_r$ is zero at the duct wall.

For inviscid and adiabatic fluids this requires that

$$\hat{u}_r\big|_{r=R} = \frac{i}{\rho_0\omega}\frac{d\hat{p}_m}{dr}\bigg|_{r=R} = 0 \Rightarrow J'_m(\Re_m R) = \hat{u}_r\big|_{r=R} = \frac{i}{\rho_0\omega}\frac{d\hat{p}_m}{dr}\bigg|_{r=R} = 0 \Rightarrow J'_m(He_m^c) = 0, \tag{41}$$

where J'_m denotes the first derivative of J_m with respect to r. The n-th solution satisfying the boundary condition Eq. (41), $He_{m,n}^c$, and the corresponding acoustic mode is known as the (m, n)th mode. The axial wavenumber $k_{\pm,m,n}$ can be calculated from (40) as

$$k_{\pm,m,n} = -\frac{Mk_0}{1-M^2} \pm \frac{k_0\left(1-(H_{m,n}^c\sqrt{1-M^2}/He)^2\right)^{\frac{1}{2}}}{1-M^2} \tag{42}$$

where $He = k_0 R$ is Helmholtz number.

There are two cases: $k_{\pm,m,n}$ is a purely real number if $He \geq He^{c}_{m,n}\sqrt{1-M^2}$, else $k_{\pm,m,n}$ contains imaginary part. The latter case is instrumental in the evanescence of sound wave since the (m, n)th mode decays exponentially in the direction of propagation. The cut-on frequency of the (m,n)th mode (i.e. the mode propagating without decaying) is $He^{c}_{m,n}\sqrt{1-M^2}$. Equations (38) and (42) presuppose that the fluid is inviscid and adiabatic, and therefore the wavenumbers of the cut-on waves are wholly real, i.e. the wave propagates without attenuation. As a rule however, the propagating waves would be unavoidably damped by the fluid or the flow.

4 Pressure and flow in open valves

The flow across a heart valve is analogous to that along a blood vessel; nevertheless, the two pressures on either side of the valve account for the pressure difference [12]. Accordingly, the pressure difference across the aortic valve that drive flow across the valve in the event of ventricular ejection is the variation between intraventricular pressure (P_{IV}) and the aortic pressure (P_{Ao}). The motion of the heart valves is usually determined via the Navier–Stokes equation wherein boundary conditions of the blood pressures, pericardial fluid, and external loading are used as the constraints. It is taken as a boundary condition in the Navier–Stokes equation in defining the fluid dynamics of blood ejection from the left and right ventricles into the aorta and the lung [8].

If the following conditions are assumed: there is conservation of inflow energy, there is stagnant region behind leaflets, there is conservation of outflow momentum, there is flat velocity profile, then the pressure drop, Δp, across an open heart valve is related to the flow rate, Q, through the valve by

$$a_1 \frac{\partial Q}{\partial t} + a_2 Q^2 = \Delta p \tag{43}$$

where a_1 and a_2 are nonzero constants. For valves assumed to have a single degree of freedom (such as studied using the aortic and mitral valves [8] the pressure and flow relationship is given by the Euler equations

$$\frac{\partial p}{\partial x} + \rho\left(\frac{\partial u}{\partial t} + u\frac{\partial u}{\partial x}\right) = 0, \tag{44}$$

$$\frac{\partial A}{\partial t} + \frac{\partial}{\partial x}(Au) = 0, \tag{45}$$

where, u = axial velocity, p = pressure, A^* = orifice area of valve. We get

$$A^*(x,t) = A_0^*\left(1 - [1 - \Lambda(t)]\frac{x}{L}\right)^2 \tag{46}$$

where, $\Lambda^2(t) = \dfrac{A^*(L,t)}{A_0^*}$ for $\Lambda(t)$being 1d.f., and L the axial length of the valve. Now,

$$\int_0^L p(x,t)\frac{\partial A^*}{\partial x}dx = \left[A_0^* - A^*(L,t)\right]p(L,t). \tag{47}$$

Note that in the case of a heart valve, the *orifice area* of the opened valve is to be used since the opening is not circular. Therefore the radius has to be given in terms of the area. Since $A = \pi r^2$, therefore $r = \sqrt{(A/\pi)} = A^*$.

To elucidate the above relationship we consider, as in [23], the effect of pressure on flow and the effect of flow on chamber pressures. Suppose Q is the flow rate of blood through the mitral valve (transmitral flow). This transmitral flow (Q) is as good as the rate of change in ventricular volume (dV_v/dt) and the negative of the rate of change in left atrial volume ($-dV_a/dt$). The time rate of change of flow can be written in the form

$$\frac{dQ}{dt} = \frac{\left(p_a - p_v - R_c Q^2 - R_v Q\right)}{M}, \tag{48}$$

where, $p_a(t)$ = Left atrial pressure (mm Hg), $p_v(t)$ = Left ventricular pressure (mm Hg), R_c = convective resistance of mitral valve (g/cm^{-7}), and R_v = viscous resistance of mitral valve (g/cm^{-4}/s^{-1}), M is a distributed mass term, $\varrho l/A^*$ with units g/cm^{-4}. Here ϱ is blood density (1.05 g/cm^3).

To decipher how chamber pressures are affected by flow, assume that at any time, the left ventricular pressure depends on the left ventricular volume, $p_v(V_v)$ and, by the same token, left atrial pressure depends on the atrial volume, $p_a(V_a)$.

We require expressions that relate the rate of change in chamber pressure (dp/dt) to the flow into or out of that chamber. The equations

$$\frac{dp_a}{dt} = \frac{\left(dV_a\right)}{dt} / \frac{dV_a}{dp_a} = -\frac{Q}{C_a} \tag{49}$$

$$\frac{dp_v}{dt} = \frac{\left(dV_v\right)}{dt} / \frac{dV_v}{dp_v} = \frac{Q}{C_v} \tag{50}$$

are the temporal left arterial and ventricular rate of change of pressure given in terms of the left arterial compliance, C_a ,and left ventricular compliance, C_v respectively.(Note that $1/C_{a,v}$ indicates chamber stiffness in each case). While equation (48) orders how pressure affects flow, equations (49-50) orders how chamber pressure is affected by flow. The coupled system of equations (49) and (50) is one that may predict the time progression of mitral flow, and atrial and ventricular pressure, together with prescribed initial pressures ($p_a(0)$ and $p_v(0)$), mitral impedance (M, R_c, and R_v) and chamber compliance.

Reduce (48)-(50) to two coupled system. Let $\Delta p = p_a - p_v$, and $C_+ = \left(\frac{1}{C_a} + \frac{1}{C_v}\right)^{-1}$,

where Δp is the transmitral gradient and C_+ is the net compliance of the two chambers. Equation (48) now takes the form

$$\frac{dQ}{dt} = \frac{\left(\Delta p - R_v Q - R_c Q^2\right)}{M}, \tag{51}$$

and subtract (50) from (49) to get

$$\frac{d\Delta p}{dt} = \frac{-Q}{C_+} \quad (52)$$

From (51) and (52) the transmitral flow (Q) may be determined.

5 Summary and result

The flow propensities in the cardiovascular structures were studied. The circulatory system is marked by laminar blood flow wherein concentric layers of blood flow in parallel down the length of a blood vessel. Nevertheless, laminar flow may transit to a chaotic (turbulent) flow under conditions of high flow velocity in which the critical Reynolds number (*Re*) is exceeded. In describing the flow characteristics in the cardiovascular structures associated phenomena such as acoustic wave and noise generation, coherent perturbation, and valvular pressure and flow relationship were discussed.The motion of the heart valves is usually taken as a boundary condition in the Navier–Stokes equation in defining the fluid dynamics of blood ejection from the left and right ventricles into the aorta and the lung.

The excerpts from this work are:

1. The pulsatile structure of flow drive the coherent perturbations (periodic waves) in any vascular region. The waveforms are vital to the determination of the physiological state of the cardiovascular parameters.
2. If the pressure drop, Δp , across an open heart valve is known the flow, Q, through the valve can be determined.

References

[1] Agarwal, N. K. and Bull, M. K. (1989). Acoustic wave propagation in a pipe with fully developed turbulent flow. Journal of Sound and Vibration, 132(2):275–298.

[2] Carley, M. Turbulence and noise, https:// people.bath.ac.uk

[3] Chenyan, W., (2015). Theoretical and numerical studies of sound propagation in low Mach-number duct flows, Doctoral Thesis in Engineering Mechanics, Stockholm: KTH Royal Institute of Technology.

[4] Farzad, A., Caldwell, E., Tawfik, P., Sue D. and Robert F.W. (2016). Audible coronary artery Stenosis. The American Journal of Medicine, 129: 515-521.

[5] Ffowcs Williams, J. E., and Hawkings, D. L. (1969). Sound generation by turbulence and surfaces in arbitrary motion, Phil. Trans. R. Soc. A 264, 321–342. doi:10.1098/rsta.1969.0031

[6] Florian, von K-B., Achudhan, K., Ralf, F.T., Barker, A.J., Blaszczyk, E., Markl, M. and Schulz-Menger J. Evaluation of aortic blood flow and wall shear stress in aortic stenosis and its association with left ventricular Remodeling, Circ Cardiovasc Imaging: Available at http://circimaging.ahajournals.org

[7] Wikipedia contributors. "Heart sounds." Wikipedia, The Free Encyclopedia.Wikipedia, The Free Encyclopedia, 23 Jun. 2022. Web. 11 Nov. 2022.

[8] Wikipedia contributors."Heart valve."Wikipedia,The Free Encyclopedia. Wikipedia, The Free Encyclopedia, 11 Sep. 2022. Web. 11 Nov. 2022.

[9] Joly, A., Violeau, D., Leroy, A., Ferrand, M. (2016). Applying Riemann solvers to open boundaries in free surface and confined flows. SPHERIC 2016, Munich, Germany. hal-01702792

[10] Jung, H.S. and Rajat, M. (2012). A coupled flow-acoustic computational study of bruits from a modelled stenosed artery, Med Biol Eng Comput . 50(10):1025-35.

[11] Khalilian, M.R.,Malekian, A, Aramesh M.R.,Dehdashtian M. and Maryam T.(2016). Innocent versus pathologic murmurs: A challenge of neonatal examination, J. Clin. Neonatol., 5: 174-8. doi: 10.1007/s11517-012-0917-5. Epub 2012 May 21.

[12] Klabunde, R.E. (2021). Hemodynamics, [In]:Cardiovascular Physiology Concepts, New 3rd ed., Wolters Kluwer Press, https://www.cvphysiology.com/Hemodynamics/H001
[13] Laufer, J. The structure of turbulence in fully developed pipe flow, Report 1174, naca.central.cranfield.ac.uk › reports ›naca-report-1174
[14] Lighthill, M. J. (1952). On Sound Generated Aerodynamically, I. General Theory, Proc. Roy. Soc. London, A 211: 564-587.
[15] Morfey C.L. and Wright M.C.M. (2007). Extension of Lighthill's acoustic analogy with application to computational aeroacoustics, Proc. R. Soc. A 463, 2101-2127, doi:10.1098/ rspa.2007.1864
[16] Pierce, A.D. (1991). Acoustics: An introduction to its physical principles and applications, The Acoustical Society of America.
[17] Reethuf, G. (1978) Turbulence-generated noise in pipe flow. Ann. Rev. Fluid Mech., 10: 333-67.
[18] Reneman, R.S., van Merode, T., Hick, P.,Muytjens, A.M., Hoeks, A.P.(1986). Age-related changes in carotid artery wall properties in men. Ultrasound Med Biol., 12:465-471.
[19] Reynolds, W.C. and Hussain, A.K.M.F. (1972). The mechanics of an organized wave in turbulent shear flow, Part 3. Theoretical models and comparisons with experiments. Journal of Fluid Mechanics, 54(02): 263–288.
[20] Sabbah, H.N. and Stein, P.D. (1976). Turbulent Blood Flow in humans, its primary role in the production of ejection murmurs. Circulation Research, 38(6):513-522.
[21] Salvatore, M. Physical diagnosis secrets (2nd ed., 2008), Elsevier Inc.
[22] Sotiropoulos, F., Trung, B. L. and Gilmanov, A. (2016). Fluid Mechanics of heart valves and their replacements, Annu. Rev. Fluid Mech., 48:259–83, doi:10.1146/annurev-fluid-122414-034314.
[23] Thomas, S.L., Heaton, J, M., Physiology, Cardiovascular Murmurs. [Updated 2020 Apr 1], Available from: https://www.ncbi.nlm.nih.gov/books/NBK525958/.
[24] Thomas, J.D. and Weyman, A.E. (1989). Fluid dynamics model of mitral valve flow: description with vitro validation, [In]: Sahn, D. J. and Yoganathan, A, P., (1989), Seminar on in vitro Studies of cardiac flow and their applications for Clinical Doppler Echocardiography-II", JACC 13(I 221): 221-33.
[25] Wei, Y., Guoyun, F., Xiaoqing Z., Yong, T., Zhenping, W. and Shiwei Z. (2018**)**. Heat transfer and friction characteristics of turbulent flow through a circular tube with Ball turbulators, Appl. Sci. 8, 776; doi:10.3390/app8050776.

International Journal of Mathematical Analysis and Modelling

Scope: The International Journal of Mathematical Analysis and Modelling (IJMAM), formerly known as the Journal of the Nigerian Society for Mathematical Biology, is the official journal of the Nigerian Society for Mathematical Biology, designed to disseminates original research findings in all areas of pure and applied mathematics. The aim of the journal is to cause to be published, original research, that shows the connection between pure and applied mathematicians, statisticians, operations researchers, physicists, engineers, computer scientists and specialists in any field of human endeavour such as in agriculture, medicine, pharmacy, life sciences, physical sciences, engineering, social sciences, humanities, arts, etc., at the crossroad of theoretical, experimental and field studies with the mathematical sciences, in order to provide solutions to problems that cut across these fields through exchange of ideas and collaborations.

Submitted papers should provide rigorous mathematical analysis of any real-world problem being discussed; at the same time, the results obtained should be useful and easily understandable by non-mathematicians. The journal will accept different kinds of articles, ranging from review articles to special invitations. All submitted manuscript will be assessed by the Editor-in-Chief before being sent out for peer-review.

Areas covered in the IJMAM include, mathematical modelling, numerical analysis, fluid mechanics, real and complex analysis, functional analysis, operator theory, statistics, algebra, computational mathematics and differential equations. Articles that show the connections between different areas of mathematics when solving real-world problems are especially welcome in the IJMAM.

Manuscript Information and guidelines for Authors

This is to invite you to submit high-quality research articles to the International Journal of Mathematical Analysis and Modelling (IJMAM), formerly known as the Journal of the Nigerian Society for Mathematical Biology.

Manuscripts should be written either using MS Word (most preferred) or in LaTeX. Initial submissions for review can be in MS Word or PDF. There will be a page restriction of a maximum of 26 pages per accepted article. The article should be concise and details of well-established mathematical methods should be omitted. Articles that do not contain significant mathematical content and results will not be accepted for publication.

Citations within the manuscript should be done using the number system i.e., “Following the idea in [7], we have that …”. Theorems, Lemmas, Propositions, Remarks, etc., should be numbered using the Section number where they appear e.g., Theorem 2.1 will appear in Section 2.

References should follow the format shown below:

[1] Anderson, R.M. and May, M. (1991). Infectious Diseases of Humans: Dynamics and Control. Oxford University Press, UK.

[2] Castillo-Chavez, C. and Song, B. (2004). Dynamical models of tuberculosis and their applications. Math. Biosci. Eng., 1:361-404.

References can be in alphabetical order in the list of references, which should be the last section in the manuscript.

Manuscripts should be submitted to the Editor-in-Chief, via the following email address: mcsb@uniben.edu. Please note that this is the **only** acceptable channel for manuscript submission at this time.

There is a publication charge for each accepted article. Payment details will be corresponded to the author(s) at the time of manuscript acceptance for publication in the IJMAM.

Subscription rates: This is subject to change from time to time. Please, contact the Editor-in-Chief for the current rates, for local and foreign subscriptions.

International Journal of Mathematical Analysis and Modelling
(Formerly Journal of the Nigerian Society for Mathematical Biology)
Volume 5, Issue 4 (November), 2022

A two-step iterative algorithm for finding common fixed point of Bregman quasi strict pseudo-contraction mappings with applications
E. Ekuma-Okereke, F.M. Okoro, and C.E. Abhulimen 109 – 131

Mathematical analysis of Ebola virus population dynamics
J. Andrawus, S. Abdulrahman, R.V.K. Singh, and S.S. Manga 132 – 163

Particle characteristics in a multi-phase Newtonian flow
F.E. Nzerem and H.C. Ugorji 164 – 174

Flow propensities in biological vessels and valves
F.E. Nzerem and H.C. Ugorji 175 - 187

International Journal of Mathematical Analysis and Modelling
(Formerly Journal of the Nigerian Society for Mathematical Biology)
Volume 5, Issue 4 (November), 2022

Contents

Analytical Method for Estimation of Black-Scholes Equation of Option Pricing
I.U. Amadi and B.E. Umoh 1 – 13

Developments in computational optimization techniques of conjugate gradient coefficient, search direction, Broyden-Fletcher-Goldfarb-Shanno, symmetric-rank one and Davidon-Fletcher-Powell quasi-Newton methods
A. Adams, U.Y. Abubakar, U. Abubakar and Y. Yakubu 14 – 24

Modeling the impact of a random perturbation on the yields of tuber crops using a computational approach
B.O. Nwala, P. Nwagor, and I.U. Amadi 25 – 37

Mathematical modelling of skilling fishery management for sustainable development of an economy
C. Nkuturum and I. George 38 – 49

Use of a generalized gamma additive model to determine the effect of monetary policy on the Nigerian stock market
O.L. Aako and O.A. Agbolade 50 – 57

Tracking oscillating edge-flames: a mathematical approach
R.O. Olayiwola, I.B.S. Mohammed, J.P. Oyubu, U. A. Abdullahi, E.O. Anyanwu, A.D. Abubakar, and E.M. Yisa 58 – 71

Statistical theories and methods: a panacea for identifying the cause of low political participation among statisticians towards enhanced national development
D.M.O. Omebo, A.Y Emmanuel, T.D Ailobhio, and A.A. Hassan 72 – 78

The spread of covid-19 disease and the health of Nigeria
R.T. Abah 79 – 88

Construction of prior probability distribution using a mollified functional
S.J. Yaga, N.P. Dibal, I.E. Gongsin, H.R. Bakari, S.C. Nwaosu, and Zara Wudiri 89 – 94

Thermal explosion with convection in porous media: a mathematical approach
R.O. Olayiwola, S.I. Yusuf, A.D. Abubakar, K.J. Audu, I.B.S. Mohammed, E.O. Anyanwu, U.A. Abdullahi, and J.P. Oyubu 95 – 108